Understanding how the Bcl-2 interactome contributes to apoptotic sensitivity

A thesis submitted to The University of Manchester for the degree of Doctor of Philosophy in the Faculty of Biology, Medicine and Health

2019

Louise E. King

School of Medical Sciences

Division of Molecular and Clinical Cancer Studies

Contents

Word count: 47,919

Index of figures

Index of tables

Abbreviations

A

AKAP1 - A-kinase anchoring protein 1

ALDH3A2 - aldehyde dehydrogenase 3 family member A2

APAF-1 - apoptotic peptidase activating factor 1

ATM - Ataxia-telangiectasia mutated

B

Bad – Bcl-2-associated agonist of cell death

Bak – Bcl-2 homologous antagonist/killer

Bat3 - HLA-B-associated transcript

Bax – BCL2 associated X protein

Bcl-2 – B cell lymphoma 2

Bcl-XL - B-cell lymphoma-extra large

BH – Bcl-2 homology

BHFDR - Benjamini and Hochberg corrected false discovery rate

Bid – BH3 interacting-domain death agonist

Bim – Bcl-2 interacting mediator of cell death

Bok – Bcl-2 related ovarian killer

C

c-FLIP - Cellular FLICE-inhibitory protein

CARD – caspase recruitment domain

CDK – cyclin dependent kinase

CDT1 - chromatin licensing and DNA replication factor 1

CISD1 - CDGSH Iron Sulfur Domain 1

CLL – chronic lymphocytic leukaemia

COX-2 - cyclooxygenase-2

CRISPR - clustered regularly interspaced short palindromic repeats

CREB - cAMP response element-binding

D

DD – death domain

DED – death effector domain

DIABLO - direct IAP binding protein with low pI

DISC – death-inducing signalling complex

DKO – double knockout

DR5 – death receptor 5

Drp1 – dynamin related protein 1

E

E2F1 - E2 transcription factor 1

EGF – epidermal growth factor

ERAD - endoplasmic-reticulum-associated protein degradation

ERK - extracellular-signal-regulated kinase

F

FCCS – fluorescence cross-correlation spectroscopy

Fis1 - mitochondrial fission protein 1

FKBP8 – FK506-binding protein 8

FLIM – fluorescence lifetime imaging

FLIP – fluorescence loss in photobleaching

FRAP – fluorescence recovery after photobleaching

FRB - Rapamycin binding domain of mTor

FRET - Förster resonance energy transfer

FUCCI - fluorescence ubiquitination-based cell cycle indicator

H

H 1/2B – histone 1/2B

HBD – hormone binding domain

HIF-1α - hypoxia-inducible factor 1-alpha

I

IAP - inhibitor of apoptosis

IRE1α - (inositol-requiring enzyme 1 alpha)

IRF-1/3 - interferon regulatory factor-1/3

M

Mcl-1 - myeloid cell leukaemia-1

MEF – mouse embryonic fibroblast

MFF – mitochondrial fission factor

Mfn 1/2 – mitochondrial fusion regulator 1/2

MOMP – mitochondrial outer membrane permeabilisation

N

NFκB – nuclear factor kappa-light-chain-enhancer of activated B cells

NOD1 - nucleotide-binding oligomerisation domain-containing protein 1

NSCLC – non-small-cell lung carcinoma

O

OMM – outer mitochondrial membrane

OPA1 - optic atrophy protein 1

P

PKA – protein kinase A

PMAIP1 - Phorbol-12-myristate-13-acetate-induced protein 1

PPIA - peptidylprolyl isomerase A

Puma – p53 upregulated modulator of apoptosis

R

ROI – region of interest

ROS – reactive oxygen species

S

SAINT - significance analysis of interactome

SCLC – small cell lung carcinoma

SLBP – stem-loop binding protein

SMAC – second mitochondria-derived activator

SNIPer - protease under small-molecule control

STAT - signal transducer and activator of transcription

T

TEV – tobacco etch virus

TKT - transketolase

TMD – transmembrane domain

TNF – tumour necrosis factor

TNFR1 - tumour necrosis factor receptor 1

TRAIL - TNF-related apoptosis-inducing ligand

TRC40 - TMD recognition complex 40

U

UV – ultraviolet

V

VDAC – voltage-dependent anion channel

X

XIAP - X-linked inhibitor of apoptosis protein

Abstract

Apoptotic sensitivity between individual cells within a population is varied and the molecular basis of this variation is unclear. Bcl-2 family proteins are the central regulators of apoptosis at mitochondria, with interactions between pro- and anti-apoptotic family members dictating the life or death decision of a cell. Bcl-2 proteins are in equilibrium between mitochondria and cytosol, which shifts to a more mitochondrial state as cells move closer to their apoptotic threshold, termed mitochondrial priming. Heterogeneity in anti-apoptotic Bcl-2 protein dynamics in live cells is predictive of priming within cell populations. What regulates the changes in interactions between pro- and anti-apoptotic proteins in a healthy cell compared to a cell that is primed to die is complex. Using live cell imaging techniques, we show that BH3-mimetics such as ABT-737 do not fully recapitulate the binding of full length BH3 proteins at the outer mitochondrial membrane (OMM). What differs between these binding mechanisms is unknown, but it is likely due to full-length Bcl-2 proteins forming part of larger regulatory complexes at the OMM. Using a proximity Biotin labelling approach to determine what other factors are involved in regulating Bcl-2 protein dynamics outside of the protein family itself reveals that mitochondrial membrane proteins are likely to play a key role. Examining these interactions in more detail will improve our understanding of the causes of apoptotic heterogeneity within cell populations and may enable improved efficacy of BH3-mimetic compounds.

Declaration

No portion of the work referred to in this thesis has been submitted in support of an application for another degree or qualification of this or any other university or other institute of learning.

Copyright Statement

i. The author of this thesis (including any appendices and/or schedules to this thesis) owns certain copyright or related rights in it (the “Copyright”) and s/he has given The University of Manchester certain rights to use such Copyright, including for administrative purposes.

ii. Copies of this thesis, either in full or in extracts and whether in hard or electronic copy, may be made only in accordance with the Copyright, Designs and Patents Act 1988 (as amended) and regulations issued under it or, where appropriate, in accordance with licensing agreements which the University has from time to time. This page must form part of any such copies made.

iii. The ownership of certain Copyright, patents, designs, trademarks and other intellectual property (the “Intellectual Property”) and any reproductions of copyright works in the thesis, for example

iv. graphs and tables (“Reproductions”), which may be described in this thesis, may not be owned by the author and may be owned by third parties. Such Intellectual Property and Reproductions cannot and must not be made available for use without the prior written permission of the owner(s) of the relevant Intellectual Property and/or Reproductions.

v. Further information on the conditions under which disclosure, publication and commercialisation of this thesis, the Copyright and any Intellectual Property and/or Reproductions described in it may take place is available in the University IP Policy (see http://documents.manchester.ac.uk/DocuInfo.aspx?DocID=2442 0), in any relevant Thesis restriction declarations deposited in the University Library, The University Library’s regulations (see http://www.library.manchester.ac.uk/about/regulations/) and in The University’s policy on Presentation of Theses.

Acknowledgments

Firstly, I would like to thank my supervisors Andrew Gilmore and Keith Brennan for all the help and advice they have provided over the past few years. It's certainly had its ups and downs, but their level-headedness and ability to laugh at my mistakes helped keep me calm during times of stress. Thank you also to my advisor, Mike White, for his incredibly useful input throughout.

Thank you also to all the members of the Gilmore, Brennan, Streuli, Swift and Ucar labs that I have had the pleasure of working with over the course of my studentship. A special thanks go to Rob Pedley and Matt Jones for not only putting up with my complaining, but for their willingness to share ideas and offer help and advice when needed, be it in the lab or in the pub.

I would also like to thank all members of the Core Facility departments for their invaluable expertise and help. In particular: Peter March, Roger Meadows and Dave Spiller in Bioimaging; Mike Jackson in Flow Cytometry; David Knight in BioMS, and Craig Lawless for proteomics data analysis.

Finally, I want to thank my parents for all the support, encouragement, and offers of trips back to Scotland when things got too stressful. You've always supported me in everything that I've chosen to do, and this no exception. I couldn't have done it without you.

Author contributions

Certain figures within this thesis have been produced in collaboration with others:

Chapter 3: Mutagenesis, immunofluorescence and apoptosis assays of anti-apoptotic ΔTM plasmids were carried out by Robert Pedley (Fig. 3.3 and 3.4). FRAP of WT and BH3 2A mCherry-BH3 proteins was carried out by Ricardo Rodriguez-Enriquez (Fig. 3.7).

Chapter 4: mCherry was cloned into the Bid^{Tev} vector by Ricardo Rodriguez-Enriquez (Fig. 4.1). Cloning of Tev-V5 into the pCDH-TRE3GS-MCS-EF1α-tagBFP-T2A-TetOn3G vector and initial creation of the stable BBT MCF10A cell line was carried out by Robert Pedley (Fig. 4.6). FCCS experiments were carried out by Ryuhei Sakabe (Fig. 4.8).

Chapter 5: MDA-MB-231 cell fate microscopy and analysis (Fig.5.5), and creation of the lentivirus containing pLL3.7m-Clover-Geminin(1-110)-IRES-mKO2-Cdt(30-120) (Fig.5.6) was carried out by Robert Pedley.

Chapter 6: BirA*Bcl-XL construct cloning, virus production, cell line creation, BioID experiments and analysis were carried out by Robert Pedley (Fig. 6.2). BirA*Bax and BirA*S184V Bax construct cloning was carried out by Jordan Morris (Fig. 6.11). Bax BioID MaxQuant and SAINTexpress analysis was carried out by Craig Lawless.

1. Introduction

1.1 General introduction

A key challenge in cancer therapy is determining how to target tumour cell populations whilst minimising impact on healthy surrounding cells. One major issue limiting the efficacy of current treatments is dose-limiting toxicity, particularly with the types of cytotoxic agents such as Taxol and Docetaxel used for more advanced tumours. The majority of cytotoxic chemotherapies used in clinics kill cancer cells by inducing apoptosis, a form of programmed cell death that is a highly-regulated and evolutionarily conserved process with no inflammatory response[1]. Whilst this can initially be very effective, resistance to such treatments can manifest over time. The increased understanding of apoptosis that has developed over the past decades is now providing new opportunities for targeting vulnerabilities in cancer, however there are still large gaps in our knowledge. How apoptotic sensitivity differs between normal tissue and tumours, between different tissue types, and within individual tissues themselves is not fully understood. How individual cells regulate their apoptotic sensitivity, and if this sensitivity is variable is unclear. Understanding the fundamentals of apoptosis more fully is crucial for improving treatment response.

Apoptosis is a fundamental process during development and maintenance of tissue homeostasis, and has also been identified as a key hallmark of cancer when incorrectly regulated[2]. Programmed cell death was initially discovered in silk moth studies in 1965[3], with the term apoptosis later being coined by Kerr and colleagues[1]. Electron microscopy analysis of apoptosis identified the key stages of the process: cell separation and condensation, membrane blebbing[1], chromatin condensation, DNA fragmentation[4], apoptotic body formation and finally clearance of cell remnants[1]. Although apoptosis occurs asynchronously throughout a cell population, the same morphological stages always occur in sequence[5]. Further studies revealed that the morphological features and kinetics of apoptosis are conserved among a wide variety of organisms, including humans, suggesting a fundamental role in maintaining cellular homeostasis[6].

Initiation of apoptosis can occur via two signalling pathways depending on whether the apoptotic initiating stimulus occurs from inside or outside the cell, termed the intrinsic pathway or extrinsic pathway, respectively. Although the initiation of these pathways occurs via distinct mechanisms, they are not mutually exclusive; both are reliant on the activation of a family of cysteine-aspartic proteases (caspases), and crosstalk can occur between the two pathways.

1.1.1 Caspases – the executioners of apoptosis

Caspases hydrolyse peptide bonds at an aspartic acid via a cysteine residue in their active site to either activate or inactivate their target proteins[7]. There are currently 11 known genes in the human genome which encode different caspase proteins[8] which have over 400 target proteins[9]. These are involved in a multitude of processes such as cell adhesion, DNA synthesis and repair, protein translation, calcium and lipid metabolism, and apoptosis[10]. Seven of these caspases (caspase-2, -3, -6, -7, -8, -9 and -10) are specifically involved in apoptosis. Caspases are classified as either sensitisers or executioners based on their mechanism of action and target substrates (discussed below). Initiator caspases are synthesised as inactive zymogens and remain inactive until a pro-apoptotic signal initiates their activation via dimerisation, whereas executioner caspases are synthesised as dimers.

Initiator caspases include caspase-2, -8 and -9. When inactive these zymogens are composed of a prodomain linked to a large p18 and a small p12 subunit[11] (Fig. 1.1A). The prodomain varies in structure between caspases, either containing a death effector domain (DED) or a caspase recruitment domain (CARD)[12]. Initiator caspases undergo autoactivation by heterodimerisation in response to apoptotic stimuli via recruitment of adaptor molecules at their prodomain[13,14]. This recruitment causes an increase in concentration of inactive caspases to the area thus allowing proximity-induced dimerisation to occur[15]. Specifically where caspases are recruited to is specific to each, with caspase-2 recruited to the PIDDosome, caspases-8 to the death-inducing signalling complex (DISC) and caspase-9 to the apoptosome[16]. After activation via dimerisation, a further autoproteolytic cleavage can occur in which the prodomain is removed in order to stabilise the catalytic domain of the caspase, at least in terms of caspase-8[17] and possibly caspase-9[18]. Caspases involved in

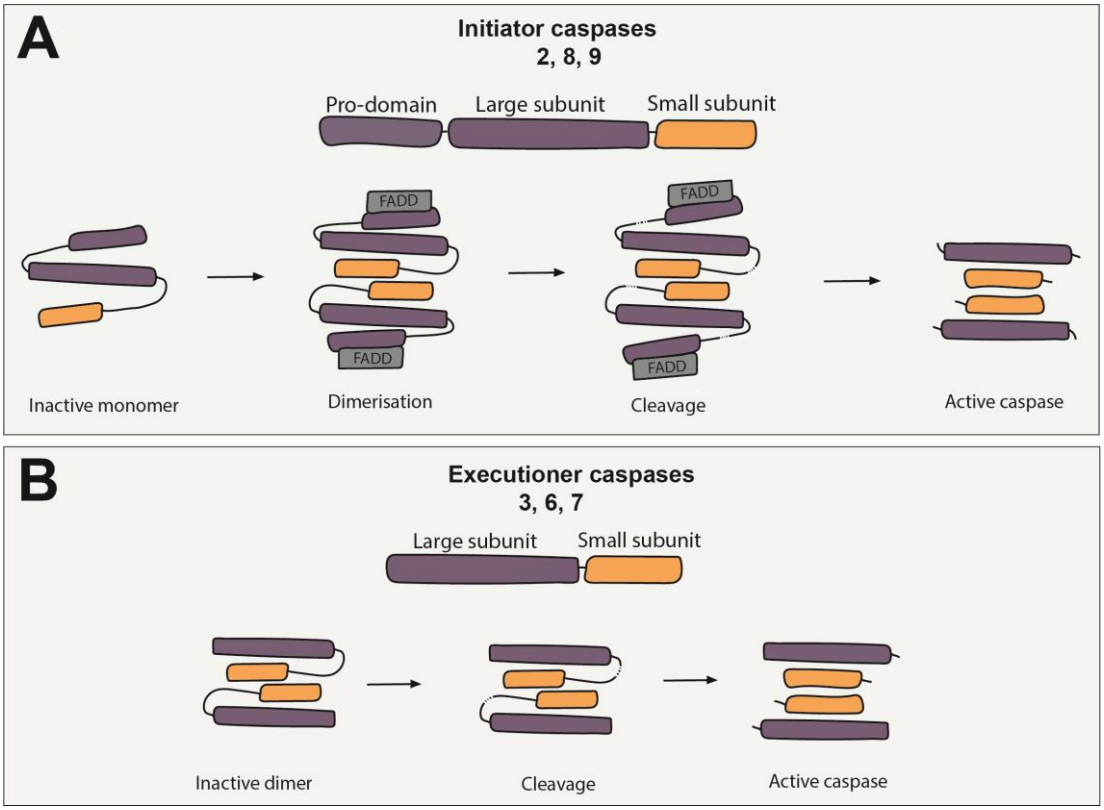

Figure 1.1. Initiator and executioner caspase activation

A. Initiator caspases are inactive as monomers composed of a pro-domain, large subunit and small subunit. Recruitment to adaptor proteins such as FADD leads to autoactivation via dimerisation. Autoproteolysis can then occur to stabilise the active form. Active initiator caspases can then cleave downstream executioner caspases.

B. Executioner caspases exist as inactive dimers and are activated upon cleavage via initiator caspases. Active caspases can then interact with a range of substrates to begin dismantling the cellular components.

regulating processes other than apoptosis (e.g. caspase-1 and the inflammatory response) are also activated via a similar mechanism[19].

The known structure of executioner caspases such as caspase-3, -6 and -7 is mainly based on structural analysis of caspase-7, which begins as an inactive dimer consisting of a small and large subunit[14,20] (Fig. 1.1B). Activation occurs upon cleavage within the linker region between the two subunits by active initiator caspases, allowing each active site of the executioner caspase to come into close-proximity. Subsequently, activated executioner caspases are capable of cleaving other executioner caspases, as well as other substrates, ultimately leading to apoptosis. Which specific caspases are activated is dependent on the type of apoptotic stimulus the cell responds to, and thus which apoptotic pathway is initiated: the intrinsic or extrinsic pathway.

1.1.2 Extrinsic apoptosis

The extrinsic apoptotic pathway, or death receptor pathway, is initiated upon binding of extracellular ligands to cell surface receptors (Fig.1.2). Apoptosis is initiated via signalling from death receptor ligands from the tumour necrosis factor (TNF) superfamily such as Fas (as well as TRAIL and TNFα). Ligands bind to their specific death receptors (e.g. Fas receptor) at the cell membrane[21]. These death receptors contain intracellular Death Domains (DD) which enable the corresponding death receptors to engage the cell's downstream death machinery[22]. In the case of Fas ligand binding to its receptor, the receptors oligomerise and recruit adaptor proteins to form the death-inducing signalling complex (DISC)[23]. DISC formation initiates procaspase-8 binding, in turn causing its homo-dimerization and cleavage into its active form, caspase-8. This process is regulated by the FLICE-inhibitory protein (c-FLIP), a protein that is structurally similar to caspase-8 but does not contain a catalytic site[24]. Upon caspase-8 activation, two distinct caspase signalling pathways can occur depending on the cell type involved. In "type I" cells (e.g. thymocytes and mature lymphocytes), caspase-8 cleaves procaspases -3 and -7 into their active forms. In "type II" cells (e.g. hepatocytes and pancreatic β cells), procaspases -3 and -7 are inhibited by the X-linked inhibitor of apoptosis, XIAP, which binds to the procaspases with high affinity to inhibit their activation[25]. Instead the pro-apoptotic protein Bid is cleaved by caspase-8, activating mitochondrial outer membrane

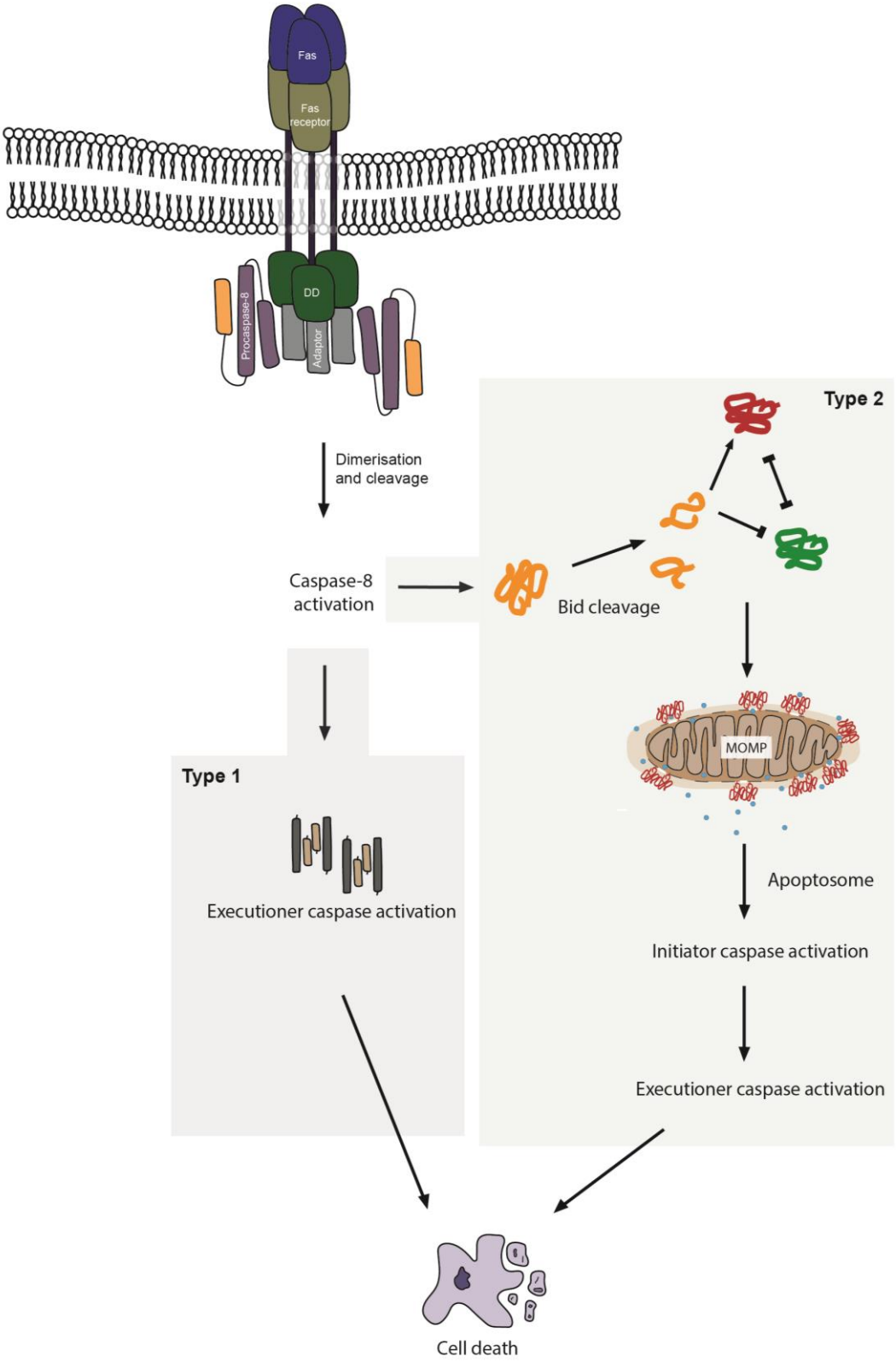

Figure 1.2. Extrinsic apoptotic pathway

External pro-apoptotic signals initiate the extrinsic apoptotic pathway via death receptor ligands (e.g. Fas) binding their specific cell surface receptors. This causes dimerisation of the intracellular DD, recruiting adaptor molecules (e.g. FADD) forming the DISC. Procaspase-8 is cleaved and activated at the DISC and either activates the type 1 response in which executioner caspases are directly cleaved, or the type 2 response in which Bid is cleaved into tBid and MOMP initiated

permeabilisation (MOMP)[26,27]. Bid cleavage also occurs in type I cells but does not induce apoptosis due to a preference for the type I pathway, most likely due to lower levels of XIAP in type I cells[28]. Bid is one member of a family of proteins called the Bcl-2 proteins which contains both pro- and anti-apoptotic members that regulate apoptotic outcome by binding to and inhibiting each other. The different family members and their mechanism of action are described in more detail later.

Death receptors have been examined as potential targets for treatment of a range of cancers. However, not all TNF receptors are appropriate targets. Fas-targeted therapy has been shown to cause severe liver damage[29,30]. Targeting TNFα also resulted in significant side-effects during clinical trials including lung or liver failure and increased blood clotting[31,32] Targeting TRAIL (TNF-related apoptosis inducing ligand) and its death receptors in cancers overexpressing the ligand (e.g. non-small cell lung cancer (NSCLC)[33] or colon carcionma[34]) has shown more positive results as it can specifically kill tumour cells without harming surrounding healthy tissue[35]. Recombinant human TRAIL and antibodies targeting TRAIL receptors have shown promise, however high levels of resistance have hampered clinical use as only a select number of patients showed successful response[36,37]. Furthermore, the majority of TRAIL receptor targeting drugs are not potent enough to sufficiently act as agonists alone, and whilst combination therapies have improved efficacy, patient toxicity is still an issue. Recent efforts have aimed at improving these issues as reviewed by de Miguel et al[38] but as of yet no effective treatment is available.

1.1.3 Intrinsic apoptosis

The intrinsic apoptotic pathway is activated via pro-death signals originating from within the cell, such as DNA damage or a lack of growth factor signalling (Fig. 1.3). Depending on the pro-apoptotic stimulus present, the various pro-apoptotic and anti-apoptotic members of the Bcl-2 protein family are activated and inhibit the functions of the other. Once the balance of the pro-death to pro-life signal shifts in favour of death, a subset of the Bcl-2 family pro-apoptotic proteins form pores in the outer mitochondrial membrane (OMM), causing a significant loss in OMM integrity, releasing apoptogenic factors from the inter- membrane space such as cytochrome c[39]. This permeabilization is considered the “point of no return” in the apoptotic

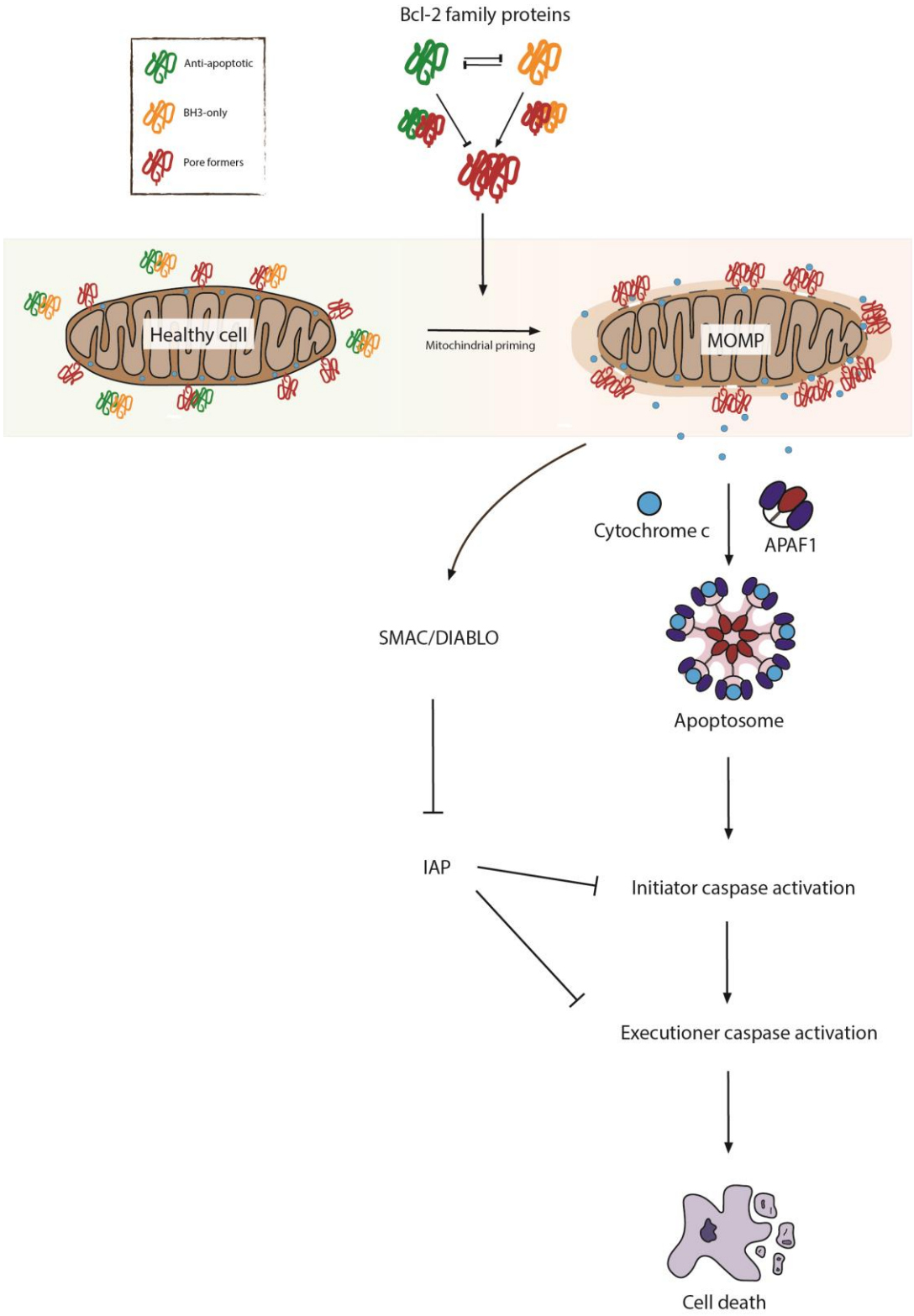

Figure 1.3. Intrinsic apoptotic pathway
Interactions between Bcl-2 family proteins are regulated by intrinsic apoptotic signals. Upon increase of an apoptotic signal, pro-apoptotic Bcl-2 proteins insert into the OMM, form pores and MOMP occurs, releasing cytochrome c and APAF1 into the cytosol. Cytochrome c, APAF1 and dATP form the apoptosome which catalyses initiator procaspase activation. This leads to cleavage of executioner procaspases which, when activated, initiate cell death. SMAC/DIABLO are also released from mitochondria during MOMP to prevent IAP inhibition of initiator and executioner caspase activation.

process, as once this occurs a cell is committed to death. Released cytochrome c can bind to the apoptotic peptidase activating factor 1 (APAF1), a cytosolic protein consisting of a caspase-recruitment domain (CARD), nucleotide binding domain and a number of WD40 repeats[40]. The cytochrome c/APAF1 complex, alongside dATP forms a complex called the apoptosome, which can in turn recruit procaspase-9 and initiate its cleavage[41,42]. Active caspase-9 can then itself cleave and activate caspase-3 and caspase-7[43], which initiates the classical biochemical disruption of the cell such as activation of DNA fragmentation. Simultaneously with cytochrome c release, the second mitochondria-derived activator (SMAC) protein (also known as the direct IAP binding protein with low pI, DIABLO) is also released[44,45]. SMAC/DIABLO advance the apoptotic process by inhibiting the inhibitor of apoptosis (IAP) proteins such as XIAP.

1.2 Bcl-2 family proteins – the guardians of life and death

The Bcl-2 family of proteins consists of at least 20 proteins that share regions of sequence homology (termed BH domains) within their structure. All family members are composed of 6-7 amphipathic α-helices surrounding two central hydrophobic α-helices. The pro- or anti-apoptotic function of each protein is largely dependent on their specific structure which dictates how they are activated, and which other Bcl-2 family proteins they interact with. Anti-apoptotic Bcl-2 proteins bind to pro-apoptotic proteins to inhibit them, keeping cells alive. When apoptotic signals increase, the levels of pro-apoptotic proteins increase, sequestering all the anti-apoptotic proteins. This allows the remaining pro-apoptotic proteins to form pores in the outer mitochondrial membrane and initiate MOMP. A brief overview of each protein examined within this thesis will be discussed below, with others reviewed elsewhere such as Youle & Strasser, 2008[46].

1.2.1 Anti-apoptotic Bcl-2 family proteins

Anti-apoptotic Bcl-2 proteins are comprised of four BH domains and a C-terminal transmembrane domain (TMD) (Fig. 1.4A). They function as inhibitors of apoptosis by binding to, and sequestering, pro-apoptotic Bcl-2 proteins, preventing MOMP. Binding to pro-apoptotic proteins occurs within the BH1-BH3 domains at a hydrophobic cleft. Whilst structurally similar to each other, individual anti-apoptotic

Bcl-2 proteins have some unique structural and functional attributes as discussed below.

1.2.1.1 Bcl-2

The first Bcl-2 family gene discovered was *BCL2* itself, when examining a frequent translocation between chromosomes 14 and 18 in B cell lymphoma patients that caused its overexpression[47,48]. This was the first oncogene to be discovered that promoted cell survival rather than increasing the rate of proliferation, introducing a new paradigm in the development of carcinogenesis[49]. Early *in vitro* studies examining the role of Bcl-2 in healthy tissues demonstrated its importance in development, including in the early development of the nervous system[50], and at specific stages during T-cell development[51], as its anti-apoptotic function is critical in ensuring specific cells survive during the high levels of apoptosis seen during development. Further analysis using immunofluorescence and cell fractionation studies revealed a higher concentration of the Bcl-2 protein present in longer-lived progenitor cells, or in mature cells with longer lifespans, compared to cells with a higher turnover rate[52]. It was also discovered to have a mainly mitochondrial localisation in cells[53] although it is also localised to the endoplasmic reticulum (ER) and nuclear envelope[54].

Homozygous Bcl-2 knockout mice are viable, however, mice show significant growth retardation, polycystic kidneys, and eventual early mortality postnatally due to developmental defects caused by deficient apoptosis regulation[55]. Overexpression of Bcl-2 in specific tissues in mice cause a number of phenotypes including brain hypertrophy[56] and resistance to sepsis-induced apoptosis in T-lymphocytes[57] due to increased resistance to apoptosis in these tissues. Furthermore, in humans, Bcl-2 levels have been shown to be elevated in a range of cancers including chronic lymphocytic leukaemia (CLL)[58], small cell lung carcinoma (SCLC)[59] and neuroblastoma[60].

The 3D structure of Bcl-2 was determined nearly 20 years after its discovery, in part due to its poor solubility[61]. After characterising the structure of another anti-apoptotic Bcl-2 protein, Bcl-XL, a soluble Bcl-2/Bcl-XL chimera was used for NMR analysis

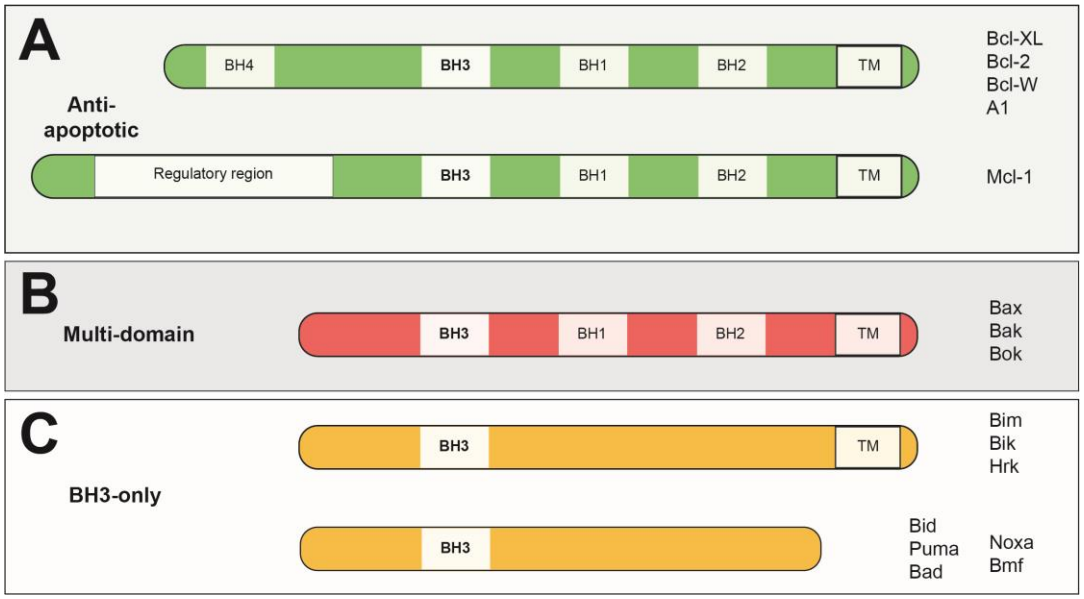

Figure 1.4. Structure of Bcl-2 family proteins

A. Anti-apoptotic Bcl-2 proteins including Bcl-XL and Bcl-2 contain four BH domains and a C-terminal TMD for membrane insertion. Mcl-1 is unique in that it does not contain a BH4 domain, but instead has a large regulatory region at its C-terminus containing four PEST sequences, within which are multiple important regulatory residues.

B. Pro-apoptotic Bcl-2 proteins are divided into 2 subgroups based on the number of BH domains present. The multi-domain proteins Bax, Bak and Bok, contain the BH1-3 domain and also the C-terminal TMD

C. The second group of pro-apoptotic proteins, the BH3-only proteins (including both activators and sensitisers), contain only the BH3 domain (e.g. Bid, Puma and Bad), whilst Bim, Bik and Hrk also contain a C-terminal TMD.

which revealed its helical structure[61]. A hydrophobic groove is present on the surface of the protein where it interacts with other Bcl-2 family members, demonstrated in studies where substitution mutations in these residues abolish Bcl-2 protein interactions and remove its anti-apoptotic function[62]. It also contains a C-terminal 19 amino acid α-helical transmembrane domain that is crucial for its mitochondrial localisation[63]. Studies examining the control of Bcl-2 have revealed that Bcl-2 can be regulated post-transcriptionally, as well as via direct binding of other Bcl-2 family proteins. For example, Bcl-2 is phosphorylated during mitotic arrest to increase apoptotic susceptability[64]. Bcl-2 also has other roles in cells apart from preventing MOMP, including regulating mitochondrial morphology, calcium homeostasis at the ER and autophagy[65,66].

1.2.1.2 Bcl-XL

The BCL2L1 gene was identified in a 1993 study characterising avian lymphoid development whilst attempting to identify Bcl-2-related genes[67]. Two distinct isoforms of Bcl-X were discovered to exist due to alternate splicing; the long 233 amino acid anti-apoptotic isoform, Bcl-XL, and the shorter 170 amino acid pro-apoptotic isoform, Bcl-XS. X-ray crystallography and NMR spectroscopy identified the full structure of Bcl-XL minus its transmembrane domain[68], highlighting its similarity to Bcl-2. Further X-ray crystallography studies have demonstrated the hydrophobic groove within the BH1-BH3 regions is important for binding pro-apoptotic proteins such as Bak[69] and Bim[70]. Like Bcl-2, Bcl-XL is found distributed between mitochondria and cytosol although a comparatively larger proportion of Bcl-XL is free in the cytosol[71]. Interestingly, although structurally and functionally similar, a direct comparison between Bcl-2 and Bcl-XL highlights significant differences in their activities. For example, Bcl-XL has been shown to be ten times more effective at protecting MCF-7 cells from doxorubicin-induced apoptosis than Bcl-2[72] suggesting differences in which pathways primarily regulate the proteins and which other proteins they interact with.

Like Bcl-2, Bcl-XL shows high tissue-specific expression during embryonic development and tissue homeostasis[73]. Bcl-XL knockout mice die at embryonic day 13 with significant levels of cell death in the developing brain, spinal cord and liver[74]. The anti-apoptotic function of Bcl-XL is further exemplified as BCL2L1 is one of the

most commonly amplified anti-apoptotic genes found in cancer (e.g. gastric cancer[75]), as well as having protein overexpression in others including breast cancer[76] and colorectal cancer[77]. Under normal circumstances, Bcl-XL is regulated transcriptionally by a number of transcription factors including NF-κB and signal transducer and activator of transcription (STAT) proteins[78], and post-translationally via numerous proteins such as cyclin-dependent kinases (CDKs) during cell cycle regulation[79]. Outside of apoptotic regulation via interaction with other Bcl-2 family proteins, Bcl-XL is known to have roles in regulating presynaptic plasticity[80] and, like Bcl-2, calcium homeostasis at the ER[81].

1.2.1.3 Bcl-W

Bcl-W was discovered using a PCR-based cloning strategy and its anti-apoptotic function originally demonstrated in lymphoid and myeloid cells[82]. NMR spectroscopy revealed a similar 3D structure to Bcl-2 and Bcl-XL, however its C-terminal transmembrane domain differs from Bcl-2 in that helix α8 is folded into its BH3 domain and can be displaced by binding of pro-apoptotic proteins such as Bid in a similar manner to the pro-apoptotic Bcl-2 protein Bax[83]. Furthermore, addition of other BH3 peptides such as Bim, or indeed a smaller 26mer Bim peptide, converts Bcl-W from being loosely associated with the OMM to an integral membrane protein via this transmembrane domain displacement[84]. Bcl-W is structurally distinct from Bcl-XL in that it contains an extra C-terminal α-helix within its hydrophobic groove which causes a comparative decrease in its affinity for BH3 protein binding[85]. The exact role this extra helix plays in the function of Bcl-W is unknown.

Mice null for Bcl-W are viable and healthy, however males are infertile – another similarity Bcl-W shares with pro-apoptotic Bax[86]. Bcl-W expression has been shown to be critical for B-cell survival, with overexpression contributing to lymphomagenesis in B-cell lymphoma and Burkitt lymphoma[87]. Bcl-W also potentially contributes to invasiveness of gastric cancer cells[88]. Both Bcl-XL and Bcl-W expression are important in sensory neuronal survival during development, however Bcl-W appears to be more effective at inhibiting apoptosis with age compared to Bcl-XL[89]

1.2.1.4 Mcl-1

Mcl-1 was originally isolated from ML-1 human myeloid leukaemia cells and is similar in structure to Bcl-2[90]. It shares a similar BH3-binding hydrophobic groove to Bcl-XL[91] but within this groove are a number of unique residues that may contribute to its binding specificity with BH3 proteins[91]. Furthermore Mcl-1 does not contain a BH4 domain but is significantly larger than its other anti-apoptotic counterparts as it contains extra regulatory regions within its N-terminus. The first 170 residues of Mcl-1 are enriched for proline, glutamic acid, serine and threonine residues (termed PEST regions)[90] which may contribute to its comparatively faster turnover time[92]. A number of significant residues within the PEST regions have been identified as being important regulatory phosphorylation sites. For example serine 155, 159 and threonine 163 are all glycogen synthase kinase-3 sites controlling Mcl-1 degradation, whereas serine 64 is a CDK1 and CDK2 site which, when phosphorylated, decreases Mcl-1's affinity for BH3 proteins[93]. Analysis via immunofluorescence in ML-1 cells initially determined that, whilst the distribution of Mcl-1 is similar to that of Bcl-2 in terms of showing significant mitochondrial localisation, some Mcl-1 is imported into the mitochondrial matrix[94], as well as being distributed to other membrane compartments (e.g. nuclear envelope)[95] and tissues at different stages of development[96].

Knockout of Mcl-1 in mice causes peri-implantation embryonic lethality suggesting a key role for the protein in early developement[97]. Conditional knockout mice caused premature apoptosis in B and T lymphoid cells and haematopoietic stem cells. Inhibiting Mcl-1 expression has been an aim in recent years for the treatment of numerous Mcl-1-overexpressing cancers including breast cancer[98], prostate cancer[99] and ovarian cancer[100]. Whilst developing an Mcl-1 specific mimetic has proven difficult, potent inhibitors have now been developed (discussed later). Outside of its roles in development, Mcl-1 is involved in cell cycle progression, with overexpression causing inhibition during S-phase[101] and a decrease in expression levels as mitosis progresses[102].

1.2.2 Multi-domain pro-apoptotic Bcl-2 family proteins

The multi-domain pro-apoptotic proteins are also known as the pore formers Bax, Bak and Bok. This subset of proteins are structurally similar to the anti-apoptotic proteins, containing the BH1-3 domains (and possibly a BH4 domain[103]) as well as a C-terminal TMD, but are responsible for permeabilising the OMM during MOMP (Fig. 1.4B). The multi-domain proteins exert their pro-apoptotic function by forming pores in the OMM causing the release of cytochrome c. Whilst initially seeming functionally redundant, all three proteins carry out specific roles within cells. Bok is the least well characterised of the pore-formers and is expressed at very low levels due to its high turnover rate[104] in a select number of tissues[105]. It is therefore not examined within the scope of this thesis, but its specific roles in ER-associated degradation leading to apoptosis are examined elsewhere[104,106].

1.2.2.1 Bax

The Bax protein was discovered in 1993 during a study identifying novel interacting partners of Bcl-2 via co-immunoprecipitation[107]. The 21kDa protein was cloned and sequenced to reveal that it was very similar in sequence to anti-apoptotic Bcl-2 but induced apoptosis rather than inhibited it. Bax is composed of nine α-helices – eight amphipathic helices surrounding hydrophobic helix α5 - with a 3D structure closely resembling that of Bcl-XL including a large flexible loop between helices α1 and α2 and a hydrophobic cleft[108]. In the same structural study, it was noted that Bax in solution is a monomer and resides predominantly in the cytosol due to occlusion of its C-terminal α9 TMD helix within its hydrophobic groove. It was suggested that only upon the presence of a pro-apoptotic stimulus does Bax localisation change to a more mitochondrial state to induce MOMP[109]. This view of Bax is beginning to change with an increasing number of studies examining Bax in live cells. It has now been shown that Bax is very dynamic in cells, continuously shuttling between cytosol and mitochondria, but becoming more mitochondrial in the presence of pro-apoptotic signalling[110–112].

The precise mechanism by which Bax is activated has been an area of much debate but is believed to be a multi-step process whereby Bax undergoes conformational

changes, mitochondrial localisation, and dimerisation at the OMM. In the case of transient apoptotic signals like extracellular matrix (ECM) detachment, Bax can translocate to the OMM within 15 minutes of signalling[113] but cannot initiate MOMP until activated by p38MAPK signalling[114]. Re-attachment to the ECM causes Bax retrotranslocation back to the cytosol[110]. Upon the presence of a more persistent pro-apoptotic stimulus, cellular levels of Bax begin to increase[115]. The initial binding step by BH3 proteins to Bax is thought to be relatively transient and thus has been historically difficult to study. A study by Gavathiotis and colleagues suggests that BH3 proteins can bind to Bax at an alternative site to the anti-apoptotic proteins, located at α-helices 1 and 6[116]. Later studies agreed with this, demonstrating that the α1 helix of Bax plays a necessary role in its ligand-induced activation by Bid and Puma[117]. BH3 protein binding induces destabilisation of the protein structure, causing the α1-helix to unfold, with the core α2-α5 helices separating from the α6-α9 segment[118]. This displacement of the C-terminal helix from the hydrophobic groove presents an opportunity for membrane insertion. Interestingly, it has also been suggested that Bax can autoactivate in the absence of BH3 protein binding when anti-apoptotic proteins are downregulated, suggesting that Bax is repressed by anti-apoptotic proteins in healthy cells but is capable of membrane insertion without BH3 binding[119]. The C-terminus of Bax is required for its apoptotic function, as mutation of proline 168 in the preceding linker region inhibits mitochondrial localisation[120], and deletion of the TMD itself also prevents mitochondrial localisation and apoptotic function. Mutation of serine 184 to valine, however, increases mitochondrial localisation[121].

Upon translocation, Bax oligomerises via a region encompassing the BH1 and BH3 domains[122]. The conformational change induced by BH3 protein binding exposes hydrophobic regions that associate with the OMM and are available to bind the hydrophobic groove of another Bax molecule, forming a symmetric homodimer[123]. Bax and Bak can then form higher order oligomers via binding at the α6 and α9 helices[124,125] to form pores, although the exact mechanism of this process is still uncertain and multiple models have been suggested. Recent STED microscopy of Bax at the OMM allowed visualisation of the distinct ring structures formed at the OMM, the formation of which correlated with cytochrome c release[126]. In terms of the structure of these rings, a study by Subburaj and colleagues using TIRF microscopy suggests Bax molecules initially bind to the OMM as monomers but rapidly form dimers and larger oligomers, and once an equilibrium has been reached a range of

oligomer sizes exists[127]. Blue native PAGE assays demonstrated that Bax forms part of complexes as large as 200kDa at the OMM[128]. Whilst molecular structures of Bax in its pore conformation are not currently available, it has previously been suggested that the α5 and α6 helices form a transmembrane hairpin perpendicular to the membrane and the remaining helices lie across the membrane surface in an "umbrella" conformation[118,129]. An "in plane" model has also been suggested in which α9 inserts fully into the membrane but α5 and α6 only partially insert to induce pore formation, although the specific arrangement of all Bax and Bak domains in this model is uncertain[123]. A further model has been proposed in which helices α6-α9 form a flexible conformation allowing formation into a dimer "clamp", with α2-α5 at the rim of the pore, and α6 orienting parallel to each other forming the transmembrane pore[129]. More high-resolution analysis will be needed to fully elucidate the exact structure of the ring formations under various levels of pro-apoptotic signalling to determine which of these models is representative of the specific pore structure.

Bax knockout mice are viable but display abnormalities across a range of cell and tissue types such as thymocyte and B-cell hyperplasia, male sterility due to a defect in sperm differentiation[130], and neuromuscular defects due to a lack of removal of excess neurons[131]. Whilst permeabilization of the OMM is the primary function of Bax, it can also localise to the ER where it regulates calcium homeostasis, as Bax/Bak double knockout MEFs display a reduced resting calcium concentration[132]. Whilst the exact role of Bax in this process is unclear, oligomerisation of Bax can still occur and initiate caspase-12 cleavage[133]. Bax also has roles in regulating mitochondrial morphology as studies have demonstrated its co-localisation at distinct foci with the mitochondrial fission regulator, Drp1, and the fusion regulator, Mfn2, at the OMM[134]

1.2.2.2 Bak

Bak was discovered in 1995 during an examination of the protein complex regulating the apoptosis-inhibiting ability of the adenovirus E1B 19K[135]. Overexpression of Bak in sympathetic neurons inhibited the effect of E1B 19K and increased levels of apoptosis. Unlike Bax, Bak is primarily located at the OMM, even in healthy cells[136]. This is partly due to exposure of its N-terminus occurring before apoptosis is

initiated[136]. Furthermore, the C-terminus of Bak is capable of targeting GFP to mitochondria[137]. The Bak BH3 domain was discovered and identified as being necessary for its pro-apoptotic function and Bcl-XL binding soon after its discovery, along with the identification of its TMD[138]. As with Bax, the exact mechanism of Bak activation and function is not fully understood but is believed to be similar to that of Bax. Examining the X-ray structure of a Bak homodimer brought to light a zinc binding site for homodimer formation[139] with subsequent crystal structure analysis identifying an alternative, pro-apoptotic homodimer structure[140]. This structure potentially relates to complexes containing both Bax and Bak that can form in the membrane upon Bax translocation to the OMM that were identified using live cell microscopy[141]. It was discovered that Bak can be activated by binding of monoclonal antibodies at its α1-α2 loop, inducing a conformational change and oligomerisation[142]. A similar mechanism was also found in mitochondrial-bound Bax, but not cytosolic Bax, suggesting localisation at the OMM is crucial for this mechanism.

Bak knockout mice displayed no abnormalities, but when crossed with Bax knockout mice, very few survived past the perinatal period, and fewer than 10% survived until adulthood[143]. Of those that did survive, a wide range of defects were evident pertaining to a lack of apoptosis, including interdigital webs, imperforate vaginal walls, and excess cells in the central nervous system and haematopoietic system. Alongside MOMP, Bak also regulates mitochondrial morphology by promoting fusion in healthy cells and fission in dying cells[144].

1.2.3 BH3-only pro-apoptotic Bcl-2 family proteins

The second group of pro-apoptotic Bcl-2 proteins are known as the “BH3-only” proteins that contain only one of the four BH domains, the BH3 domain (Fig. 1.4C). This region of homology is required for interaction with the anti- apoptotic Bcl-2 proteins via a conserved LXXXGDE motif[69]. The BH3-only proteins are classified into two groups depending on their mechanism of action – sensitisers and activators. Sensitisers bind to and sequester anti-apoptotic Bcl-2 proteins, allowing the activators to bind to and activate Bax and Bak, which is discussed in more detail later. As with the anti-apoptotic Bcl-2 proteins, structural similarities between BH3 proteins are present, but differences in the sequence of individual BH3 domains and

protein structure make these a diverse group of proteins with differing roles in apoptotic regulation.

1.2.3.1 Bad

The Bcl-2-associated agonist of cell death (Bad) protein was discovered during a screen of yeast two-hybrid cDNA libraries examining binding partners of Bcl-2[145]. Bad shared some homology with Bcl-2 but did not have a C-terminal TMD and was found to contain two putative PEST sequences similar to those found in Mcl-1, thought to be required for its regulation via post-translational modifications. Subsequent studies identified that phosphorylation is a key mechanism by which Bad is regulated. Several studies have been carried out to determine which specific sites are phosphorylated, and the function of these individual modifications. Zha and colleagues used a set of nested deletions of the Bad protein plus site directed mutagenesis to determine key residues in the BH3 domain of Bad that were required for heterodimerisation with Bcl-2 proteins and thus pro-apoptotic function[146]. It wasn't until 2009 that further phosphorylation sites of human Bad were established via mass spectrometry and sequence alignment to mouse Bad[147]. It was established that the human Bad protein had a number of consensus sites with the mouse protein, namely serine-75 (mouse serine-112), serine-99 (mouse serine-135) and serine-118 (mouse serine-155). In the presence of IL-3, Bad is phosphorylated on Ser-112 and Ser-136 initiating binding of 14-3-3 scaffold proteins, sequestering it in the cytosol[148]. Only non-phosphorylated Bad can bind to Bcl-XL and exert its pro-apoptotic activity. Phosphorylation at serine-155 by PKA prevents binding of Bad and Bcl-XL[149].

Mice null for Bad are viable with the majority of cell types developing normally[150]. Older mice do, however, develop diffuse B cell lymphoma suggesting a role for Bad protein in protecting against lymphocyte tumorigenesis. Overexpression studies in non-small cell lung cancer cell lines demonstrated inhibition of proliferation in certain cell lines, and induction of anoikis in the epithelial MDCK and COS-7 cell lines[151]. Studies in multiple other cell lines have shown Bad overexpression caused an increased propensity to undergo apoptosis[152–154]. Outwith direct regulation of Bcl-2 family proteins, Bad plays a role in cell cycle regulation in response to growth factor signalling[155], glucokinase activity, ATP production and respiration[156]

1.2.3.2 Noxa

Pro-apoptotic Noxa (gene name *PMAIP1*) was discovered during a study identifying p53 target genes involved in the DNA damage-induced apoptotic response[157], with its pro-apoptotic function later confirmed in Noxa deficient MEFs[158]. Noxa exerts its pro-apoptotic function by binding to anti-apoptotic proteins, but as the smallest protein in the Bcl-2 family, comprising of only 54 residues, it is not believed to interact with Bcl-XL, Bcl-2 or Bcl-W[159]. Therefore, Noxa is activated and binds to Mcl-1 in response to multiple types of pro-apoptotic stimuli including DNA damage and hypoxia[160] in response to a range of transcription factors including E2F1[161] and c-myc[162].

Northern Blot analysis from mouse tissue mRNA showed tissue-specific expression of Noxa with inherently low levels of expression in numerous tissues including the brain, thymus, testes, lung and intestinal tract[157]. Knockout Noxa mice have no developmental defects and appear normal apart from having increased resistance to DNA damage-induced apoptosis, suggesting its main function is indeed to initiate apoptosis in response to p53 activation[163]. Overexpression of Noxa in HeLa cells caused high levels of mitochondrial localisation and as a result, large levels of apoptosis[157]. Noxa is also found to function in glucose metabolism by stimulating glucose turnover, and is also suppressed by Cdk5-mediated phosphorylation on serine 13 in the presence of glucose[164].

1.2.3.3 Bid

The BH3 interacting-domain death agonist (Bid) was first characterised in 1996 through its ability to interact with both Bcl-2 and Bax[165]. It was noted during these experiments that Bid localised to both cytosol and mitochondria, even though it lacks a C-terminal TMD. Elucidating the solution structure of Bid identified its similarity in structure to Bcl-XL and Bax, with two central hydrophobic helices surrounded by six amphipathic helices, although sequence similarity is limited to only the BH3 domain[166]. This structure is unique to Bid as other BH3 proteins are intrinsically unstructured proteins[167]. Another unique property of Bid compared to other BH3 proteins is that it can be cleaved within its large flexible loop between helices 2 and

3 by caspase-8[168]. This forms two fragments: a C-terminal 14kDa fragment and a 15kDa N-terminal fragment, tBid. This cleavage causes the localisation of tBid to the OMM where it exerts its pro-apoptotic effect via binding Bcl-XL with ten times higher affinity than uncleaved Bid, and direct activation of Bax and Bak[169]. Interestingly, full length Bid can also exert pro-apoptotic activity, as it still has affinity for Bcl-XL, and a Bid mutant containing a non-cleavable caspase cleavage site can still induce apoptosis in primary embryonic fibroblasts[170]. Furthermore, full-length Bid can translocate to mitochondria during anoikis and regulate apoptosis without the need for interaction with other Bcl-2 proteins[171], as well as regulate apoptotic sensitivity during mitosis via phosphorylation on serine-66[172]. Therefore, whilst the primary recognised role of Bid is linking the extrinsic and intrinsic apoptotic pathways, it can also function solely within the intrinsic pathway.

Bid-null mice are resistant to Fas-induced apoptosis, and a proportion of the mice present with moderate liver damage[173]. Outside of its pro-apoptotic function there is evidence within the literature suggesting Bid is also important in the regulation of a diverse range of processes such as lipid transfer between mitochondria and other membranes[174], regulation of the inflammatory response via interaction with NOD1[175] and interestingly, anti-apoptotic roles in the NFκB pathway via COX-2 induction[176].

1.2.3.4 Bim

Another direct activator BH3 protein, Bim, was discovered during an expression screen aimed at identifying proteins that bind to Bcl-2[177]. Although Bim only contains one BH domain, unlike the aforementioned pro-apoptotic proteins, it was found to contain a C-terminal TMD and was thus localised between both mitochondria and cytosol. During its initial discovery, three splice variants of Bim were identified: 110 amino acid Bim_S, 140 amino acid Bim_L, and 196 amino acid Bim_{EL}. Later examination identified additional isoforms denoted Bimα1, Bimα2, Bimβ1 and Bimβ4, with only the alpha variants containing a BH3 domain and none of which contained a C-terminal TMD[178]. Bim was identified as being pro-apoptotic via sequestration of Bcl-2, Bcl-XL and Bcl-W and apoptosis induction upon overexpression of Bim_L. Within the same screen it was also identified that the short Bim_S isoform more effectively antagonised Bcl-2 than its longer counterparts and is thus the more potent apoptosis inducer. Characterisation of Bim, and indeed several

other BH3 proteins as a direct activator of Bax took a number of years to achieve. A significant advance was made by Gavathiotis and colleagues using NMR and stabilised α-helix of Bcl-2 domains (SAHBs) to identify direct interaction between Bim SAHB and Bax at a binding groove distinct from that occupied by anti-apoptotic Bcl-2 proteins[116].

Bim has been identified in multiple studies as a particularly important regulator of T-cell apoptosis[179,180]. Knockout studies in mice provided some of the first evidence that Bim is essential in regulating apoptosis during development in haematopoietic cells and in protecting against the autoimmune response[163,181]. Conversely, overexpression of Bim via E2F1 is found in multiple breast and prostate cancer cells alongside Bcl-XL and Mcl-1[182]. The three isoforms of Bim have each been shown to have distinct roles from each other, with Bim_L and Bim_{EL} most abundantly expressed in most cell lines and tissues[183]. For example, Bim_{EL} and Bim_L bind to LC8 of the microtubule-associated dynein motor complex which inhibits its pro-apoptotic function[184]. Furthermore, Bim_L is involved in IL-7-dependent lysosomal positioning and induces autophagy, whereas Bim_S and Bim_{EL} induce apoptosis upon IL-7 withdrawal[185]. In addition to regulatory roles in apoptosis, Bim has also been identified as part of a regulatory network of proteins involved in unfolded protein response signalling through IRE1α[186], although whether this is an upstream effect rather than downstream is controversial[187].

1.2.3.5 Puma

The p53 upregulated modulator of apoptosis (Puma) was identified via microarrays of cells with or without the p53 tumour suppressor to identify p53 inducible target genes involved in apoptotic regulation[188]. Puma, therefore, is activated in response to a plethora of pro-apoptotic stimuli including, but not limited to, DNA damage[189,190], cytokine withdrawal[191,192], glucocorticoids, and downstream of various oncogenes[193,194]. Multiple Puma transcripts were subsequently identified from the original screen with only two – PUMA-α and PUMA-β – containing a BH3 domain which localised to mitochondria and induced apoptosis. Direct activation of Bax via the BH3 domain of Puma was identified via bacteria two-hybrid assays and pulldown assays[117,195]. Furthermore, surface plasmon resonance has been used to assess the ability of Puma to induce Bak-mediated permeabilisation of mitochondria[196]. Indeed,

the generation of Bid/Bim/Puma triple knockout mice demonstrated that each of the three BH3 proteins are required for activation of MOMP through Bax and Bak[197].

Similarly to Noxa, Puma-null mice demonstrate an increase in resistance to DNA-damage induced apoptosis, as well as resistance to cytokine deprivation, glukocorticoids and staurosporine treatment[190]. Overexpression of Puma is involved in a range of diseases such as apoptosis of spinal cord cells in rat neurogenic intermittent claudication[198], and generation of ROS and degradation of the cytoskeletal regulator stathmin in colorectal cancer[199]. As well as direct regulation of apoptosis, evidence is present that suggests Puma also regulates angiogenesis of vascular and microglial cells via control of autophagy[200], and, like Bim, is involved in the unfolded protein response[186].

1.3 Models of Bcl-2 family protein interactions

Induction of MOMP is controlled via interactions of Bcl-2 family proteins. As mentioned previously, this occurs via the single domain common to all Bcl-2 family members – the BH3 domain[138]. This domain is comprised of a 26 residue α-helix which has been defined in pro-apoptotic proteins as having a consensus sequence L-X(3)-G-D that can interact with the hydrophobic binding groove of anti-apoptotic proteins[201]. Whilst all Bcl-2 proteins interact via this domain, each protein has a specific affinity for its counterpart, and a lot of conflicting data is present within the literature as to which proteins bind which (Fig. 1.5). The currently accepted binding map suggests that Bid, Bim and Puma are considered “promiscuous” as they bind all anti-apoptotic proteins to some extent, as well as Bax and Bak. Bad can bind to Bcl-2, Bcl-XL and Bcl-W, whereas Noxa can only interact with Mcl-1 (reviewed in [46]). Bax has been shown to interact with all anti-apoptotic proteins, whereas Bak only has known interactions with Bcl-XL and Mcl-1[135,202].

Whilst a significant amount of research has been carried out examining how Bcl-2 proteins bind and interact via their BH3 domain, precisely how these interactions culminate in the activation or inhibition of apoptosis is a contentious issue. Previously, two competing interaction models were proposed: direct activation and derepression. The direct activation model proposes that Bax and Bak are inactive,

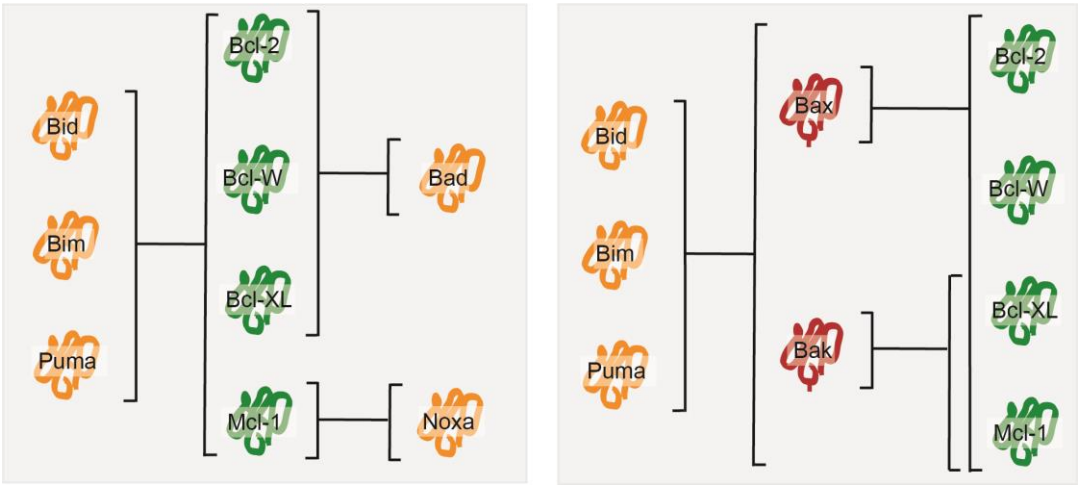

Figure 1.5. Bcl-2 protein binding specificities

Schematic representation of the current map of Bcl-2 family protein binding specificities. The promiscuous binders Bid, Bim and Puma bind all the anti-apoptotic proteins and both Bax and Bak, whereas Bad binds Bcl-2, Bcl-XL and Bcl-W, and Noxa only binds Mcl-1. All anti-apoptotic proteins can bind to Bax, but only Bcl-XL and Mcl-1 can bind to Bak.

unable to initiate apoptosis until activated by BH3 protein binding. A select group of pro-apoptotic BH3 proteins, namely Bid, Bim and Puma, directly bind to Bax, Bak or Bok in order to activate them and initiate MOMP (Fig. 1.6A)[203,204]. The remaining BH3 proteins such as Noxa and Bad are termed sensitisers, the role of which is to bind to and sequester the anti-apoptotic proteins, preventing them from inhibiting the direct activators. The derepression model differs from the direct activation model in that this model assumes that Bax and Bak are not inactive in the cytosol, but are constitutively active and remain in check by anti-apoptotic protein binding (Fig. 1.6B)[205,206]. When the cell is then targeted for apoptosis, the BH3 proteins displace the anti-apoptotic proteins from Bax and Bak, freeing them to induce MOMP.

The culmination of studies examining both models suggest that perhaps apoptosis is regulated by a combination of both models – termed the unified model[207]. This theory postulates that both direct activation and derepression are occurring concurrently within cells, with differences in Bcl-2 protein interactions dictating how susceptible a cell is to undergoing apoptosis (Fig. 1.6C). Bax and Bak, therefore, are found both in the cytosol and bound to the OMM and are kept in check by anti-apoptotic proteins. When the apoptotic signal increases, the concentration of Bax and Bak at the OMM increases as anti-apoptotic proteins are displaced by BH3 proteins, activating their oligomerisation and inducing MOMP. This idea is exemplified by the creation of a cell line by O'Neill and colleagues in which Bid, Bim, Puma, Bad, Noxa, Bik, Hrk and Bmf have been knocked out, termed the "OctaKO"[208]. Even in the absence of activator and sensitiser BH3 proteins, Bax and Bak could still permeabilise the OMM upon the removal of Bcl-XL and Mcl-1, suggesting they are repressed via anti-apoptotic protein binding.

The argument in support of the unified model is, in part, thanks to our increased understanding of the intricacies of apoptotic sensitivity regulation in greater depth, due to a shift in experimental methodologies, with more focus on examining Bcl-2 protein interactions in live cells rather than the more traditional *in vitro* methods. It is well-known that detergents used when extracting Bcl-2 proteins from lipid bilayers can cause conformational changes in the proteins, either disrupting protein-protein interactions or inducing artificial interactions[108,209]. Furthermore, many studies examining specific Bcl-2 protein interactions use truncated forms of the proteins (for example, proteins lacking their transmembrane domain) or BH3 peptides rather than

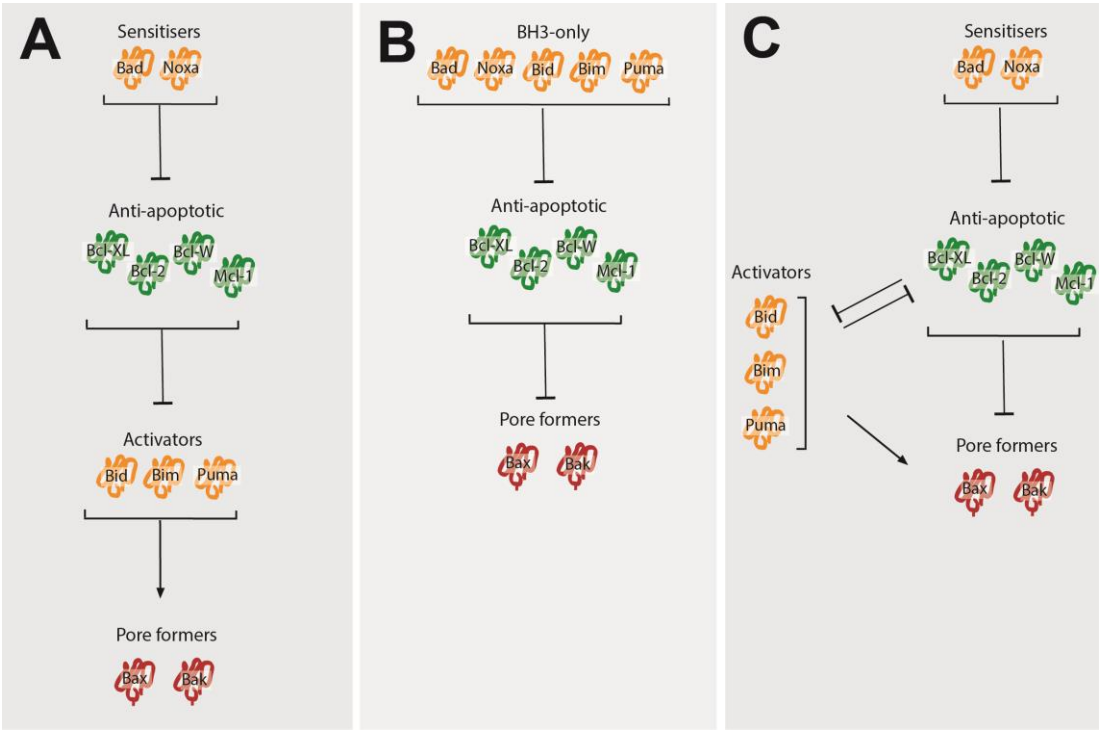

Figure 1.6. Models of Bcl-2 protein regulation of MOMP

A. Direct activation. Bax and Bak are inactive until bound by activator BH3 proteins. This binding causes mitochondrial localisation and oligomerisation. In the absence of a pro-apoptotic stimulus, the activators are sequestered by the anti-apoptotic proteins, and are only available to activate Bax and Bak if displaced by the sensitiser BH3 proteins.

B. Derepression. Bax and Bak are constitutively active but remain unable to carry out MOMP due to sequestration by anti-apoptotic Bcl-2 proteins. In the presence of an apoptotic stimulus, the BH3-only proteins displace Bak and Bax from the anti-apoptotic proteins, freeing them to carry out MOMP.

C. Unified model. A combination of both A and B occurs. Bax and Bak can be activated directly by BH3 proteins and inhibited by anti-apoptotic proteins. The anti-apoptotic proteins can be displaced by both the sensitiser BH3 proteins or the activators.

the full-length proteins. Hydrocarbon stapled BH3 domains (SAHBs) have been shown to cause increased binding affinity of Bcl-2 proteins at the BH3 domain[210]. Even when full-length proteins are used, different variants of the same Bcl-2 protein can have significantly different binding affinities for other Bcl-2 family members[211]. Additionally, recent live cell studies have highlighted the importance of the TMD for Bcl-2 protein function, with membrane localisation of Bcl-XL having a direct influence on how tightly it can bind to BH3 domains and thus how effective it is at blocking apoptosis[212]. This suggests that the appropriate *in vivo* protein conformation is needed for BH3 binding. What other factors on the OMM are involved in regulating whether or not a Bcl-2 protein is stably inserted or only transiently interacts with the membrane is also poorly understood, although studies have shown that Bax forms part of a much larger complex when inserted into the OMM[128]. Thus there is a significant amount of conflicting data in the literature as to the binding specificities between Bcl-2 family proteins[213], where they bind, and how these interactions culminate in either survival or death.

1.4 Mitochondrial priming – setting the threshold for apoptosis

Recent work in live cells using fluorescently tagged full-length Bcl-2 family proteins is beginning to shed some light on some of the conflicting Bcl-2 protein interaction data within the literature. For example, most models suggest that Bax is an inactive monomer in the cytosol, activated upon BH3 protein binding to displace its TM domain. However, Bax is thought to be able to interact with BH3 proteins only when both are associated with a membrane and thus must localise to the OMM before BH3 binding[214]. Bax can also be retrotranslocated from the OMM back to the cytosol by Bcl-XL[215]; a process which is both rapid and reversible as demonstrated when cells detached from their ECM are subsequently re-attached[216]. Bax is therefore unlikely to be an inactive monomer within the cytosol, but instead in an active dynamic equilibrium between mitochondria and cytosol[110], constantly targeting to the mitochondria and being removed by anti-apoptotic Bcl-2 proteins. As levels of pro-apoptotic proteins like Bax increase their mitochondrial localisation, cells become more susceptible to apoptosis – termed mitochondrial priming. When a cell is relatively unprimed, Bax retrotranslocation is rapid as it is removed from the OMM (Fig. 1.7). In a primed cell, anti-apoptotic proteins are sequestered and Bax is much more stable on the OMM in preparation for MOMP. Therefore whilst *in vitro* studies

have provided invaluable information so far, they provide only a snapshot in time and thus do not represent the dynamic priming landscape within cells

The concept of mitochondrial priming arose when developing a method to predict the effectiveness of chemotherapeutics on patient outcome. Testing where the apoptotic threshold of a patient's tumour sample lies *in vitro* can provide a method by which we can predict the response of the patient to various drugs or drug combinations, rather than subjecting the patient themselves to a potentiality prolonged and ineffective treatment. A technique termed BH3 profiling was developed in which mitochondrial priming of primary patients samples was measured by exposing mitochondria from these samples to BH3-only protein peptides and measuring mitochondrial depolarisation[217]. This allows the apoptotic threshold of cells to be calculated in a relatively rapid test; the more primed a sample is, the more sensitive that sample will be to treatment. Indeed, BH3 profiling has shown that the level of mitochondrial priming prior to therapy is predictive of therapeutic response[218]. For example, treatment of primary AML patient samples with Bim BH3 induces significantly more mitochondrial depolarisation than cells from healthy patients, suggesting these AML cells are more mitochondrially primed[219]. Indeed, these patients responded significantly better to treatment than those whose samples were unresponsive to Bim BH3. Similar results were found in other cancers, including lymphoma cell lines[218], primary acute lymphoblastic leukemia (ALL)[220] and CLL[221].

One point to consider when relating the dynamic nature of Bcl-2 proteins to the apoptotic models outlined above is how the transient interactions between Bcl-2 proteins and the OMM occur to set the level of the apoptotic threshold. Due to the specific charged residues and hydrophobic nature of the TMD, insertion into the OMM would require relatively little energy[222,223]. However, a significant amount of energy would then be required to remove such proteins from the OMM. In a cell where levels of apoptotic priming are high, Bcl-2 proteins are stably inserted into the OMM. However, in a cell with low levels of priming, the dynamic nature of the proteins suggests that, perhaps, full TMD membrane insertion does not take place as proteins are rapidly retrotranslocated to the cytosol. Studies have indicated that certain mitochondrial membrane proteins are thought to interact with various Bcl-2 family members. For example, the mitochondrial fission regulator Drp1 has been

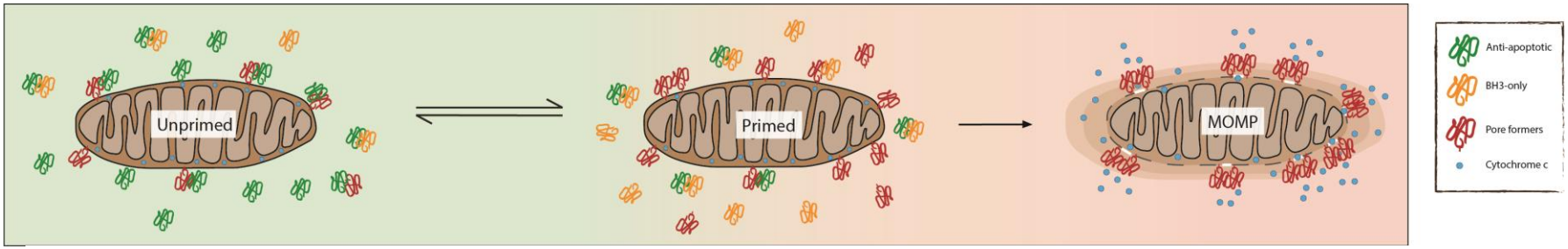

Figure 1.7. Mitochondrial priming is a dynamic process

In an unprimed cell, levels of pro-apoptotic Bcl-2 proteins are low and are sequestered by anti-apoptotic proteins which retrotranslocate them from mitochondria. In the presence of a pro-apoptotic stimulus, levels of pro-apoptotic proteins increase, and anti-apoptotic proteins are sequestered by BH3 proteins. This leaves pore formers such as Bax free to localise to the OMM. As the levels of Bax at the OMM increase, the cell eventually reaches its apoptotic threshold and MOMP is initiated. Up until the threshold is reached, priming is dynamic, and cells can revert to an unprimed state if the apoptotic stimulus is removed.

shown to regulate Bax translocation to the OMM upon irradiation[224] where it forms foci with both Drp1 and the mitochondrial fusion regulator Mfn2[134]. How these and other membrane proteins regulate the dynamics of Bcl-2 proteins is an interesting question that needs further examination in the future.

The dynamic nature and intricate balance between pro- and anti-apoptotic Bcl-2 family proteins allows them to act as a buffer against the multitude of signals reaching the cell, killing cells that are no longer required and keeping healthy cells alive. As cells acquire damage, the equilibrium of the Bcl-2 landscape changes due to increased expression or function of the pro-apoptotic proteins, and downregulation or neutralisation of anti-apoptotic ones. This ultimately increases or decreases mitochondrial priming and thus apoptotic sensitivity. An interesting phenomenon has also recently been uncovered whereby MOMP does not occur in every mitochondria concurrently, but only a small proportion undergo permeabilization, termed minority MOMP[225]. This causes partial caspase activation without inducing apoptosis, This, in combination with the fine balance of Bcl-2 protein activity required to maintain healthy cells, makes it perhaps unsurprising that cancer cells show alteration in their Bcl-2 landscape, with overexpression of anti-apoptotic proteins or reduced expression of pro-apoptotic proteins.

1.5 Targeting Bcl-2 proteins in cancer therapeutics

Bcl-2 was originally discovered in B-cell lymphoma patients and has since been found to be overexpressed in multiple cancers including chronic lymphocytic leukaemia (CLL)[58], small cell lung carcinoma (SCLC)[59] and neuroblastoma[60]. Overexpression of Bcl-XL has been found in breast cancer[76], colorectal cancer[77] and increases chemotherapeutic resistance in prostate cancer[226]. In particular, Mcl-1 overexpression is prevalent in a particularly large number of human cancers, such as 36% of breast cancers and 54% of lung cancers[227]. Despite overexpression of multiple anti-apoptotic Bcl-2 proteins being present in a range of cancers, this by itself is certainly not the sole cause of oncogenesis. Indeed, the Bcl-2 t(14;18) translocation is also present in healthy lymphocytes[228,229] and when Bcl-2 has been overexpressed in mouse models it is not by itself oncogenic[230]. When found in combination with other oncogenes such as Myc, amplification of Bcl-2 can contribute to oncogenesis[231].

Conversely to upregulation of anti-apoptotic proteins, downregulation of pro-apoptotic Bcl-2 proteins is also found in a range of cancers. Loss of Bim alone is present in renal cell carcinoma[232], and alongside Puma in Epstein-Barr virus-positive patient samples[233]. Loss of Puma alone is also found in Burkitt lymphoma[193] and glioblastoma[234]. The role of Puma in the p53 response would fit with its downregulation promoting genetic instability and resistance to genotoxic therapies. Changes in the BH1-3 proteins are also found in cancer. Frameshift mutations in Bax are found in colon cancer[235,236], and a loss of function due to silencing by miR-365 is seen in cutaneous squamous cell carcinoma[237]. However, as with the anti-apoptotic proteins, mouse models where individual BH1-3 and BH3-proteins have been deleted have not significantly predisposed those animals to tumours[46]. Gene deletion studies in mice show that Bax and Bak are largely redundant, and loss of one or the other has no overt oncogenic effect. Bad and Bid knockout mice are predisposed to lymphoma and myeloid tumours respectively, but again with a long latency. As with anti-apoptotic Bcl-2 proteins, loss of pro-apoptotic proteins can cooperate with other oncogenes to accelerate tumour development and progression.

A significant problem in cancer therapy development is how to specifically target a tumour cell population whilst minimising impact on the surrounding healthy cells. Dose limiting toxicity is a major hurdle preventing the use of cytotoxic agents to treat patients with more advanced tumours. Although resistance to apoptosis is a well-established hallmark of cancer, how and why sensitivity differs between normal tissue compared to tumours is a more complex issue than just that cancer cells are more resistant to cell death. The increased understanding of apoptosis that has developed over the past decades is now providing new opportunities for targeting vulnerabilities in cancer, in particular by targeting specific members of the Bcl-2 family of proteins.

1.5.1 Narrowing the chemotherapeutic target with BH3 mimetics

Thanks to novel research relating Bcl-2 protein dynamics and expression levels to apoptotic resistance, much more research has gone into targeting specific anti-apoptotic Bcl-2 proteins as a chemotherapeutic target. A major breakthrough came with the development of BH3 mimetics – compounds that target the binding groove of Bcl-2 proteins with high affinity. The first BH3-mimetic to be developed was the

Bcl-2 and Bcl-XL inhibitor ABT-737 in 2005. A “SAR by NMR” method was used to screen a chemical library to identify any small molecules that bound to the BH3 domain of Bcl-XL in a similar manner to endogenous BH3 proteins[238]. Two molecules were identified that bound to distinct regions within the BH3 domain using key residues that were known to be used by Bak. Slight structural modifications were introduced to one of the compounds to prevent human serum albumin binding and improve overall binding affinity. Clinical studies using ABT-737 showed promise for the regression of solid tumours in xenografts of lymphoma and SCLC[238], as well as part of a combination therapy for HNSCC[239]. Its lack of oral bioavailability, however, prevented it from being clinically useful. This led to the development of its counterpart ABT-263, made orally bioavailable by modifying three key residues in its backbone[240], which was highly successful in inducing regression of SCLC and ALL xenografts[241]. However, acute thrombocytopenia was observed in multiple *in vivo* studies in mice, dogs, rats[242] and clinical trials in patients with lymphoid tumours[243,244]. The realisation that platelets require Bcl-XL for survival[245] due to high levels of albumin binding[246] led to modifying ABT-263 to increase its specificity for Bcl-2, thus creating the Bcl-2-specific inhibitor ABT-199[247].

Thus far, ABT-199 (venetoclax) has been approved in clinics for treatment of CLL patients with a 17p deletion who have had at least one prior therapy. Furthermore, in November 2018 venetoclax was granted accelerated approval by the FDA for treatment of AML as a combination therapy in adults aged 75 or older, or who have comorbidities that prevent the use of other treatments. However, as it is not only Bcl-2 which is aberrantly regulated in cancer, understanding the precise mechanisms by which all Bcl-2 proteins are regulated in healthy cells versus cancer cells is crucial in targeting Bcl-2 protein-dependent cancers.

Multiple Bcl-XL-specific mimetics have been developed and research is still ongoing to ensure effective targeting for treatment of Bcl-XL-dependent tumours[248,249]. Of note, the design of WEHI-539 has shown Bcl-XL targeting specificity in Bcl-XL-dependent mouse embryonic fibroblasts[250]. WEHI-539 has so far demonstrated effectiveness in a study examining approaches to target medulloblastoma and paediatric glioblastoma solid tumours in combination with the Aurora kinas A inhibitor MLN8273[251]. An NMR and structural based design approach was taken to create a Bcl-XL inhibitor which was more potent than WEHI-539, leading to the

creation of A-1155463[252], with studies ongoing. Mcl-1 is also a target of high interest due to its expression in a range of cancers, such as breast tumours that currently do not have effective treatments[24]. Although it has proven challenging to specifically target Mcl-1, a number of potent inhibitors have now been developed, recently reviewed by Xiang et al[253]. Of those currently under examination, S63845 from Servier shows the greatest specificity over Bcl-2 and Bcl-XL[55] and is currently undergoing early phase clinical trials. Thus, advances in recent years are showing promise for targeting a much broader range of cancers using BH3 mimetics.

1.5.2 Measuring mitochondrial priming using the BH3 profiling toolkit

Understanding the dynamics of Bcl-2 proteins in live cells is crucial when determining how to most effectively therapeutically target the Bcl-2 proteins, as conventional chemotherapies kill cells via Bcl-2 protein-regulated mitochondrial apoptosis. Understanding how the myriad of variations in expression and function of Bcl-2 proteins combines in a cancer cell, in comparison to normal cells, will determine how effective a drug will be at initiating apoptosis specifically in tumour cells. BH3 profiling has shown to be successful in predicting the apoptotic outcome of patients[220,221]. This technique was later modified to determine the effect of pre-treatment priming on patient sample response to specific drugs or drug combinations – termed dynamic BH3 profiling[254]. Cells are incubated with specific drug combinations, permeabilised, and exposed to various BH3 peptides to induce MOMP. By comparing with untreated cells, the most effective drug combinations can be identified, as well as if cancers are dependent on specific Bcl-2 proteins for survival. Should the cancer cells in question be reliant on a specific anti-apoptotic Bcl-2 protein, or indeed a subset of these proteins for survival, this can be identified via the specific BH3 peptide used[255]. This technique demonstrated, for example, that double-hit lymphomas are reliant on Bcl-2, and in some cases, Bcl-XL or Mcl-1, for survival[256]

BH3 profiling uses mitochondrial depolarisation as a readout for susceptibility to apoptosis, and therefore measures apoptotic sensitivity at a specific timepoint. As discussed, mitochondrial priming is dynamic, and therefore the efficacy of drugs may vary over time, which could potentially be missed using this method. Apoptosis is also induced using BH3 peptides rather than full-length proteins which, as

previously highlighted, may not fully recapitulate the interactions of full-length BH3 proteins. Patient samples are also tested *in vitro*, and Bcl-2 protein signalling may change in the time taken between obtaining the primary patient sample and measuring priming. As a diagnostic tool, dynamic BH3 profiling has so far proven highly successful, but why variation in response to treatment occurs within patient samples is still unclear.

1.5.3 Dynamic heterogeneity of apoptosis in healthy tissues and in chemotherapeutic resistance

Mitochondrial priming is regulated by an intricate balance of interactions between Bcl-2 family proteins in the cytosol and on mitochondria. These interactions are highly dynamic, and thus the apoptotic landscape is constantly shifting across a spectrum of priming. This variation is present on multiple levels. Significant levels of apoptosis occur during embryonic development where expression levels of Bcl-2 proteins vary greatly between tissues and at different developmental stages. For example, in the developing nervous system of mice, neuronal Bcl-2 levels significantly decrease by 5 months of age[46]. Bcl-XL and Mcl-1 play key roles in the survival of immature B-cells during development, whereas Bcl-2 is required for survival of mature B-cells[257]. The balance of priming during development is also influenced by changes in pro-apoptotic Bcl-2 proteins, as exemplified in a recent study demonstrating that subtle changes in the balance of pro- and anti-apoptotic Bcl-2 proteins has profound effects on tissues during craniofacial development[258].

BH3 mimetics are defined as functioning under two specific criteria: they bind with high affinity to their target protein and induce mitochondrial apoptosis[259]. Therefore, design of new or improved BH3 mimetics to target specific cancers is based on current knowledge of Bcl-2 protein interactions, thus the abundance of conflicting data in the literature may cause issues. Another concern recently coming to light with targeting Bcl-2 proteins via mimetics is the development of chemotherapeutic resistance over time. There has been recent evidence of both experimental and clinical occurrences of venetoclax resistance from two independent studies. These found that acquired resistance in patients on long term venetoclax treatment resulted from similar mutations in the Bcl-2 gene which significantly reduced the

affinity of ABT-737 and ABT-199 for Bcl-2, but did not affect binding to BH3 proteins like Bim[260,261]. This has significant implications on how exactly BH3-mimetics interact with endogenous Bcl-2 family proteins as the mimetics do not fully recapitulate the binding of full-length BH3-only proteins. Interestingly, several recent *in vitro* studies have come to a similar conclusion. One such study found that Bim binds to Bcl-XL, not only via the classic BH3-groove, but at another site on the protein[262]. This "double-bolt locking" of Bcl-XL and Bcl-2 means Bim is more resistant to displacement by ABT-263 than initially expected. The development of newer BH3-mimetics may help to overcome such resistance. For example, another Bcl-2 selective drug, S55746 has recently been described which binds in the same groove as venetoclax, but has interactions with distinct amino acids [263]. Thus, there is potential that novel mimetics may provide an approach to overcome resistance, but a more in-depth knowledge of the specific interactions between anti- and pro-apoptotic proteins may be required to fully utilize such compounds.

1.6 Project aims and objectives

Apoptotic priming in normal cells and tissues varies dynamically at multiple levels; between different adult tissues or within the same tissue at distinct developmental stages, between individual cells within a tissue, and in the same cell at different times as the cell is exposed to changes in signalling. Overall, our understanding of how apoptosis is controlled in mammalian cells has reached a level of maturity whereby it is now being applied in drug development and thus in a clinical setting. However, there is still a level of complexity in understanding how apoptosis is dynamically controlled within single cells, and populations of those cells. Why do cells within a population respond differently to apoptosis-stimulating treatments? Even within clonal cell populations, the apoptotic outcome of cells is varied, with some cells showing resistance to drug treatments where others die[264]. It would not be unreasonable to postulate that Bcl-2 protein interactions play a role in this variation. The Bcl-2 family themselves are diverse, activated by, and interacting with, a vast range of signalling pathways, not least showing selectivity for binding within their own protein family.

To improve the efficacy of Bcl-2 protein-targeting chemotherapeutics, we first need to have a more complete understanding of how the dynamic changes in apoptotic

regulation are controlled. This requires a more in-depth understanding of how the localisation and interactions between Bcl-2 family proteins themselves changes temporally, and determining other potential regulatory proteins involved in the processes leading up to apoptosis. Previous work in our laboratory used live cell imaging techniques to measure the dynamics of Bcl-XL and Mcl-1 in live cells and found both proteins to retrotranslocate from mitochondria to the OMM, similarly to Bax (Ricardo Rodriguez-Enriquez, unpublished data). These dynamics were slowed upon addition of multi-domain Bax and Bak or activator BH3 proteins. Whether other anti-apoptotic proteins behave in the same manner is unclear. Furthermore, whether all pro-apoptotic proteins can alter anti-apoptotic protein retrotranslocation, and if BH3-mimetics recapitulate these interactions in live cells, is also unknown. We therefore questioned if we could develop these live cell techniques to further interrogate Bcl-2 family interactions in live cells in more detail to determine how their behaviour is regulated in both healthy cells, and in the lead up to apoptosis.

Therefore, the aims of this project are to:

- Develop a method to measure Bcl-2 proteins dynamics in live cells, in real time, to identify changes in these dynamics in unprimed versus primed cells
- Develop a system where competition in binding between Bcl-XL and BH3 proteins can be measured
- Identify factors contributing to heterogeneity in apoptotic priming and Bcl-2 protein dynamics
- Identify novel interactors of Bcl-2 proteins using BioID proximity labelling

2. Materials and Methods

2.1 Cell culture techniques

2.1.1 Reagents

Plastic cell culture dishes and multi-well plates were from Corning. Glass bottom dishes were from IDT. Dulbecco's Modified Eagle's Medium (DMEM), DMEM-F12, and Ham's F-12 were from Lonza. Foetal bovine serum (FBS) and horse serum (HS) were from Biosera. Phosphate buffered saline (PBS), penicillin & streptomycin (P/S), trypsin-EDTA, human insulin, choleratoxin, hydrocortisone, epidermal growth factor (EGF), dimethyl sulfoxide (DMSO), HEPES, Etoposide, Doxycycline, Taxol, and 4-hydroxytamoxifen (4-OHT) were from Sigma Aldrich. S63845, and WEHI-539 were from Selleckchem. *Trans*IT-X2 was from Mirus Bio LLC. Lipofectamine RNAiMAX was from Invitrogen. ABT-737 and ABT-199 were from Abbott Laboratories. Polybrene was from Merck Millipore. siRNA were purchased as a pre-designed SMARTpool from Dharmacon.

2.1.2 Cell lines

MEF, MCF10A, MDA-MB-231, MCF7, BT-474, SK-BR-3 and HEK-293T cells were from ATCC (Virginia, USA). $Bax^{-/-}Bak^{-/-}$ MEF were originally gifted from Stanley Korsmeyer and Nika Danial (Harvard Medical School, USA). $Drp1^{-/-}$ MEF were gifted from Tomomi Kuwana (La Jolla Institute for Immunology, USA).

2.1.3 Cell maintenance

MEF, MDA-MB-231, MCF7, BT-474, SK-BR-3, and HEK-293T cells were cultured in DMEM supplemented with 10% FBS. MCF10A cells were grown in DMEM-F12 supplemented with 5% HS, 20ng/ml EGF, 0.5mg/ml hydrocortisone, 100ng/ml choleratoxin and 10µg/ml insulin. All cells were cultured in a humidified incubator at 37°C with 5% CO_2. When subculturing cells, growth medium was removed, and cells washed with PBS before adding trypsin-EDTA. Cells were left to incubate at 37°C until all had detached. Detached cells were diluted in full growth medium and centrifuged at 350rpm for 5 minutes to pellet. Pelleted cells were resuspended in an appropriate volume of full growth medium and plated as required.

2.1.4 Freezing and thawing cells

Cells were grown to approximately 70-80% confluency before being trypsinised and centrifuged as previously described. Pelleted cells were resuspended in the appropriate volume of freezing medium. For MEF and MDA-MB-231 cells, complete growth medium was supplemented with 10% DMSO. For MCF7, SK-BR-3, HEK-293T and BT-474 cells, complete growth medium was supplemented with 5% DMSO. For MCF10A cells, 70% complete growth medium was supplemented with 20% HS and 10% DMSO. Cells were then aliquoted into cryotubes and slowly frozen to -80°C at -1°C/min in a Mr Frosty Freezing Container (ThermoFisher Scientific). For thawing, cells were quickly thawed in a 37°C water bath and diluted in complete growth medium before centrifuging at 350rpm for 5 minutes. Cells were then resuspended in fresh growth medium.

2.1.5 Transient DNA transfection

24 hours before transfection cells were seeded into a 6-well plate to achieve 70% confluency on the day of transfection. 0.5-1µg of plasmid DNA per well was transfected using 100µl of serum free medium and 3µl of *Trans*-IT X2 reagent into 1ml total complete growth medium, following manufacturer's instructions. Cells were then assayed 24 hours post-transfection.

2.1.6 siRNA transfection

24 hours before transfection cells were seeded into a 6-well plate in antibiotic-free complete medium to achieve approximately 60% confluency on the day of transfection. On the day of transfection, the appropriate volume of siRNA was transfected using Lipofectamine RNAiMAX reagent following manufacturer's instructions. The siRNA transfection mix was incubated at room temperature for 5 minutes before adding dropwise to cells. Cell were incubated 24 hours before assaying.

2.1.7 Lentivirus production

HEK-293T cells were seeded into T-75 flasks to achieve 70% confluency the next day, two flasks per virus. On the day of transfection, 6µg pMD2.G envelope vector, 9µg psPax2 packaging vector and 12µg of appropriate pCDH vector were diluted in 500µL of blank DMEM and mixed with 1µg/µL PEI in 500µL blank DMEM, and

incubated at room temperature for 30 minutes. Transfection mix was then added dropwise to HEK-293T cells in 5ml total complete growth medium, and cells were incubated overnight. The next day, virus transfection medium was removed and replaced with 10ml complete growth medium containing 0.5M sodium butyrate. Cells were subsequently incubated at 37°C for 6-8 hours before replacing sodium butyrate medium with complete growth medium and leaving cells to incubate for 48 hours. 48 hours later, virus medium was filtered through a 0.45µm filter and 4°C PEG solution added to a 1X concentratoin. PEG medium was then left to incubate at 4°C between 12 hours to a maximum of 4 days. Medium was then centrifuged at 1500xg for 30 minutes at 10°C and supernatant collected. The supernatant was then spun at 1500xg for a further 5 minutes to remove any residual virus. Virus pellets were pooled and resuspended in 100µL cold PBS before storing 50µL aliquots in cryotubes at -80°C until required for infection.

2.1.8 Lentiviral infection

24 hours before infection cells were seeded into a 6-well plate to achieve 40% confluency on the day of infection. On the day of infection, the appropriate volume of virus was diluted into 1ml of complete growth medium per well plus 8µg/ml Polybrene. 24 hours post-infection, virus medium was replaced with complete growth medium and cells were incubated at 37°C overnight. Infection efficiency was tested 2 weeks post-infection via immunofluorescence and western blotting.

2.1.9 Fluorescence activated cell sorting (FACS)

Cell that were stably expressing fluorescently-tagged proteins (at least 2 weeks post-lentiviral infection) were trypsinised, pelleted and resuspended in sorting medium (serum-free complete growth medium supplemented with 25mM HEPES, 100U/ml penicillin and 100µg/ml streptomycin) to obtain a concentration in the range of $5x10^6$ – $10x10^6$ cells/ml. Cells were then filtered through a 50µm filter to obtain single cells. Cells were sorted using a FACS Aria Fusion (BD Biosciences) using the appropriate emission bandpass filter for the fluorophore being sorted. Sorted cells were either plated into 10cm dishes, or for single cells, round-bottom 96-well plates.

2.1.10 Drug treatments

4-OHT stocks were dissolved in ethanol and used at a working concentration of 10µM. Cells were incubated for 1 hour before assaying live cells, or 18 hours before carrying out apoptosis assays. ABT-737, ABT-199, WEHI-539 and S63845 stocks were dissolved in DMSO and assayed at a working concentration of 5µM for 24 hours. Etoposide stocks were dissolved in DMSO and used at a working concentration of 800µM. Taxol stocks were dissolved in DMSO and used at a working concentration of 1µM for 50 hours. Doxycycline stocks were dissolved in ddH_2O and used at assay-dependent working concentrations as stated

2.2 Microscopy-based techniques

2.2.1 Reagents

Formaldehyde (methanol free) was from Sigma. Triton X-100 was from VWR International. Fluorescent mounting medium was from DAKO. Superfrost Plus adhesion slides and Polysine coated slides were from Thermo Scientific.

2.2.2 Immunofluorescence staining of adherent cells

Cells on coverslips were washed in PBS before being fixed in 4% formaldehyde in PBS for 5 minutes and permeabilised in 0.2% Triton X-100 in PBS for 5 minutes. Cells were then washed in PBS before adding primary antibody (Table 2.1) diluted to working concentration in 10% horse serum in PBS. Cells were incubated in primary antibody for 1 hour, then washed 3 times in PBS. Secondary antibody (Table 2.2) was then diluted to working concentration in 10% horse serum and added to cells for 1 hour at room temperature, in darkness. Cells were subsequently washed 3 times in PBS before adding DAPI for 5 minutes, 1:10,000 dilution in PBS. Cells were washed a final three times in PBS and once in ddH_2O before being left to air-dry overnight. Dried coverslips were then mounted onto glass slides using Dako fluorescent mounting medium and left to set. Slides were imaged using a Zeiss Axioplan 2 using a 63X, 1.4NA Plan Achromat objective and Image J software.

2.2.3 Immunofluorescence staining of non-adherent cells

Growth medium from cells grown in dishes was collected before washing in PBS. The PBS wash was also collected and pooled with the appropriate growth medium sample, and cells trypsinised. Trypsinised cells were also pooled with removed medium from the appropriate sample. Samples were cytospun at 400rpm for 5 minutes onto polysine coated slides. Cells were then fixed in 4% formaldehyde for 5 minutes before being stained and imaged as previously outlined.

2.2.4 Fluorescence recovery after photobleaching (FRAP)

Cells were plated onto glass bottom dishes at the appropriate density for imaging, then transfected or treated with drugs 1-2 days prior to imaging. Before imaging, cells were washed with PBS before adding 2ml of movie medium (Ham's F12 supplemented with 10% FBS, 1% penicillin & streptomycin, and 25mM HEPES), then placing in the microscope chamber for at least 1 hour prior to imaging to allow cells to equilibrate. For FRAP, a 2.5μm^2 ROI within the cell encompassing both the cytosol and mitochondria was selected and photobleached for 10ms, 100% laser power, using either 488nm for GFP or YFP, and 594nm for mCherry. Images were captured every 5 seconds for 30 seconds pre-bleach and at 5 second intervals post-bleaching. Images were acquired using a CSU-X1 spinning disc confocal (Yokagowa) on a Zeiss Axio-Observer Z1 microscope with a 63x/1.40 Plan-Apochromat objective, Evolve EMCCD camera (Photometrics) and motorised XYZ stage (ASI). The 488nm and 561nm lasers were controlled using an AOTF through the laserstack (Intelligent Imaging Innovations (3I) allowing both rapid 'shuttering' of the laser and attenuation of the laser power. Slidebook software (3I) was used to capture images. Images were analysed using Image J and GraphPad Prism software. Briefly, background fluorescence was subtracted and fluorescence within the photobleached region quantified for each cell. Fluorescence was then normalised to 100% pre-bleach and one-phase association curves fitted.

2.2.5 Photoactivation

Cells were plated onto glass bottom dishes as with FRAP. For photoactivation analysis, a 2μm^2 region close to the nucleus (identified via the red H2B fluorescence) was selected and photoactivated using the 405nm laser for 10ms, 100% laser power. Images were captured every 5 seconds for 30 seconds pre-bleach and at 5 second intervals post-bleaching. All microscope components used

were the same as for FRAP. Images were analysed using Image J and GraphPad Prism software. Briefly, background fluorescence was subtracted and fluorescence within the photoactivated region quantified for each cell. Fluorescence was then normalised to 100% post-photoactivation and one-phase dissociation curves fitted.

2.2.6 Fluorescence cross-correlation spectroscopy

FCCS measurements were performed on an LSM 510 META equipped with the ConfoCor 3 system through a C-Apochromat 40×/NA1.2 Korr. UV-VIS-IR water-immersion objective (Carl Zeiss, Jena, Germany). Cells were maintained in the stage incubator at 37°C and 5% CO_2. Measurements were taken on regions of mitochondrial GFP-Bcl-XL. GFP and mCherry fluorescent signals that were excited at 488 and 594 nm were separated through a NFT600 dichroic mirror; they were then recorded through a BP505-540 and BP615-680 bandpass filter, respectively. The pinhole was set to 73 mm. After the structure parameter determination using rhodamine 6G and Alexa Fluor 594 solutions as standards, optical settings in the measurement day were adjusted. The measurement period was 10s. Autocorrelation and cross-correlation functions were fitted to Eq. 1 and Eq. 2, respectively.

$$G(\tau) = 1 + \left[1 + \frac{T}{1-T}\exp\left(-\frac{\tau}{\tau_{\text{triplet}}}\right)\right]\frac{1}{N}\left[\sum_{i}^{m} F_i\left(1+\frac{\tau}{\tau_i}\right)^{-1}\left(1+\frac{\tau}{s^2\tau_i}\right)^{-\frac{1}{2}}\right] \qquad [1]$$

$$G(\tau) = 1 + \frac{1}{N}\left[\left(1+\frac{\tau}{\tau_i}\right)^{-1}\left(1+\frac{\tau}{s^2\tau_i}\right)^{-\frac{1}{2}}\right] \qquad [2]$$

where F_i and t_i are the fraction and diffusion time of component i, respectively; N is the average number of fluorescent molecules in the analysed volume defined by the beam waist w_0 and the axial radius z_0; s is the structure parameter representing the ratio of w_0 to z_0; m is the number of components (m = 2, here); T is the triplet fraction; and $t_{triplet}$ is the relaxation time of the triplet state. Relative cross-correlation amplitude (RCA) was calculated using Eq. 3.

$$\text{RCA} = \frac{G_{\text{C}}(0) - 1}{G_{\text{R}}(0) - 1} \qquad [3]$$

where $G_C(0)$ and $G_R(0)$ are the cross-correlation and autocorrelation function of mCherry at delay time zero, respectively.

2.2.7 Time-lapse microscopy

For cell fate analysis, cells were plated into 12-well plates at the appropriate density and incubated for 24 hours. 30 minutes prior to imaging, cells were treated with various drug combinations. Appropriate ROIs were selected within each well and imaged every 15 minutes for 50 hours. Cells were maintained at 37°C and 5% CO_2 throughout imaging. Images were acquired on an Eclipse Ti inverted microscope (Nikon) using a 20x/ 0.45 SPlan Fluar objective, and a pE-300 LED (CoolLED) fluorescent light source, and NIS Elements AR.46.00.0 The images were collected using a Retiga R6 (Q-Imaging) camera. Images were analysed using NIS Elements software. Individual cells were followed manually across the whole imaging timeframe and cell fate recorded based on cell morphology. Cells were considered mitotic from the point of initial rounding until the first point of cytokinesis, membrane blebbing, or returning to original morphology.

For FUCCI imaging, cells were plated onto a 30mm glass-bottom dish to achieve approximately 30% confluency the next day. Cells were placed in the microscope chamber at least 16 hours after plating and maintained at 37°C with 5% CO_2 throughout imaging. Images were collected on a Zeiss LSM 780 confocal microscope using a 40x / 1.3 Plan-Apochromat objective and 0.6x confocal zoom. The confocal settings were as follows: pinhole 1 airy unit, scan speed 400Hz unidirectional, format 9 x 512x512 tile scan. Images were collected using a PMT detector with the following spectral channel settings; FITC 490-533nm; Texas red 563-625nm using the 488nm (3%), 594nm (1%) laser lines respectively.

2.3 Molecular techniques

2.3.1 Reagents

JM109 bacteria cells were originally purchased from Promega and made competent in-house. Phusion HF DNA polymerase, dNTPs, restriction enzymes, T4 DNA ligase and T4 polynucleotide kinase were from NEB. SybrSafe, Ampicillin, Kanamycin and SOC medium was from Invitrogen. Agarose was from Melford Labs.

2.3.2 Plasmids

mCherry-tagged tBid, BimEL and Bad, along with the BH3-domain variants, were generous gifts from David Andrews (McMaster University). mCherry-PUMA and Noxa were generated by PCR amplification of the coding sequences and cloning into mCherryC1. Full-length Bid^{Tev} and pcDNA-Tev-V5 were gifts from Douglas Green (St. Judes, Memphis). The Bid^{Tev}mCh-GFP-Bcl-XL vector was created by cloning Bid^{Tev} into pmCherryN1, and then the fusion cloned upstream of the T2A sequence in pCDH-EF1-T2A-GFP-Bcl-XL. $BadER^{Tam}$ was generated by cloning the coding sequence for Bad into pCDH-EF1-T2A-GFP-Bcl-XL, and subsequently inserting the coding sequence for the oestrogen receptor hormone binding domain[265] in frame between Bad and the T2A sequence. Site directed mutagenesis was used to substitute the codons for S112 and S136 to those for alanine. The pLL3.7m-Clover-Geminin(1-110)-IRES-mKO2-Cdt(30-120) plasmid was generously gifted from Matthew Jones (University of Manchester). GFP-BaxWT and GFP-BaxS184V have been previously described[110]. The lentiviral pCDH expression vector was from SystemBiosciences. pMD2.G, psPAX2 and pVenus were kindly donated by D. Trono. pSpCas9(BB)-2A-GFP was kindly donated by F. Zhang. The BioID plasmid was kindly donated by K. Roux. Lentivirus expression vectors were generated using pCDH-EF1-MCS-T2A. GFP and paGFP-Bcl-2 proteins were inserted downstream of the T2A sequence. For the paGFP variants, H2B-mRFP was inserted upstream of the T2A sequence[110].

2.3.3 Bacterial transformation and DNA extraction

All bacterial transformations were carried out using JM109 cells made competent in house. 0.5µg of DNA was added to 50µl of bacteria and incubated on ice for 10 minutes. Cells were then heat shocked at 42°C for 45 seconds before being returned to ice for a further 5 minutes. 150µL of LB or SOC medium was then added before incubating at 37°C for 1 hour with shaking. 50µL of bacteria were then plated on LB agar plates containing the appropriate antibiotic at 100µg/ml and incubated overnight at 37°C. Single colonies were then picked and cultured in 5ml or 100ml of LB broth overnight at 37°C with shaking. Cultures were then centrifuged, and DNA amplified using either the Qiagen Plasmid Purification Miniprep or Maxiprep kit following manufacturer's instructions.

2.3.4 Genomic DNA extraction

Cells were trypsinised and spun down at 5000rpm for 5 minutes. Supernatant was removed and the cell pellet resuspended in 200µL lysis buffer (1M Tris pH8, 0.5M EDTA pH8, 5M NaCl, 10%SDS, 0.05mg/ml proteinase K, ddH_2O) before incubation overnight at 56°C. After incubation, 280µL isopropanol was added and the mixture shaken vigorously to precipitate the DNA. The sample was centrifuged at 4500rcf for 30 minutes then the supernatant discarded before washing the DNA pellet in 500µL of 70% ethanol. The sample was then centrifuged again at 4500rcf for 5 minutes before fully removing the supernatant, using a tissue to remove excess. The pellet was then air dried for approximately 10 minutes before resuspending in 50µL TE buffer (1M Tris pH 7.2, 0.5M EDTA pH8, ddH_2O) at 56°C.

2.3.5 Polymerase Chain Reaction (PCR)

PCR reactions were carried out under the conditions specific to the individual reaction. For genotyping, MyTaq Red mix was used following manufacturer's instrcutions. For higher fidelity reactions such as cloning and sequencing, Phusion DNA polymerase was used following manufacturer's instructions. Primers were designed using DNA Dynamo and produced by Sigma. All PCR reactions were carried out using a Veriti 96 well thermal cycler (Applied Biosystems).

2.3.6 DNA restriction enzyme digestion and ligation

Restriction digests of DNA were carried out using enzymes from New England Biolabs, following manufacturer's instructions for each individual enzyme. Ligations were carried out using T4 DNA ligase following manufacturer's instructions. Typically, a 3:1 molar ratio of insert to plasmid was used per reaction.

2.3.7 Agarose gel electrophoresis

Linearised DNA was analysed on either a 1% or 2.5% agarose gel depending on the size of the DNA fragments being analysed. Gels were prepared by mixing the appropriate quantity of agarose with 1X TAE (2M Tris, glacial acetic acid, 0.05M EDTA pH8.0, ddH_2O) and heated until all the agarose had dissolved. SYBR safe was added before setting. Following electrophoresis, gels were imaged on an LED Safe Imager Blue-light transilluminator (Invitrogen) and DNA extracted using a QIAQuick Gel Extraction Kit (Qiagen).

2.3.8 Site-directed mutagenesis

Mutagenesis reactions were carried out using the QuickChange Lightning Site-Directed Mutagnensis Kit (Agilent) following manufacturer's instructions.

2.3.9 CRISPR-Cas9 knockout

Genes were targeted for knockout following the protocol outlined in Ran et al., 2013[266]. sgRNA sequences were found located in the closest appropriate exon to the gene start codon and selected using an online CRISPR design tool (http://tools.genome-engineering.org). Primers were designed to target directly upstream of an NGG PAM site and cloned into a modified form of pX458 (pSpCas9(BB)-2A-GFP) in which the GFP was replaced with mCherry to allow FACS selection of positively transfected clones already expressing a GFP-tagged protein. Low passage MCF10A cells were transfected as outlined previously, and 24 hours post transfection were selected via FACS into single cells in 96-well plates. Cells were grown for approximately 4 weeks in 50% conditioned medium to aid growth. Once cells had been expanded up to a near-confluent 10cm plate, genomic DNA was extracted and a PCR carried out using primers designed to target 100-200bp either side of the target sequence. PCR products were run on a 2.5% agarose gel to visualise any indels. Potentially edited gDNA was then gel extracted, purified, and cloned into the pGEM-T easy vector as per manufacturer's instructions. The ligation was transformed into competent bacteria, purified and sequenced to genotype any edits in the gDNA compared to WT gDNA. These knockouts were then confirmed via Western blot.

2.4 Protein techniques

2.4.1 Reagents

30 % acrylamide-bisacrylamide, glycine, methanol, NaCl, KCl, and Tris were from Fisher Scientific. 10x casein blocking buffer, SDS, bromophenol blue, glycerol, DTT, Tween, NaF and Na_3VO_4 were all from Sigma. Protein inhibitor cocktail was from Calbiochem.

2.4.2 Cell lysis

Cells were washed three times in ice cold PBS, 5 minutes each, before being lysed in ice cold 1X RIPA buffer (250mM Tris HCl pH 7.4, 750mM NaCl, 0.5% SDS, 5% NP40, 5% sodium deoxycholate, ddH_2O) with added 1X protease inhibitor cocktail, 100mM Na_3VO_4 and 500mM NaF. The appropriate volume of RIPA was added to cells and incubated on ice for 5 minutes before scraping cells from the bottom of the dish. Cells were incubated on ice for a further 5 minutes before being collected into an Eppendorf and centrifuged at 14,000rcf for 15 minutes at 4°C. Supernatant was transferred to a fresh Eppendorf and stored at -20°C until needed.

2.4.3 BCA assay

BCA assays were carried out using the Pierce BCA protein assay kit following manufacturer's instructions. Assays were carried out in 96-well plates and absorbance at 562nm measured using a BP800 microplate reader (BIOHIT).

2.4.4 SDS-PAGE and immunoblotting

Protein samples were run on 10-15% gels depending on the size of proteins to be analysed. Gels of the appropriate percentage were made by combining 10-15% acrylamide/bisacrylamide, 0.37M Tris-CL pH8.8, 0.1% SDS, 0.1% ammonium persulphate and 0.0001% TEMED for the resolving gel, and 3% acrylamide/bis solution, 0.125M Tris-CL pH6.8, 0.1% SDS, 0.1% ammonium persulphate, 0.001% TEMED for the stacking gel. 20-40 µg of lysate were mixed with 10µL 5x sample buffer (10% glycerol, 50mM Tris pH 6.8, 10% SDS, 100mM DTT and 0.2% bromophenol blue) and heated to 95°C for 5 minutes. Samples were then loaded into the SDS-PAGE gel and run at 35mA per gel for approximately 90 minutes in running buffer (25 mM Tris, 192 mM glycine, 0.1 % SDS (w/v)). Samples were subsequently transferred onto nitrocellulose membrane (Amersham Protran, Merck) at 100V for 1 hour in transfer buffer (48 mM Tris, 39 mM glycine, 20% methanol (v/v)). Membranes were blocked in 1% casein in TBS-T (20mM Tris, 150mM NaCl, pH7.5, 0.1% Tweet-20) for 1 hour at room temperature. Primary antibodies were dilute to the appropriate concentration in blocking buffer and incubated overnight at 4°C (Table 2.1). Primary antibody was washed 3 times for 15 minutes each in TBS-T before adding secondary antibody (Table 2.2). This was incubated for one hour at

room temperature in darkness before three more TBS-T washes. Membranes were visualised using a LI-COR Odyssey CLX and LI-COR Image Studio software.

2.4.5 Membrane stripping

To strip proteins off membranes for reprobing, membranes were washed once with 1M NaOH for 5 minutes, then two rounds of 5 minutes ddH_2O followed by 5 minutes of TBS, before blocking and probing as previously described.

Target	Host	Supplier	Catalogue number	Dilution
AKAP1	Rabbit	Cell Signalling Technologies	5203	1:500
β-actin	Mouse	Abcam	Ab8224	1:1000
Bad	Rabbit	Cell Signalling Technologies	9292	1:500
Bcl-XL	Rabbit	Cell Signalling Technologies	2762	1:500
Bid	Rabbit	Cell Signalling Technologies	2002	1:500
Bim	Rabbit	Cell Signalling Technologies	2819	1:500
mCherry	Mouse	Abcam	Ab125096	1:500
Active caspase-3	Rabbit	R&D Systems	AF835	1:500
GFP	Rabbit	Life Technologies	A-11122	1:1000
mitoHsp70	Mouse	Thermofisher	MA3-028	1:1000
Oestrogen receptor	Rabbit	Abcam	Ab16660	1:500
Streptavidin (Alexa Fluor 488 conjugate)	-	Thermofisher	S32354	1:1000
Vinculin	Mouse	Abcam	Ab9532	1:1000
V5	Rabbit	Abcam	Ab9116	1:500

Table 2.1 Primary antibodies used for immunofluorescence and Western blotting

Target	Host	Conjugate dye	Supplier	Catalogue number	Dilution
anti-rabbit	Donkey	Alexa Fluor 488	Life Technologies	A-21206	1:1000
anti-rabbit	Donkey	Alexa Fluor 594	Life Technologies	A-21207	1:1000
anti-rabbit	Donkey	Alexa Fluor 647	Life Technologies	A-31573	1:1000
anti-mouse	Donkey	Alexa Fluor 488	Life Technologies	A-21202	1:1000
anti-mouse	Donkey	Alexa Fluor 594	Life Technologies	A-21203	1:1000
anti-mouse	Donkey	Alexa Fluor 647	Life Technologies	A-31571	1:1000

Table 2.2 Secondary antibodies used for immunofluorescence

Target	Conjugate dye	Host	Supplier	Catalogue number	Dilution
Anti-rabbit	680LT	Donkey	Li-Cor	926-68023	1:5000
Anti-rabbit	800CW	Donkey	Li-Cor	926-32213	1:5000
Anti-mouse	680LT	Donkey	Li-Cor	926-68022	1:5000
Anti-mouse	800CW	Donkey	Li-Cor	926-32212	1:5000

Table 2.3 Secondary antibodies used for Western blotting

2.5 Biotin proximity labelling techniques

2.5.1 Reagents

D-biotin and streptavidin-agarose beads were from Sigma Aldrich.4X Laemmli sample buffer was from BioRad. InstantBlue was from Expedeon.

2.5.2 BioID labelling

Cells expressing BirA* fusion proteins were seeded so that they were approximately 60% confluent the next day. 24 hours later, growth medium was replaced with complete growth medium supplemented with 50µM biotin and cells were incubated for 16 hours. Biotin medium was replaced with complete growth medium for one hour to allow free biotin to diffuse out of the cells. Cells were then lysed as described previously

2.5.3 Streptavidin-agarose affinity purification

Protein concentration of labelled lysates was determined via BCA assay and the appropriate volume of streptavidin-agarose bead slurry (10:1 total protein mass:volume of beads) was washed twice with lysis buffer, centrifuging for 2 minutes at 4000rpm between washes to remove supernatant. After the final supernatant was removed, lysate was added to the beads and samples were incubated overnight on and end-over-end tumbler at 4ºC. The next day, samples were centrifuged for 2 minutes at 4000rpm and supernatant removed and stored as the flowthrough. Beads were washed twice with lysis buffer, once with urea wash buffer (2M Urea, 10mM, Tris-HCl pH8.0), and twice more with lysis buffer, centrifuging for 2 minutes at 4000rpm between each wash. Pellets were then resuspended in the appropriate volume of elution buffer (1X SDS-PAGE sample buffer, 2mM D-biotin) and incubated at 95ºC for 5 minutes. Beads were then pelleted, the supernatant removed and either loaded into and SDS-PAGE gel or concentrated using a vacuum concentrator.

2.5.4 Sample preparation

Samples were loaded into an SDS-PAGE gel briefly until the entire sample had completely entered the resolving gel (approximately 5 minutes). Proteins were then fixed in the gel and stained using InstantBlue for 1 hour, with gentle shaking. Gels were then destained with ddH_20 overnight, or until all background staining was removed. Gel tops were then submitted to the University of Manchester Bio-MS facility for further preparation and liquid chromatography-tandem mass spectrometry using a Thermo Orbitrap Elite coupled with a Thermo nanoRSLC system (Thermo Fisher Scientific).

2.5.5 Data processing

All processing of raw data was carried out by Craig Lawless. Using MaxQuant v1.6.2.101[267], data was searched against the human proteome downloaded from Uniprot (July 2019) and appended to the mouse Bax sequence for each bait protein. As a data-level quality control, the pairwise comparisons of all samples and replicates and the PCA of the control vs each of the bait experiments was examined to ensure significant agreement across biological repeats between the experiments. SAINT (SAINTexpress)[268] was then used to identify interacting preys. High-confidence proximity interactions against negative control samples were determined using a BHFDR threshold of 0.05.

3. Mitochondrial priming can be measured via retrotranslocation of anti-apoptotic Bcl-2 proteins in live cells

3.1 Introduction

Our current understanding of how Bcl-2 proteins regulate apoptosis is lacking in many areas, largely due to the previous methodology used to examine Bcl-2 protein interactions. Measuring interactions between truncated BH3 peptides or on synthetic lipid membranes has created a lot of conflicting data in terms of the mechanisms of activation of Bcl-2 proteins in response to a pro-apoptotic stimulus. For example, one important outstanding question is where Bcl-2 protein-protein interactions occur; is localisation at the OMM critical for anti- and pro-apoptotic protein interactions, or does this occur in the cytosol? Is localisation of anti-apoptotic proteins at the OMM crucial for their function, and how does the mechanism of retrotranslocation occur? Due to the conflicting nature of our current understanding of Bcl-2 protein regulation of apoptosis, more studies of protein-protein interactions in live cells are required to elucidate the mechanisms of apoptotic induction between cell populations, and between individual cells. Furthermore, how these interactions differ in live, healthy cells versus the interim period leading up to apoptosis, and if this differs between different cell types has not been well characterised. To this end, we first need a method of examining Bcl-2 protein dynamics in live cells.

Using fluorescence loss in photobleaching (FLIP), it has been shown that pro-apoptotic Bax[215] and Bak[111] dynamics and their interactions are not binary, but are continually changing around an equilibrium depending on the apoptotic signals reaching the cell. However, using these live cell methods has also demonstrated that Bax and Bak dynamics are fundamentally different from each other in an unprimed cell, as Bak is inherently more stably localised at the OMM than Bax[111]. The functional purpose of these differences in localisation is still not fully understood, but swapping the TMDs of Bak and Bax also switches their distributions suggesting that the composition of the TMD is important in regulating these dynamics. Bax is believed to undergo a conformational change whereby its TMD is released from its hydrophobic groove to allow insertion into the OMM[121]. Whether this occurs in the cytosol as a precursor to OMM localisation, or whether this

conformational change is dependent on membrane localisation is unclear. The changes in Bax dynamics are regulated, at least in part, by anti-apoptotic Bcl-2 proteins such as Bcl-XL, as measured via a change in FLIP dynamics[215,269]. However, the mechanism of these interactions is also contentious. FRET has also been used previously to examine interactions between Bcl-2 proteins in live cells, for example when studying the interactions or pro-apoptotic and anti-apoptotic Bcl-2 proteins in MCF-7 cells[270] or indeed between Bcl-2 family proteins and other interactors, such as Bcl-XL and E2F1[271]. Whilst this method is useful in measuring protein-protein interactions in live cells, it requires both proteins to be fluorescently tagged which can limit the types of experiments that can be performed. Using FLIP, Edlich and co-workers state that the Bcl-XL-Bax interaction serves to retrotranslocate Bax from the mitochondria to prevent apoptosis in healthy cells[215]. Conversely, previous work in our laboratory has also demonstrated that Bcl-XL and Bax stabilise each other at the OMM as cells become more stressed[110]. Thus, the mechanism of Bax activation and Bcl-XL anti-apoptotic function requires further examination. What is known is that changes in mitochondrial priming relate to changes in Bax dynamics, with a decrease in FLIP correlating with an increase in Bax mitochondrial localisation, and an increase in priming[110]. Whilst FLIP does not necessarily indicate a direct interaction between the proteins being measured, proteins are in close-proximity can be visualised.

It was also demonstrated that fluorescence recovery after photobleaching (FRAP) can be used to measure mitochondrial translocation of proteins that show both cytosolic and mitochondrial distribution[110]. As Bcl-XL has been identified as a regulator of Bax, we wished to examine the dynamics of it, and other anti-apoptotic Bcl-2 proteins in healthy, live cells to determine if their dynamics vary, with some preferentially localising to the OMM like Bak. We also questioned whether these dynamics would also be altered when exposed to various pro-apoptotic signals. Similarly to FLIP, FRAP does not necessarily indicate direct binding between proteins, but close proximity proteins can be visualised, and further FRAP analysis of non-binding versions of the proteins can indicate whether direct binding is a likely cause of changes in FRAP measurements. We therefore chose to utilise FRAP as well as photoactivation to measure both the translocation onto, and retrotranslocation off mitochondria (Fig. 3.1).

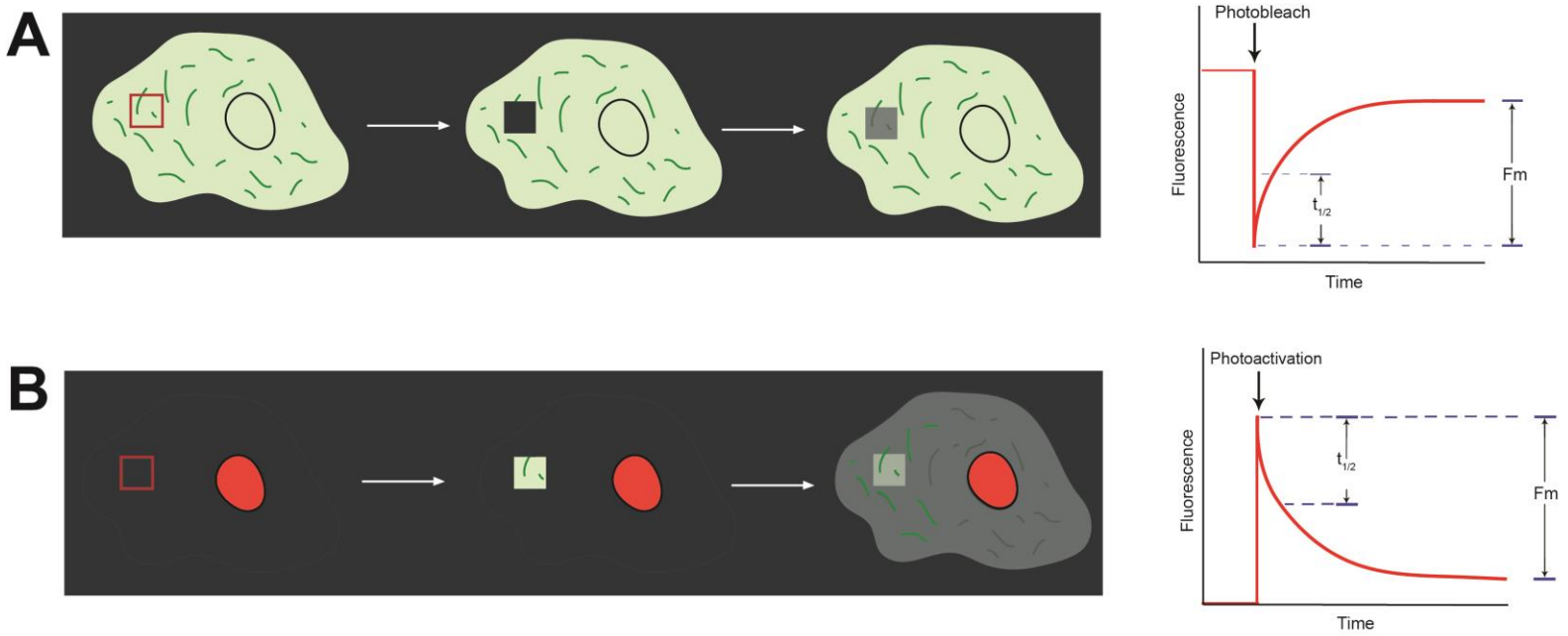

Figure 3.1. FRAP and photoactivation

A. During FRAP, cells expressing a fluorescently tagged protein are photobleached within an area of the cell encompassing both mitochondria and cytosol (red square). Over time, fluorescence recovers as the unbleached mobile fraction of protein replaces the bleached fraction. The fluorescence recovery within the same area is measured over time and plotted on a graph. The area under the curve represents the mobile fraction of the protein (Fm) and can be used to measure the halftime of fluorescence recovery ($t_{1/2}$).

B. For photoactivation, cells expressing a photoactivatable fluorescently tagged protein are photoactivated within an area of interest (red square). The area is selected relatively close to the nucleus, identifiable by a fluorescent histone 2B. Over time, mobile photoactivated proteins leave the bleached are and are replaced but the non-photoactivated fraction. The decrease in fluorescence is measured over time and plotted on a graph. As with FRAP, both the mobile fraction and halftime of fluorescence loss can be calculated from the graph.

3.2 Anti-apoptotic Bcl-2 proteins have different mitochondrial translocation rates

As Bax and Bak have significantly different mitochondrial localisation and retroanslocation rates between mitochondria and cytosol in healthy cells, and Bax interacts with Bcl-XL at the OMM, we wanted to investigate whether anti-apoptotic proteins also varied in their mitochondrial dynamics. In order to investigate this, MEFs null for Bax and Bak (herein referred to as DKO MEFs) transiently expressing N-terminal Venus- or YFP-tagged full-length Bcl-2, Bcl-XL, Bcl-W and Mcl-1 were subjected to FRAP analysis to measure the dynamics of the individual proteins in heathy cells (Fig 3.2A). Cells were photobleached within the yellow region of interest (ROI) encompassing a proportion of the mitochondrial protein and the recovery of fluorescence within the same ROI measured over time. Any differences in fluorescence recovery levels or rates indicates differences in the translocation of the proteins onto the mitochondria. Recovery of fluorescence of each protein was measured in multiple cells and one phase association curves fitted to the data (Fig 3.2B). All four proteins measured showed some recovery of fluorescence, indicating that all of them are relatively dynamic within live cells. Interestingly, only Bcl-2 had different dynamics from the other proteins. Analysis of both the average mobile fraction (Fig 3.2C) and halftime of fluorescence recovery (Fig. 3.2D) showed that Bcl-2 has a significantly lower mobile fraction than the other three proteins, and fluorescence recovers significantly slower.

3.3 The transmembrane domain of anti-apoptotic Bcl-2 proteins is essential for maintaining their protective function

The difference in FRAP dynamics between Bcl-2 and the other anti-apoptotic Bcl-2 proteins tested could be explained due to differences in their transmembrane domain (TMD) sequences. The TMD of Bak is predicted to be more hydrophobic than that of Bax based upon predicted free energy (ΔG_{app}) values for ER insertion, potentially explaining its more mitochondrial localisation[272]. Bcl-2 is also predicted to be have a more hydrophobic TMD than other anti-apoptotic proteins, thus Bcl-2 could be more tightly inserted into the OMM. When the TMDs of Bcl-XL and Bcl-2 are interchanged, so too are their localisations[273]. This agrees with previous data

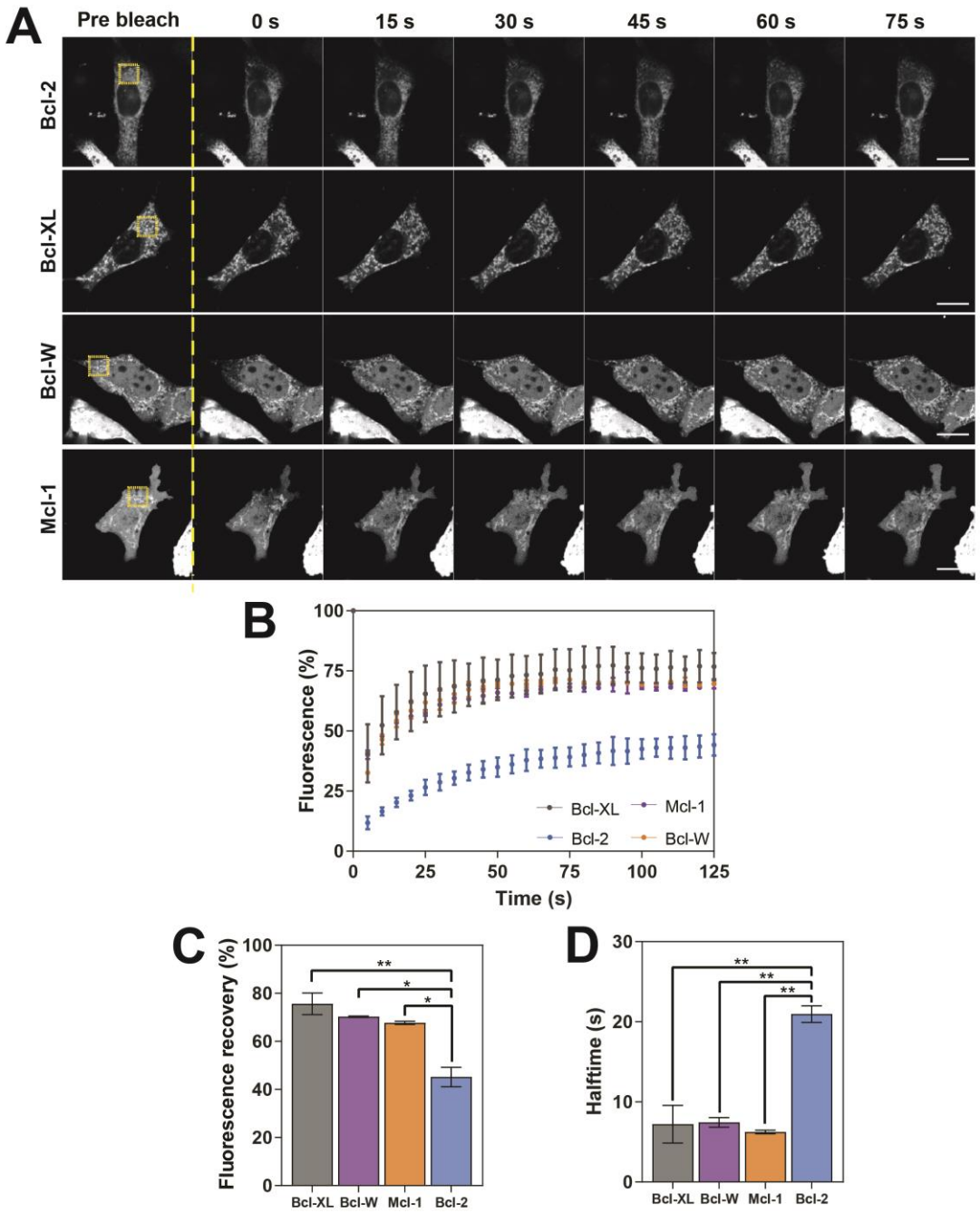

Figure 3.2. The major anti-apoptotic Bcl-2 proteins are in equilibrium between cytosol and mitochondria

A. Representative images showing FRAP analysis carried out on DKO MEFs transiently expressing GFP- or Venus-tagged Bcl-2 proteins. A ROI within the cell containing both mitochondria and cytosol was photobleached for 10ms using a 488nm laser, and the recovery of fluorescence in the same area measured over time. Images were taken every 5 seconds.

B. Recovery in fluorescence was plotted over time and non-linear regression carried out.

C. The average fluorescence recovery was calculated and plotted from data in B.

D. The average halftime for fluorescence recovery was calculated and plotted from data in B. Data represents values from 2 independent experiments, n=30 cells per condition. Error bars represent standard deviation and data was analysed via ANOVA.* = $p<0.05$; ** = $p<0.01$.

from our laboratory which demonstrated via FRAP that making the TMD of Bcl-XL more hydrophobic slowed its retrotranslocation dynamics to levels comparable to that of Bcl-2 (Ricardo Rodriguez-Enriquez, unpublished data), further suggesting the composition of the TMD is integral in regulating retrotranslocation dynamics. How these differing localisations between mitochondria and cytosol relate to specific apoptotic functions is still unclear. Original examination of Bcl-XL anti-apoptotic function by Borner and colleagues demonstrated that the TMD of Bcl-XL was not required for its pro-survival function[274]. However, more recent studies examining Bcl-XL interactions in live cells have demonstrated that its membrane localisation contributes towards its ability to resist derepression by inhibitors such as WEHI-539, and influence its affinity for BH3 domain binding[212]. We therefore wanted to examine the requirement of the TMD of anti-apoptotic Bcl-2 proteins for maintaining their anti-apoptotic function.

In order to investigate this, comparison of full-length proteins against those lacking a TMD is required. Expression vectors containing N-terminal Venus- or YFP-tagged anti-apoptotic Bcl-XL, Bcl-2, Bcl-W and Mcl-1 had previously been mutated to introduce a premature stop codon upstream of the C-terminal TMD - as indicated in Fig. 3.3A - to delete the transmembrane helix (termed ΔTM). Both full-length and ΔTM proteins were transiently expressed in DKO MEFs, which were then fixed, and immunostained for their Venus or YFP tag alongside a mitochondrial marker, mHsp70 (Fig. 3.3B). As expected, all four full-length proteins were distributed between mitochondria and cytosol, to varying degrees. All of the ΔTM forms of the proteins, however, showed a completely cytosolic localisation, presumably due to their inability to insert into the OMM. These results are in agreement with previous data examining ΔTM localisation of Bcl-XL and Bcl-2 via fractionation of HEK293T cells[273].

The TMD of Bax is essential for its execution of apoptosis[275]. To determine whether the TMD of Bcl-XL and the other anti-apoptotic proteins is required for their protective function, we examined the effect a lack of TMD had on protection against pro-apoptotic tBid-induced apoptosis. WT MEFs were transfected with expression vectors containing either full-length or ΔTM Bcl-2 protein sequences in the presence of transiently expressed tBid-mCherry. Both live and dead cells were collected and immunostained, and apoptotic cells were identified by nuclear morphology (Fig.

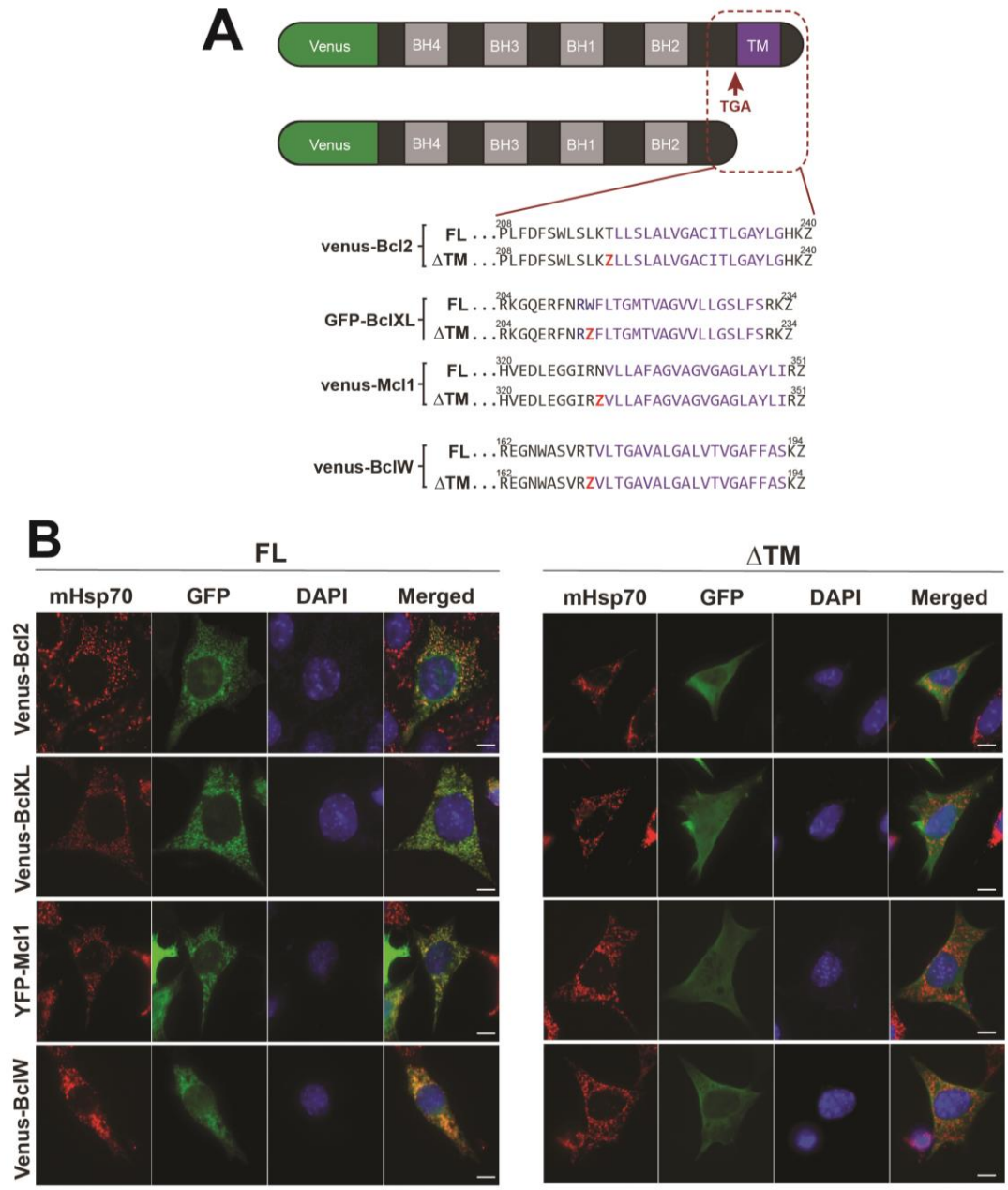

Figure 3.3. Bcl-2 proteins require their transmembrane domain for mitochondrial localisation

A. Plasmids containing full-length GFP- or Venus-tagged Bcl-2 proteins were mutated to introduce a premature stop codon directly upstream of the transmembrane domain.

B. Full-length or ΔTM Bcl-2 protein plasmids were transiently transfected into DKO MEFs. Cells were subsequently fixed and stained for the Venus- or GFP-tagged Bcl-2 proteins and the mitochondrial marker mHsp70. All full-length Bcl-2 proteins showed both mitochondrial and cytosolic localisation, whereas all ΔTM mutants were completely cytosolic. Scale bars represent 10μm.

3.4A). Full-length Bcl-2 proteins offered levels of protection similar to that seen when a BH3-inactive form of tBid, tBidG94E was transfected (Fig. 3.4B). Removal of the transmembrane domain, however, caused a significant decrease in anti-apoptotic function of all four proteins when expressed in the presence of tBid-mCh, comparable to that of tBid-mCh alone. Interestingly, Mcl-1ΔTM-expressing cells had significantly lower levels of apoptosis than cells expressing tBid-mCh alone, suggesting Mcl-1 can still retain some anti-apoptotic function even in the absence of its TMD. To ensure the differences in levels of apoptosis were not due to differences in the expression levels of transfected proteins, a Western blot of each transfection was carried out (Fig. 3.4C). Bcl-XL, Bcl-2, and Bcl-W lysates contained comparable levels of the transfected Bcl-2 proteins suggesting similar expression levels between conditions. The Mcl-1ΔTM lysate also showed similar levels of expression, however, the full-length Mcl-1 lane showed much lower expression at the correct size, with a stronger expressing band at a much lower molecular weight. Subsequent Western blot analysis showed a further decrease in expression levels of the full-length Mcl-1 and a stronger presence of the smaller protein, perhaps suggesting a degradation of the full-length protein over time (data not shown). Due to this inconsistency, Mcl-1 was no longer pursued for the remainder of this thesis.

The lack of ability of the ΔTM Bcl-2 proteins to localise to the OMM suggested a complete inability to insert into the OMM. To test this, DKO MEFs transiently expressing either full-length or ΔTM Bcl-2 proteins were subjected to FRAP analysis (Fig. 3.5A & 3.5B). Both Bcl-2 and Bcl-XL ΔTM variants showed significantly higher mobile fractions than their full-length counterparts (Fig. 3.5C). Interestingly, full-length Bcl-W dynamics were slightly, but not significantly lower compared to the ΔTM variant. To test whether the ΔTM protein dynamics measured were purely diffusion or if some interactions were still occurring at other regions of the protein, the halftime of recovery of fluorescence of each ΔTM protein was compared to that of GFP (Fig. 3.5D). Bcl-XL ΔTM and Bcl-W ΔTM had significantly slower dynamics than GFP, whereas Bcl-2 ΔTM had slightly, but not significantly slower dynamics. This suggests that even without the presence of the C-terminal transmembrane helix, there is some interaction of anti-apoptotic proteins either with components at the OMM or in the cytosol that prevent free diffusion of the proteins. Together these data suggest that the ability of the full-length Bcl-2 proteins to insert into the OMM via their transmembrane domain is important in maintaining membrane localisation and full anti-apoptotic function. It also suggests that, even without a C-terminal

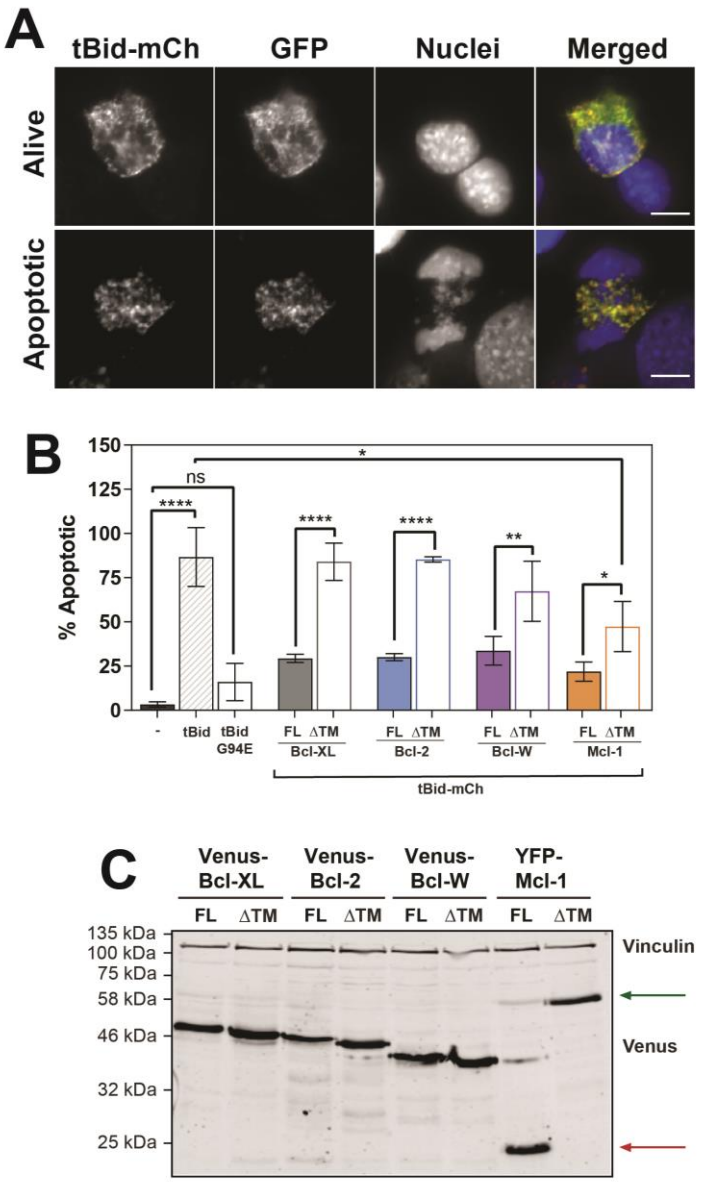

Figure 3.4. The transmembrane domain of Bcl-2 proteins is essential for maintaining anti-apoptotic function

A. MEFs were transiently transfected with either FL or ΔTM Bcl-2 proteins in the presence of wildtype or inactive pro-apoptotic tBid-mCh, and cytospun onto slides 24 hours later. Apoptotic cells were identified via immunofluorescence by changes in nuclear morphology.

B. Apoptosis was quantified for positively transfected cells and analysis comparing FL versus ΔTM mutants carried out. Data represents values from 3 independent experiments. Error bars represent standard deviation and all data were analysed via ANOVA. * = $p<0.05$; ** = $p<0.01$; **** = $p<0.001$.

C. Transient expression levels of FL and ΔTM Bcl-2 proteins were compared via Western blot by blotting for GFP, using vinculin as a loading control. The green arrow indicates full-length and ΔTM Mcl-1, and the red arrow indicates the lower molecular weight full-length Mcl-1 degradation band.

transmembrane helix, anti-apoptotic Bcl-2 proteins can still interact with other proteins to some degree. Which proteins these are, whether these interactions occur in the cytosol or at the OMM, and whether they are BH3-dependent remains to be studied.

3.4 Anti-apoptotic Bcl-2 proteins have specific individual binding specificities for pro-apoptotic BH3 proteins in live cells

Previous work from our laboratory has shown that Bcl-XL and pro-apoptotic multi-domain Bax can stabilise each other at the OMM, and that mitochondrial Bax sensitises cells to apoptosis[110]. This is contradictory to other live cell studies which demonstrate that Bcl-XL exerts its anti-apoptotic activity by removing Bax from the OMM back to the cytosol[215]. Both arguments agree that localisation at the OMM is important for the Bcl-XL and Bax interaction, but whether the mitochondrial complex stabilises this interaction or not is unclear. We therefore wanted to determine whether binding of other BH3 proteins would demonstrate a shift in the localisation and dynamics of Bcl-XL or indeed other anti-apoptotic Bcl-2 proteins, and whether all BH3 proteins bind to all anti-apoptotic proteins to the same degree. To examine this, a photoactivatable form of GFP-tagged Bcl-XL was transiently expressed in DKO MEFs on a vector which also expressed H2B-mRFP in order to locate positively transfected cells. Cells were also co-transfected with vectors containing mCherry-tagged BH3 proteins tBid, Bim_{EL}, Puma, Bad or Noxa. An area near to the nucleus was targeted for photoactivation using a 405nm laser, and the dissociation of paGFP within this region was measured over time (Fig. 3.6A). The loss of fluorescence after photoactivation of GFP-Bcl-XL was slowed in the presence of all the pro-apoptotic proteins tested, although not all to the same degree. tBid and Puma had the most dramatic effect on the loss of fluorescence, and Noxa the least. This was somewhat surprising as the majority of literature suggests that Bcl-XL does not interact with Noxa[159]. As endogenous anti-apoptotic Bcl-2 proteins are still present in the DKO MEFs, it is possible that endogenous Mcl-1 could be binding to Noxa and slowing its dynamics, rather than Bcl-XL itself, and Bcl-XL is binding to other pro-apoptotic proteins within the cell. Using a cell line devoid of all anti-apoptotic Bcl-2 proteins and transfecting them back in separately would clarify this observation.

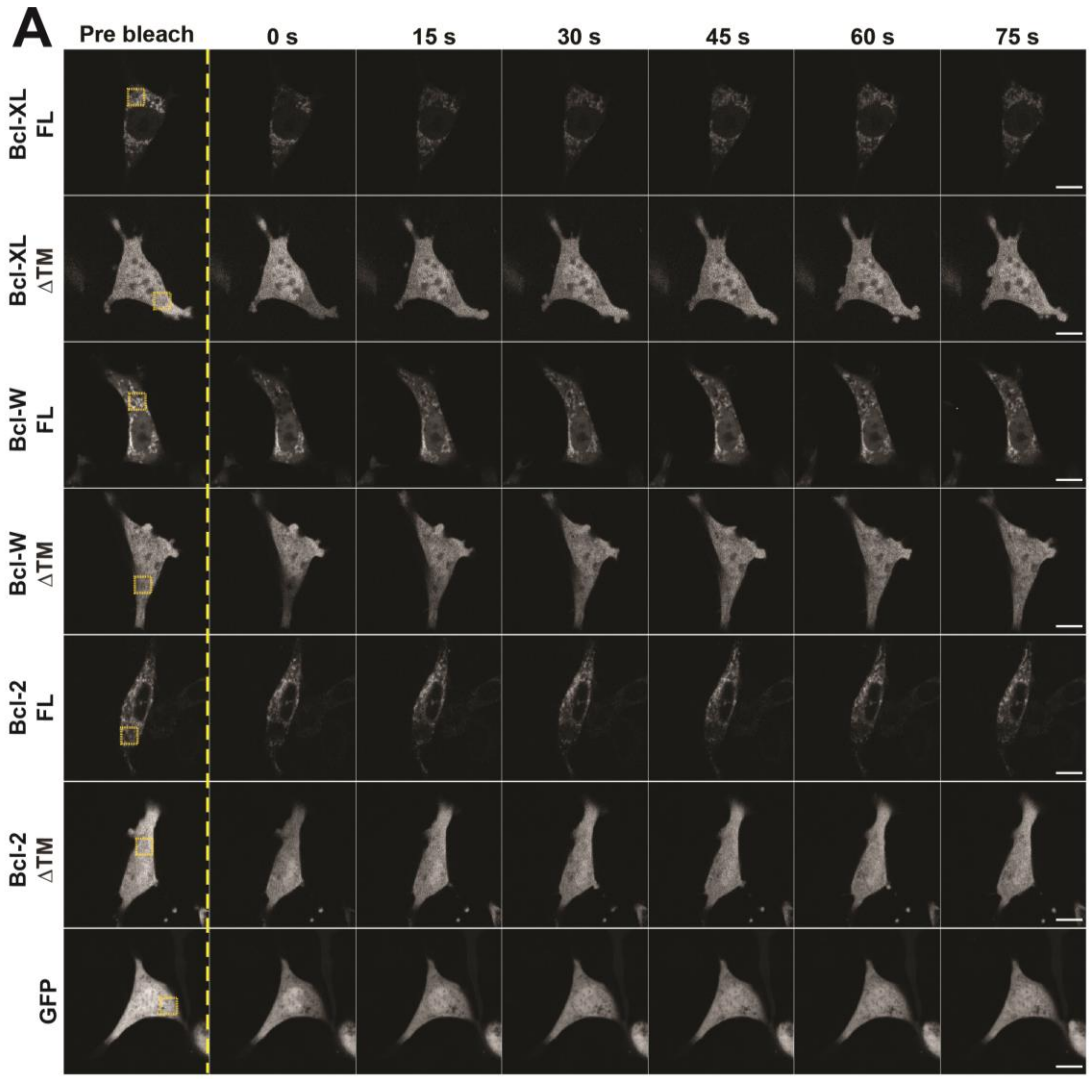

Figure legend on next page.

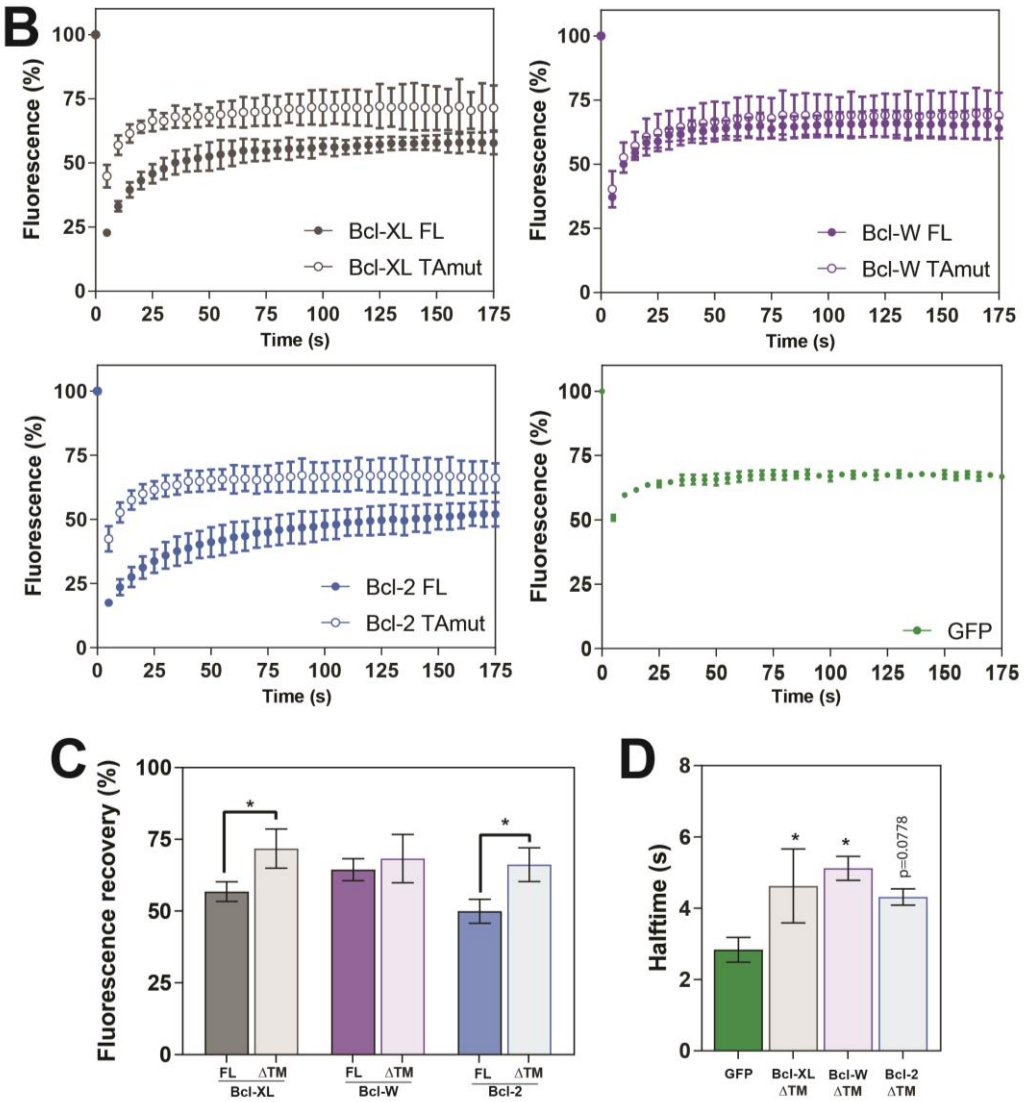

Figure 3.5. Bcl-2 protein dynamics are altered in the absence of a transmembrane domain.

A. DKO MEFs were transiently transfected with plasmids containing FL or ΔTM Bcl-2 proteins, or GFP, and FRAP carried out. Cells were photobleached within the yellow ROI for 10ms and fluorescence recovery within the same ROI measured.

B. Graphs of average FRAP data from A.

C. Non-linear regression analysis was carried out on data from B and the average fluorescence recovery plotted. The difference between the FL and ΔTM variant of each protein was compared.

D. The average halftime of recovery of same ΔTM data as in C was calculated and compared to FRAP data of DKO MEFs transiently expressing GFP. Data represents values from 3 independent experiments, n=50 cells per condition. Error bars represent standard deviation and fluorescence recovery was analysed via ANOVA. * =$p<0.05$

To confirm this binding specificity was not cell line-specific or due to differences in expression of the transiently expressed proteins, FRAP analysis was carried out on MCF10A cells stably infected with GFP-Bcl-XL alone, or transiently expressing each of the previous mCherry BH3 proteins (Fig. 3.6.B). In agreement with the previous photoactivation data, all five mCh-BH3 proteins tested significantly reduced Bcl-XL FRAP dynamics, including Noxa. This suggests that examining full-length Bcl-2 proteins in live cells reveals protein-protein interactions that differ to the current accepted Bcl-XL-model.

Whilst the TMD of anti-apoptotic proteins is required for their function, pro-apoptotic BH3-only proteins have also been shown to require a functional BH3 domain to exert their pro-apoptotic effect. Interactions between anti- and pro-apoptotic Bcl-2 family proteins are well-defined within the BH3 domain; the solution structure of Bak and Bcl-XL demonstrated that the BH3 domain forms an amphipathic α-helical structure that can bind with high affinity to the hydrophobic groove created by the BH1, BH2 and BH3 domains of Bcl-XL[69]. Studies in live cells have shown that single amino acid substitutions in the BH3 domain of tBid, Bim and Puma can inhibit the release of cytochrome c in MEFs[276]. Previous FRAP experiments have been carried out in our laboratory by Ricardo Rodriguez-Enriquez which measured the dynamics of Bcl-XL in the presence of either tBid or Bim_{EL} or 2A mutants of each, in which two residues in the BH3 domain - leucine 146 and phenylalanine 153 – were substituted with alanine, abolishing any direct interaction at the BH3 domain. tBid reduced Bcl-XL dynamics, in agreement with our FRAP data, whereas the tBid2A had no effect (Fig. 3.7A). Bim also decreased Bcl-XL dynamics, and, unlike Bid2A, Bim2A caused a slight decrease in the mobility of Bcl-XL, although this was not as pronounced as full-length mCherry-Bim (Fig. 3.7B). This is in agreement with data measuring Bcl-XL interaction with full-length and 2A mCherry Bim in MCF-7 cells via FRET[277] and with a more recent study demonstrating that Bim can bind Bcl-XL and Bcl-2 at two separate binding sites[262]. To confirm this difference in Bcl-XL dynamics between WT and 2A mutants was functional, WT MEFs were transfected with either mCherry-tBid or -Bim, 2A mutants of each, or mCherry, and levels of apoptosis were assayed via immunofluorescence. Both FL tBid and Bim_{EL} induced significant levels of apoptosis compared to mCherry (Fig. 3.7C). tBid2A and Bim2A induced apoptosis in a significantly smaller proportion of cells. tBid2A caused comparable levels of apoptosis to mCherry alone, whereas Bim_{EL}2A caused significantly more apoptosis, although not to the same level as the BH3-functional Bim. This agrees with our

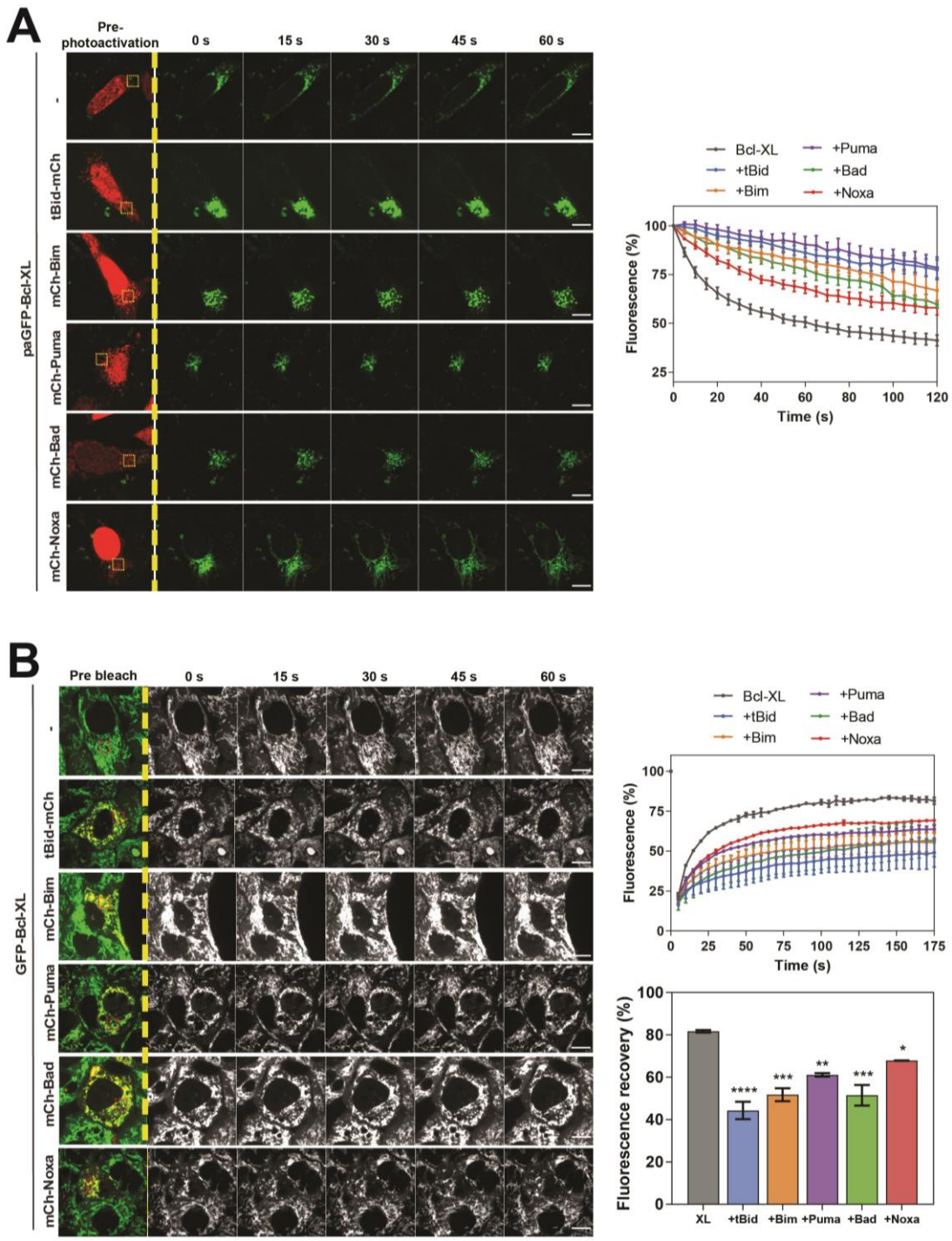

Figure 3.6. Bcl-XL interacts with multiple pro-apoptotic BH3 proteins

A. DKO MEFs transiently expressing photoactivatable Bcl-XL and mCherry-tagged BH3 proteins were photoactivated within the yellow ROI and images captured every 5 seconds. The loss of fluorescence within the same ROI was measured and average loss of fluorescence curves plotted.

B. MCF10A cells stably expressing GFP-Bcl-XL and transiently expressing mCherry-tagged BH3 proteins were photobleached within the yellow ROI and fluorescence recovery measured over time. Fluorescence recovery curves were plotted and analysed as previously described. Data represents values from 3 independent experiments. Error bars represent standard deviation and data was analysed via ANOVA.* = $p<0.05$; ** = $p<0.01$; *** = $p<0.005$; **** = $p<0.001$. Scale bars represent 10µm.

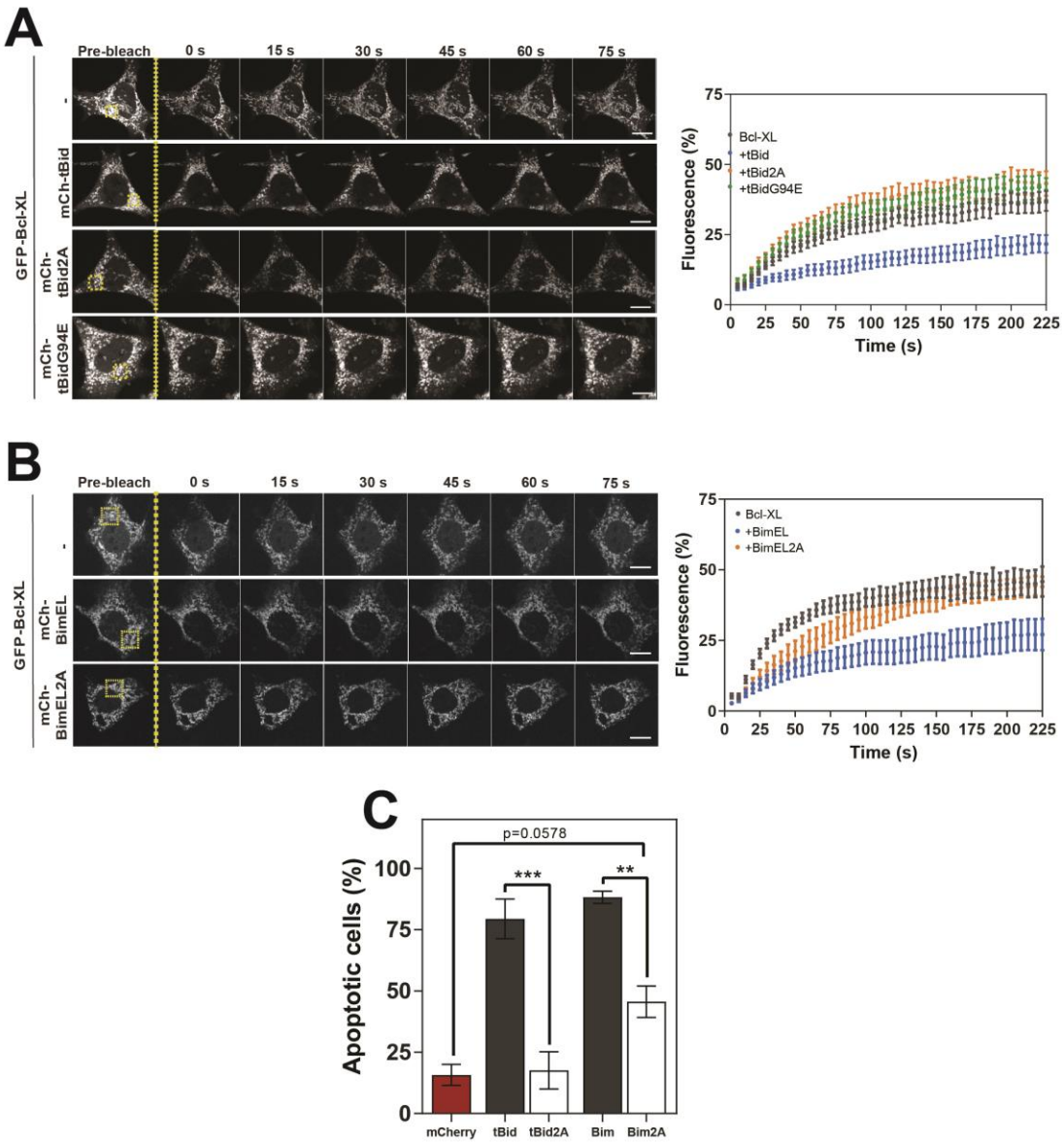

Figure 3.7. A functional BH3 domain is required for pro-apoptotic Bcl-2 protein interactions and maintenance of pro-apoptotic function

A.DKO MEFs transiently expressing GFP-Bcl-XL and either mCherry-tagged tBid, tBid2A or tBidG94E were subjected to FRAP analysis as described previously. Fluorescence recovery was plotted over time, with images taken every 5 seconds. Data represents averages of 10 cells per condition.

B. DKO MEFs transiently expressing GFP-Bcl-XL and either mCherry-tagged Bim or Bim2A were subjected to FRAP analysis as in A. Data represents averages of 10 cells per condition.

C. MEFs transiently transfected with vectors containing GFP-Bcl-XL and either FL or 2A mCherry-tBid, -Bim or mCherry were cytospun and levels of apoptosis quantified via immunofluorescence. Data represents values from 3 independent experiments. Error bars represent standard deviation and all data were analysed via ANOVA. ** = $p<0.01$; **** = $p<0.001$.

previous FRAP data and recent FLIM-FRET data[262], suggesting that Bim2A can still interact with Bcl-XL and exert its pro-apoptotic function in cells to a degree, whereas tBid requires a functional BH3 domain to exert its pro-apoptotic function.

Having demonstrated that Bcl-XL can interact with tBid, Bim, Puma, Bad and Noxa, we next wanted to assess whether the binding profiles of other anti-apoptotic proteins in live cells agree with previous binding assay data. Photoactivation was therefore carried out on Bcl-W and Bcl-2 in the presence of the BH3 proteins. Unlike Bcl-XL, Bcl-W did not have a strong interaction with the full panel of BH3 proteins tested (Fig 3.8A). mCherry-tBid, -Bim and -Puma all decreased the rate of Bcl-W dissociation from mitochondria. Bad and Noxa, however, had little effect on Bcl-W dynamics. This again differs from previously published non-live cell assay data which suggests that Bcl-W and Bad are strong interactors and therefore indicates not all Bcl-2 proteins share the same binding specificities to BH3 proteins.

FRAP data showed that Bcl-2 was significantly less mobile than the other Bcl-2 proteins analysed (c.f. Fig. 3.2). When its dynamics were analysed via photoactivation, none of the BH3 proteins tested significantly altered its retrotranslocation dynamics (Figure 3.8B), most likely due to its relatively stable insertion into the OMM. Therefore, BH3 proteins slow the dynamics of mobile anti-apoptotic Bcl-2-proteins to varying degrees, which is dependent on the presence of a functional BH3 domain.

3.5 Mitochondrial priming via serum starvation reduces Bcl-XL dynamics

Transiently expressing mCh-BH3 proteins in cells aims to, as far as possible, mimic the activation of BH3 proteins that would normally occur when a cell is exposed to apoptotic stresses. We wanted to test whether a reduction in Bcl-XL dynamics occurs in the presence of other, more representative pro-apoptotic stimuli. Serum starvation causes a decrease in growth factor signalling which, in turn, can have a direct effect on pro-apoptotic Bcl-2 family protein activation. For example, a decrease in EGF signalling causes increased Bim expression[278] and a decrease in Bad phosphorylation leading to an increase in its activation[279]. We therefore

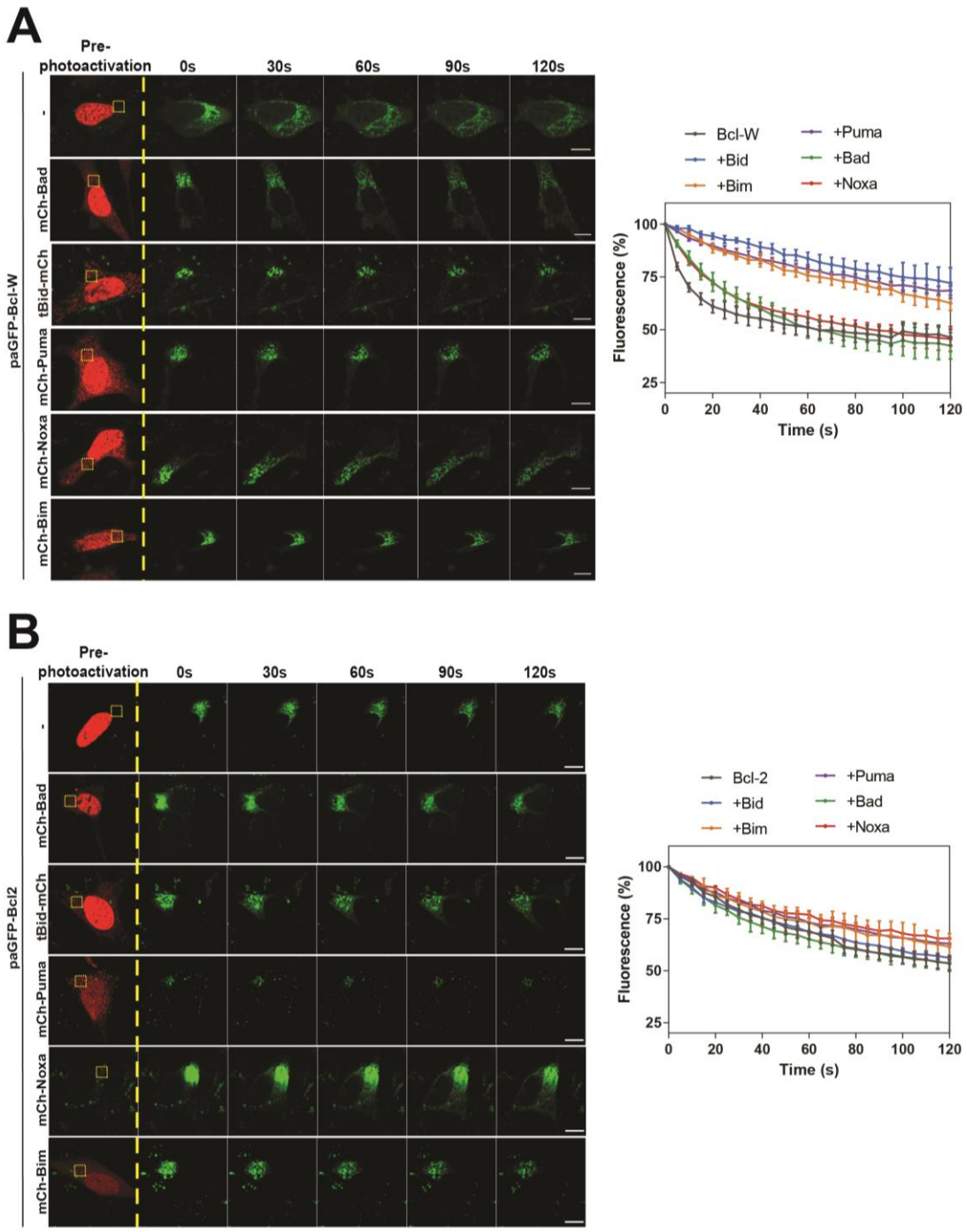

Figure 3.8. Individual anti-apoptotic Bcl-2 proteins have different BH3 protein binding preferences

A. DKO MEFs transiently expressing photoactivatable Bcl-W and mCherry-tagged BH3 proteins were photoactivated within the yellow ROI and images captured every 5 seconds. The loss of fluorescence within the same ROI was measured and average loss of fluorescence curves plotted.

B. DKO MEFs were transiently transfected with photoactivatable Bcl-2 and mCherry-tagged BH3 proteins and photoactivation analysis was carried out as in A. Data represents values from 3 independent experiments, n=50 cells per condition. Error bars represent SEM. Scale bars represent 10µm.

hypothesised that growing cells without serum would increase pro-apoptotic Bcl-2 protein activity, which in turn would cause a stabilisation of Bcl-XL at the OMM. This could then be measured via a reduction in the recovery of fluorescence of GFP-Bcl-XL during FRAP analysis. To examine this, stable GFP-Bcl-XL MCF10A cells were cultured in either complete medium or serum-free medium for 7 days before carrying out FRAP analysis (Figure 3.9A). Cells grown in serum-free medium showed significantly slower Bcl-XL dynamics compared to those cultured in complete medium (Fig. 3.9B and 3.9C). This suggested that a decrease in Bcl-XL dynamics was a result of an increase in levels of activated pro-apoptotic proteins due to a lack of growth factor signalling.

3.6 Discussion

Based on current literature, the general perception of the mechanism of Bcl-2 protein function is that they are cytosolic until induction of apoptosis, after which they become localised to the OMM. This very black and white view of Bcl-2 protein apoptotic regulation is more recently coming into question following an increase in live cell studies which demonstrate that pro-apoptotic Bax is continuously shutting between cytosol and mitochondria[109,110,121]. This also highlights differences in protein regulation between different pro-apoptotic family members, such as Bak being inherently more mitochondrial. Anti-apoptotic Bcl-2 proteins appear to play a role in these differing dynamics as Bcl-XL can interact with and inhibit Bax pro-apoptotic function. In healthy cells, whether Bax is removed from the OMM by Bcl-XL[215], or whether Bcl-XL stabilises Bax at the OMM but inhibits its activation is still under question[110]. Furthermore, whether variation between anti-apoptotic Bcl-2 protein dynamics is important for function is unclear. To investigate how Bcl-2 proteins interact with each other and with the OMM in healthy cells and in the lead up to apoptosis, we needed to establish an assay by which we could measure the dynamics and interactions of Bcl-2 proteins in live cells, in real-time. We thus utilised FRAP and photoactivation of fluorescently tagged full-length Bcl-2 proteins to measure protein dynamics in live cells. FRAP analysis allows measurement of recovery of fluorescence of a portion of photobleached proteins as they are replaced with a non-bleached fraction[280,281]. Photoactivation, on the other hand, allows measurement of loss of fluorescence of a photoactivated fraction of proteins as they leave the OMM and move throughout the cell[282]. Utilising a combination of both

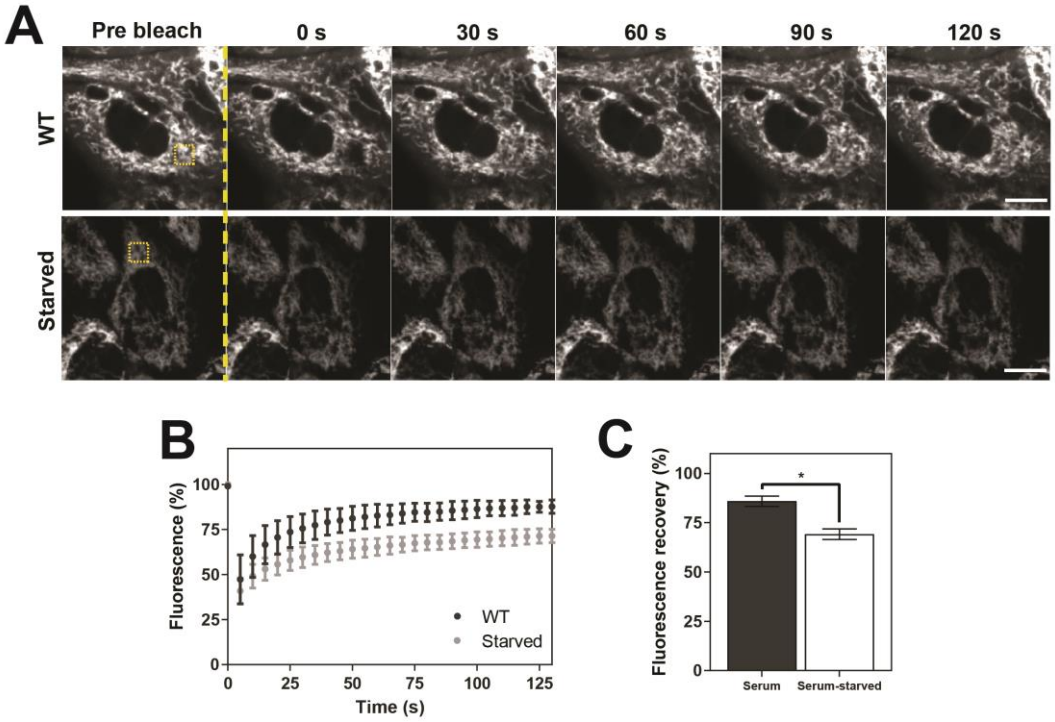

Figure 3.9. Serum starvation slows the FRAP dynamics of Bcl-XL

A. MCF10As stably expressing GFP-Bcl-XL were cultured in either complete growth medium, or serum-free medium for 7 days before carrying out FRAP analysis. Cells were photobleached within the yellow ROI and imaged every 5 seconds.

B. Fluorescence recovery from cells in A was plotted over time.

C. Non-linear regression of the average fluorescence recovery was carried out from data in B. Data represents values from 3 independent experiments, n=75 cells per condition per repeat. Error bars represent standard deviation and data was analysed via Student's t-test. * = $p<0.05$. Scale bars represent 10µm.

methods gives an overall picture of how anti-apoptotic Bcl-2 proteins are constantly moving on and off mitochondria, regulating individual cells' apoptotic responses.

FRAP analysis of transiently expressed anti-apoptotic proteins revealed that Bcl-2, Bcl-XL, Bcl-W and Mcl-1 are all mobile, constantly shuttling between cytosol and mitochondria in healthy cells. Of the four proteins examined, Bcl-2 was the least mobile. This is perhaps not surprising, as examination of its transmembrane domain identifies it as having a predicted lower ΔG_{app} value for insertion into the ER membrane than other anti-apoptotic proteins[272] (Fig. 3.10). Whilst this value may not directly apply to the OMM, it could be inferred that Bcl-2 would insert into the OMM more readily than the others. Proteins containing C-terminal TMDs have been shown to have structurally similar domains, with 17-23 hydrophobic residues followed by a sequence rich in basic amino acids[222,283]. The distinct structure of the residues surrounding the TMD between different Bcl-2 proteins is believed to play a key role in their specific localisation. For example, the TMD of Bcl-XL is encompassed by more basic amino acids than Bcl-2, and this more basic structure is thought to be the bona fide OMM localising sequence[273]. Immunoelectron-based studies have shown that between 55-85% of Bcl-2 is localised to the ER membrane rather than the OMM[284]. Fusing the TMD of Bcl-XL to GFP targets GFP to the OMM, whereas the TMD of Bcl-2 targets GFP to both mitochondria and the ER[273]. Potentially, when measuring Bcl-2 dynamics via FRAP, the rate at which it is translocating onto ER membranes is also being measured, thus showing a significantly lower mobile fraction than its more mitochondrial counterparts. Use of a live cell mitochondrial marker during FRAP may help to determine whether or not this is the case.

The differing dynamics of anti-apoptotic proteins also highlights a key question with regards to Bcl-2 protein regulation of MOMP – why are Bcl-2 proteins dynamic between cytosol and mitochondrial or ER membranes? Retrotranslocation of proteins to the cytosol is not an OMM-specific mechanism. For example, during the endoplasmic-reticulum-associated protein degradation (ERAD) response, misfolded proteins are retrotranslocated from the ER to the cytosol for degradation[285]. There is potential for proteins with the correct 3D structure to transiently bind to the ER membrane before being released back to the cytosol. Potentially, part of the

Protein	C-terminal sequence	Predicted ΔG
Bcl-2	FDFSWLSLKTLLSLALVGACITLGAYLGHK	-1.356
Bcl-W	NWASVRTVLTGAVALGALVTVGAFFASK	-0.418
Bcl-XL	GQERFNRWFLTGMTVAGVVLLGSLFSRK	-0.355
Mcl-1	LEGGIRNVLLAFAGVAGVGAGLAYLIR	-0.275

Figure 3.10. Predicted free energy of Bcl-2 protein transmembrane domains
Analysis of the amino acid sequence of Bcl-2 protein tail anchors. Potential transmembrane domains are highlighted in red based on their hydrophobicity. ΔG values shown are as calculated by the ΔG prediction server. Of note, Bcl-2 has a much lower ΔG value compared to the other proteins.

measured retrotranslocation dynamics is purely a result of mobile proteins encountering a non-specific hydrophobic membrane. When considering the OMM, the concept that anti-apoptotic proteins are continually buffering the cell against low levels of apoptotic signals would also account for these dynamics; anti-apoptotic proteins are moving between the OMM and cytosol to “mop up” any excess pro-apoptotic proteins in order to inhibit apoptosis in healthy cells. Both hypotheses rely on the ability of Bcl-2 proteins to extract from lipid membranes rapidly once inserted. How this occurs is not well studied, but there may be mitochondrial proteins involved in the membrane insertion and extraction process. For example, a recent CRISPR-Cas9 genome-wide screen identified that Bax requires the presence of the OMM voltage-dependent anion channel 2 protein (VDAC2) to localise to the OMM and carry out MOMP[286]. More investigation is needed to fully understand how proteins like this regulate the dynamic insertion and extraction process, and how this differs from more stably inserted Bcl-2 proteins.

The importance of the TMD of Bcl-2 proteins is further highlighted when this domain is removed from the full-length proteins, as both localisation and anti-apoptotic function are disrupted. Previous *in vitro* and live cell studies have shown similar lack of mitochondrial localisation when the TMD is removed[63,287] and Bax loses its pro-apoptotic function when there is no functional TMD[120,121]. It is interesting to note that, of the four anti-apoptotic proteins tested, cells expressing the Mcl1ΔTM mutant had significantly lower levels of apoptosis in the presence of tBid than tBid-mCh alone, suggesting even without the TMD some of its anti-apoptotic function remained. Mutation studies examining the N-terminal amino acids of Mcl-1 demonstrated that the S162 residue, which is still present in the Mcl1ΔTM mutant, is crucial for retaining anti-apoptotic function[288], and that Bcl-2 proteins can still bind to BH3 proteins even when lacking their TMD[212]. Mcl1ΔTM may therefore have the potential to maintain some mitochondrial localisation and thus still offer minor protection from apoptosis. However, due to what appeared to be a gradual degradation of the YFP-Mcl-1 plasmid over time, any potential conclusions made about Mcl-1 must be approached with caution.

The current map of Bcl-2 protein BH3 binding partners is mainly based on data gained from studies utilising techniques such as affinity measurements using BH3

peptides and truncated Bcl-2 proteins, immunoprecipitation, and NMR using recombinant proteins[46,213]. How well this reflects the live cell environment is unclear. Measuring the FRAP and photoactivation dynamics of full-length anti-apoptotic Bcl-2 proteins in the presence of full-length BH3 proteins elucidated differences in binding compared to the current understood model. Bcl-XL appeared to interact with all the BH3 proteins analysed including Noxa, previously thought not to interact with Bcl-XL. The majority of studies examining the Bcl-XL-Noxa interaction have been carried out using a Noxa BH3 peptide rather than the full-length protein[159,204,206,257,289]. However, some studies have shown an interaction between Bcl-XL and Noxa, for example in HeLa cells after UV- or CPT-induced DNA damage[290], Thapsigargin-induced ER stress or proteasomal inhibition[291], or via surface plasmon resonance measurements[292]. Bcl-W also showed differences in binding interactions, showing little interaction with Bad and Noxa. A lack of Bcl-W-Bad interaction has been shown in a study examining Bcl-W interactions in adult rat testis[293], suggesting that perhaps there may be tissue-specific differential binding of Bcl-2 proteins with their BH3 counterparts. Another factor to consider when examining Bcl-2 protein interactions is the specific protein variants used. Multiple studies have identified differences in binding affinities of different Bcl-2 variants with pro-apoptotic proteins within the same experiments[211,292]. Furthermore, when examining interactions in live cells, the expression levels of the proteins in question may also play a key role. Live cell studies have demonstrated that overexpression of Bcl-XL reduces effectiveness of the BH3 mimetic WEHI-539[212], and thus differences in BH3 binding specificity may exist between endogenously versus exogenously expressed proteins. One question that is still unclear is where exactly in the cell interactions between pro- and anti-apoptotic proteins take place. Based on examination via FRAP and photoactivation, binding of proteins appears to occur at the OMM, however, whether the initial binding occurs in the cytosol before mitochondrial localisation or can occur without any membrane association at all is unclear.

Increased expression of pro-apoptotic BH3 proteins occurs in response to various pro-apoptotic stimuli, thus transiently overexpressing BH3 proteins in cells aims to mimic this mitochondrial priming response. Serum starvation was also used as an alternative method to prime cells that did not involve directly manipulating Bcl-2 family proteins, as removal of serum decreased growth factor signalling, which in

turn, activates BH3 proteins. Although the change in endogenous pro-apoptotic Bcl-2 protein levels upon serum starvation was not directly shown, this could be achieved via Western blot of Bim and phosphorylated Bad. Alternatively, knocking down endogenous Bim should, at least partially, prevent changes in apoptotic priming in the absence of serum. A decrease in Bcl-XL retotranslocation was measured under serum-free conditions, similar to the change seen in the presence of mCh-BH3 proteins. Therefore, measuring changes in the dynamics of Bcl-2 proteins between mitochondria and cytosol can be used as a measure of levels of mitochondrial priming within live cells.

4. BH3 proteins compete for binding to Bcl-XL

4.1 Introduction

Results from the previous chapter demonstrated that FRAP or photoactivation can be used to measure variations in dynamics of Bcl-2 family proteins in live cells. Using these techniques, we demonstrated that a decrease in anti-apoptotic protein retrotranslocation dynamics mirrors increased levels of mitochondrial priming, induced either by exogenously expressing BH3 proteins or serum starvation. It also revealed that the binding specificities between anti-apoptotic and pro-apoptotic Bcl-2 proteins may differ from the currently accepted model. We therefore wanted to determine if BH3 proteins that do bind to Bcl-2 proteins have differing affinities for binding, and if so, whether these proteins displace other BH3 proteins from binding.

The concept that BH3-only proteins are in competition for binding anti-apoptotic proteins is most apparent in the proposed models of action for the induction of MOMP. The division of BH3-only proteins into sensitisers and activators relies on the concept that sensitisers such as Bad or Noxa can displace activators like Bid or Bim from anti-apoptotic proteins[294], and these proteins must then displace anti-apoptotic proteins from Bax and Bak to initiate MOMP. These differences in affinities have been attributed, in part, to interactions at the OMM, which can cause structural changes that alter binding affinities[295]. Understanding the precise mechanism of MOMP initiation requires detailed studies of binding affinities between Bcl-2 family proteins. For example, it has been shown that, between cBid, Bcl-XL and Bax, Bcl-XL can outcompete cBid for binding to Bax[296], and that Bad can release cBid from Bcl-XL to activate Bax[214]. Studies like these give a detailed insight into the series of events leading up to Bax activation, but are carried out in cell-free systems using liposomes and BH3 peptides, which may not be representative of the interactions occurring in live cells.

Gaining a more representative understanding of competition between Bcl-2 protein binding is important when considering the development of BH3-mimetics, particularly with the recent approval of ABT-199 for clinical use in the treatment of CLL. BH3-mimetic development is based on the concept that sensitisers can displace activator BH3 proteins from sequestration by anti-apoptotic proteins.

Recent studies are beginning to analyse the specificity of these interactions. For example, co-expressing equal concentrations of a pro- and an anti-apoptotic Bcl-2 proteins in cells causes the cells to become sensitive to BH3-mimetic treatment – a method termed mito-priming[297]. Using this technique to engineer cells dependent on specific anti-apoptotic proteins, the specificity of BH3-mimetics can be assayed using apoptosis as an output. Such experiments have demonstrated that ABT-737 is ineffective at displacing Bim from Bcl-XL, recently shown to be due to the "double-bolt locking" binding mechanism of Bim[262]. To gain a better understanding of competition between Bcl-2 family proteins and BH3-mimetics, as well as determine whether BH3-mimetics can bind to anti-apoptotic proteins as effectively as endogenous proteins, analysis of these interactions in live cells is necessary. However, controlling expression levels of both anti-apoptotic and pro-apoptotic proteins using transient expression is difficult, and thus may contribute to cell-to-cell variation between binding of different proteins. To solve this issue, we aimed to develop inducible systems in which both anti- and pro-apoptotic proteins were expressed at equal levels, to allow measurements of competition between multiple BH3 proteins within the same system.

4.2 Creation of inducible BH3-only protein cell lines

Using FRAP to measure changes in anti-apoptotic protein retrotranslocation dynamics allows us to measure changes in mitochondrial priming. As pro-apoptotic protein binding causes slowed anti-apoptotic protein FRAP dynamics, we could theoretically simultaneously measure a shift in fluorescently labelled pro-apoptotic protein dynamics. Competition between pro-apoptotic proteins could therefore be measured by activating a second BH3 protein and measuring any changes in FRAP dynamics of the fluorescently labelled BH3 protein. To achieve this, a system was required in which cells co-expressed both an anti-apoptotic protein and an inducible pro-apoptotic protein. Bcl-XL was chosen as the anti-apoptotic protein to measure as it was the only Bcl-2 protein tested that showed a significant decrease in dynamics with all of the BH3 proteins tested (see Fig. 3.6). We wished to select an activator and a sensitiser BH3 protein to assay for competition. The classification of Puma as a direct activator is still widely debated and thus was not selected. The regulation of both Bim expression and activation is complex, with regulation of mRNA transcription, stability and post-translational modifications[298–300], thus

modifying the regulatory residues of Bim to create an inducible form would be difficult. We therefore selected Bid as the activator protein to analyse as manipulation of the caspase 8 cleavage site would render the protein inducible. Sensitiser Noxa is regulated transcriptionally via a range of signalling pathways including HIF-1α, AKT and E2F1, and post-translationally via IRF-1, IRF-3 and CREB[301]. Furthermore, the stability of Noxa is also regulated post-translationally via ubiquitylation. Conversely, Bad is mainly regulated via phosphorylation at key residues Serine-112 and -136, and thus is easier to manipulate into an inducible form. Two approaches were therefore taken to create inducible BH3 protein systems – one involving Bid, and another other using Bad.

A lentivirus had previously been created that contained GFP-tagged Bcl-XL preceded by a T2A cleavage sequence (Fig. 4.1A). Directly upstream of the T2A sequence was Bid-mCh in which the caspase 8 cleavage site was replaced with a humanised tobacco etch virus (TEV) protease recognition sequence (herein referred to as Bid^{Tev}mCh)[302]. Bid^{Tev}mCh cleavage and activation could be induced via transient transfection of pCDNA-Tev-V5. This created an inducible form of tBid which was expressed in equal ratios with Bcl-XL but was inactive until Tev-V5 was expressed. Any positively transfected cells would be evident by an increase in both tBid and Bcl-XL mitochondrial localisation. To prevent either the process of transfection or the activation of Bid^{Tev}mCh inducing apoptosis and preventing measurement of competition, DKO MEFs stably expressing Bid^{Tev}mCh were transfected with Tev-V5 and either lysed for protein extraction or fixed and immunostained to examine the localisation of Bid in the absence and presence of Tev-V5. Western blot analysis showed expression of both GFP-BclXL and Bid^{Tev}mCh at similar levels (Fig. 4.1B). Immunofluorescence of both untransfected and transfected cells showed that, upon Tev-V5 transfection there was an increase in both Bcl-XL and Bid^{Tev}mCh co-localisation (Fig. 4.1C).

Having established that Bid cleavage and activation could be induced by transiently expressing Tev-V5, we next wanted to test the effect of Tev-V5 transfection on Bcl-XL and Bid dynamics in live cells. Previous FRAP data in DKO MEFS showed a decrease in Bcl-XL dynamics in the presence of tBid-mCh, thus a similar reduction in the mobility of Bcl-XL would be expected using the inducible system. FRAP analysis was carried out on both GFP-BclXL and Bid^{Tev}mCh in untransfected and

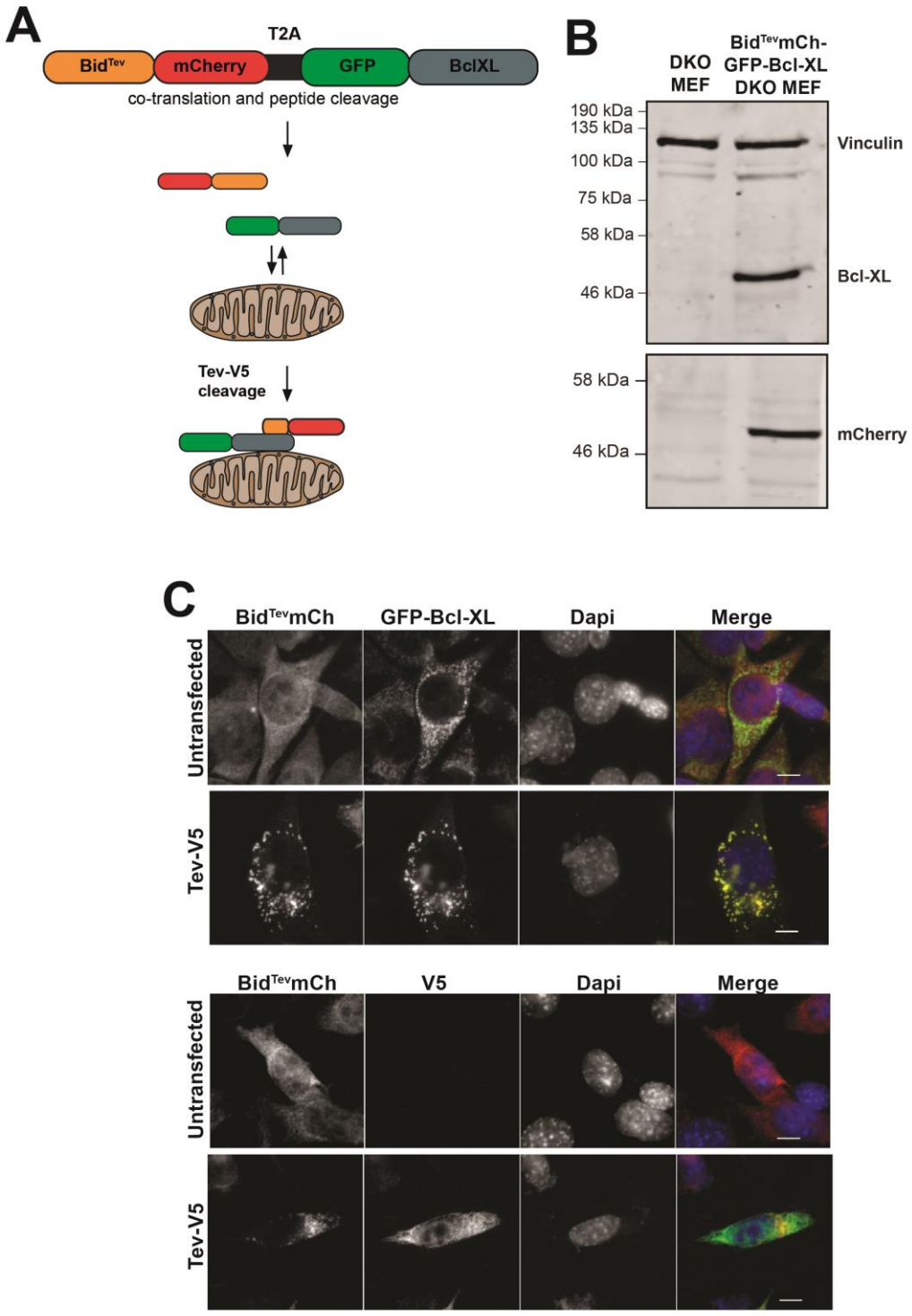

Figure 4.1. Bid^{Tev}mCh is localised to mitochondria upon Tev-V5 transfection

A. Schematic of the Bid^{Tev}mCh-GFP-Bcl-XL system. Bid^{Tev}mCh and GFP-Bcl-XL are post-translationally cleaved at the T2A site giving equimolar expression of each protein. Bid^{Tev}mCh is inactive until Tev-V5 transfection which causes binding of the two proteins and localisation at the OMM.

B. Western blot analysis of lysates of DKO MEFs stably expressing the construct. The membrane was probed for Bcl-XL and mCherry. Vinculin was used as a loading control.

C. Immunofluorescence of the same cell line as in B, showing both untransfected and Tev-V5 transfected cells. Cells were stained against GFP, mCherry or V5-tag. Scale bar represents 10µm.

Tev-V5 transfected cells (Fig. 4.2A). Similarly to the immunofluorescence data, positively transfected cells were easily distinguished by the mitochondrial localisation of Bid^{Tev}mCh. In positively transfected cells the mobile fraction of both Bcl-XL and Bid^{Tev}mCh significantly decreased (Fig. 4.2B). The reduction in retrotranslocation of Bcl-XL in the presence of active Bid^{Tev}mCh suggested that Bcl-XL dynamics could be used as a readout for the activation and binding of Bid.

An issue with the Bid^{Tev} system was that activation of Bid required transfection of Tev-V5, which meant a long induction timeframe and a lack of ability to reverse the activation. Our laboratory had previously attempted to create a much faster inducible system utilising a split protease SNIPer system in which the Tev protease was split into two fragments fused to FRB and FKBP (FRB-N-Tev and FKBP-C-Tev, respectively), which can be induced upon treatment with Rapamycin[303]. By transducing cells with Bid^{Tev}mCh and both Tev fragments, Bid cleavage and activation can be induced over shorter timeframes (Rodriguez-Enriquez R. unpublished data). By also expressing GFP-Bax in these cells, Bid^{Tev} cleavage can induce apoptosis via direct activation of Bax. Bid^{Tev} cleavage was observed in a time- and dose-dependent manner in NIH-3T3 cells stably expressing all parts of the inducible system, however the activation was not particularly robust and thus levels of apoptosis were low (data not shown). This was potentially due to lack of humanisation of the plant-optimised split Tev sequences, or a lack of equimolar expression of FRB-N-Tev and FKBP-C-Tev within individual cells.

Due to the poor kinetics and low expression of Bid activation in the previous system, a different approach was chosen for creating the inducible Bad system. A lentivirus had previously been created that contained GFP-tagged Bcl-XL preceded by a T2A cleavage sequence (Fig. 4.3A). Directly upstream of the T2A was pro-apoptotic Bad in which regulatory serines 112 and 136 were substituted with alanine, and the C-terminus fused with the oestrogen receptor (ER) hormone binding domain (HBD)[265]. In the absence of the 17β-oestradiol ligand, the ER HBD is bound to the chaperone protein Hsp90. In the presence of its ligand, receptor dimerisation occurs, allowing DNA binding and transactivation[304]. The HBD used contains a modified murine G525R domain which cannot bind the 17β-oestradiol ligand, and in which the endogenous ligand-dependent transactivation activity (TAF-2) does not occur, but is instead highly responsive to 4-hydroxytamoxifen (4-OHT)[304]. This created an

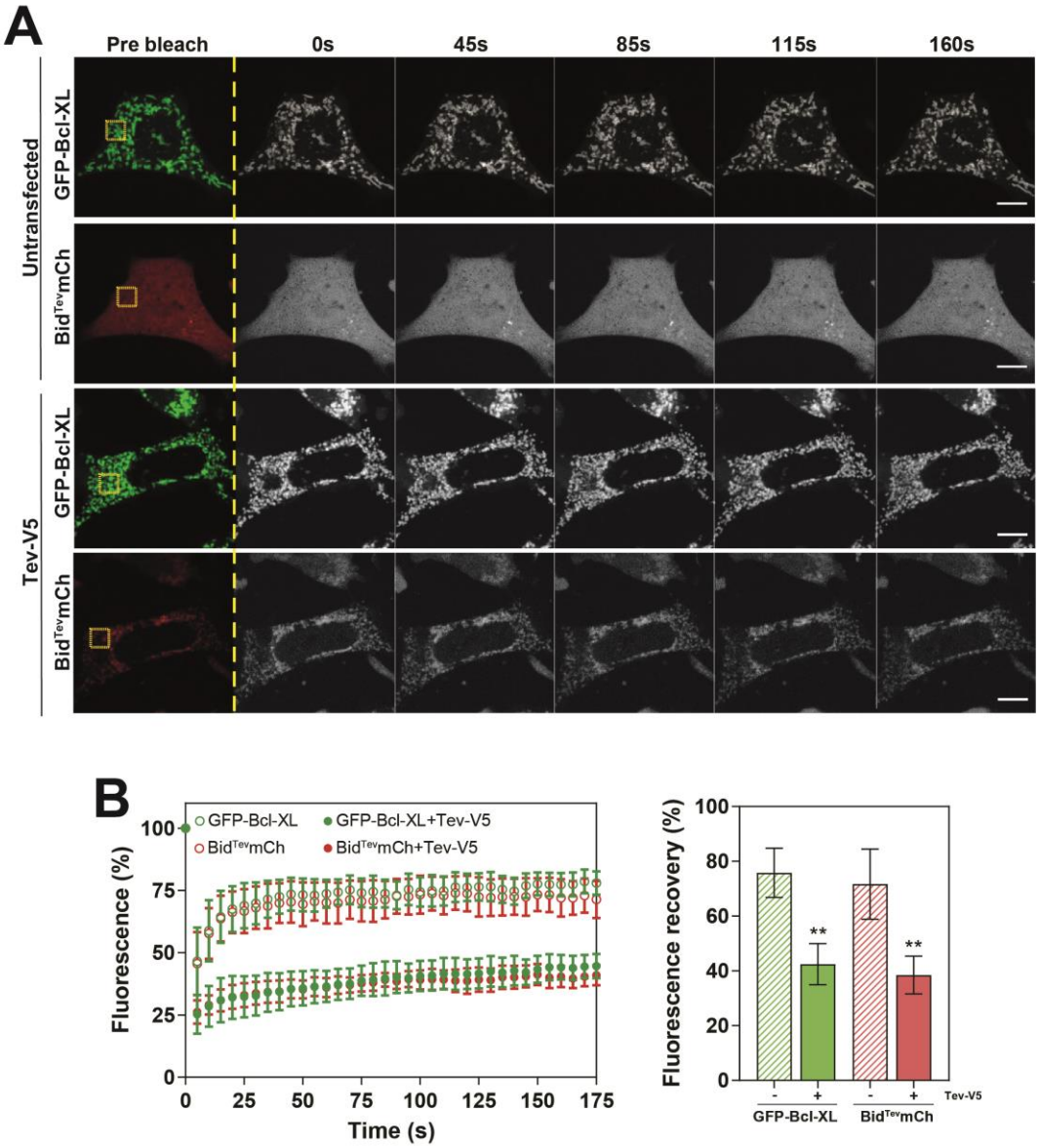

Figure 4.2. Bcl-XL dynamics can be used as a readout of pro-apoptotic Bid activity
A. DKO MEFs stably expressing Bid^{Tev}mCh-GFP-Bcl-XL were untransfected or transfected with Tev-V5 and FRAP carried out on both Bcl-XL and Bid^{Tev}mCh. Cells were photobleached within the yellow ROI and imaged every 5s.
B. Data from A averaged and plotted.
C. Non-linear regression on the average fluorescence recovery was carried out from data in B. Data represents values from 3 independent experiments. n=50 cells per condition. Error bars represent standard deviation and data was analysed via ANOVA.** = $p<0.01$. Scale bars represent 10µm.

inducible form of Bad (BadER^{Tam}) which was also expressed in equal ratios with Bcl-XL but remained inactive in the absence of 4-OHT as the HBD is bound to Hsp90. Thus, when 4-OHT was added, Bad should activate, bind to Bcl-XL and stabilise it at the OMM in a relatively short timeframe. DKO MEFs that had previously been infected with the BadER^{Tam}-GFP-Bcl-XL virus were tested for expression via Western blot and immunofluorescence. Western blot analysis showed GFP-Bcl-XL and BadER^{Tam} at the correct molecular weights in the stable cell line, and were not present in the DKO MEFs (Fig. 4.3B). Immunofluorescence identified that stable cells had cytosolic BadER^{Tam} via staining against ER and GFP-Bcl-XL was localised between mitochondria and cytosol (Fig. 4.3C). After 1 hour of 4-OHT treatment there was a noticeable increase in mitochondrial Bcl-XL and BadER^{Tam}. We next examined any changes in Bcl-XL dynamics in live cells via FRAP. FRAP was carried out in BadER^{Tam}-GFP-Bcl-XL DKO MEFs both before and after 4-OHT treatment (Fig. 4.3C). Activation of Bad via 4-OHT significantly decreased the level of recovery of Bcl-XL fluorescence on mitochondria and increased the length of time for fluorescence recovery (Fig. 4.3D). Together these data suggest that the change in Bcl-XL dynamics can be used as a readout of Bad activation, in real time.

We next wanted to determine if the change in localisation and FRAP dynamics of Bcl-XL upon Bad activation directly related to mitochondrial priming. To test this, MCF10As were selected for infection as apoptosis could be induced in these cells due to the presence of Bax and Bak, and as MCF10As do not express the oestrogen receptor, the use of 4-OHT should not have any effect other than activation of BadER^{Tam}. MCF10As infected with the BadER^{Tam}-GFP-Bcl-XL vector were selected via FACS (data not shown). Successful expression was tested via immunofluorescence against GFP and ER, and via Western blot. Western blot analysis showed expression of both GFP-Bcl-XL and BadER^{Tam} at the correct molecular weight after blotting against GFP and ER (Fig. 4.4A). Both Bcl-XL and BadER^{Tam} became more mitochondrial after 4-OHT treatment when viewed via immunofluorescence (Fig. 4.4B). FRAP was also carried out to confirm similar changes in Bcl-XL translocation rates after Bad activation. To ensure any changes in dynamics measured was due to activation of Bad rather than an artefact of 4-OHT treatment, WT MCF10A cells were transiently transfected with either GFP-Bcl-XL or BadER^{Tam}-GFP-Bcl-XL and dynamics measured in the absence and presence of 4-OHT (Fig. 4.4C). In the transient cells, 4-OHT had no effect on Bcl-XL dynamics (Fig. 4.4D). In the BadER^{Tam}-GFP-Bcl-XL cells, treatment with 4-OHT caused a

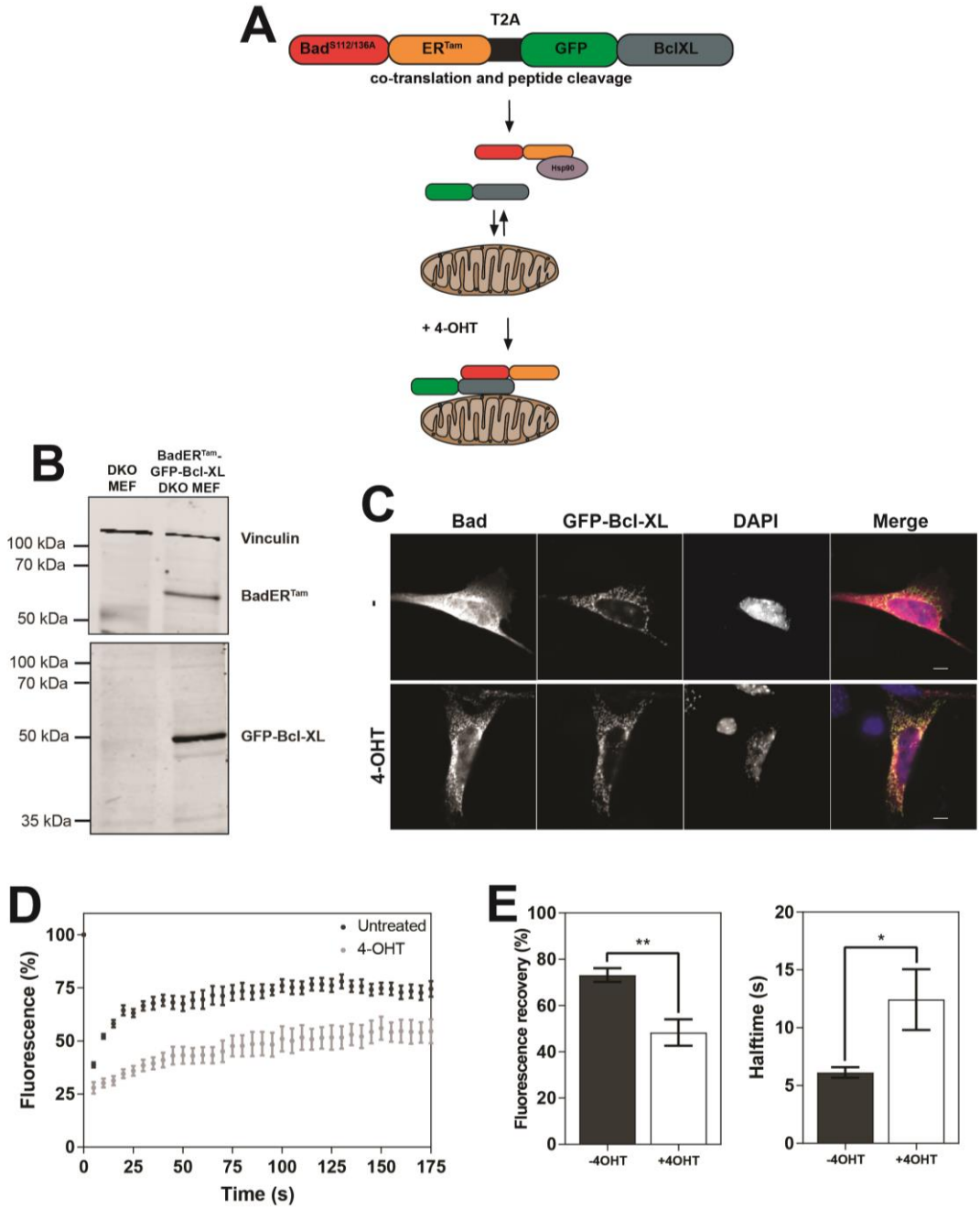

Figure 4.3. Bcl-XL dynamics can be used as a readout of pro-apoptotic Bad activity

A. Schematic of the BadER^{Tam}-GFP-Bcl-XL system. BadER^{Tam} and GFP-Bcl-XL are post-translationally cleaved at the T2A site giving equimolar expression of each protein. BadER^{Tam} is inactive until 4-OHT treatment which causes binding of the two proteins and localisation at the OMM.

B. Western blot of DKO MEF and BadER^{Tam}-GFP-Bcl-XL DKO MEF lysates. Membranes were probed for Bad and GFP. Vinculin was used as a loading control.

C. Immunofluorescence of stable BadER^{Tam}-GFP-Bcl-XL MEFs in both untreated and 4-OHT treated cells. 4-OHT treatment increases both Bcl-XL and Bad co-localisation. Scale bar represents 10µm.

D. The stable DKO MEF line was subject to FRAP in the absence and presence of 4-OHT. Images were taken every 5s and plotted.

E. Non-linear regression was carried out and the average fluorescence recovery and halftime calculated from data in D. Values represent data from 3 independent experiments. Error bars represent standard deviation and data was analysed via T-test.* = $p<0.05$; ** = $p<0.01$.

significant decrease in Bcl-XL dynamics compared to untreated cells, with Bcl-XL appearing more mitochondrial. This demonstrated successful creation of a cell line in which Bad can be activated rapidly to prime cells, which can be quantified via measurement of GFP-Bcl-XL FRAP dynamics.

As activation and binding of BH3 proteins is a dynamic process which can be reversed upon removal of a pro-apoptotic stimulus, we wanted to test whether this could be achieved with the BadER^{Tam}-GFP-Bcl-XL MCF10A cells. To test this, an assay was set up in which the BadER^{Tam}-GFP-Bcl-XL MCF10A cells were subjected to FRAP analysis then treated with either EtOH (Fig. 4.5A) or 4-OHT (Fig.4.5B) for 24 hours. After this 24-hour incubation, EtOH and 4-OHT were washed out and another round of FRAP immediately carried out (day 1) (Fig. 4.5C). 48 hours later, FRAP was again carried out (day 3), and then again 72 hours later (day 6). EtOH was used as a vehicle control. Cells were re-plated after day 3 to prevent them becoming over-confluent. The average recovery in fluorescence was calculated each day for both conditions. EtOH-treated cells showed no difference in Bcl-XL FRAP recovery throughout the course of the experiment. Cells treated with 4-OHT showed highly reduced Bcl-XL dynamics immediately after the initial 4-OHT washout, which subsequently increased 48 hours later, and further increased back to untreated levels by day 6. This demonstrated that the change in Bcl-XL dynamics induced by 4-OHT treatment is a reversible process that can be reverted to normal levels by removing the Bad-activating stimulus.

To confirm that the change in Bcl-XL dynamics observed after 4-OHT treatment was due to the activation of Bad binding to Bcl-XL and thus was causing increased mitochondrial priming, an apoptosis assay was carried out. BadER^{Tam}-GFP-Bcl-XL MCF10A cells were treated with either DMSO or Etoposide in the absence or presence of 4-OHT and apoptosis analysed via immunofluorescence. Etoposide is a topoisomerase II inhibitor that induces DNA damage by inhibiting the repair of DNA double strand breaks created by topoisomerase II during the unwinding of DNA during replication[305]. Etoposide-treated cells accumulate at the G2/M phase of the cell cycle, mediated by p53[306]. Upon failure of DNA repair, Bcl-2 family proteins like Puma and Noxa are upregulated to initiate apoptosis. We hypothesised that treatment of Etoposide would cause binding of Noxa and Puma to Bcl-XL, and that activation of Bad via 4-OHT treatment would displace Noxa and Puma from Bcl-XL

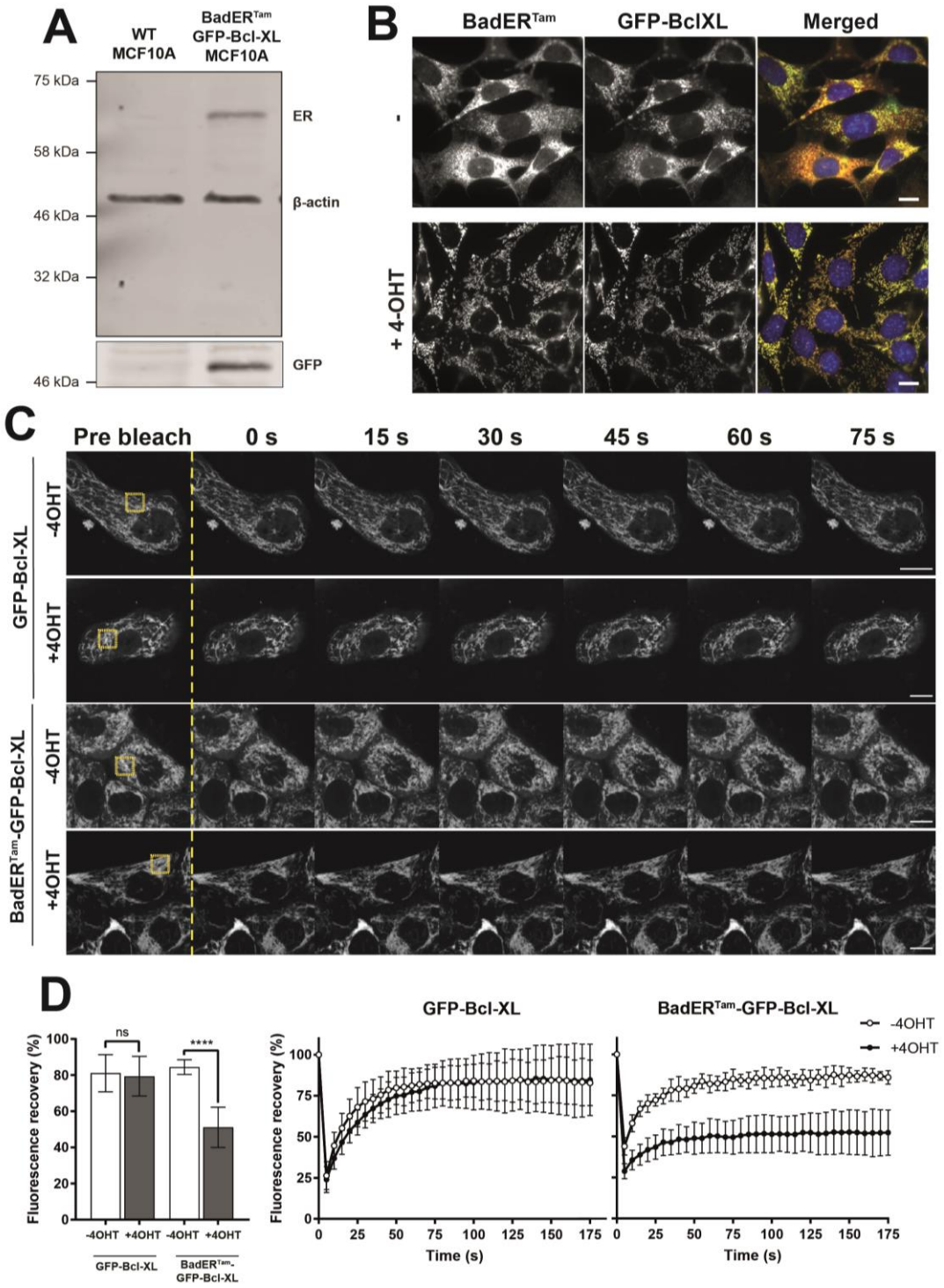

Figure 4.4. Creation of a BadER^{Tam}-GFP-Bcl-XL MCF10A cell line

A. Western blot of WT and BadER^{Tam}-GFP-Bcl-XL MCF10A cell lysates show expression of both ER^{Tam} and GFP-Bcl-XL at the correct molecular weights in the infected cells only, but not in WT MCF10A. β-actin was used as a loading control.

B. Immunofluorescence of cells in A both untreated and treated with 4-OHT stained for GFP and ER. Scale bar represents 10µm

C. Representative images of FRAP carried out on MCF10As expressing either GFP-Bcl-XL or GFP-Bcl-XL-BadER^{Tam} treated with 4-OHT. Cells were bleached within the yellow ROI and fluorescence measured every 5s. Scale bars represent 10µm.

D. Non-linear regression was carried out and average fluorescence recovery plotted. Only the BadER^{Tam} cell line was affected by 4-OHT treatment. Values represent data from 2 independent experiments. Error bars represent SD and data was analysed via ANOVA. **** = p<0.001.

to induce apoptosis. Cells treated with either DMSO or a combination of DMSO and Etoposide showed minimal apoptosis (Fig. 4.5D). Treatment with Etoposide alone caused a slight increase in apoptosis levels which was significantly increased in the presence of 4-OHT. This suggested that activation of Bad alone primes cells but does not induce apoptosis, and that the pro-apoptotic effects of Etoposide are mostly inhibited by the over-expression of Bcl-XL binding to activated BH3 proteins like Puma or Noxa. We would therefore hypothesise Bad activation with 4-OHT causes it to bind to Bcl-XL, displacing Puma or Noxa to kill the cells. These data suggest that inducing Bad in this system causes an increase in mitochondrial priming, which can be measured via a change in Bcl-XL FRAP dynamics.

Finally, to try to use this inducible system to directly measure competition between BH3 proteins, we aimed to create a cell line that contained both the inducible BadER^{Tam} and a more rapidly activated Bid^{Tev}. A Doxycycline-inducible Bid^{Tev}mCh system was previously created by Robert Pedley by cloning the Tev protease into the multiple cloning site of a pCDH-TRE3GS-MCS-EF1α-tagBFP-T2A-TetOn3G vector (generously gifted by Stuart Cain). This would allow a more rapid induction of Bid cleavage compared to transient transfection. Stable BadER^{Tam}-GFP-Bcl-XL MCF10A cells had previously been transduced with the Bid^{Tev}mCh-GFP-Bcl-XL vector and the tagBFP-TetOn-Tev protease vector, and positively infected cells sorted for both mCherry and tagBFP expression (data not shown). To test whether Doxycycline treatment induced cleavage of Bid, the BadER^{Tam}-GFP-Bcl-XL-Bid^{Tev}-mCherry-TetOn-Tev cells (herein referred to as BBT MCF10As) were treated with 0.3µM Doxycycline for 24 hours before lysing cells and carrying out a Western blot to assay Tev induction. Probing for Bid revealed equal expression of endogenous hBid between WT and BBT MCF10As, and the presence of Bid^{Tev}mCh in the BBT MCF10A lysate (Fig. 4.6A). A lower molecular weight band was also present at the appropriate molecular weight for cleaved Bid^{Tev} in the BBT MCF10A lysate, suggesting treatment with Doxycycline induces Tev-mediated Bid^{Tev} cleavage.

We next set up a concentration gradient of Doxycyline treatment to determine the appropriate concentration to use for maximal Bid^{Tev} cleavage. BBT cells were treated with a range of concentrations of Doxycycline for 24 hours, lysed and Western blot analysis carried out (Fig. 4.6B). No Tev-V5 expression was visible in untreated cells, or cells treated with up to 1ng/ml Doxycycline. Cell treated with

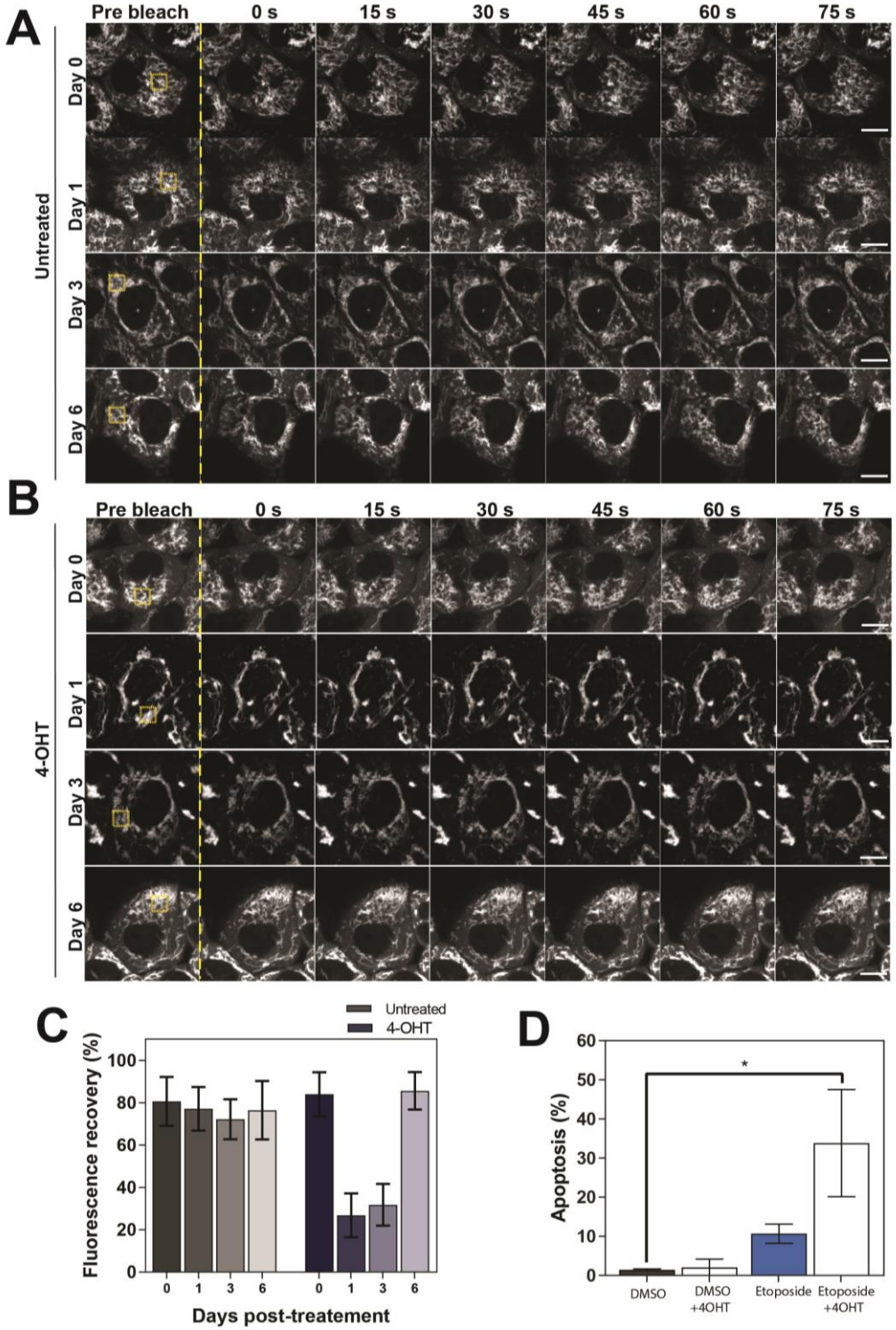

Figure 4.5. Activation of BadER^{Tam} reversibly increases mitochondrial priming

A. BadER^{Tam}-GFP-Bcl-XL MCF10A cells were subjected to FRAP (day 0) before being treated with EtOH for 24 hours. Treatment was washed out and a second round of FRAP was carried out immediately afterwards (day 1). Subsequent FRAP was performed 3 days and 6 days post-washout. The ROI within the yellow box was photobleached for 5ms and recovery in fluorescence measured every 5s.

B. Cells underwent the same analysis as in A except they were treated with 4-OHT instead of EtOH.

C. The average recovery in fluorescence for cells in A and B was calculated for each condition and plotted. Values represent 60 cells per condition. Error bars represent SD.

D. BadER^{Tam}-GFP-Bcl-XL MCF10A cells were treated with combinations of 4-OHT and/or Etoposide for 24 hours and apoptosis quantified via immunofluorescence. Values represent data from 3 independent experiments, analysed via ANOVA. Error bars represent SD. * = $p<0.05$

10ng/ml or greater showed clear Tev-V5 expression, which did not increase with increasing concentration. Cells were also treated for 48 hours before lysing and Western blotting to determine if a longer treatment time caused increased Tev-V5 expression levels (Fig. 4.6C). Treatment time did not appear to affect the levels of Tev-V5 expression. To confirm that expression of Tev-V5 induced Bid activation and therefore increased mitochondrial localisation, BBT cells were treated with a range of concentrations of Doxycycline before fixation and staining against GFP and mCherry (Fig. 4.6D). Bid^{Tev}mCh was mainly cytosolic in the majority of cells imaged, regardless of Doxycycline treatment. The localisation of Bcl-XL also did not differ after treatment with Doxycycline. This suggested that, whilst Tev-V5 expression was being induced after Doxycycline treatment, the activation of Bid was not occurring effectively across all cells. Further optimisation of the system is needed before it can be used in competition assays, but this was not possible within the timeframe of this thesis.

4.3 Bad and tBid are in competition for binding to Bcl-XL

Treating the BadER^{Tam}-GFP-Bcl-XL cell line with Etoposide suggested that competition between BH3 proteins was occurring, as Etoposide treatment induced a significant amount of apoptosis only when BadER^{Tam} had been activated. This suggested displacement of direct activators Puma and Noxa from Bcl-XL, as proteins that bind more strongly to Bcl-XL will outcompete weaker ones. Stronger binding implies that the association of protein-protein interactions occurs rapidly whereas dissociation is slow[307], thus displacing a protein-protein interaction will cause a measurable shift in the displaced protein's kinetics. We wanted to examine competition between BH3 proteins in more detail. To do this we began by examining if competition existed between BadER^{Tam} and tBid; if tBid binds more strongly to Bcl-XL than BadER^{Tam}, this can be measured via a change in tBid-mCh FRAP dynamics (Fig. 4.7A). DKO MEFs stably expressing BadER^{Tam}-GFP-Bcl-XL were used for this assay to prevent expression of pro-apoptotic BH3 proteins from killing the cells. DKO MEFs were transfected with tBid-mCh, and FRAP analysis carried out in the absence or presence of 4-OHT. FRAP of Bcl-XL showed that tBid significantly lowered Bcl-XL dynamics compared to tBid2AmCh (Fig. 4.7B). The addition of 4-OHT did not affect this stabilisation. tBidmCh FRAP was also significantly lower than tBid2AmCh (Fig. 4.7C). The addition of 4-OHT increased the levels of mobile tBid

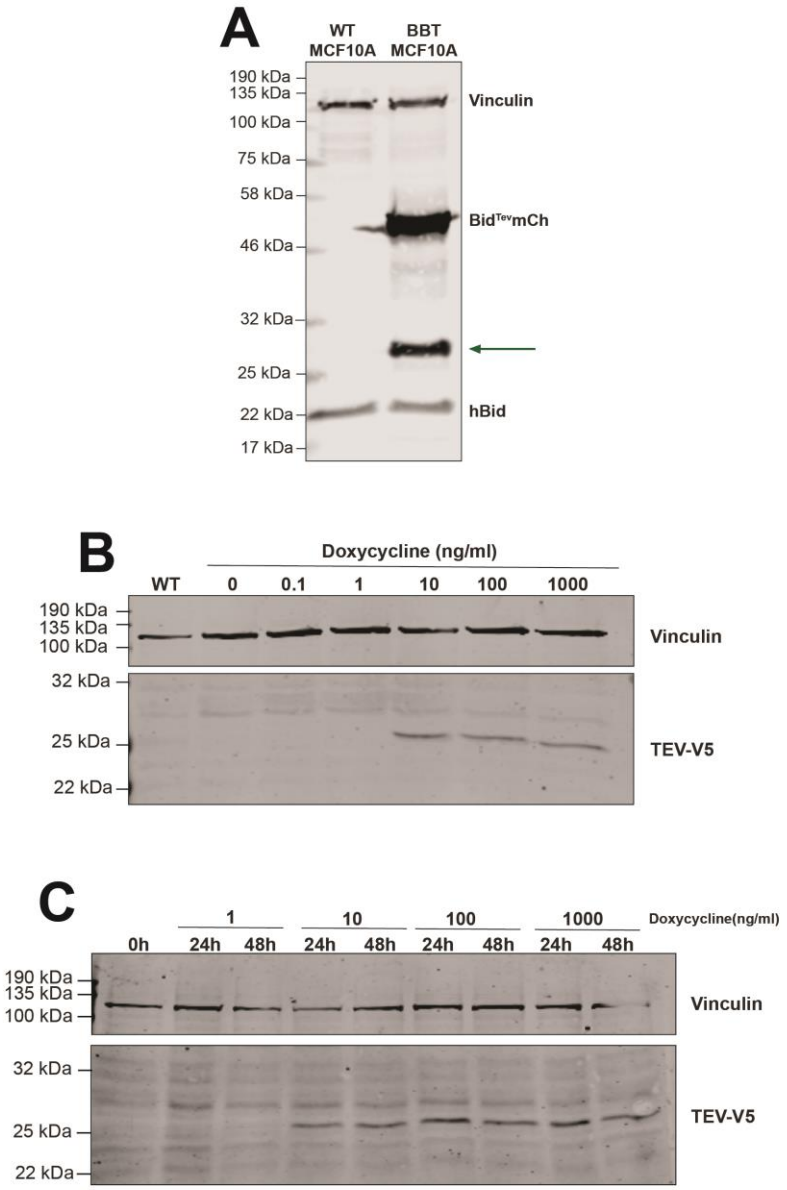

Figure legend on next page.

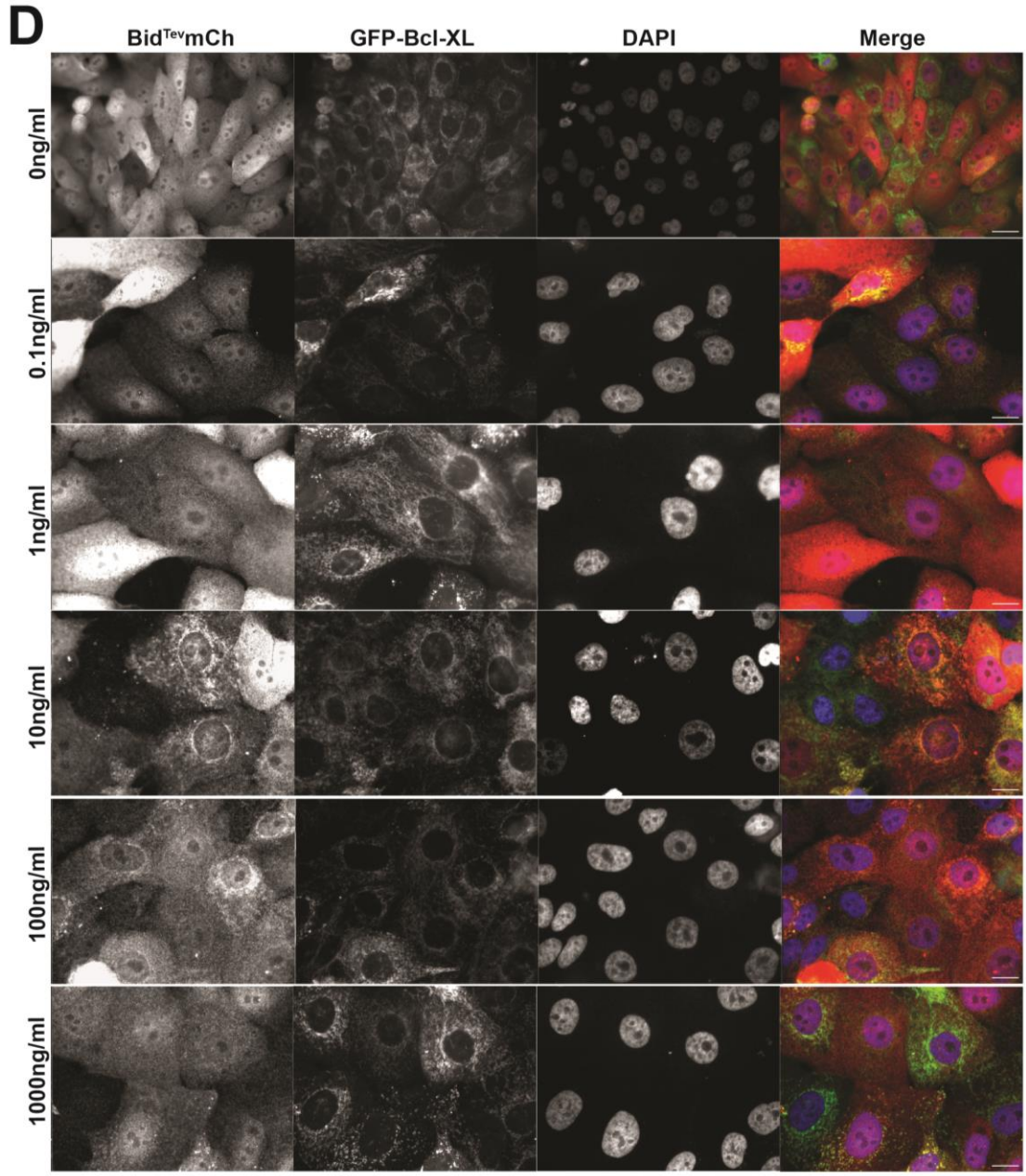

Figure 4.6. Creation of a double inducible BadER^{Tam} Bid^{Tev}mCh GFP-Bcl-XL MCF10A cell line

A. Western blot of WT and BBT MCF10A cell lysates treated with Doxycycline for 24 hours and probed for Bid. Endogenous hBid is present in both lanes. FL and cleaved Bid^{Tev}mCh (green arrow) are present in the BBT MCF10A cell lysate. Vinculin was used as a loading control.

B. Western blot of BBT MCF10A cells treated with increasing concentrations of Doxycycline and probed for the V5 tag. Tev-V5 is present from 10ng/ml Doxycycline upwards. Vinculin was used as a loading control.

C. Western blot of BBT MCF10A cells treated with increasing concentrations of Doxycycline for 24 or 48 hours and probed for the V5 tag. As in B, Tev-V5 is present from 10ng/ml Doxycycline upwards and levels are not increased after 48 hours of incubation compared to 24 hours. Vinculin was used as a loading control.

D. Immunofluorescence of BBT MCF10A cells treated with increasing concentrations of Doxycycline for 24 hours before fixation. Cells were stained against mCherry, GFP and DAPI. Scale bar represents 20µm.

mCh, although not significantly, but this level of fluorescence was also no longer significantly different to tBid2AmCh. This suggested that there may be competition for binding between Bad and tBid, with Bad potentially having a higher affinity for Bcl-XL than tBid.

To try and confirm this observation with more controlled expression levels, FRAP analysis was also performed in the MCF10A cells stably expressing BadER^{Tam}-GFP-Bcl-XL. Cells transiently expressing tBid-mCh were analysed via FRAP both without and with 4-OHT treatment. Bcl-XL was significantly stabilised at the OMM in the presence of tBid-mCh or 4-OHT to equal levels (Fig. 4.8A). There did appear to be a slight increase in stability of GFP-Bcl-XL in the presence of both tBid-mCh and 4-OHT although this was not significant. Due to GFP-Bcl-XL stable expression within this cell line, FRAP measurements of the mCherry BH3 proteins alone could not be carried out, but there was no difference in tBid-mCh dynamics in the absence or presence of 4-OHT (Fig. 4.8B). In cells expressing mCh-Bad, Bcl-XL was more stable upon activation of BadER^{Tam} than in the presence of mChBad, and GFP-Bcl-XL dynamics were unchanged in the presence of both (Fig. 4.8C). As with tBid-mCh, mCh-Bad dynamics were unchanged in the presence of active BadER^{Tam} (Fig. 4.8D). It is interesting to note that the addition of 4-OHT in the DKO MEF line transiently expressing tBidmCh had no effect on GFP-Bcl-XL dynamics, whereas in the MCF10A cell line there appeared to be a cumulative effect. This suggests that the Bcl-XL in the DKO MEFs is saturated with BH3 proteins and thus Bcl-XL dynamics cannot decrease further. These cells would potentially undergo apoptosis in the presence of Bax or Bak. In the MCF10A line, Bcl-XL may not be saturated and therefore the further decrease in dynamics in the presence of Bad is visible. Together this data suggests that alterations in either GFP-Bcl-XL or mCh-BH3 protein dynamics upon competition for binding are perhaps relatively subtle and as such they cannot be measured accurately via FRAP.

As FRAP was not a sensitive enough method, we aimed to asses competition via fluorescence cross-correlation spectroscopy (FCCS). FCCS measures the cross-correlation of two fluorescently tagged proteins by measuring fluctuations in fluorescence levels of both fluorophores within a confocal volume over time[308]. Whenever GFP and mCherry pass through the confocal volume, individually or simultaneously, the fluorescence is measured, and the correlation calculated. This

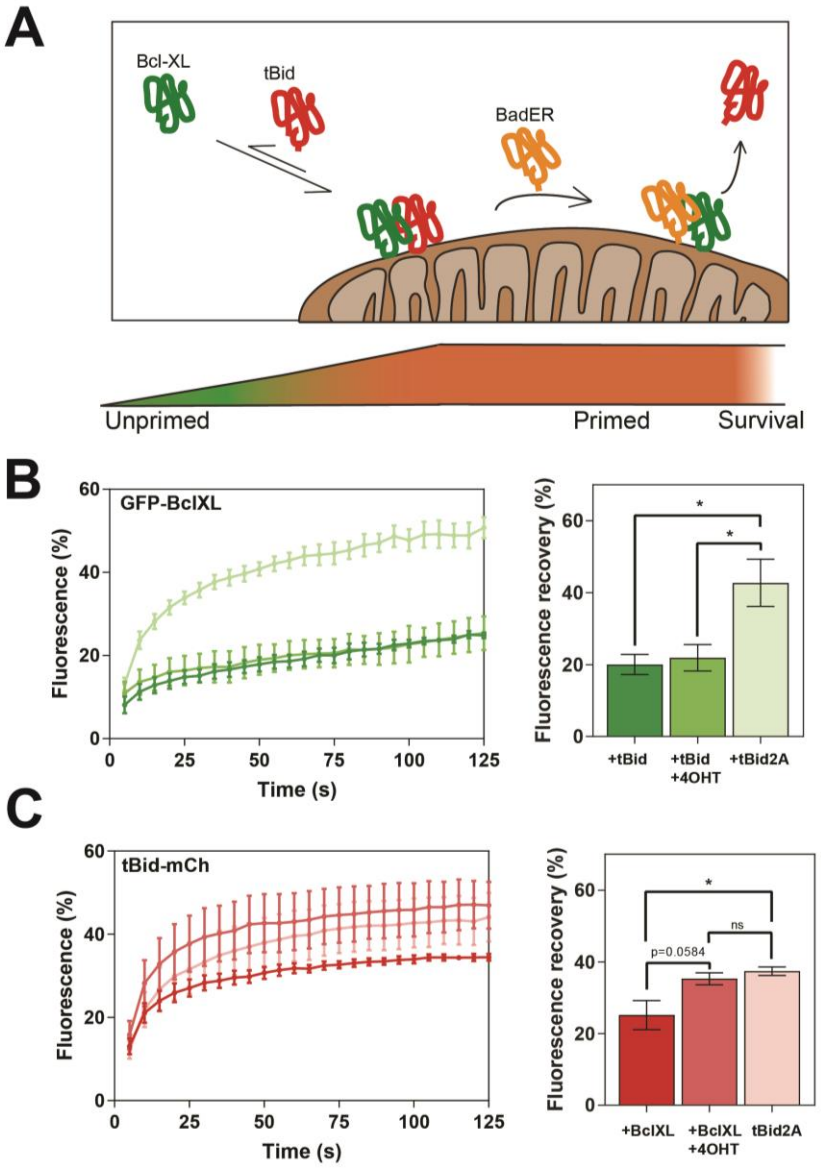

Figure 4.7. Bad competes with tBid for binding to Bcl-XL

A. Schematic of the experimental setup. tBid stabilises Bcl-XL at the OMM. If Bad has a higher affinity for Bcl-XL than tBid, activation of BadER^{Tam} would displace tBid from Bcl-XL and increase the levels of mobile tBid within the cell.

B. Results from FRAP analysis of Bid^{Tev}mCh-GFP-Bcl-XL DKO MEF cells. Curves were plotted and non-linear regression used to calculate the average GFP fluorescence recovery.

C. mCherry FRAP data from the same experiment, analysed as in B. Values represent data from 3 independent experiments, n=30 cells per condition, and error bars represent SD. Data was analysed via ANOVA. * = $p<0.05$.

technique is more sensitive for measuring protein-protein interactions than FRAP as it uses much lower excitation power and therefore requires much lower expression levels of the fluorophores, and so can be used to quantify absolute concentrations of proteins within cells. The BadER^{Tam}-GFP-Bcl-XL MCF10A cell line was transfected with expression vectors containing either mCherry tBid, Bad or Bim, or the non-binding 2A mutants of each. Vectors containing either GFP or a GFP-mCherry fusion were used as negative and positive controls, respectively. The average relative cross amplitude (RCA) values calculated from individual cell measurements showed a high cross-correlation in cells expressing the GFP-mCherry fusion, and a very low RCA value in cells expressing just GFP (Fig. 4.8D). Cells expressing either tBid, Bim or Bad all demonstrated high levels of cross-correlation with GFP-Bcl-XL, similar to the positive GFP-mCherry control, suggesting a high level of binding between Bcl-XL and the BH3 proteins. All three 2A mutants had considerably lower RCA values. Upon treatment with 4-OHT, the RCA values of mCherry-tBid, Bim and Bad were greatly reduced, suggesting that activated BadER^{Tam} was displacing the mCherry-BH3 proteins from GFP-Bcl-XL. Therefore, in using more sensitive live cell microscopy techniques like FCCS, displacement of BH3 proteins for anti-apoptotic Bcl-2 proteins can be measured, and thus binding competition can be assessed.

4.4 Breast cancer cells are more readily primed than normal breast cells

Studies have demonstrated that various cancer cells are dependent on specific Bcl-2 proteins for survival (e.g. Bcl-2 in CLL[58] and SCLC[59], or Mcl-1 in breast and lung cancers[227]) and as such are inherently more mitochondrially primed than normal, healthy cells[217]. BH3 mimetics were developed to model the interactions of BH3 proteins with the specific anti-apoptotic proteins that cancer cells are dependent on, with the aim of displacing the endogenous BH3 proteins to allow them to activate the pore formers and kill the cells. This assumes that the mimetics interact with the targeted anti-apoptotic proteins via the same mechanism as the endogenous proteins, and with the same, if not higher, affinities. As demonstrated, binding competition between Bcl-2 family proteins can be measured using live cell fluorescence microscopy, therefore examining Bcl-2 protein dynamics in the presence of mimetics could give insight into the specifics of these interactions. Before carrying out competition assays using BH3-mimetics we wanted to confirm

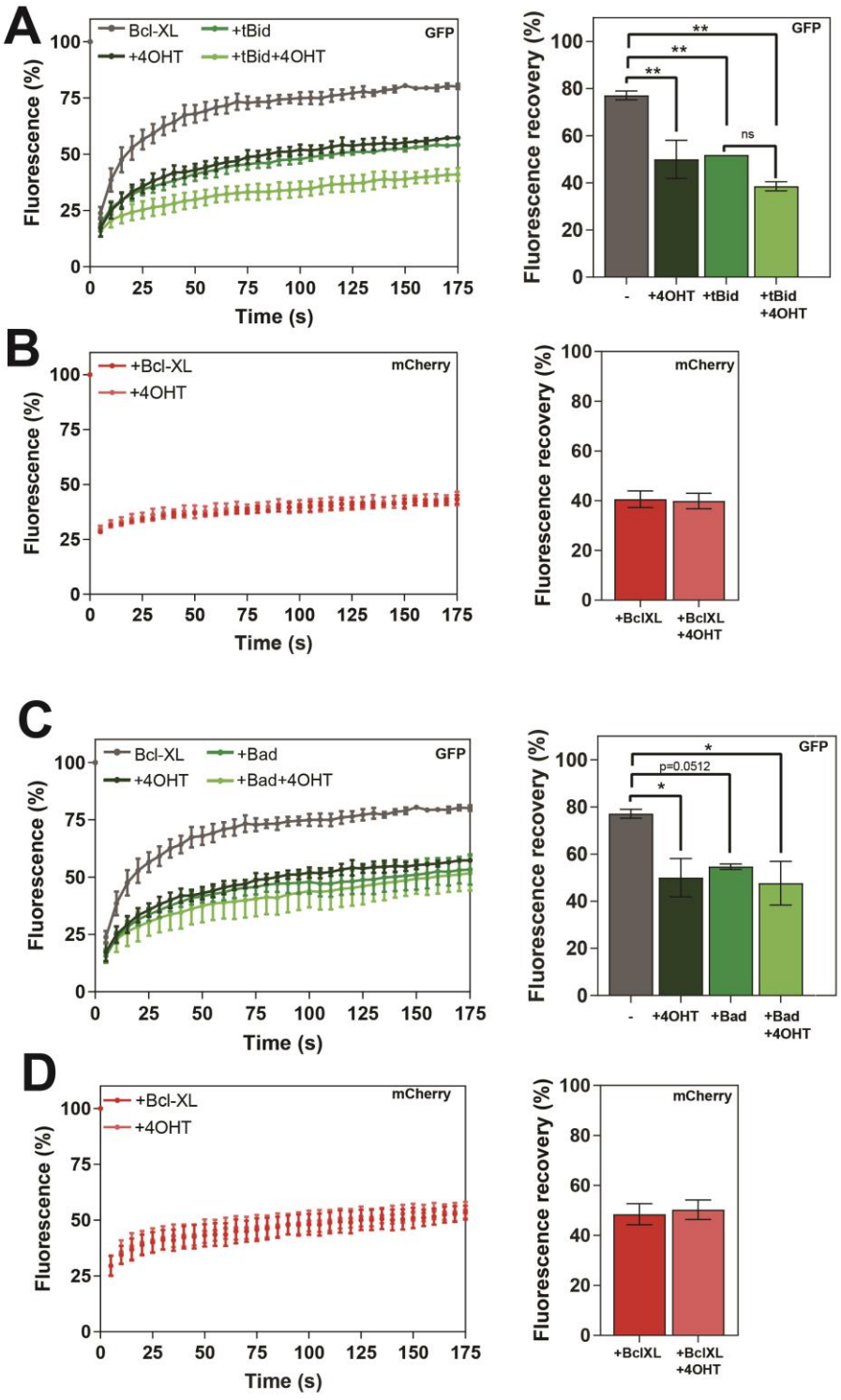

Figure legend on next page.

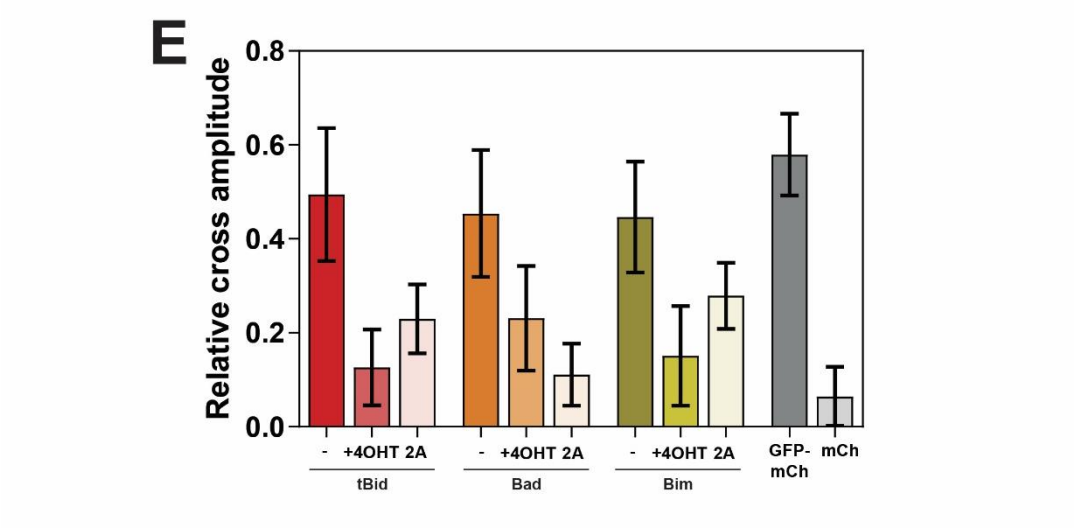

Figure 4.8. Bad can displace pro-apoptotic BH3 proteins from Bcl-XL

A. GFP-Bcl-XL-BadER^{Tam} MCF10A cells were transiently transfected with tBidmCh and FRAP carried out on GFP-Bcl-XL in the absence and presence of 4-OHT. Average fluorescence recovery curves were plotted and average fluorescence recovery calculated via non-linear regression.

B. FRAP was also carried out on tBid-mCh in the same cells as in A and analysed as above.

C. Within the same experiment as in A. cells were also transfected with mChBad and the same FRAP analysis carried out on GFP-Bcl-XL. A and C are shown as separate graphs for clarity.

D. FRAP was also carried out on mCh-Bad in the same cells as in C and analysed as above. B and D are shown as separate graphs for clarity. Values represent data from 2 independent experiments and error bars represent SD. All data was analysed via ANOVA. * = $p<0.05$; ** = $p< 0.01$.

E. FCCS analysis was carried out on GFP-Bcl-XL-BadER^{Tam} MCF10A cells transiently expressing mCherry-tagged tBid, Bad or Bim in the absence and presence of 4-OHT. The 2A mutants of each mCherry-BH3 protein were also analysed. Either mCherry or a GFP-mCherry fusion were also subject to FCCS analysis as controls. Data represents values from 30-60 cells per condition.

that the different mimetics being used were specifically inhibiting the correct anti-apoptotic proteins.

We began by testing the function of a panel of BH3-mimetics in Bcl-2-protein-dependent cancer cells lines – S63845 (Mcl-1 inhibitor), ABT-199 (Bcl-2 inhibitor), WEHI-539 (Bcl-XL inhibitor) and ABT-737 (Bcl-2, Bcl-XL and Bcl-W inhibitor). A recent study by Soderquist and colleagues determined the Bcl-2-dependency of a large panel of cell lines from a range of tissues and cancers by inhibiting specific Bcl-2 proteins individually or in combination with BH3-mimetics[309]. Among the panel of cell lines tested, SK-BR-3 cells were shown to be Mcl-1-dependent, and MDA-MB-231 cells were Bcl-XL- and to a degree, Mcl-1-dependent, as levels of apoptosis were high when these specific proteins were inhibited in these cell lines (Fig 4.9A). We wanted to assess whether we could recapitulate these results. Both cell lines were exposed to the panel of BH3-mimetics targeting different combinations of Bcl-2 proteins for 24 hours before quantifying levels of apoptosis via immunofluorescence. In agreement with the study, SK-BR-3 cells showed significantly higher levels of apoptosis in the presence of S63845 compared to DMSO treated cells (Fig. 4.9B). Levels of apoptosis were not increased upon inhibiting Bcl-2 proteins other than Mcl-1. This suggested that SK-BR-3 cells are dependent on Mcl-1 for survival, and the S63845 inhibitor is Mcl-1 specific. MDA-MB-231 cells, were not significantly affected when any individual Bcl-2 protein was targeted (Fig. 4.9C). Large levels of apoptosis occurred when both Bcl-XL and Mcl-1 were inhibited in combination using either S63845 and WEHI-539, or when treated with ABT-737 plus S63845. This suggested that MDA-MB-231 cells are dependent on both Bcl-XL and Mcl-1 for survival. This differs slightly from the Soderquist study, as in their assays, inhibition of Bcl-XL alone was sufficient to induce apoptosis in MDA-MB-231 cells, but also suggested that the mimetics were specifically inhibiting the correct proteins. Given that our assay used higher concentrations of each mimetic for a shorter timeframe, this could account for the slight differences in levels of apoptosis measured between our assay and theirs.

To examine whether competition between BH3 proteins and BH3-mimetics occurs in normal or cancer cell lines, we wanted to create inducible BadER^{Tam}-GFP-Bcl-XL cancer cell lines to measure competition via changes in Bcl-XL FRAP dynamics. Three breast cancer cell lines were selected to represent different subtypes of

A

	Bcl-2	Bcl-XL	Mcl-1	Bcl-2 Bcl-XL	Bcl-2 Mcl-1	Bcl-XL Mcl-1	Bcl-2 Bcl-XL Mcl-1
SK-BR-3	-	-	+	-	+	+	+
MDA-MB-231	-	+	-/+	+	-/+	+	+

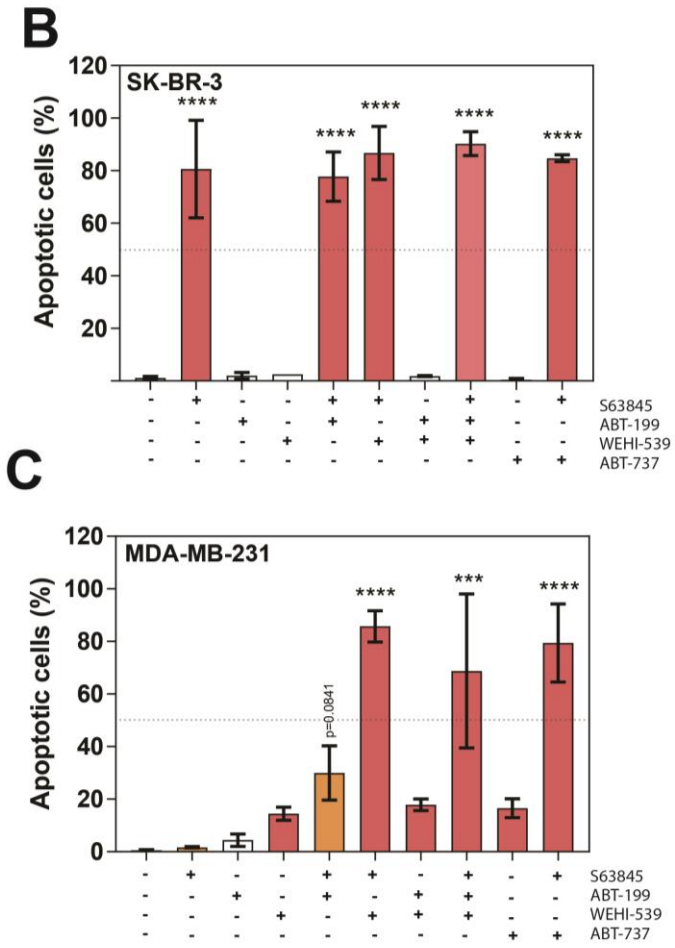

Figure 4.9. SK-BR-3 and MDA-MD-231 cells show specific Bcl-2 protein dependency
A. Predicted Bcl-2 protein dependencies of SK-BR-3 and MDA-MB-231 cell lines based on a BH3-mimetics screen from Soderquist et al, with dependence defined as over 50% of cells undergoing apoptosis after BH3-mimetic treatment. + indicates dependence; - indicates non-dependence; -/+ indicates partial dependence.
B. Levels of apoptosis in SK-BR-3 cells induced by various combinations of BH3-mimetics, measured via immunofluorescence. Individual bar colours indicate predicted outcome based on the study in A. and the dotted line indicates a 50% apoptosis cut-off of sensitivity.
C. Levels of apoptosis in MDA-MB-231 cells assayed as in B. Values represent data from 3 independent experiments and error bars represent SD. All data was measure via ANOVA compared to DMSO treated cells. *** = p<0.005; **** = p<0.001.

breast cancer; MCF-7 (ER^+, $Her2^-$), BT-474 (ER^+, $Her2^+$) and MDA-MB-231 (ER^-, $Her2^-$) and stable $BadER^{Tam}$-GFP-BclXL lines created. Expression was confirmed via immunofluorescence (Fig. 4.10A) and Western blot (Fig. 4.10B). FRAP was carried out on each cancer cell line and MCF10As in the absence and presence of 4-OHT. All cell lines showed a significant decrease in Bcl-XL dynamics in the presence of 4-OHT compared to untreated cells (Fig. 4.10C). Whilst there was no significant difference in levels of priming pre-4OHT treatment, after $BadER^{Tam}$ activation both the MDA-MB-231 and MCF-7 cells showed a significantly lower proportion of mobile Bcl-XL compared to MCF10As. This demonstrates that breast cancer cell lines are more mitochondrially primed than normal cells, which can be measured using our inducible $BadER^{Tam}$ system.

4.5 ABT-737 does not recapitulate the binding of full-length Bad to Bcl-XL

After confirming the specific targeting of the BH3-mimetics and creating cancer cell lines containing the inducible $BadER^{Tam}$-GFP-Bcl-XL system, we next wanted to examine the effect of the Bad mimetic, ABT-737 on GFP-Bcl-XL in live cells to determine whether it alters Bcl-XL dynamics in the same way as full-length Bad. To test this, an assay was used in which $BadER^{Tam}$-GFP-Bcl-XL MDA-MB-231 cells were treated with combinations of 4-OHT and/or ABT-737. If ABT-737 does indeed act in a similar manner to full-length Bad, addition of ABT-737 should displace the $BadER^{Tam}$ from Bcl-XL (Fig. 4.11A). To ensure 4-OHT treatment did not affect MDA-MB-231 cells outside of activating $BadER^{Tam}$, WT MDA-MB-231 cells were transfected with GFP-Bcl-XL and FRAP carried out in the absence and presence of 4-OHT (Fig. 4.11B). MDA-MB-231 cells do not contain the oestrogen receptor and therefore should not be affected by 4-OHT treatment. Indeed, 4-OHT treatment had no effect on Bcl-XL FRAP dynamics in the WT cell line.

We began by first measuring levels of apoptosis in the $BadER^{Tam}$-GFP-Bcl-XL MDA-MB-231 cells with either drugs alone, or in the presence of transiently transfected tBid-mCh (Fig. 4.11C). In the absence of tBid, 4-OHT treatment did not induce any apoptosis. ABT-737 alone induced a significant amount of apoptosis, which was not significantly increased upon activation of $BadER^{Tam}$. Expression of tBid-mCh caused levels of apoptosis comparable to ABT-737 and 4-OHT. The addition of 4-OHT

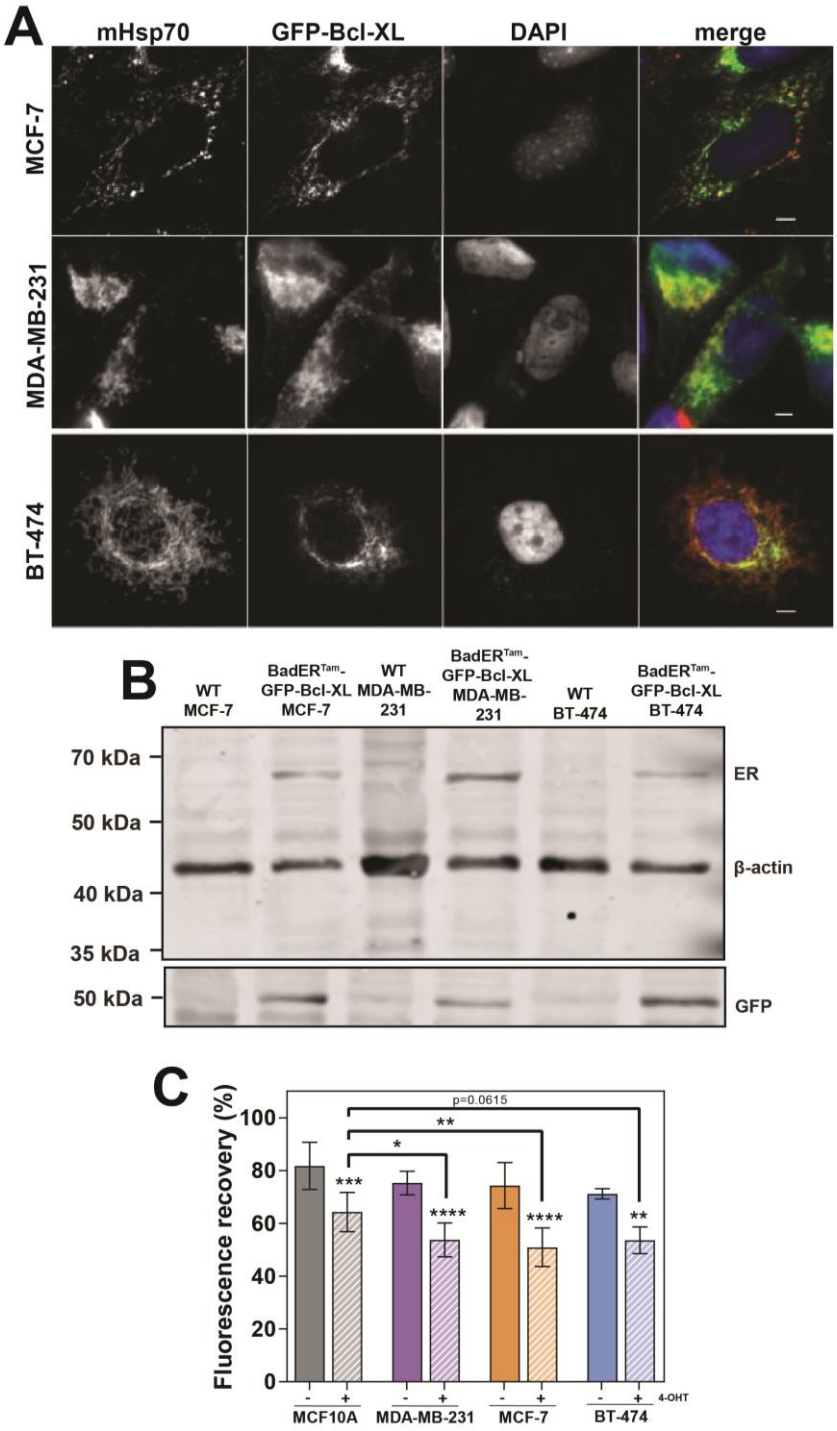

Figure 4.10. Breast cancer cell lines are more primed than MCF10As

A. Immunofluorescence of stable BadER^{Tam}-GFP-Bcl-XL breast cancer cell lines demonstrating successful lentiviral infection. Cells were stained against GFP, mHsp70 and DAPI. Scale bar represents 10µm.

B. Western blot of cell lysates from A showing expression of both ER^{Tam} and GFP-Bcl-XL at the correct molecular weights in the infected cells, but not in WT counterparts. β-actin was used as a loading control.

C. Stable cell lines were subjected to FRAP in the absence and presence of 4-OHT and average fluorescence recovery calculated. All lines showed significantly altered Bcl-XL dynamics in the presence of 4-OHT compared to untreated. MDA-MB-231 and MCF-7 lines were significantly more primed post-4-OHT treatment compared to MCF10As. Values represent data from 4 independent experiments, n=100 cells per condition. Error bars represent SD and data was analysed via ANOVA. * = p<0.05; ** = p<0.01; *** = p<0.005; **** = p<0.001.

further increased levels of apoptosis, suggesting that BadER^{Tam} was displacing tBid from Bcl-XL to induce apoptosis. ABT-737 also increased levels of apoptosis in the presence of tBid, suggesting that it too could displace tBid from Bcl-XL. The addition of both 4-OHT and ABT-737 did not increase levels of apoptosis further, which could imply that all of the Bcl-XL in the cells is saturated for binding. We next carried out FRAP analysis in the presence of 4-OHT and ABT-737 to determine if we could measure changes in Bcl-XL dynamics in the presence of ABT-737, or competition between ABT-737 and BadER^{Tam} in live cells. Bcl-XL dynamics were significantly reduced in the presence of 4-OHT alone, but surprisingly, ABT-737 alone had no significant effect on Bcl-XL dynamics compared to untreated cells (Fig. 4.11D). Treatment with a combination of both 4-OHT and ABT-737 did not alter dynamics compared to 4-OHT treatment alone. This suggested that ABT-737 was not stabilising Bcl-XL at the OMM and therefore potentially not interacting with Bcl-XL via the same mechanism as full-length Bad in live cells.

We wanted to confirm whether this observation was also true in the non-cancerous BadER^{Tam}-GFP-Bcl-XL MCF10A cell line. As with the MDA-MB-231 line, we began by measuring apoptosis levels in the absence and presence of tBidmCh. In the absence of tBidmCh, treatment with either 4-OHT or ABT-737 alone or in combination did not induce apoptosis (Fig. 4.12A). This would be expected as MCF10A cells are not known to be dependent on any specific Bcl-2 proteins for survival. Whilst tBid-mCh transfection induced a significant level of apoptosis, the addition of 4-OHT or ABT-737 did not significantly increase this further. This agrees with previous competition data suggesting that MCF10As are less primed than MDA-MB-231s and therefore addition of 4-OHT or ABT-737 does not fully saturate Bcl-XL. FRAP analysis revealed similar results to the MDA-MB-231 cell line, with ABT-737 having no effect on Bcl-XL dynamics (Fig. 4.12B). Together these data suggest that ABT-737 can compete with full-length BH3 proteins like Bad and tBid for binding to Bcl-XL, but ABT-737 does not bind to Bcl-XL via the same mechanism as full-length proteins as FRAP dynamics are not altered.

4.6 Discussion

The concept of mitochondrial priming and activation of apoptosis is based upon models of competition between Bcl-2 family proteins sequestering anti-apoptotic

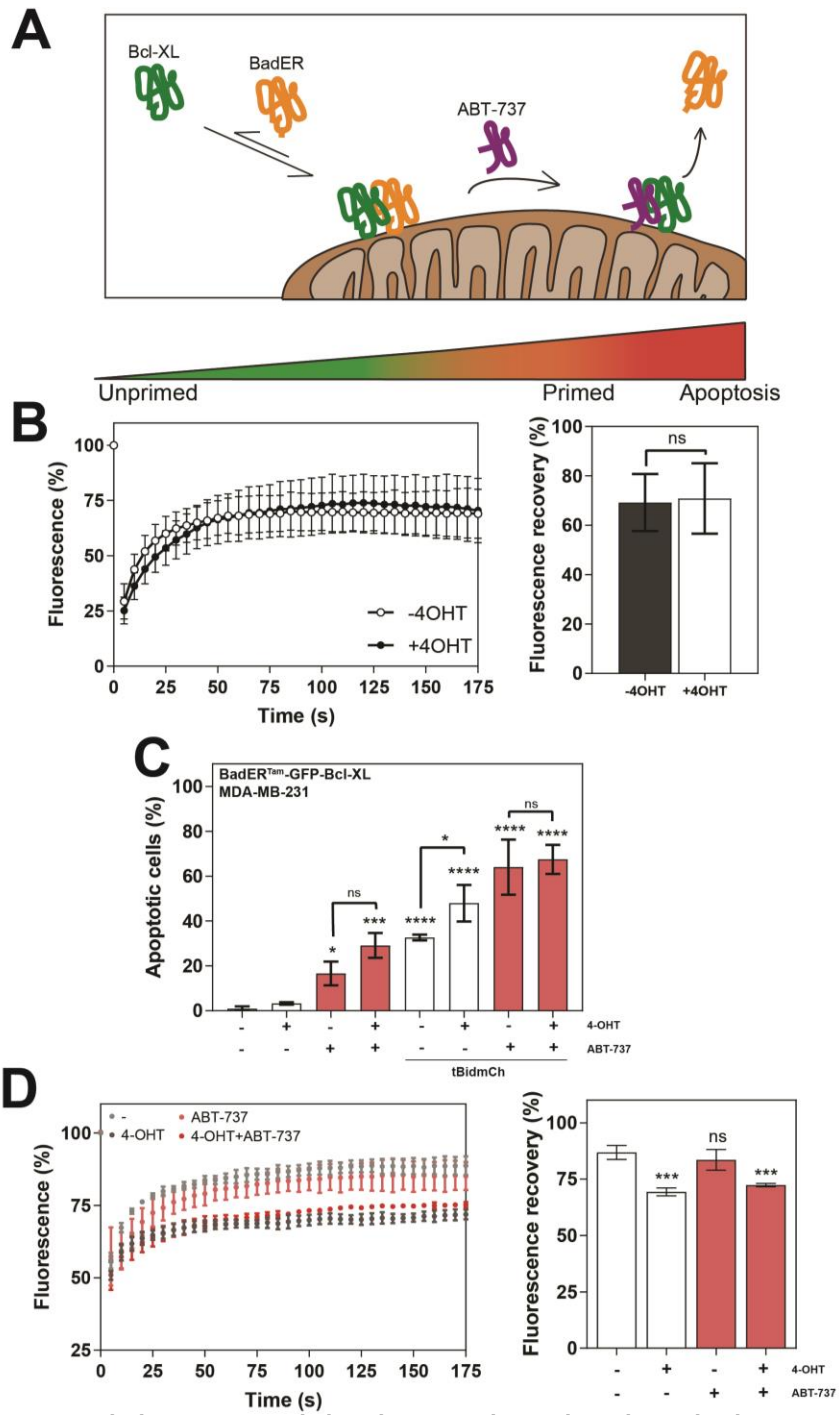

Figure 4.11 ABT-737 induces apoptosis but does not alter Bcl-XL dynamics in MDA-MB-231 cells

A. Schematic of the experimental setup. Activated BadER^{Tam} stabilises Bcl-XL at the OMM. If ABT-737 has a higher affinity for Bcl-XL than BadER^{Tam}, treatment with ABT-737 would displace BadER^{Tam} from Bcl-XL, maintaining Bcl-XL localisation at the OMM and freeing up BadER^{Tam} to induce apoptosis.

B. FRAP analysis was carried out on WT MDA-MB-231 cells transiently transfected with GFP-Bcl-XL in the absence and presence of 4-OHT and fluorescence recovery data was plotted. The average fluorescence recovery was calculated via non-linear regression curve fitting. Data was analysed using a Student's t-test and error bars represent SD.

C. Levels of apoptosis in GFP-Bcl-XL-BadER^{Tam} MDA-MB-231 cells induced by combinations of 4-OHT, ABT-737 and tBid-mCh, measured via immunofluorescence. Values represent data from 3 independent experiments and error bars represent SD.

D. FRAP analysis of BadER^{Tam}-GFP-Bcl-XL MDA-MB-231 cells treated with combinations of 4-OHT and ABT-737. Average fluorescence recovery curves were plotted, and average fluorescence recovery calculated via non-linear regression. All data was measured via ANOVA compared to DMSO treated cells unless otherwise indicated and error bars represent SD. *=p<0.05; *** = p<0.005; **** = p<0.001.

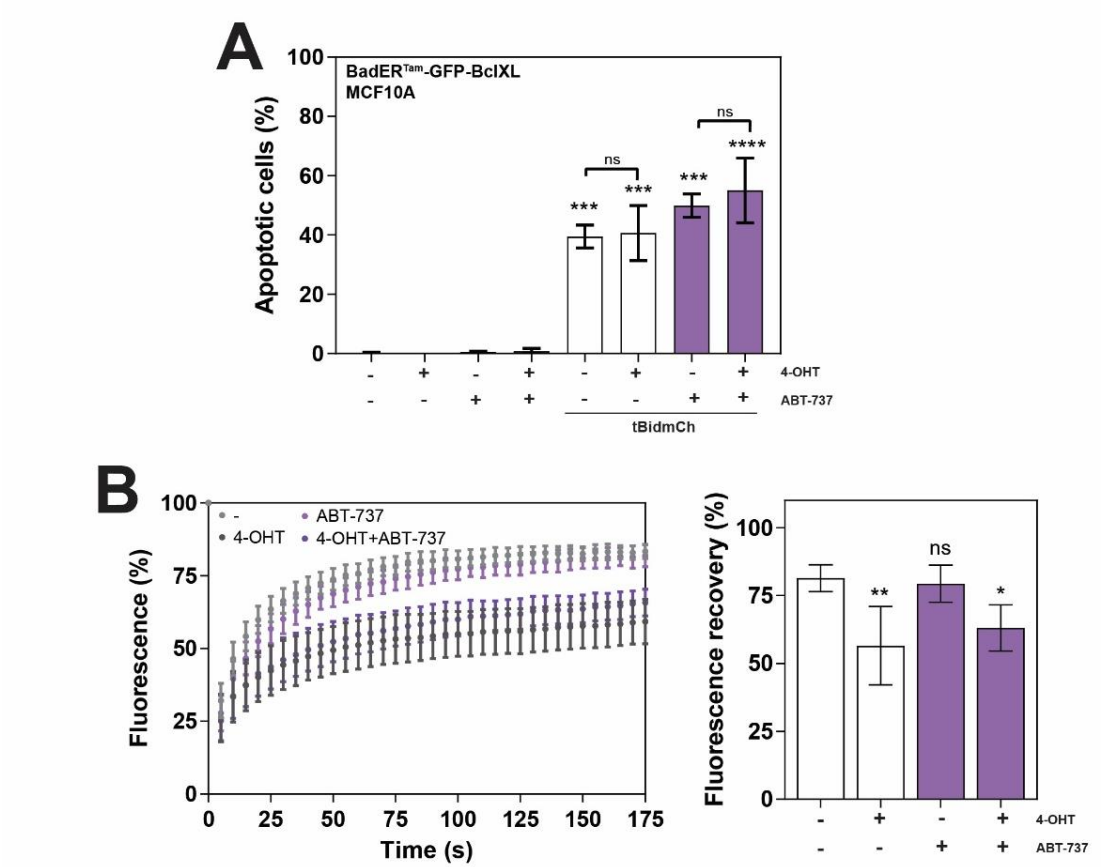

Figure 4.12. Mitochondrial priming in MCF10A cells is not significantly affected by ABT-737 treatment

A. Levels of apoptosis in BadER^{Tam}-GFP-Bcl-XL MCF10A cells induced by combinations of 4-OHT, ABT-737 and tBid-mCh, measured via immunofluorescence. Values represent data from 3 independent experiments and error bars represent SD.

B. FRAP analysis of BadER^{Tam}-GFP-Bcl-XL MCF10A cells treated with combinations of 4-OHT and ABT-737. Average fluorescence recovery curves were plotted, and average fluorescence recovery calculated via non-linear regression. All data was measured via ANOVA compared to DMSO treated cells and error bars represent SD. *=p<0.05; ** = p<0.01; *** = p<0.005; **** = p<0.001.

proteins to free up direct activator BH3 proteins. Treatment of cancer cells with BH3-mimetics assumes that the mimetics work by fully recapitulating the interactions of the endogenous BH3 proteins they were designed to mimic. To fully understand the specifics of these interaction, examining the interactions of full-length proteins in comparison to BH3-mimetics in live cells is required. We therefore wished to determine whether FRAP could be used to assay these interactions in live cells over relatively short timeframes. To this end we developed two inducible mitochondrial priming systems based on the mitopriming assays developed by Lopez and colleagues[297] that allowed activation of a sensitiser or activator BH3 protein via two distinct methods. Activation of tBid via Tev-V5 transfection allowed measurement of both Bcl-XL and tBid dynamics, and demonstrated that, upon activation, both proteins bind and stabilise each other at the OMM. The long transfection timeframe, however, made measurements of competition between Bcl-2 proteins difficult. The BadER^{Tam} system allowed measurement of competition for Bcl-XL binding between different BH3 proteins, and induction of Bad was capable over a much shorter timeframe, which could be reversed after washing out 4-OHT. This not only allowed measurement of the same cells both before and after BadER^{Tam} activation, but due to the lack of fluorophore on the BadER^{Tam}, competition with other BH3 proteins could be measured. Both Bid^{Tev}mCh and BadER^{Tam} being expressed at equal ratios to Bcl-XL also ensured activation of the proteins would not kill the cells, but induce priming whilst avoiding apoptosis.

Understanding if, and how, competition exists between BH3 proteins for binding Bcl-2 proteins is important to understand as apoptotic induction by BH3 mimetics is based upon this principle. Inducing apoptosis in the BadER^{Tam}-GFP-Bcl-XL MCF10A cells using Etoposide demonstrated that activation of Bad significantly increased levels of apoptosis compared to Etoposide alone. This suggested that BadER^{Tam} could compete with activated BH3 proteins like Puma or Noxa for binding to Bcl-XL. It would be interesting to measure levels of Puma and Noxa in these cells after Etoposide treatment and compare the localisation of these proteins before and after 4-OHT treatment to visualise this competition. Examining these interactions in live cells would also confirm this hypothesis.

FRAP analysis of competition between tBid and Bad for binding to Bcl-XL appeared to show that both proteins were relatively similar in their binding affinities for Bcl-XL,

although tBid did seem to be displaced from Bcl-XL by BadER^{Tam} in DKO MEFs. This would agree with the current apoptosis activation model that sensitiser BH3 proteins can displace the direct activators from anti-apoptotic proteins. FRAP of the stable BadER^{Tam}-GFP-Bcl-XL MCF10A cell line showed no competition between tBid or Bad with BadER^{Tam}. It was interesting to note that, although not significant, GFP-Bcl-XL dynamics did appear slower in the presence of both tBid and 4-OHT, suggesting that not all of the free Bcl-XL had been saturated with BH3 proteins when either 4-OHT or tBid were present individually. One caveat of this particular experimental setup is the lack of control over levels of tBid- or Bad-mCh expression in comparison to Bcl-XL. Due to transient transfection of tBid-mCh, higher expression of tBid compared to Bcl-XL/BadER^{Tam} could mask measurement of competition between the proteins. As FRAP analysis of competition appeared not to be sensitive enough to measure the more subtle changes in dynamics of Bcl-2 proteins, we utilised the more sensitive FCCS to measure changes in binding in MCF10A cells. FCCS demonstrated much more clearly competition between BadER^{Tam} for mCherry-tagged BH3 proteins via a decrease in RCA values between Bcl-XL and all the mCherry proteins assayed. FCCS measurements are more accurate at lower expression levels and cross-correlation measurements are taken over a more precise confocal volume. It would be interesting to use FCCS to examine interactions between BH3 proteins and other anti-apoptotic proteins, or to determine if cancer cells show distinct Bcl-2 protein binding affinities compared to WT cells.

Certain cancer cells types are inherently more mitochondrially primed than normal cells due to their dependency on specific anti-apoptotic Bcl-2 proteins for survival[217]. Using the inducible BadER^{Tam}-GFP-Bcl-XL system in multiple cancer cell lines revealed that, upon sequestration of Bcl-XL after 4-OHT treatment, both MDA-MB-231 and MCF-7 cells were significantly more primed than the MCF10A line. This would therefore agree with this theory as neutralising Bcl-XL overexpression with BadER^{Tam} activation reveals this apoptotic pressure. A number of studies have analysed Bcl-2 family protein expression in cancer cell lines, for example, studies using immunohistochemistry and microarrays suggest that MDA-MB-231 cells overexpress Bcl-2[310], Bcl-XL, Bax, and Bim[311]. A more recent study by Soderquist and colleagues examined Bcl-2 protein dependency across a large panel of cancer cell lines and primary samples via measuring response to BH3 mimetics[309]. Results showed that inhibition of Mcl-1 with A-1210477 was enough to induce significant cell

death. This agreed with our results using S63845 as the Mcl-1 inhibitor. MDA-MB-231 cells were predicted to be susceptible to Bcl-XL inhibition alone as treatment with WEHI-539 was sufficient to induce significant apoptosis, whereas Mcl-1 inhibition by A-1210477 induced moderate levels of apoptosis. Whilst our results show that MDA-MB-231 cells are relatively resistant to inhibition of individual Bcl-2 proteins, inhibiting both Mcl-1 and Bcl-XL induced significant apoptosis. It is important to note that the experimental setup in terms of treatment times and concentrations differs here, which could contribute to differences observed between results.

Although ABT-737 was designed to target Bcl-2, Bcl-XL and Bcl-W, it had no effect on the mitochondrial translocation rate of Bcl-XL in either BadER^{Tam}-GFP-Bcl-XL MCF10A and MDA-MB-231 cells. BadER^{Tam}-GFP-Bcl-XL MCF10As were unaffected by ABT-737 in terms of both apoptosis and Bcl-XL FRAP dynamics. MCF10As are a non-cancerous cell line and as such are not dependent on a specific individual or set of Bcl-2 proteins for survival. FRAP analysis of different cell lines demonstrated that MCF10As are inherently less primed than cancer cells, and thus BH3 mimetics would not necessarily be expected to have any significant effect on mitochondrial priming. Recent studies in Bcl-XL-dependent HCCT116 p21$^{-/-}$ cells demonstrated that treatment with WEHI-539 was much more effective in cells expressing lower levels of Bcl-XL compared to those which overexpressed Bcl-XL[212]. The same group also showed that derepression of Bcl-XL by both WEHI-539 and ABT-737 is more effective when Bcl-XL is not bound to the OMM. This could potentially explain the lack of change in FRAP dynamics in the both cell lines. However, ABT-737 still induced apoptosis in the MDA-MB-231 cells, suggesting it could prime cells. A number of susceptible cells may have undergone apoptosis before FRAP was carried out, and thus the remaining cells would be less susceptible to treatment, however the fact that there was no difference in Bcl-XL dynamics in any of the cells measured implies that a different binding mechanism is the more likely cause.

Live cell studies have also demonstrated that not all pro-apoptotic BH3 proteins bind to anti-apoptotic proteins via the same mechanism; Bim is resistant to displacement from Bcl-XL and Bcl-2 by ABT-263 due to interacting at two distinct binding sites[262]. Furthermore, both WEHI-539 and ABT-737 are ineffective at displacing Puma from Bcl-XL[297]. In our FRAP studies, if full-length Bad can alter Bcl-XL FRAP dynamics

but ABT-737 cannot, this also suggests that ABT-737 is not fully recapitulating the binding mechanism of endogenous BH3 proteins. This therefore warrants the question; what is different in the binding mechanism of ABT-737 compared to full-length Bad? The activation of endogenous Bad is a complex process, with its phosphorylation regulated by a range of different kinases from different signalling cascades[312]. Endogenous Bad also has a rapid turnover rate, and studies have demonstrated that ABT-737 treatment increases levels of Bad in a range of human cell lines due to a decrease in this high turnover rate[313]. Bad has been shown to be inherently unfolded in cells and contains two regulatory PEST sequences, which could play a role in its rapid turnover. How the 3D conformation of Bad is altered when bound to Bcl-XL or when localised at the OMM is not well studied, but if ABT-737 does not fully recapitulate binding and therefore does not alter the 3D structure or phosphorylation status of Bad, its binding mechanism may be different. It is possible that the interaction between ABT-737 and Bcl-XL does not involve the BH3 binding groove, but a distinct site elsewhere in the protein like the alternative binding domain found in Bim for binding to Bcl-XL[262]. Binding at this alternative site could prevent endogenous Bad binding but not alter Bcl-XL FRAP kinetics like endogenous, full-length Bad. It is also important to note that ABT-737 also interacts with Bcl-2 and Bcl-W, and could therefore be binding to these proteins with higher affinity in these experiments. Analysing the effect of more specific Bcl-XL inhibitors such as WEH1-539 on Bcl-XL FRAP dynamics would help determine if this is the case. Whilst there was not enough time within the scope of this thesis, it would also be interesting to use FCCS to determine whether ABT-737 or other BH3-mimetics have any measurable effect on Bcl-XL binding to BH3 proteins, and whether cross-correlation in the presence of BH3-mimetics differs between mitochondria and cytosol.

5. Single-cell heterogeneity in Bcl-XL dynamics predicts apoptotic outcome

5.1 Introduction

Analysing differences in Bcl-2 protein dynamics in live cells has so far given insight into variation in dynamics between individual proteins and demonstrated subtle differences in the hierarchy of binding that can be measured. However, analysing average population dynamics alone does not give a complete picture of how Bcl-2 proteins regulate apoptosis. Apoptotic sensitivity at a single cell level can vary hugely within a population of cells, and this is not necessarily due to genetic differences between cells. For example, cancer cells do not all respond in the same manner to anti-mitotic drug treatment, with some undergoing apoptosis and others escaping mitotic arrest and surviving (termed slippage)[314]. Even when separated into clonal populations, cells within each subclone show varied apoptotic responses. High throughput analysis of multiple cancer cell lines in response to a range of anti-mitotics demonstrated that subclonal populations of cells all have complex cell fate profiles that cannot be explained by genetic differences between cells[315]. In this example, the variations in apoptotic outcome observed appeared to be due to variations in levels of cyclin B1 during mitosis.

Further examples of non-genetic apoptotic heterogeneity have also been observed in non-cancerous cell lines. For example, a study by Flusberg and colleagues demonstrated that a population of MCF10A cells have an inherent equilibrium in apoptotic sensitivity[264]. Cells that survive treatment of a dose of TRAIL that kills approximately 80% of the population exhibit only a transient resistance to subsequent treatments, after which time the 20% survival rate re-establishes itself. This again implies the variation in apoptotic response is regulated by non-genetic factors. Other studies from the Sorger laboratory showed that non-genetic cell-to-cell variability in the apoptotic outcome of cells in response to TRAIL can be explained, at least partly, by variation in protein levels[316]. This includes Bcl-2 family proteins, the expression levels of which became more divergent as time post-cell division increased. This divergence may be a result of differing growth rates or noise in gene expression between individual cells. Mathematical modelling approaches

have been applied to identify causes of heterogeneity in apoptotic response within patient samples and between different cell types[317]. This also led to the conclusion that variations in protein expression levels were the cause, with HeLa cells showing a more robust resistance to fluctuations in levels of apoptotic regulators such as procaspases, XIAP and APAF-1, than cancer cell lines.

Apoptotic outcome is not the only source of heterogeneity present in the apoptosis pathway. The time between receipt of an apoptotic signal like TRAIL and the initiation of MOMP can also vary considerably between cells, ranging from timespans of hours to days until caspase-8 activation occurs[5,318]. This heterogeneity is controlled by variations in Bcl-2 protein interactions and pore formation dynamics of Bax and Bak between cells[319]. Fast cellular imaging techniques combined with mathematical modelling have shown that variations in the onset time of MOMP is due to differences in the diffusion-adsorption rates and production kinetics of MOMP inducers, as well as variation in pore formation kinetics, induced by both intrinsic and extrinsic signals[320].

Therefore, several interesting questions about the role of Bcl-2 proteins in regulating apoptosis at a single cell level remain unanswered: what is causing cell-to-cell variations in levels of Bcl-2 family proteins? What is setting the equilibrium for survival versus death? What differs in the interactions of Bcl-2 proteins between cells that survive in the lead up to apoptosis, compared to those which die? When Bcl-XL is at the OMM it is exerting its anti-apoptotic function, therefore, what is regulating the proportion of Bcl-XL that is located at the OMM? In order to answer some of these questions, we aimed to examine potential causes of cell-to-cell variation by measuring Bcl-2 protein dynamics at a single cell level. We have shown that the mobile fraction of Bcl-XL and other anti-apoptotic proteins decreases in the presence of pro-apoptotic BH3 proteins measured via FRAP. We therefore wished to examine whether these changes in dynamics occur homogeneously between cells within a population using this technique, and try to determine causes of heterogeneity in apoptotic outcome that regulate Bcl-2 proteins.

5.2 Variation in Bcl-XL dynamics is an inherent property of cell populations

Previous studies have shown that within a cell population, there is considerable heterogeneity in the time taken to initiate MOMP, and in the apoptotic outcome between individual cells[264,315–317]. Throughout all of the FRAP and photoactivation experiments carried out previously in this thesis it was noticed that there was significant cell-to-cell variation in Bcl-2 protein dynamics within each experiment, with some cells showing much faster moving GFP-Bcl-XL than others. Some example FRAP data from BadER^{Tam}-GFP-Bcl-XL MCF10A cells either untreated or treated with 4-OHT is shown in Fig. 5.1. GFP-Bcl-XL FRAP plots show a large variation in Bcl-XL dynamics in both untreated and treated cells (Fig. 5.1A). Analysing the average mobile fraction of Bcl-XL in individual cells reveals significant overlap between untreated and treated cells, with a large proportion fitting both a primed and unprimed profile (Fig 5.1B).

We wanted to determine whether this variation was an inherent property of the cell populations and not an artefact of differing levels of expression of Bcl-XL or variations in the gene insertion during the transduction of the cells. To examine this, the BadER^{Tam}-GFP-Bcl-XL MCF10A cells were plated as single cells and ten individual clonal populations expanded. Expression levels of GFP were tested via flow cytometry (Fig. 5.2A) and Bcl-XL expression probed via Western blot (Fig. 5.2B). Both methods revealed very similar levels of expression between each clonal population, suggesting variation in expression levels was unlikely to be the cause of variation.

FRAP analysis of each clonal population was carried out to examine whether the same level of variation in Bcl-XL dynamics is present in comparison to the mixed population of cells (Fig. 5.3A). Plotting of FRAP data showed that in all cell populations, treatment with 4-OHT significantly decreased Bcl-XL dynamics (Fig. 5.3B). All clonal populations also had similar levels of priming both before and after 4-OHT treatment in comparison to the mixed population. Interestingly, analysis of the cell-to-cell variability in Bcl-XL dynamics also revealed similar levels of heterogeneity in the clonal populations compared to the mixed population (Fig.

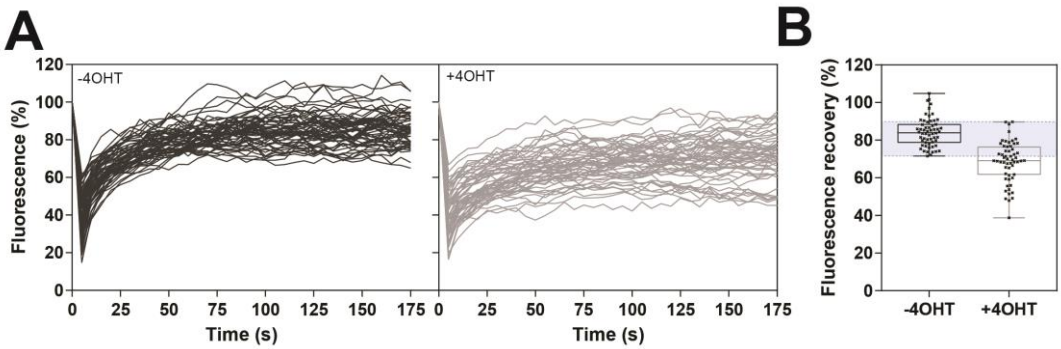

Figure 5.1. A large cell-to-cell variation is present in GFP-Bcl-XL FRAP dynamics
A. Example FRAP data of stable BadER^{Tam}-GFP-Bcl-XL MCF10A cells untreated or treated with 4-OHT. There is a large variation in the recovery of GFP-Bcl-XL fluorescence.
B. The mobile fraction of Bcl-XL within each cell was calculated from data in A and plotted. The area highlighted in blue indicates overlap in mobile fraction values between untreated and 4-OHT treated cells. n=60 cells per condition.

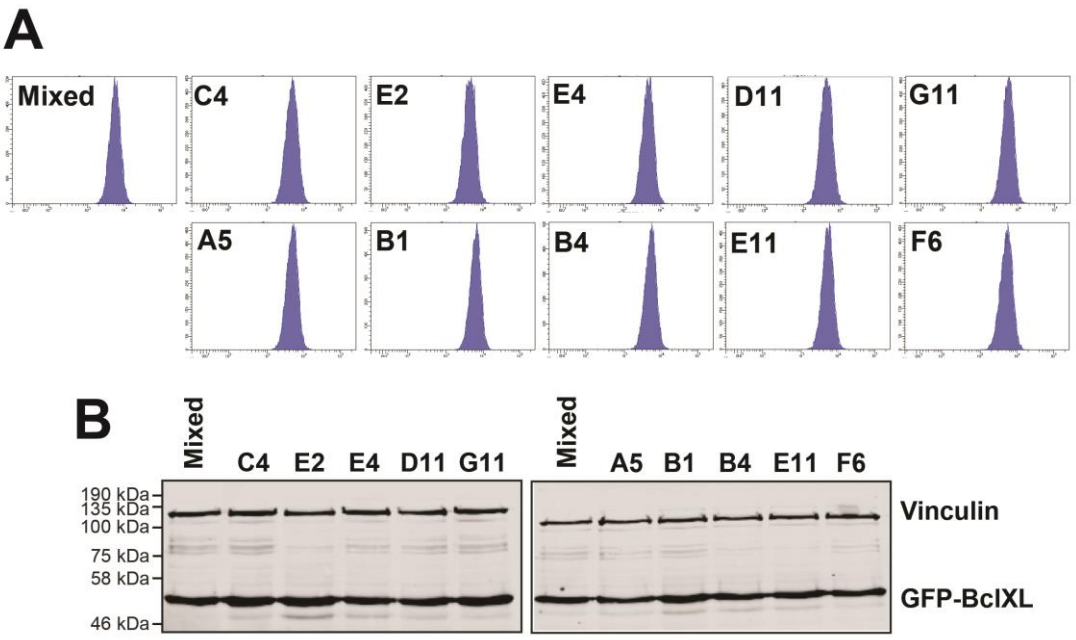

Figure 5.2. Clonal BadER^{Tam}-GFP-Bcl-XL MCF10A cells have comparable levels of GFP-Bcl-XL expression

A. Flow cytometry data of a mixed population of BadER^{Tam}-GFP-Bcl-XL MCF10A cells and 10 clonal populations. Expression of GFP is similar between all populations.

B. Western blot of lysates from populations in B probed for GFP. Vinculin was used as a loading control

5.3C). Together these data suggest that neither variation in expression levels of GFP-Bcl-XL nor differences in GFP-Bcl-XL integration between clonal populations of cells were causes of heterogeneity in Bcl-XL dynamics, suggesting this was an inherent property of the MCF10As.

5.3 Cell-to-cell variation in Bcl-XL dynamics predicts the heterogeneity in apoptotic outcome of the population

We have previously shown in this thesis that slower Bcl-XL dynamics are related to increased BH3 protein activity, which in turn relates to increased mitochondrial priming in response to pro-apoptotic stimuli like Etoposide. Furthermore, basal levels of Bcl-XL retrotranslocation dynamics vary significantly within populations of cells. We therefore wanted to investigate whether we could use these FRAP measurements to predict the apoptotic outcome of a population of cells to a pro-apoptotic stimulus like Taxol. Taxol is an anti-mitotic chemotherapeutic that disrupts spindle assembly during mitosis by stabilising microtubules, disrupting tension on the kinetochores[321]. This maintains the spindle assembly checkpoint and prolongs mitosis. This eventually leads to apoptosis of the cell due to degradation of cyclin B1[315], degradation or inactivation of Mcl-1, Bcl-2 and Bcl-XL, and activation of pro-apoptotic proteins such as Bid and Bad[322]. Cells resistant to treatment undergo mitotic slippage rather than apoptosis, and previous studies have demonstrated high inter- and intraline variation in response to Taxol in multiple different cell lines[315].

To begin we performed an assay to analyse the apoptotic outcome of 90 individual cells in response to different combinations of pro-apoptotic stimuli. BadER^{Tam}-GFP-Bcl-XL MCF10A cells were treated with either DMSO, 4-OHT, Taxol, or both 4-OHT and Taxol, and imaged every 15 minutes for 50 hours post-treatment (Fig. 5.4A). Individual cells were tracked through interphase and mitosis, and the fate of each cell after mitosis recorded – successful mitotic division, slippage or apoptosis. In DMSO treated cells, all cells proceeded through a rapid mitosis displaying successful division. Activation of BadER^{Tam} with 4-OHT had no effect on time in mitosis or mitotic division. Treatment with Taxol significantly increased the length of time cells were in mitosis. Approximately 25% of cells underwent death in mitosis or apoptosis after mitotic slippage (Fig. 5.4B). The remaining 75% of cells slipped

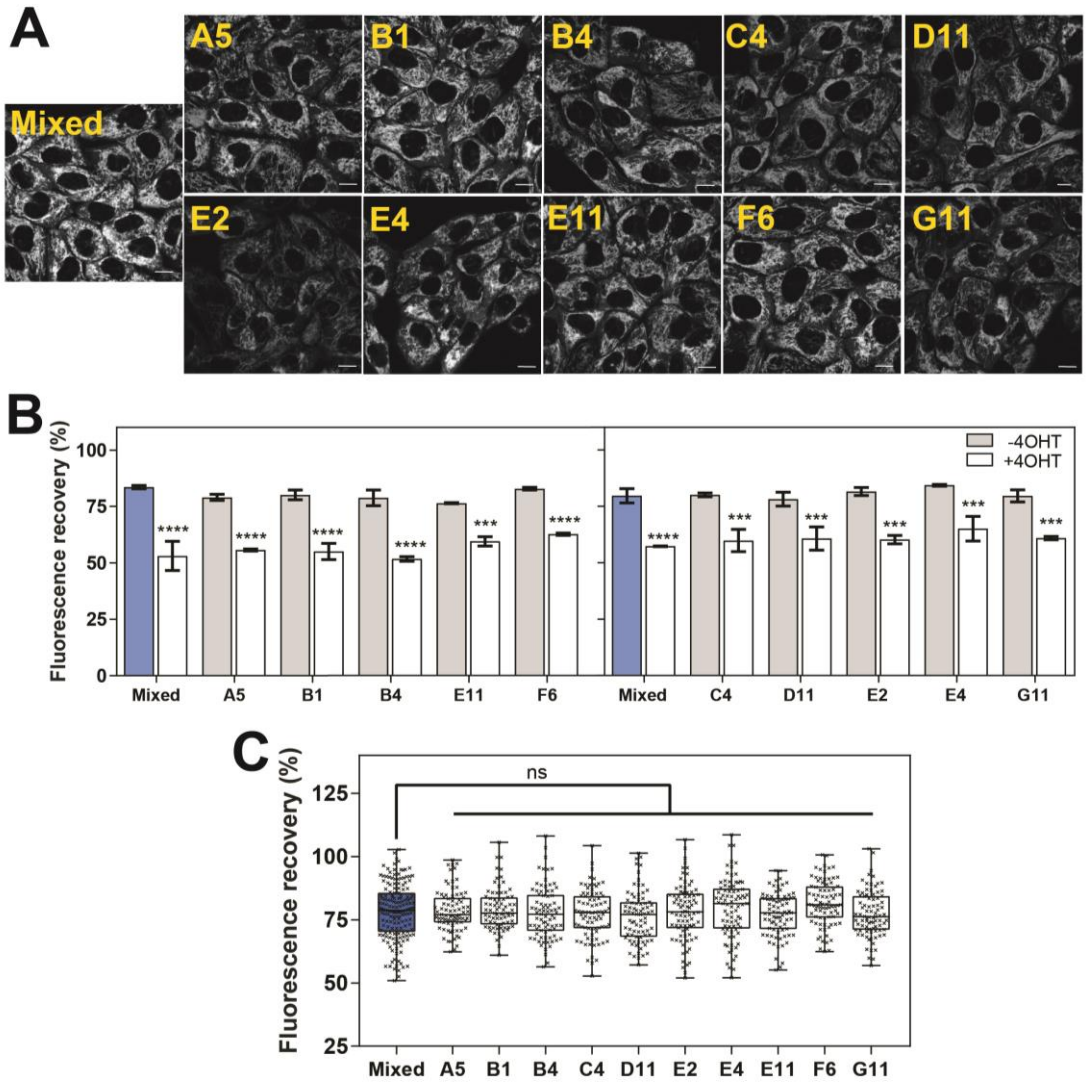

Figure 5.3. Heterogeneity in Bcl-XL dynamics is comparable between clonal cells and a mixed population

A. FRAP was performed on a mixed population of GFP-Bcl-XL-BadER^{Tam} MCF10A cells and 10 clonal populations. Example images from each population are shown. Scale bars represent 10µm.

B. Average fluorescence recovery for each population in A was calculated for both untreated and 4-OHT treated cells. All populations showed significantly more stable GFP-Bcl-XL after 4-OHT treatment. Values represent data from 3 independent experiments and error bars represent SD. Data was analysed via ANOVA. *** = $p<0.005$; **** = $p<0.001$.

C. GFP-Bcl-XL mobile fraction data from B plotted for each individual cell. The range in priming was calculated for each experimental repeat and averaged. There is no difference in the average range in priming between cell populations. Data was analysed via ANOVA. Error bars represent 10µm.

out of mitosis and survived. When cells were treated with both 4-OHT and Taxol, the length of time cells were in mitosis was comparable to cells treated with Taxol alone. The proportion of cells undergoing death in mitosis or death post-slippage increased to approximately 60%, with the other 40% slipping out of mitosis and surviving. This suggested that activation of BadER^{Tam} displaced pro-apoptotic proteins like Bid to kill cells that were primed during mitotic arrest.

In parallel to the cell fate assay described above, FRAP analysis was carried out on BadER^{Tam}-GFP-Bcl-XL MCF10A cells in the absence and presence of 4-OHT (Fig. 5.4C). This provided a measure of the pre-primed state of Bcl-XL dynamics within the cell population. Combining both FRAP and cell fate analysis, the top 75% of cells with the highest FRAP values were identified and used to set the value for the pre-mitotic apoptotic threshold of the population (Fig. 5.4D). This threshold was then used to estimate the proportion of cells that would undergo apoptosis in the presence of Taxol after priming with 4-OHT (red dotted line), with any cells whose dynamics fall below this line after 4-OHT treatment being considered sensitive to Taxol treatment. This led to a prediction that approximately 60% of cells would fall below the apoptotic threshold after pre-treatment priming via BadER^{Tam} activation. This value agreed with cell fate data, in which 60% of the MCF10As underwent apoptosis in the presence of Taxol and 4-OHT. This data suggests that, whilst there is significant heterogeneity in Bcl-XL dynamics, this variation is relative to mitochondrial priming and thus predicts the variation in apoptotic outcome of a cell population.

To determine whether Bcl-XL FRAP dynamics could be used to predict the apoptotic fate in another cell line, the BadER^{Tam}-GFP-Bcl-XL MDA-MB-231 stable cell line was also examined. The MDA-MB-231 cell line was treated with combinations of 4-OHT and Taxol and imaged over a period of 50 hours (Fig 5.5A). DMSO treatment alone did not induce apoptosis but did reveal that MDA-MB-231 cells have a longer mitosis than MCF10As (see Fig. 5.4A for comparison). 4-OHT treatment induced a small amount of apoptosis, with a proportion of cells undergoing slippage. This observation agrees with previous FRAP data showing MDA-MB-231 cells are inherently more primed than MCF10As, as pre-treatment priming with 4-OHT can induce apoptosis without further stimulus. Treatment with Taxol increased the length of time cells were in mitosis and induced a similar level of apoptosis to the 4-OHT

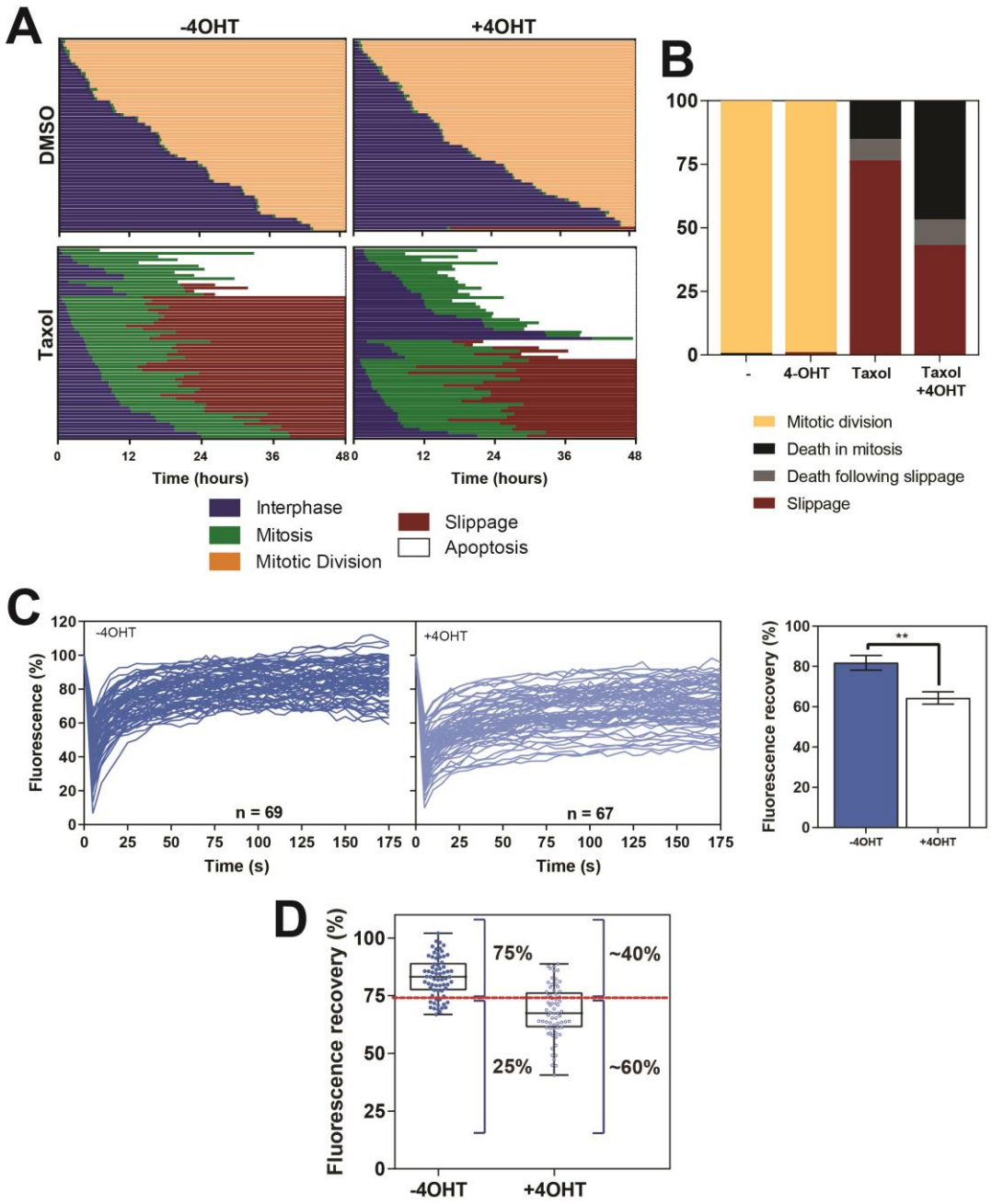

Figure 5.4. Cell-to-cell variation in Bcl-XL dynamics predicts apoptotic outcome in MCF10A cells

A. Cell fate plots of BadER^{Tam}-GFP-Bcl-XL MCF10A cells treated with DMSO, Taxol, 4-OHT or both 4-OHT and Taxol and imaged every 15 minutes for 48 hours. Each horizontal line represents the fate of a single cell. Data from 3 independent experiments, 20 cells per experiment, is shown.

B. Data from A plotted as stacked bars indicating mitotic division, slippage or apoptosis.

C. FRAP plots of the same cell line as in A with or without 4-OHT treatment. The average fluorescence recovery was calculated from a non-linear regression curve fit from 3 independent experiments. Error bars represent SD. ** = $p<0.01$.

D. Data from C plotted as box and whisker plots showing average Ymax values for both untreated and 4-OHT treated cells. Each point on the graph is the Ymax of a single cell. The red line indicates the apoptotic threshold set for the untreated cells determined following Taxol treatment. Data represents values from 3 independent experiments.

treated cells – approximately 20% - with the remainder undergoing mitotic slippage (Fig. 5.5B). Treatment with a combination of 4-OHT and Taxol increased levels of apoptosis to approximately 70%, with the remaining 30% undergoing slippage.

FRAP analysis was also carried out in parallel, in the absence and presence of 4-OHT (Fig. 5.5C). 20% of the MDA-MB-231 cells underwent apoptosis in the presence of Taxol alone, and this was used to set the value for the pre-primed apoptotic threshold of the population in the absence of 4-OHT (Fig. 5.5D). Based on the FRAP data, using this value it was predicted that approximately 70% of cells would undergo apoptosis when treated with both 4-OHT and Taxol. Indeed, cell fate analysis once again agreed with this prediction as 70% of cells died when treated with both 4-OHT and Taxol. Together these data suggest that Bcl-XL dynamics are an indication of levels of apoptotic priming of single cells, and these dynamics can be used to predict the apoptotic outcome of a population of cells in multiple cell lines.

5.4 Heterogeneity in Bcl-XL dynamics does not vary according to cell cycle stage

Now that it had been established that cell-to-cell variation in Bcl-XL dynamics correlated with heterogeneity in apoptotic outcome, we wanted to investigate potential causes and regulators of this heterogeneity. We have shown that Bcl-XL exerts its anti-apoptotic function at the OMM, as when cells become more primed, Bcl-XL retrotranslocation dynamics slow. Mitochondria themselves are highly dynamic organelles, with their morphology changing depending on the physiological state of the cell. In healthy cells the rates of mitochondrial fusion and fission are balanced[323], however during apoptosis mitochondria become highly fragmented around the same time as Bax localises at the OMM[324]. Mitochondrial fusion is regulated by the dynamin-related protein, Drp1, and the mitochondrial fission protein, Fis1, which divide mitochondria through “drawstring constriction” of the organelles[325]. Bax, Drp1 and the mitochondrial fusion regulator, Mfn2, have been shown to form large foci at the OMM which can be inhibited by Bcl-XL[134,326]. Mitochondrial morphology has also been shown to change at differing stages of the cell cycle. Hyperfused mitochondria have been observed at G1-S phase[327] and

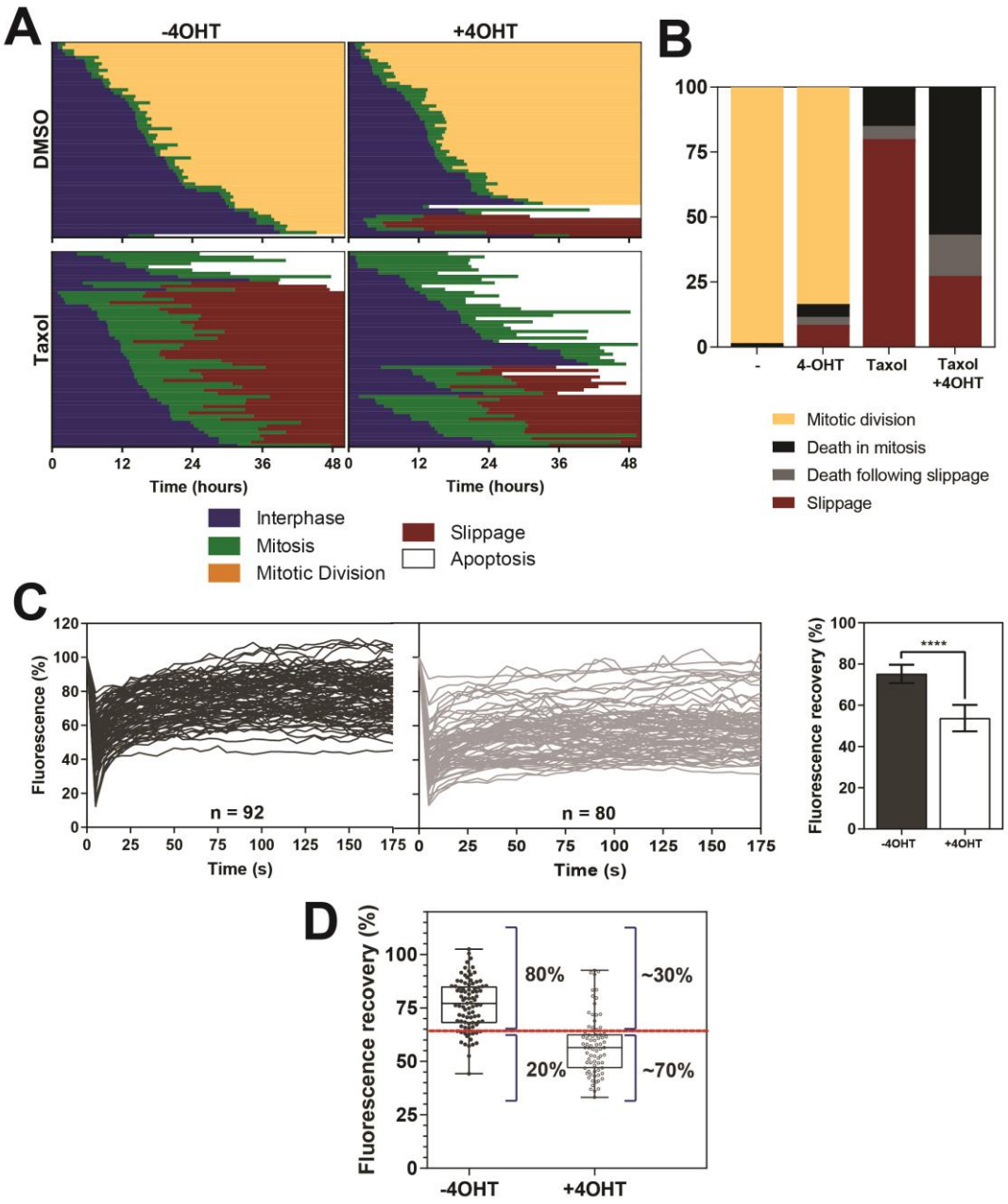

Figure 5.5. Heterogeneity in Bcl-XL dynamics predicts the apoptotic outcome of BadER^{Tam}-GFP-Bcl-XL MDA-MB-231 cells

A. Cell fate plots of BadER^{Tam}-GFP-Bcl-XL MDA-MB-231 cells treated with DMSO, Taxol, 4-OHT or both 4-OHT and Taxol and imaged every 15 minutes for 50 hours. Each horizontal line represents the fate of a single cell. Data from 3 independent experiments, 20 cells per experiment, is shown.

B. Data from A plotted as stacked bars indicating mitotic division, slippage or apoptosis.

C. FRAP plots of the same cell line as in A with or without 4-OHT treatment. The average fluorescence recovery was calculated from a non-linear regression curve fit from 3 independent experiments. Error bars represent SD. **** = $p<0.001$.

D. Data from C plotted as box and whisker plots showing average Ymax values for both untreated and 4-OHT treated cells. Each point on the graph is the Ymax of a single cell. The red line indicates the apoptotic threshold set for the untreated cells determined following Taxol treatment. Data represents values from 3 independent experiments.

fission occurs during mitosis[328]. How these changes in mitochondrial morphology alter Bcl-XL dynamics at different cell cycle stages has not been well characterised. Cell cycle and apoptosis are also known to be linked as highly proliferating cells are more susceptible to apoptosis[329]. This relationship is also evident in cancer treatment where quiescent cells are more resistant to chemotherapy-induced apoptosis than cycling cells[330]. Overexpression of oncogenes such as c-Myc can block serum-starvation induced growth arrest and induces apoptosis in the highly proliferating cell population[331]. We therefore questioned whether specific cell cycle stages correlate with higher or lower levels of mitochondrial priming. If this were true, heterogeneity in Bcl-XL dynamics could be due to individual cells within a population being in different stages of the cell cycle when FRAP measurements are being taken.

To study cells in various stages of the cell cycle, the population in question needs to be synchronised. Traditional chemical methods of synchronising cells at specific cell cycle stages involve using drugs such as nocodazole (a microtubule polymerisation inhibitor) or double thymidine block (DNA replication inhibitor) which, whilst effective at synchronising cells, can have an indirect effect on Bcl-2 protein dynamics. Nocodazole disrupts polymerisation of microtubules, arresting cells in M phase[332], which activates and degrades a number of Bcl-2 family proteins as mentioned above. Double thymidine blocks function by arresting cells at G1/S by inhibiting DNA synthesis[333] and activating the DNA damage response[334], thus activating BH3 proteins like Puma and Noxa.

We therefore decided to utilise the modified fluorescence ubiquitination-based cell cycle indicator (FUCCI) system[335], FUCCI4, as a reporter of cell cycle stage rather than synchronising populations of cells. This system utilises the ubiquitin-protease system to degrade reporter proteins which are fused to other proteins involved in cell cycle regulation – CDT1 (involved in the formation of the pre-replication complex during DNA replication), Geminin (inhibitor of CDT1), SLBP (histone stem-loop binding protein) and H1 (histone 1) (Fig. 5.6A)[336]. Due to specific temporal expression of each protein, cell cycle stage is reported via nuclear fluorescence of each protein at a single cell cycle stage. This allows identification of which stage of the cell cycle an individual cell is in without the need for synchronisation. To simplify the experimental setup, we chose to express only one set of reporters – Geminin

A

Protein	Cell cycle stage	Fluorophore
$CDT1_{30-120}$	G1	mKO2
$SLBP_{18-126}$	S	mTurquoise2
$Geminin_{1-110}$	G2	Clover
H1.0	M	mMaroon1

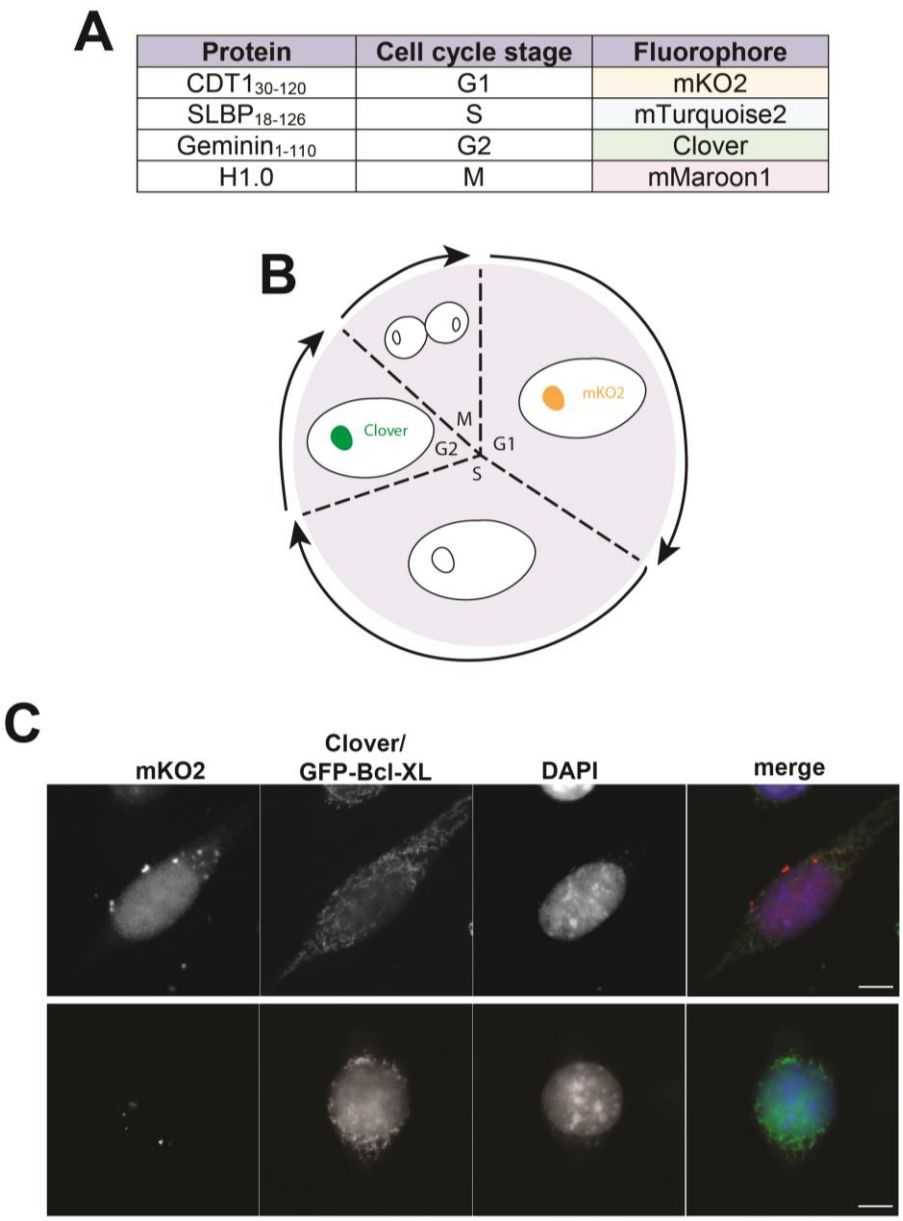

Figure 5.6. The FUCCI reporter system indicates cell cycle stage

A. Cell cycle reporter proteins used in the FUCCI4 system and their respective fluorophores.

B. Schematic of the FUCCI reporters used to indicate cell cycle stage. mKO2 indicates G1, Clover G2, S phase has no colour and M phase is recognised via cell morphology.

C. Example immunofluorescence images of DKO MEFs transiently expressing GFP-Bcl-XL and the pLL3.7m-Clover-Geminin(1-110)-IRES-mKO2-Cdt(30-120) plasmid. One mKO2-expressing and one Clover-expressing cell is shown. Scale bar represents 10µm.

and CDT1. Using only these two reporters would still maintain the ability to visualise cells at each stage in the cell cycle, as G1 and G2 would be evident via mKO2 and Clover expression, respectively, and S phase would be apparent due to lack of any nuclear fluorescence (Fig. 5.6B). M phase cells would be identified via their rounded morphology. Initial expression was tested by transient transfection of the pLL3.7m-Clover-Geminin(1-110)-IRES-mKO2-Cdt(30-120) plasmid into DKO MEFs alongside transfection of GFP-Bcl-XL, and reporter fluorescence examined via immunofluorescence (Fig. 5.6C). Fluorescence of either reporter was observed only in the nucleus of positively expressing cells.

We next created a cell line stably expressing the FUCCI reporters by infecting WT MCF10As with the pLL3.7m-Clover-Geminin(1-110)-IRES-mKO2-Cdt(30-120) lentivirus and cultured the infected cells for 2 weeks to ensure stable infection. Stably infected cells were sorted via FACS for cells containing either Clover or mKO2 fluorescence, but not both, as cells showing both colours would most likely be overexpressing the reporters (Fig. 5.7A). WT MCF10As were chosen over the BadER^{Tam}-GFP-Bcl-XL MCF10A cell line as the presence of GFP-Bcl-XL prevented sorting for mClover fluorescence, meaning only a small proportion of the total cell population could be sorted for mKO2 expression. To ensure the fluorescent reporters were cycling at the appropriate stages of the cell cycle, the FUCCI-MCF10A line was imaged every 6 minutes over a period of 72 hours and individual cells followed through each cell cycle stage (Fig. 5.7B). A representative example of a cycling cell is shown in Fig. 5.7C, with both mKO2 and Clover fluorescence visible before a loss of fluorescence during mitosis.

We next wanted to determine whether we could measure differences in Bcl-XL dynamics and variation in dynamics at difference stages of the cell cycle. The stable FUCCI-MCF10A cells were transduced with the BadER^{Tam}-GFP-Bcl-XL lentivirus to create stable lines. Whilst positively transduced cells could not be FACS sorted due to the presence of mClover fluorescence, cells expressing GFP-Bcl-XL could still be selected for FRAP analysis. There were no obvious differences in the ability of cells to progress through the cell cycle between those that were expressing GFP-Bcl-XL and those that were not. Cells expressing GFP-Bcl-XL were then subjected to FRAP analysis, measuring Bcl-XL dynamics in cells in either G1 (red nuclear fluorescence), G2 (green nuclear fluorescence) or S phase (no nuclear

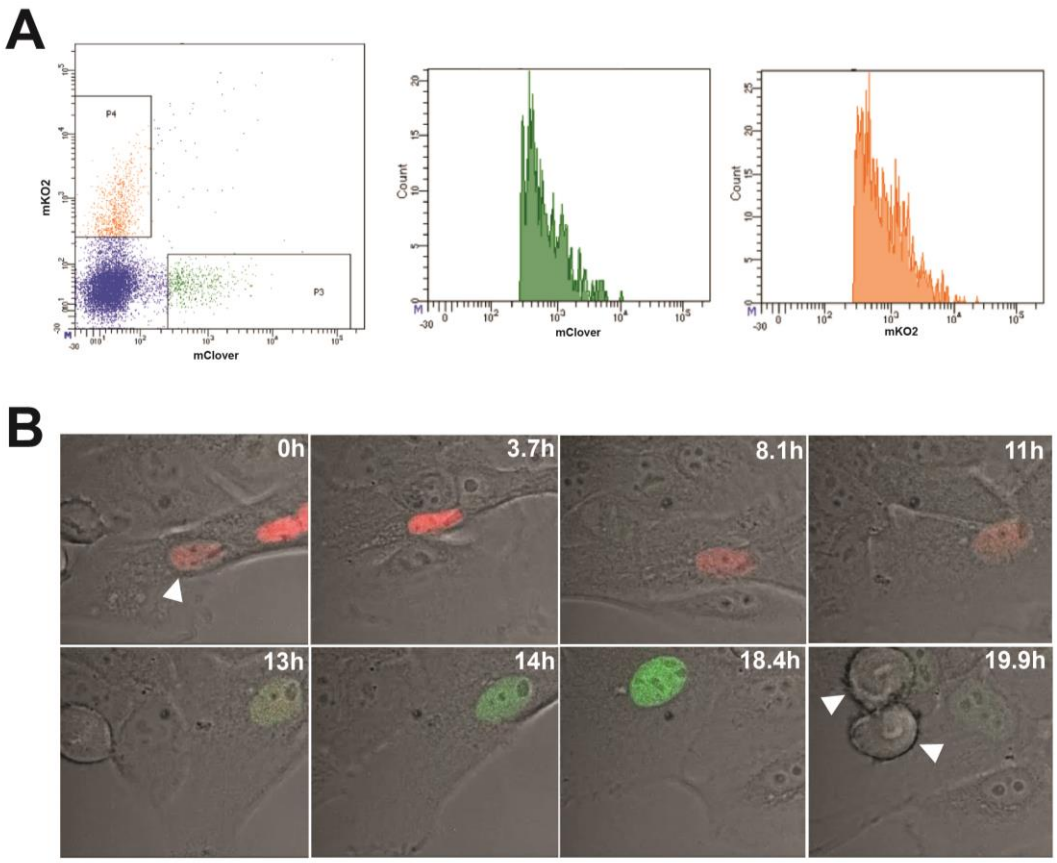

Figure 5.7. Creation of an MCF10A cell line stabley expressing the FUCCI system
A. Flow cytometry plots of FACS cells, sorted for both Clover and mKO2 fluorescence but not both.
B. Example images of a cell progressing through the cell cycle expressing the appropriate FUCCI markers. White arrows indicate the cell of interest.

fluorescence) (Fig. 5.8A). No differences were apparent between the average dynamics of Bcl-XL between each cell cycle stage (Fig. 5.8B). Measuring cell-to-cell variation in Bcl-XL dynamics between different cell cycle stages also revealed no differences (Fig 5.8C). Together these data suggest that cell cycle stage does not directly regulate Bcl-XL dynamics in MCF10A cells, and thus is not a major regulator of cell-to-cell variation in Bcl-XL mitochondrial translocation.

5.5 Endogenous pro-apoptotic Bad does not significantly regulate heterogeneity in Bcl-XL dynamics

As cell cycle stage did not appear to regulate heterogeneity in Bcl-XL dynamics, we questioned what other factors could regulate apoptotic heterogeneity. Studies have shown that levels of growth factor signalling in cells is very variable. For example, ERK signalling has been shown to occur in asynchronous pulses based on extracellular EGF concentration[337]. Breast cancer cell lines have been shown to vary in their responsiveness to AKT and ERK signalling, even within the same breast cancer subtype, based on factors such as the abundance of surface receptors which varies from cell to cell[338]. Bcl-2 family proteins are responsive to changes in growth factor signalling, as demonstrated previously when Bcl-XL dynamics were significantly slowed in serum starved MCF10A cells. Pro-apoptotic Bcl-2 proteins are regulated by growth factor signalling, for example Bad phosphorylation by AKT and PKA[279], and the inhibition of Bim via ERK signalling inhibiting anoikis[278]. Whilst *in vivo* mouse studies have demonstrated that knocking out individual BH3 proteins does not significantly affect growth and development, Bad knockout in primary mammary epithelial cells makes them less sensitive to changes in growth factor signalling[150]. As Bcl-XL dynamics are altered in the presence of BH3 proteins, and BH3 proteins are regulated by growth factor signalling, we postulated whether changes in growth factor-regulated BH3 protein levels cause heterogeneity in Bcl-XL dynamics. To investigate this, we therefore chose to examine the role of Bad and Bim on Bcl-XL dynamics.

We initially wanted to reduce levels of endogenous human Bad in the BadER^{Tam}-GFP-Bcl-XL MCF10A cell line to examine the effect on Bcl-XL dynamics. An siRNA designed to specifically target human Bad was transfected into the MCF10A cell line

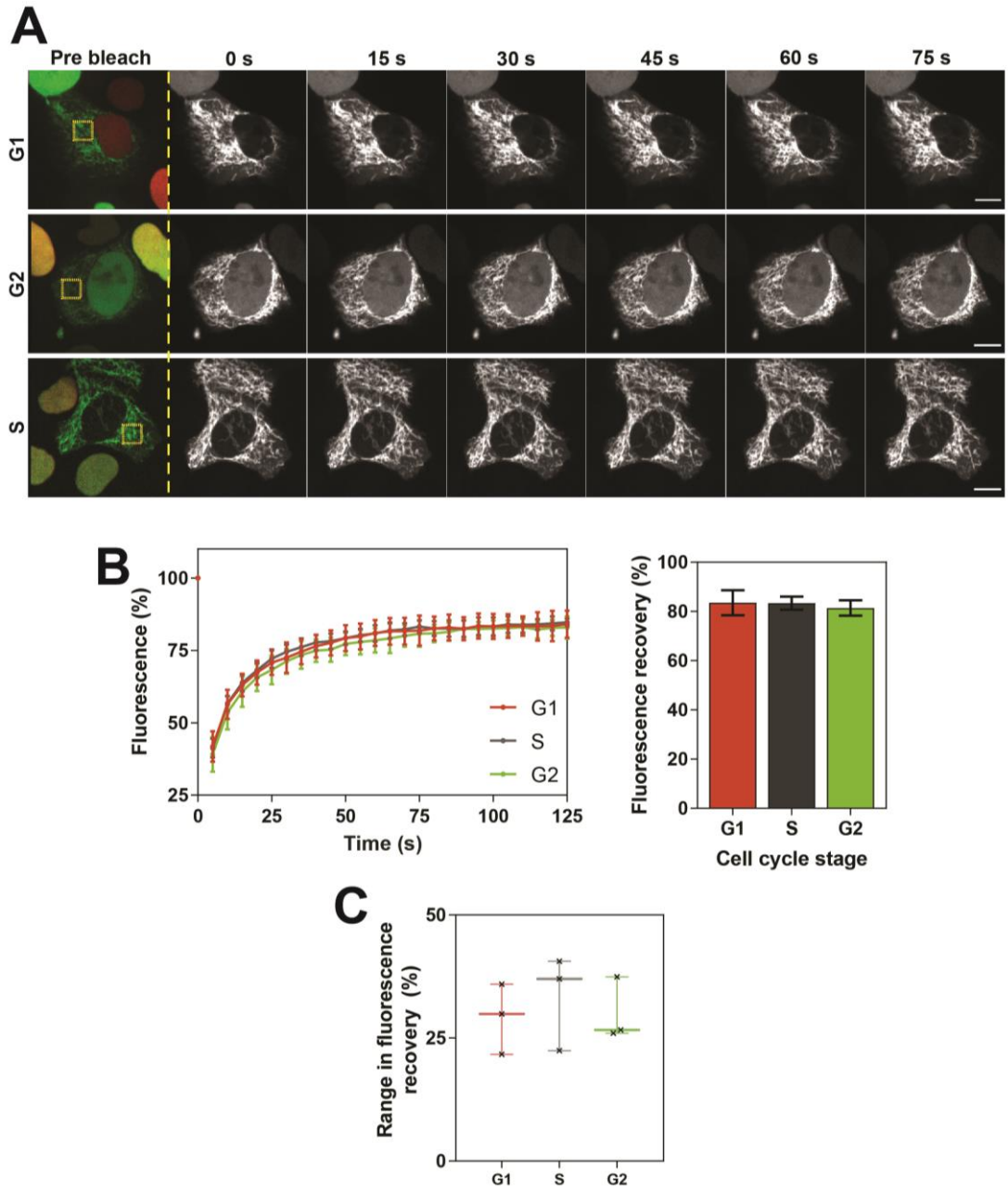

Figure 5.8. Cell cycle stage does not affect Bcl-XL dynamics

A. Representative images showing FRAP analysis carried out on FUCCI-Bcl-XL MCF10A cells. The ROI within the yellow box was photobleached for 10ms using a 488nm laser, and the recovery of fluorescence in the same area measured over time. Images were taken every 5 seconds. Scale bars represent 10µm.

B. Recovery in fluorescence was plotted over time and non-linear regression analysis carried out. There is no significant difference in mobile fraction of Bcl-XL. Data was analysed via ANOVA and values represent data from 3 independent experiments, n=90 cells per condition. Error bars represent SD.

C. The range in GFP-Bcl-XL fluorescence recovery was calculated for each experimental repeat from B and each value plotted. There is no significant difference in the range between cell cycle stages. Data was analysed via ANOVA.

and knockdown efficiency examined via Western blot (Fig.5.9A). Unfortunately, levels of endogenous Bad remained at equal levels to untransfected cells, but exogenous mouse BadER^{Tam} levels were significantly reduced. This also reduced levels of GFP-Bcl-XL expression in live cells (Fig. 5.9B). We instead chose to remove endogenous Bad completely by utilising the CRISPR-Cas9 system to knockout hBad in the MCF10A cells. Guide sequences were designed targeting exon 2 close to the start codon of the gene but avoiding targeting the G Protein-Coupled Receptor 137 gene sequence running anti-sense to Bad (Fig. 5.9C). These guides were cloned into the pX458 vector and transfected into BadER^{Tam}-GFP-Bcl-XL MCF10A cells. Positively transfected cells were subsequently single cell sorted via FACS and surviving clones grown and genotyped via PCR and DNA sequencing. Due to poor transfection efficiency and poor survival during clonal growth only 5 clones were successfully expanded up for genotyping. Two clones – clone 2 and clone 8 - were identified with indels that caused frame-shift mutations in the DNA, with these frameshift mutations confirmed via sequencing (Fig. 5.9D). The absence of Bad protein was confirmed via Western blot, with clone 8 showing a complete lack of protein, and clone 2 showing a protein of increased molecular weight (Fig. 5.9D). Both Bad KO clones still expressed the exogenous BadER^{Tam} protein at equal levels to the WT cell line.

As Bad-deficient primary mammary epithelial cells have been shown to become less sensitive to growth factor removal-induced apoptosis, and growth factor removal alters Bcl-XL dynamics, we carried out FRAP to determine if the absence of Bad in the KO cell line had any effect on Bcl-XL dynamics in healthy cells due to an inability to respond to growth factor signalling. WT, clone 2 and clone 8 cell lines underwent FRAP analysis in the absence and presence of 4-OHT (Fig. 5.10A). 4-OHT treatment significantly reduced Bcl-XL dynamics in all three cell lines (Fig. 5.10B). Comparison of Bcl-XL mobile fraction before or after 4-OHT treatment revealed no significant differences between WT and hBad KO cell lines. To determine if the absence of hBad had any effect on heterogeneity of Bcl-XL dynamics, the range in levels of Bcl-XL dynamics within each experiment and for each cell line was quantified and plotted (Fig. 5.10C). Whilst there were no significant differences between any of the cell lines, clone 8 did trend towards a larger cell-to-cell variation post-4-OHT treatment. Plotting every datapoint from each experiment revealed that, in untreated cells, the WT cell line had a small number of cells with much more stable Bcl-XL compared to both knockout lines (Fig. 5.10D). Interestingly, after 4-

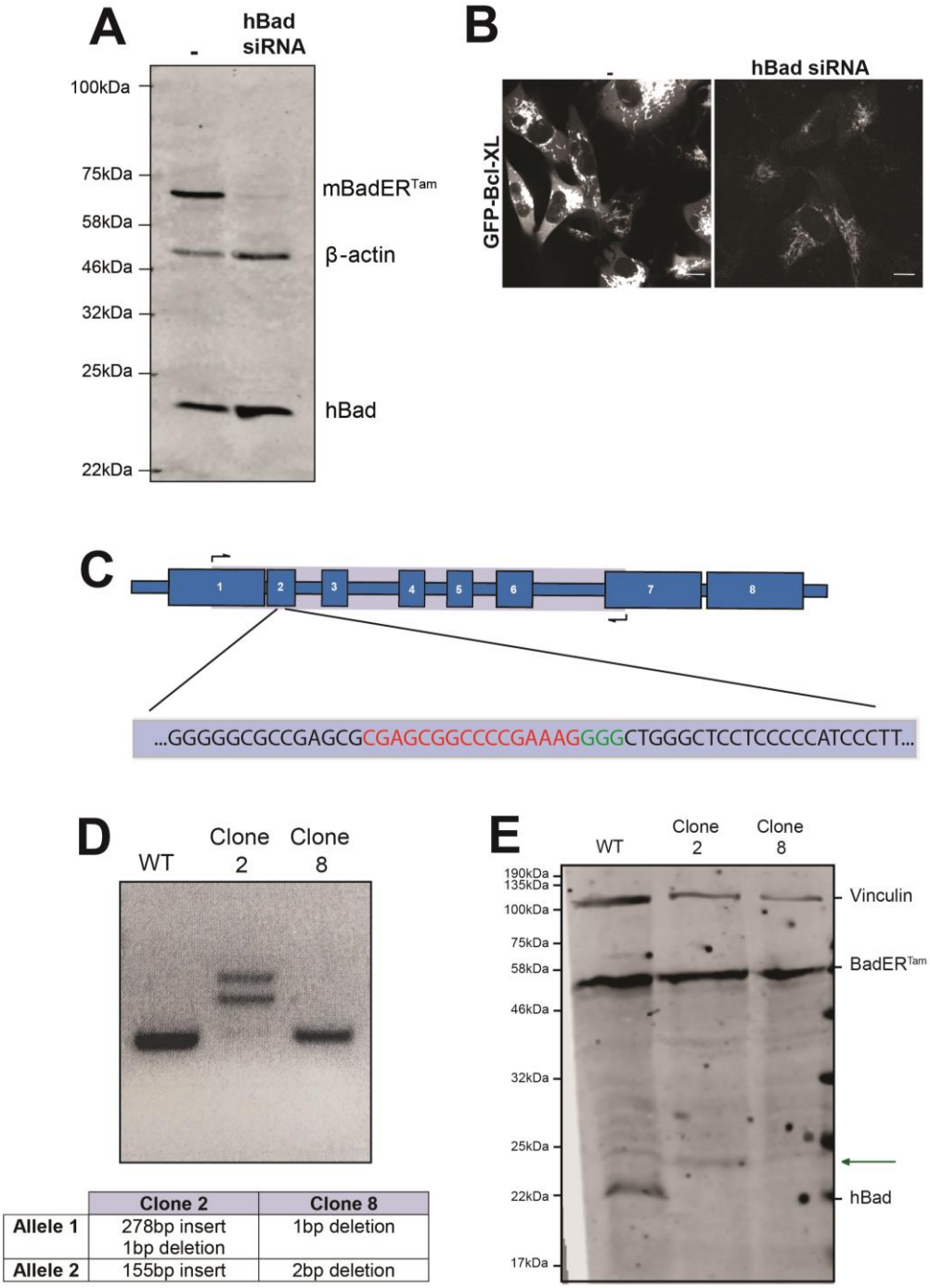

	Clone 2	Clone 8
Allele 1	278bp insert 1bp deletion	1bp deletion
Allele 2	155bp insert	2bp deletion

Figure 5.9. Creation of a hBad knockout cell line using CRISPR-Cas9

A. Western blot of BadER^{Tam}-GFP-Bcl-XL MCF10A cells untreated or treated with an siRNA designed to target human Bad. The membrane was probed against Bad. β-actin was used as a loading control.

B. Example live cell images of untreated and siRNA treated cells showing GFP-Bcl-XL expression. Scale bar represents 10μm.

C. Schematic of CRISPR targeting site and guide sequence. The Bad gene was targeted in exon 2 (blue box). The red text represents the guide sequence and the green text represents the PAM site directly downstream.

D. Agarose gel of PCR amplicons of DNA extracted from WT GFP-Bcl-XL MCF10As and two CRISPR clones. The table below indicates specific indels in the CRISPR clones.

E. Western blot of lysates extracted from the same clones as in B. The membrane was probed against Bad and vinculin was used as a loading control. Green arrow indicates larger molecular weight band in Clone 2.

OHT treatment both knockout lines had a small number of cells with much more mobile Bcl-XL compared to WT cells. This suggested that endogenous Bad may be priming a small subset of cells when BadER^{Tam} is inactive, and when BadER^{Tam} is activated and sequesters excess Bcl-XL, the lack of endogenous Bad in the knockout cells leaves a small subset of cells less primed that WT cells.

Bad sensitises cells to apoptosis via binding Bcl-XL upon increased levels of stress[339] and the Bad KO cells appeared to show minor differences in heterogeneity after 4-OHT treatment when excess Bcl-XL was sequestered. As FRAP experiments were being carried out in an overall unprimed, healthy population of cells (with the equilibrium of Bcl-XL favouring its most cytosolic distribution), we questioned whether this would mask any significant differences between WT and BadKO cells. Potentially, inducing an initial level of priming in the populations would uncover differences in either heterogeneity or mobility in Bcl-XL. To test this, WT and hBad KO clone 8 cells were serum starved for 7 days before carrying out FRAP analysis, as Bad induces apoptosis via interaction with Bcl-XL upon serum starvation[340] (Fig. 5.11A). Clone 8 was selected as it showed the larger number of unprimed cells between the two KO lines in the previous FRAP experiment. Serum-starved cells were significantly more primed than those which were grown in complete growth medium for both cell lines (Fig. 5.11B). There was no difference in priming between WT and Bad KO cells in either condition. There was also no significant difference in the single cell variation in Bcl-XL dynamics between WT and hBadKO MCF10As (Fig. 5.11C).

As removal of Bad alone appeared to affect GFP-Bcl-XL dynamics in a small sub-population of cells, we tested whether knocking down an activator BH3 protein as well would have any effect on heterogeneity in Bcl-XL dynamics. An siRNA against Bim was used to knockdown Bim expression levels either in WT or BadKO clone 8 cells. Knockdown efficiency was measured via Western blot analysis which showed Bim had been knocked down to almost undetectable levels in both lines (Fig. 5.12A). FRAP analysis was carried out on WT and BadKO lines with Bim siRNA. Knocking down Bim did not affect overall levels of priming between the cell lines (Fig. 5.12B) or heterogeneity in Bcl-XL FRAP dynamics (Fig. 5.12C). Together these data suggest that, whilst Bad may have a partial role in the regulation of a

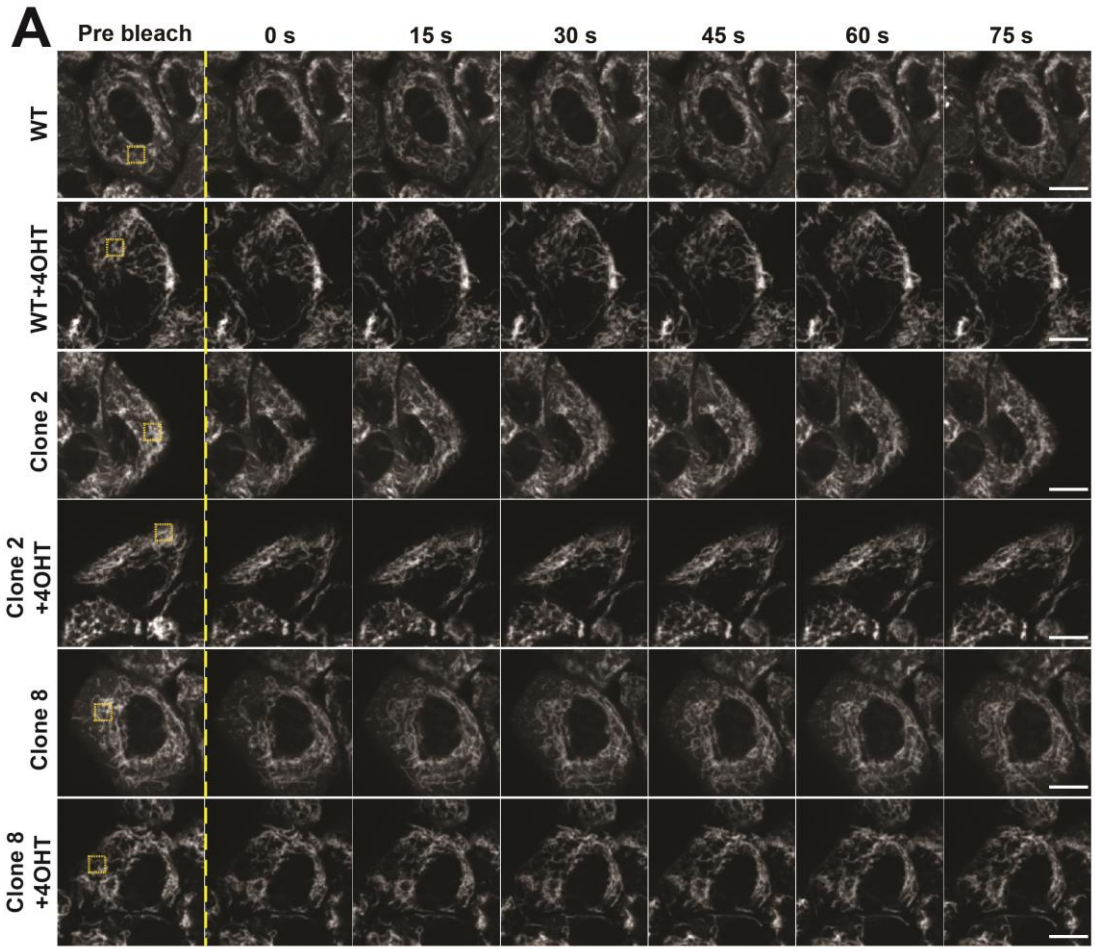

Figure legend on next page.

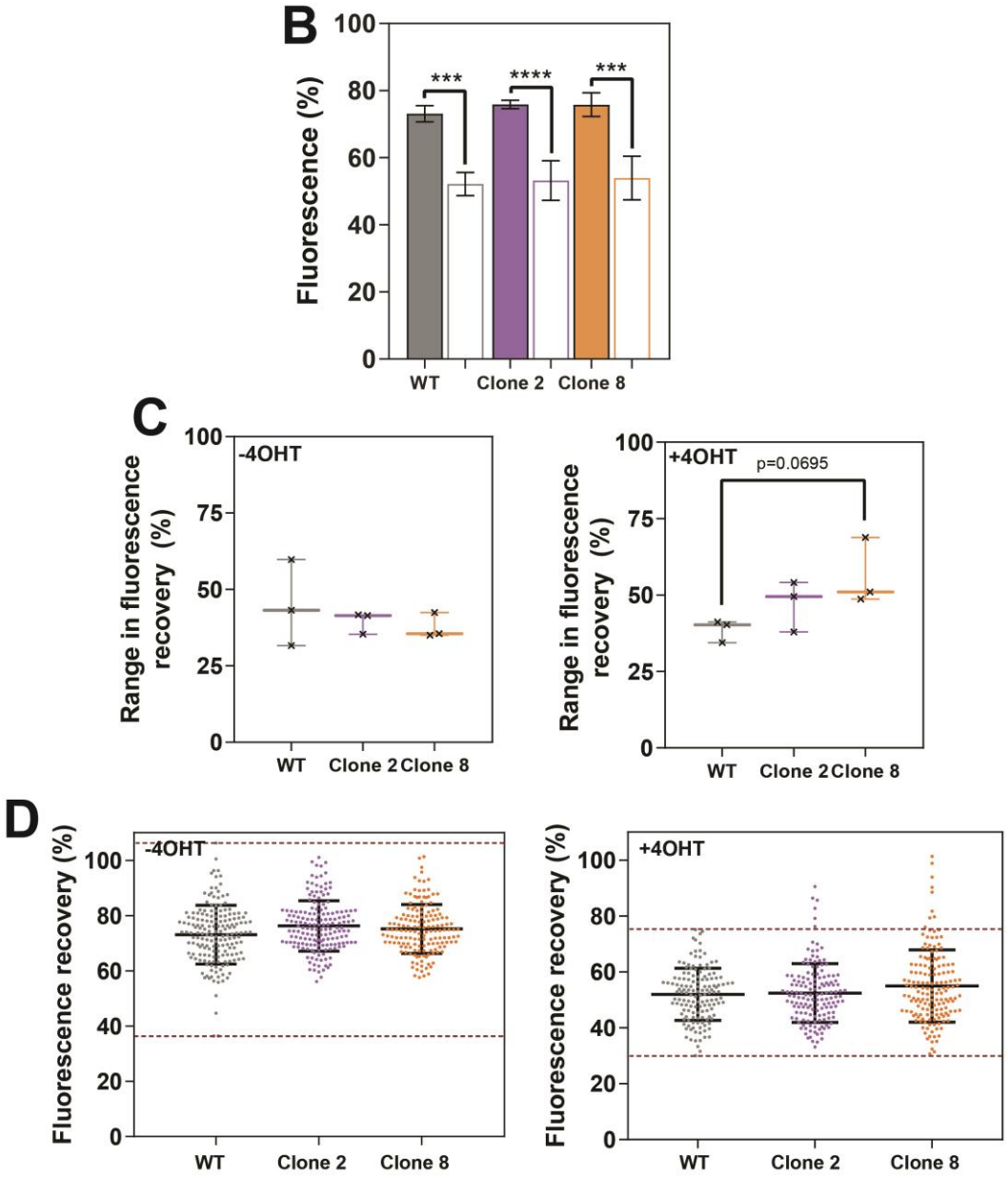

Figure 5.10. Bad regulates Bcl-XL dynamics in a small subset of MCF10A cells

A. FRAP was carried out in WT and Clone 8 Bad KO GFP-Bcl-XL-BadER^{Tam} MCF10A cells in the absence and presence of 4-OHT. The yellow ROI was photobleached for 10ms and fluorescence recovery within the same ROI measured every 5 seconds afterwards. Scale bars represent 10µm.

B. Non-linear regression curves were fit to data from A and the average fluorescence recovery calculated for each condition. All three cell lines were significantly primed in the presence of 4-OHT. Data represents values from 3 independent experiments and was analysed via ANOVA. Error bars represent SD. *** = $p<0.005$; **** = $p<0.001$.

C. The range in GFP-Bcl-XL fluorescence recovery was calculated for each experimental repeat from B and each value plotted. There is no significant difference in the range between WT and Bad KO cell lines. Data was analysed via ANOVA.

D. Every mobile fraction datapoint from each experiment was plotted to identify any outlying points. The red dotted lines indicate the range in values in WT cells for reference.

small subset of cells, individual BH3 proteins are not the sole regulator of heterogeneity in Bcl-XL dynamics.

5.6 Discussion

Single cells within a population differ in their response to pro-apoptotic stimuli, and in many cases this is not due to genetic differences between cells[264,315,341]. Significant cell-to-cell variation also exists in the translocation of Bcl-XL to the OMM, with slower dynamics indicative of more mitochondrially primed cells, and vice versa. Even in a primed cell population, however, there is a vast range in Bcl-XL translocation rates, with many cells showing similar dynamics to those in an unprimed population. It is interesting that this variation is present to the same extent within a clonal population of cells and is therefore most likely an inherent property of cell populations. Here we have shown that heterogeneity in pre-primed Bcl-XL dynamics is predictive of heterogeneity in apoptotic outcome in response to Taxol in both MCF10As and MDA-MB-231s. These results are similar to those measured via BH3 profiling using BH3 peptides to prime cells before treating with chemotherapeutic agents[217]. Patient response highly correlates with levels of pre-treatment priming. Our FRAP method of measuring apoptotic sensitivity is distinct from BH3-profiling as Bcl-2 protein dynamics can be measured in the lead up to apoptosis and so comparisons can be made between cells which eventually die to those which survive, rather than using mitochondrial depolarisation as the output[218,257]. This also permits addition of further pro-apoptotic stimuli to measure the effect of subsequent treatments, or removal of stimuli to reset the equilibrium. Although Bcl-XL dynamics are being used as a measure of mitochondrial priming, the effect of pro-apoptotic stimuli on other anti-apoptotic proteins could also be measured using this system. Predicting the apoptotic outcome of individual cells within a population using this technique would confirm that slow translocation dynamics correlate with apoptotic sensitivity, as any single cells falling below the calculated apoptotic threshold should undergo apoptosis. This was attempted by carrying out FRAP of individual cells, then subsequently following the fate of the same cells after drug treatment. However, the logistics of the equipment setup meant that tracking the same cells after FRAP was not possible.

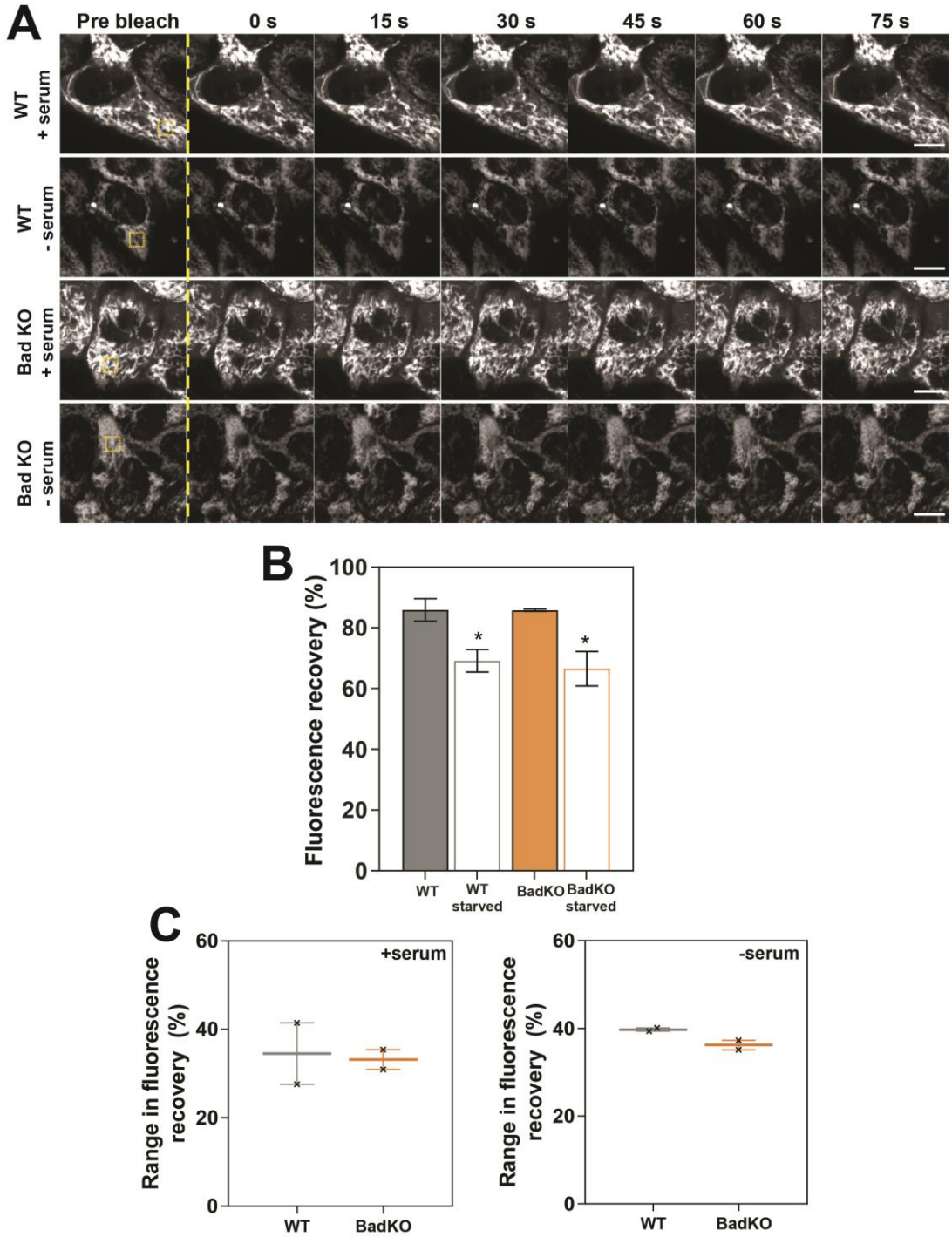

Figure 5.11. Endogenous Bad knockout does not affect Bcl-XL dynamics in serum-starved cells
A. Representative images showing FRAP analysis carried out on WT and Bad KO BadER^{Tam}-GFP-Bcl-XL- MCF10A cells grown in either complete medium or serum-free medium for 7 days. The ROI within the yellow box was photobleached for 10ms using a 488nm laser and the recovery of fluorescence in the same area measured over time. Images were taken every 5 seconds. Scale bars represent 10µm.
B. Average recovery in fluorescence was calculated via non-linear regression. Serum starvation significantly stabilised Bcl-XL at the OMM in both lines, but there is no significant difference between cell lines. Data was analysed via ANOVA and values represent data from 2 independent experiments, n=150 cells per condition. Error bars represent SD. * = $p<0.05$.
C. The range in GFP-Bcl-XL fluorescence recovery was calculated for each experimental repeat from B and each value plotted. There is no significant difference in the range between WT and Bad KO cell lines, with or without serum. Data was analysed via Student's t-test.

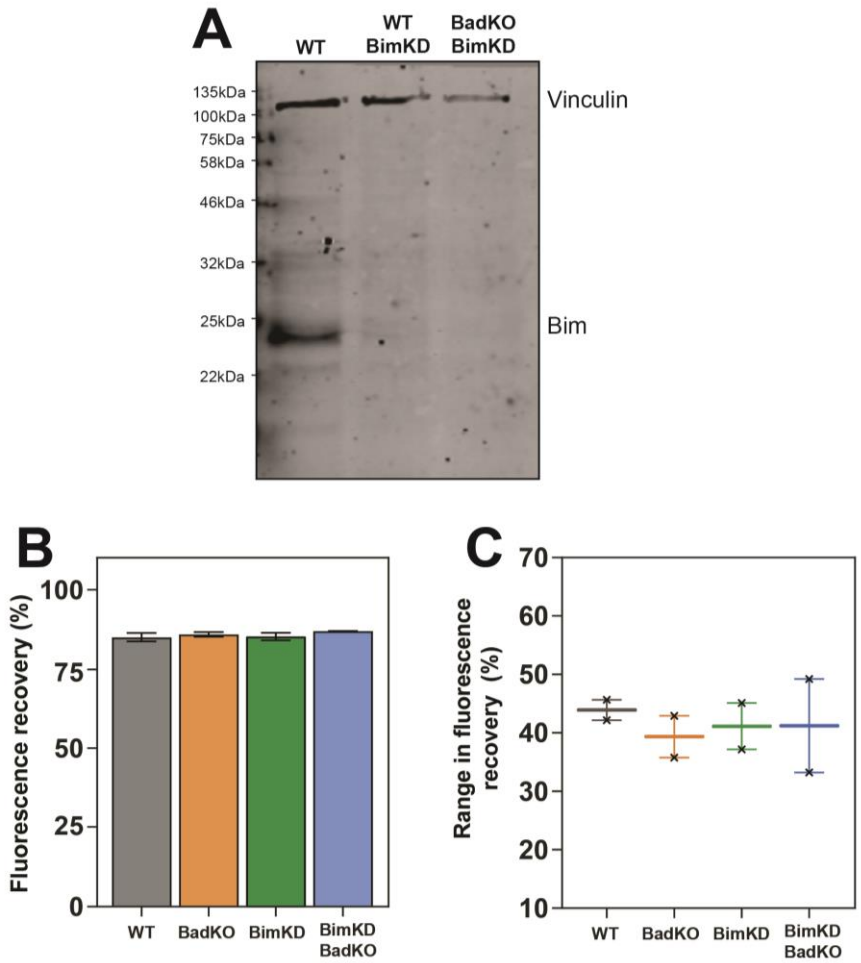

Figure 5.12. Bim alone, or in combination with Bad, does not regulate Bcl-XL dynamics

A. WT and BadKO GFP-Bcl-XL-BadER^{Tam} MCF10As were transfected with siRNA against Bim, protein extracted, and a Western blot carried out to test knockdown efficiency. Vinculin was used as a loading control.

B. FRAP was carried out on WT and Bad KO cells as above and average fluorescence recovery calculated. There is no significant difference between conditions, Data represents values from 2 independent experiments and was analysed via ANOVA. Error bars represent SD.

C. The range in GFP-Bcl-XL fluorescence recovery was calculated for each experimental repeat from B and each value plotted. There is no significant difference in the range between WT and Bad KO cells in either condition. Data was analysed via ANOVA.

It has been shown that cell populations reach an equilibrium in terms of their sensitivity to pro-apoptotic stimuli[264], however how this equilibrium is established and regulated at a single cell level has not been elucidated. Both pro- and anti-apoptotic Bcl-2 proteins have been linked to regulating mitochondrial priming during different stages of the cell cycle. For example, cells entering mitosis become more primed for apoptosis to ensure that any cells that fail to divide properly are targeted for death. This is, in part, due to activities of Bcl-2 family proteins. For example, Bid is phosphorylated on serine-66 as cells enter mitosis and is dephosphorylated during the metaphase-to-anaphase transition[172]. This phosphorylation increases mitochondrial priming if cells are delayed in mitosis. Mcl-1 is also degraded during mitotic arrest, which contributes to increased priming[342,343]. Activating BadER^{Tam} in our system induced apoptosis in Taxol-treated cells, potentially by displacing Bid from Bcl-XL to activate apoptosis. Bcl-2 and Bcl-XL are also known to play a role in the regulation of cell cycle progression, in particular by delaying entry into S-phase in quiescent cells as shown in both tissue culture systems[344,345] and mouse models[346,347]. In cancer cells the role of anti-apoptotic proteins is less clear, as Bcl-2 is known to promote tumourigenesis by inhibiting apoptosis, but overexpression is also associated with better prognosis[348]. If, and how, the regulation of apoptosis and cell cycle progression are intimately linked is still uncertain. Mutational studies of tyrosine 28 (Bcl-2) and tyrosine 22 (Bcl-XL) residues in the BH4 domain show normal anti-apoptotic functionality, but the delay into S-phase is eliminated, suggesting the two processes are distinct from each other[349]. FRAP analysis of Bcl-XL at differing cell cycle stages showed no difference in either the translocation rate of Bcl-XL or the variation in Bcl-XL dynamics measured. This would agree that cell cycle and apoptosis regulation are distinct processes, at least in terms of Bcl-XL in non-cancerous cells. However, Bcl-XL is overexpressed in our system and as such, may be masking more subtle changes occurring in Bcl-XL dynamics between different stages. Measuring dynamics after the addition of 4-OHT may highlight more subtle differences present, however there was not time to carry out these experiments within the timeframe of this thesis.

As pro- and anti-apoptotic proteins are known to bind to each other to regulate apoptosis, we questioned whether removal of individual BH3 proteins would alter the balance of the remaining proteins. Using CRISPR-Cas9 we created two MCF10A Bad knockout cell lines containing BadER^{Tam}-GFP-Bcl-XL. Whilst there were no significant differences in Bcl-XL dynamics between the WT and knockout cell lines,

there did appear to be subtle differences when examining all data points together. Under stress-free conditions both knockout cell lines lacked any cells with particularly high levels of priming, of which there were a small number in the WT cells. As all three cell lines are overexpressing Bcl-XL, a large amount of the protein would be expected to be very mobile within the cell, and thus may mask subtle differences between conditions. Any outlying cells with particularly stable Bcl-XL in the WT line could be due to stabilisation at the OMM from endogenous Bad. Due to a lack of Bad in the KO cells, these cells are no longer present. Furthermore, post-4OHT treatment (and thus after sequestration of excess levels of Bcl-XL) both knockout lines had a small proportion of cells with particularly low levels of apoptotic priming. Due to the lack of Bad to prime these cells, Bcl-XL is still mobile. As knockout mice cell lines develop normally[150], this suggests there may be some functional redundancy between Bad and other BH3 proteins, and so perhaps only cells at the furthest ends of the priming spectrum, or cells primed by Bad-specific pathways may be affected by a lack of Bad protein.

Serum starvation of WT and Bad KO cells did not reveal any differences between both cell lines in Bcl-XL dynamics even though Bad is known to contribute to regulating apoptosis via direct interaction with Bcl-XL under serum-free conditions. Previous experiments examining this interaction were carried out in cells transiently overexpressing both Bcl-XL and Bad[340]. Apoptosis was measured via caspase-3 activation in these experiments and thus how apoptosis is regulated before MOMP is not known. As with FUCCI FRAP experiments, the excess concentration of Bcl-XL in our experimental setup could mask any changes that may occur when the proteins are expressed at more endogenous levels. This could also be true for Bim KD experiments where again, no differences were seen. Many of these assumptions are only taking into consideration the Bcl-2 family proteins themselves and how they regulate apoptotic outcome between inter-family interactions. O'Neill and colleagues developed an "OctaKO" cell line in which Bid, Bim, Puma, Bad, Noxa, Bik, Hrk and Bmf had been removed, and these cells were still able to undergo Bax/Bak-mediated apoptosis upon the removal of Bcl-XL and Mcl-1[208]. This suggests that pro-apoptotic Bcl-2 family proteins alone are not the sole regulator of apoptosis, and therefore knocking out or reducing levels of only one or two may not have a significant impact on Bcl-XL dynamics. As discussed earlier, mitochondria themselves play a crucial role in apoptotic regulation as this is the site of the "point of no return" in the apoptotic pathway, and Bcl-2 family proteins associate with the

OMM during fission and fusion. Exactly if and how mitochondria regulate Bcl-2 protein-protein interactions and retrotranslocation dynamics is not fully understood, but may contribute to the heterogeneity in apoptotic outcome of a population of cells.

6. Using proximity biotin labelling to investigate the wider Bcl-2 interactome

6.1 Introduction

Studies over the past 20 years have demonstrated that the regulation of apoptosis via Bcl-2 family proteins is a complex and dynamic process. Understanding the intricacies of how an apoptotic cell fate is reached in non-transformed, healthy cells is crucial for subsequently understanding how a cancer cell's apoptotic signalling is disrupted. In particular, what regulates heterogeneity in the apoptotic response of a population of cells to a pro-apoptotic stimulus is still unclear. To date, the majority of literature has focussed on interactions between the Bcl-2 family proteins themselves, and how their interactions with one another between cytosol and mitochondria set the apoptotic threshold. However, the subcellular localisation of Bcl-2 proteins is crucial in determining apoptotic outcome[350] and as such, what factors regulate the localisation of Bcl-2 proteins at the OMM may play an important role in regulating apoptotic heterogeneity. There is evidence demonstrating that, when localised to the OMM, Bax forms part of complexes of up to 200kDa when not in its active conformation[128]. Bad can also form complexes of a similar size with glucokinase and other proteins at the OMM as part of glycolysis and apoptosis regulation[156]. This may, at least partly, explain why ABT-737 does not seem to fully recapitulate the function of endogenous Bad – if interaction with other proteins in a larger complex is required for apoptosis initiation, ABT-737 may not have the ability to form these complexes. A role for these complexes in regulating apoptosis is exemplified as cells deficient in all BH3 proteins can still undergo Bax/Bak-mediated apoptosis when Bcl-XL and Mcl-1 are inhibited, suggesting that other factors present at the OMM can initiate Bax/Bak-dependent MOMP[208]. What these complexes are comprised of, and what specific role they play in regulating the mechanism of Bcl-2 protein dynamics is not completely understood.

Previous experiments aimed at identifying novel interactors of Bcl-2 family proteins utilised techniques such as co-immunoprecipitation assays or native PAGE gels. An issue with these methods is that they require the use of detergents to extract membrane-embedded proteins, which can induce artificial interactions or disrupt genuine ones[209]. Live cell microscopy techniques such as FRAP[281] and FRET[351] are

advantageous in that they examine protein-protein interactions within the context of a live cell, however this requires the proteins of interest to be fluorescently tagged and thus they are inadequate for identifying novel protein-protein interactions. We therefore decided to use a biotin proximity labelling assay termed “BioID” which has been used previously in our laboratory to identify novel interacting partners of Bcl-2 proteins such as Bid[352]. Based on other work in our laboratory which identified that Bid phosphorylation during prolonged mitosis increased apoptotic priming[172], BioID was used to examine proteins which were responsible for regulating this phosphorylation during mitosis. This approach identified a number of non-canonical candidate proteins outwith the Bcl-2 family including the mitochondrial porin VDAC2. Knocking out VDAC2 in HeLa cells increased the propensity of cells to undergo mitotic slippage over apoptosis when treated with Taxol, thus identifying VDAC2 as a regulator of dynamic changes in apoptotic priming in mitosis.

The BioID system utilises an *E.coli* biotin ligase, BirA, modified with a R118G substitution (referred to as BirA*) fused with the protein of interest (the “bait”)[353] (Fig. 6.1A). In the presence of excess Biotin added to culture medium, BirA* binds biotin and ATP to produce biotinyl-5’-AMP (termed “reactive biotin”). Reactive biotin can biotinylate proteins on primary amines within a range of approximately 10nm. By fusing BirA* to a protein of interest and incubating with biotin, any proteins in close-proximity over the labelling period are biotinylated (Fig. 6.1B). Labelled proteins can then be isolated via streptavidin affinity purification and identified by mass spectrometry analysis. This particular approach has shown to be successful in identifying novel protein complexes in centrioles[354], the inner nuclear membrane[355] and focal adhesions[356]. We therefore wanted to use this approach to identify potential novel proteins interacting with Bcl-XL, to try and understand more fully what regulates its dynamics between mitochondria and cytosol.

6.2 Identification of Bcl-XL-interacting proteins using BioID

An experiment had previously been carried out using BioID to identify novel interactors of Bcl-XL, which we wished to then knockout individually using CRISPR-Cas9, and examine what effect this has on Bcl-XL dynamics. We designed an assay using BioID in which Bcl-XL was used as the bait protein. Cells expressing

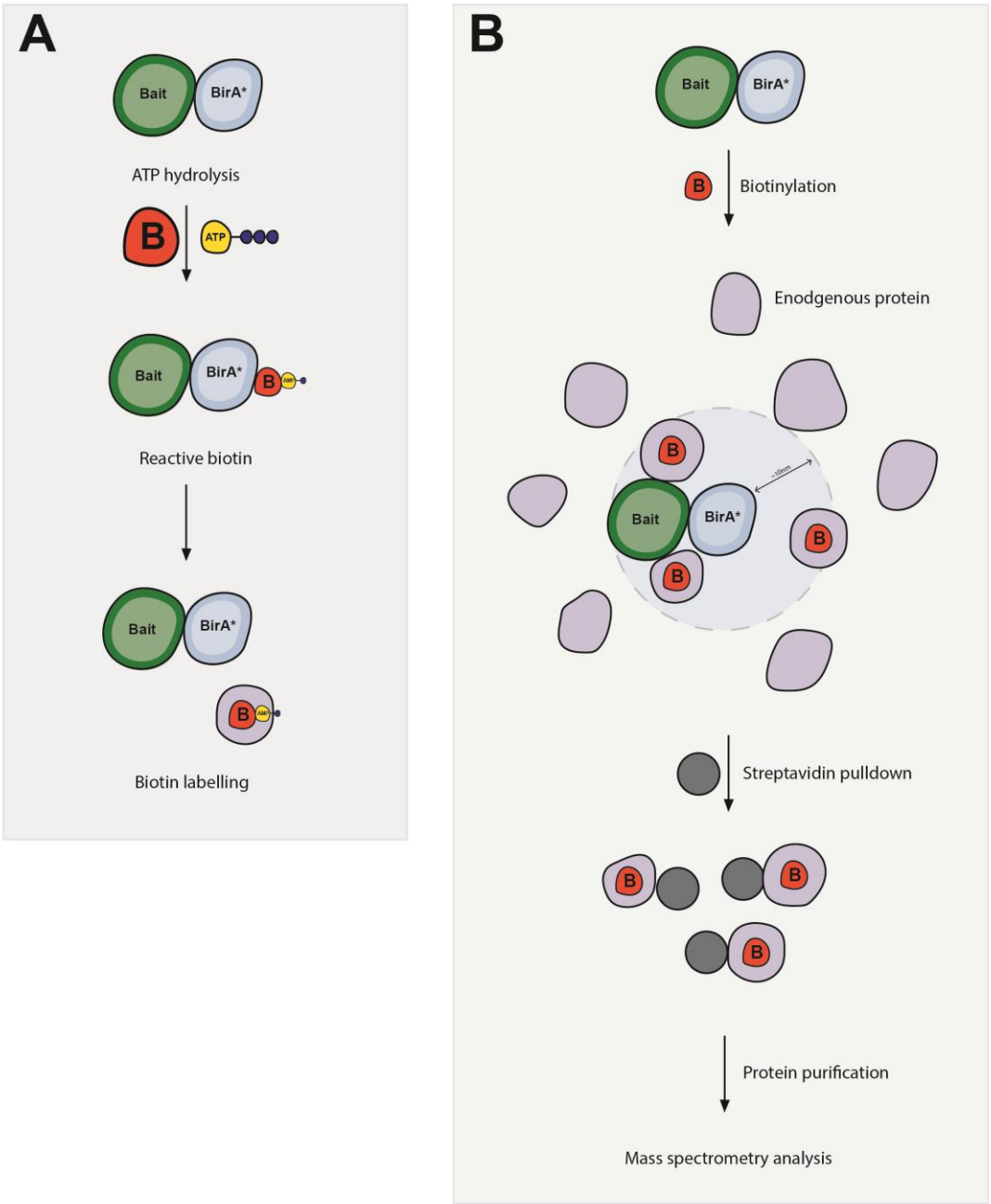

Figure 6.1 Schematic of the BioID BirA* labelling mechanism

A. BirA* is fused to a protein of interest (the "bait"). In the presence of biotin and ATP, the BirA* active site binds both biotin and ATP, hydrolysing ATP into AMP which subsequently covalently bonds to biotin. The now "reactive biotin" is briefly held in the BirA "holding site" before being released. Reactive biotin can then biotinylate nearby proteins via covalent bonding on primary amine residues. Due to the short half-life of reactive biotin, only proteins in close proximity will be labelled.

B. Schematic of experimental setup. Cells containing the bait protein fused to BirA* are incubated with excess biotin overnight to allow labelling of close-proximity endogenous proteins. As biotin binds with high affinity to streptavidin, labelled proteins can be purified using streptavidin beads. Proteins are then purified, digested and sent for mass spectrometry analysis.

BirA*Bcl-XL were cultured with biotin to induce labelling overnight and any proteins in close-proximity to Bcl-XL, either in the cytosol or on the OMM were labelled. To account for non-specific background interactions, BirA*Venus was used as a control. Two constructs were cloned containing either a myc-tagged BirA* fused to Bcl-XL, separated from a tagBFP fluorophore by a T2A sequence, or the same construct with Venus in place of Bcl-XL (Fig. 6.2A). Lentiviruses containing each construct were created and stably expressing MCF10A cell lines were generated. MCF10A cells were stably transduced with either construct and FACS sorted for low expression levels (data not shown). Assays were set up in triplicate in which the stable BirA* MCF10A cells were incubated with biotin overnight and labelled proteins isolated via streptavidin pulldown. Labelled proteins were then purified and sent for mass spectrometry analysis. Raw data was then analysed using MaxQuant[267] against the human proteome and principal component analysis carried out to ensure consistency between replicates before using SAINTexpress to identify interacting prey[268]. SAINT (Significance Analysis of INTeractome) is a statistical tool used to separate genuine bait-prey interactions from false positives. SAINT analysis identified 1249 enriched proteins compared to the BirA*Venus control experiments (Fig. 6.2B). A list of proteins considered significantly enriched based on the Benjamini-Hochberg false discovery rate corrected p-value (BHFDR) are shown in Table 6.1.

Interestingly, only two Bcl-2 family proteins – Bax and Bcl-Rambo - were identified. We hypothesised that this could be explained as the cells were labelled in an unprimed, healthy state, and as such any interactions with Bcl-2 family proteins were most likely very transient. We chose to focus on the 16 most significantly enriched proteins ($p<0.001$) to prioritise for further investigation. Among these, 10 were identified as localising to mitochondria (highlighted in Table 6.1). As mitochondrial proteins are likely to regulate Bcl-2 protein binding at the OMM and may therefore have a role in Bcl-XL retrotranslocation regulation, we chose to examine these in more detail to establish potential candidates to investigate further.

There were multiple mitochondrial proteins enriched that have previously been identified to interact with Bcl-XL specifically, or other members of the Bcl-2 family proteins. Drp1 is a cytosolic GTPase that can translocate to mitochondria via interaction with the OMM receptor MFF, where it couples GTP hydrolysis with

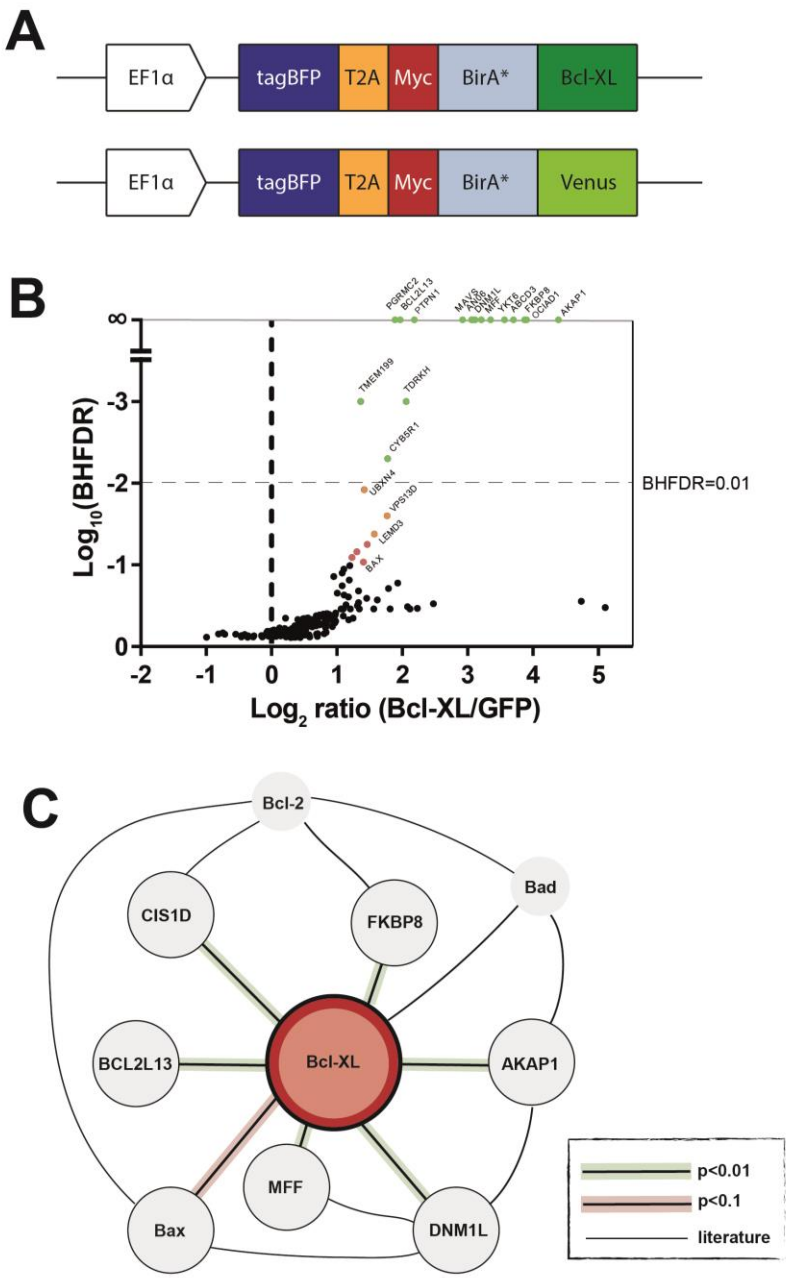

Figure 6.2. Results from Bcl-XL BioID mass spectrometry

A. Schematic of BirA* constructs expressed in cells used for BioID. Under the EF1α promoter, tagBFP is fused to Bcl-XL via a T2A self-cleaving sequence. This allows FACS sorting of stable cells and normalisation of expression levels. BirA* is fused to the N-terminus of Bcl-XL, which itself is fused to a Myc-tag. As a control for non-specific interactions, Bcl-XL is replaced with Venus.

B. Results from mass spectrometry displayed as a volcano plot. Data shows the mean ratio of biotinylated protein abundance for Bcl-XL versus Venus control. A positive ratio indicates enrichment in the Bcl-XL sample. Green values represent p<0.001, orange values represent p<0.05, red values represent p<0.1

C. Diagram summarising the significantly enriched proteins, highlighting the highly enriched proteins from SAINT analysis and interactions between these proteins identified from previous literature.

Gene name	Description/protein name	Log_2 fold change	BHFDR
DNM1L	**Dynamin 1-like (DRP1)**	**3.21**	**0**
YKT6	Synaptobrevin homolog YKT6	3.56	0
PTPN1	Tyrosine-protein phosphatase non-receptor type 1	2.18	0
ABCD3	ATP-binding cassette sub-family D member 3	3.70	0
FKBP8	**FK506 binding protein 8**	**3.87**	**0**
ANO6	Anoctamin 6	3.12	0
AKAP1	**A-kinase anchor protein 1**	**4.39**	**0**
MFF	Mitochondrial fission factor	3.35	0
OCIAD1	OCIA domain containing 1	3.90	0
CISD1	CDGSH iron sulfur domain 1	3.08	0
TDRKH	Tudor and KH domain-containing protein	2.06	0
PGRMC2	Progesterone receptor membrane component 2	1.89	0
EXD2	Exonuclease 3'-5' domain-containing protein 2	2.92	0
BCL2L13	BCL2 like 13 (Bcl-Rambo)	1.97	0
MAVS	Mitochondrial antiviral-signaling protein	3.06	0
TMEM199	Transmembrane protein 199	1.37	0.001
CYB5R1	NADH-cytochrome b5 reductase 1	1.78	0.005
UBXN4	UBX domain protein 4	1.42	0.012
VPS13D	Vacuolar protein sorting 13 homolog D	1.77	0.025
LEMD3	LEM domain containing 3	1.57	0.042
ZC3HAV1	Zinc finger CCCH-type containing, antiviral 1	1.46	0.056
VRK2	VRK serine/threonine kinase 2	1.31	0.069
PEX11B	Peroxisomal biogenesis factor 11 beta	1.23	0.081
BAX	BCL2 associated X, apoptosis regulator	1.41	0.092

Table 6.1 Significantly enriched proteins in Bcl-XL BioID screen

Significantly enriched proteins identified from SAINT analysis of BirA*Bcl-XL mass spectrometry data. Highlighted proteins are known to localise to mitochondria. Proteins in bold have been previously associated with Bcl-XL from literature. BHFDR of 0 indicates $p<0.001$ due to rounding.

regulation of mitochondrial fission[357,358]. Drp1 knockout mice are embryonic lethal due to developmental defects in the brain[359,360] and downregulation of Drp1 has been shown to inhibit mitochondrial fragmentation and has also shown partial inhibition of cytochrome c release during apoptosis[361]. Whilst MFF has no direct associations with Bcl-2 family proteins, Drp1 co-localises with Bax[134] and Bcl-XL in neurons[362] during mitochondrial fission. Furthermore, Drp1 has also been identified as a key substrate of AKAP1[363,364]. This suggests that Bcl-XL, AKAP1 and Drp1 may function together at the OMM (Fig. 6.2C). AKAP1 is a scaffold protein involved in recruitment of signalling molecules such as protein kinase A (PKA) to the OMM[365–367]. PKA is a serine-112-specific Bad kinase and thus promotes cell survival[368] demonstrated in neurones where overexpression of AKAP1 decreases serum-starvation-induced apoptosis by phosphorylating and inhibiting pro-apoptotic Bad[369]. AKAP1 overexpression in hippocampal neurones has been shown to promote mitochondrial elongation and cell survival through regulation of Drp1[363]. Conversely, AKAP1 knockdown in hippocampal neurones promotes mitochondrial fragmentation and increases levels of apoptosis. The effect of AKAP1 on other Bcl-2 family proteins, including Bcl-XL, in other tissues has not been well characterised.

FK506-binding protein 38 (FKBP8) is a peptidyl-prolyl *cis-trans* isomerase which catalyses the rate-limiting protein folding step at peptidyl bonds preceding proline residues[370,371]. FKBP8 is predominantly localised to mitochondria, and is activated in the presence of calcium-bound calmodulin[370,372]. Previous studies suggest that FKBP8 acts as a Bcl-2 inhibitor via direct binding[373]. However, FKBP8 has also been shown to co-localise at mitochondria with Bcl-2 and Bcl-XL, and when downregulated, causes an increase in levels of apoptosis in mammalian cells[374]. FKBP8 is a Bcl-2 and Bcl-X[375] chaperone and forms larger complexes with calcium and calmodulin at the OMM[373,376]. The CDGSH iron-sulfur domain-containing protein 1 (CISD1) is also primarily localised to mitochondria where it inhibits ferroptosis by preventing mitochondrial iron uptake and lipid peroxidation[377]. It has also been shown to bind to Bcl-2 at the ER to inhibit anti-apoptotic function, and can be displaced by Bik[378,379]. There is currently no evidence of any direct interaction with Bcl-XL.

As Bcl-Rambo was the only Bcl-2 family protein identified other than Bax, this was also selected for further investigation. Bcl-Rambo is a potential pro-apoptotic

member of the Bcl-2 family containing all four BH4 domains and a unique 250 amino acid sequence (BHNo domain) upstream of its C-terminal transmembrane domain[380]. Interestingly, Bcl-Rambo does not require its BH3 domains to initiate apoptosis, but does require mitochondrial localisation via its transmembrane domain[381] where it can regulate mitochondrial fission in the absence of Drp1[382]. Furthermore, it has been suggested that Bcl-Rambo does not directly interact with other Bcl-2 family proteins to induce apoptosis, but rather interacts with the adenine nucleotide translocator to induce the mitochondria permeability transition pore (MPT). The involvement of Bcl-XL in the induction of OMM permeabilisation by Bcl-Rambo is unknown.

From this list of interacting proteins, candidates were selected and targeted for knockout using CRISPR-Cas9. Due to previous evidence from the literature we chose to target Drp1 and AKAP1, as these are known to bind Bcl-XL and are potentially both part of the same complex with Bcl-XL at the OMM. FKBP8 was also selected as it is known to interact with Bcl-XL and also forms part of larger complexes at the OMM. We also selected to target Bcl-Rambo as it was the only Bcl-2 family protein identified other than Bax, and interaction with Bcl-XL has to date not yet been identified. Interactions are summarised in Fig. 6.2C.

6.3 Creating knockout lines from prioritised mass spectrometry candidates

We utilised the CRISPR-Cas9 system to create knockout cell lines of each of the 4 genes identified above. To begin, guides were designed to knockout AKAP1 by targeting exon 9 - the first coding exon in the AKAP1 gene (Fig. 6.3A). These guides were cloned into a pX458 vector in which the GFP fluorophore was replaced with mCherry to allow identification of positively transfected BadER^{Tam}-GFP-Bcl-XL MCF10A cells. The MCF10As were transfected with AKAP1KO-mChpX458 and single clones sorted via FACS. Clones were expanded and initially genotyped via PCR. Two clones were identified that had obvious indels when run on an agarose gel (Fig. 6.3B). Both were sequenced to confirm that one clone, clone 8, contained two frameshift mutations, and clone 17 contained one frameshift and one in-frame deletion. Knockout of the AKAP1 protein was subsequently confirmed via Western

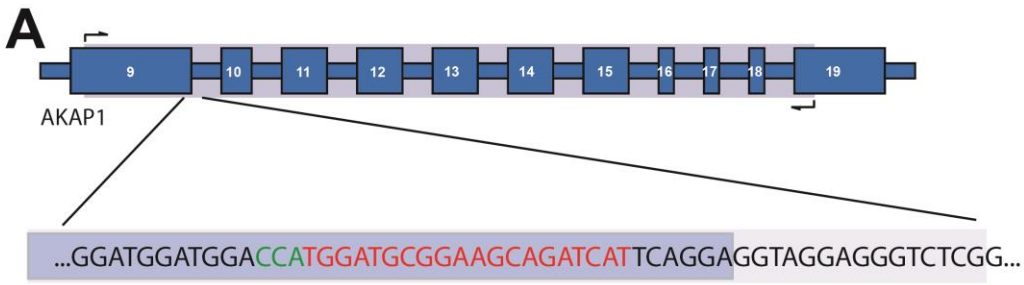

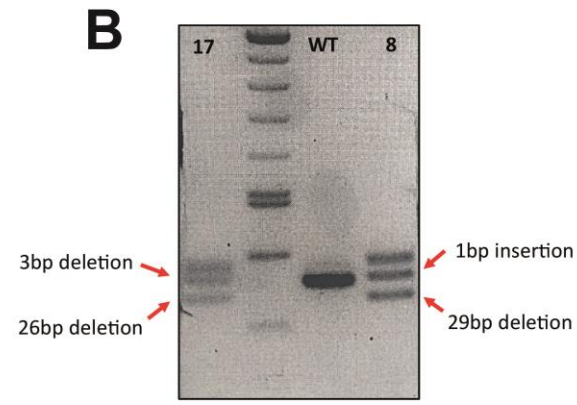

	Clone 8	Clone 17
Allele 1	1bp insertion	3bp deletion
Allele 2	29bp deletion	26bp deletion

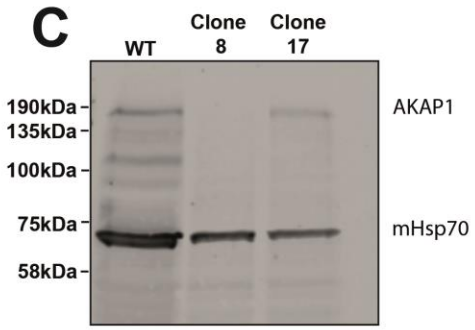

Figure 6.3. Validation of the creation of an AKAP1 knockout MCF10A cell line

A. Schematic of CRISPR targeting site and knockout guide sequence. The AKAP1 gene was targeted in the first coding exon, exon 9. Red text indicates the guide sequence and green text indicates the PAM site.

B. Agarose gel of PCR amplicons of DNA extracted from WT BadER^{Tam}-GFP-Bcl-XL MCF10As and two CRISPR clones. The table below indicates specific indels in the CRISPR clones.

C. Western blot of lysates extracted from the same clones as in B. The membrane was probed against AKAP1 and mHsp70 was used as a loading control.

blot, with clone 8 showing a complete loss of protein, and clone 17 showing decreased expression levels (Fig. 6.3C).

We next targeted Drp1 by designing guides to target exon 2 of the Drp1 gene (Fig. 6.4A). As with AKAP1 KO CRISPR cell line generation, the guides were cloned into mChpX458 and positively transfected cells were FACS sorted into single clones. Clones were then expanded, and genomic DNA extracted for PCR genotyping. Agarose gel electrophoresis of extracted genomic DNA revealed four clones that appeared to have acquired indels, which were subsequently sequenced (Fig. 6.4B). Unfortunately, sequencing revealed that all clones contained either one or two indels containing a non-frameshift mutation and therefore no complete knockout clones. As an alternative to creating a knockout in MCF10As, MEFs which had previously been edited to produce a Drp1 knockout line were used for subsequent analysis (gifted from Tomomi Kuwana, La Jolla Institute for Immunology).

Finally, guides were designed targeting the second coding exon of the FKBP8 gene, exon 6 (Fig. 6.5A) and upstream of the start codon of Bcl-Rambo in exon 4 (Fig. 6.5C). The guides were cloned into mChpX458, transfected into BadER^{Tam} GFP-BclXL-MCF10As, and FACS sorted as above. In total, 4 clones were successfully expanded from the FKBP8 transfection and screened for edits via PCR, however no indels were present (Fig. 6.5B). 24 BCL2L13 potential KO clones were examined, none of which had any obvious indels evident from agarose gel electrophoresis (Fig. 6.5D). It was apparent that the current CRISPR-Cas9 method for creating knockout cell lines was inefficient, with few clonal populations surviving post-FACS sort, and very low DNA editing efficiency. A more high-throughput methodology is required to efficiently target candidate genes for further assay, but optimisation of such techniques was not possible within the scope of this thesis.

6.4 AKAP1 does not significantly regulate Bcl-XL mitochondrial localisation or dynamics

After confirmation that an AKAP1 knockout line had been successfully created, we next wanted to determine whether a lack of AKAP1 would have any effect on the

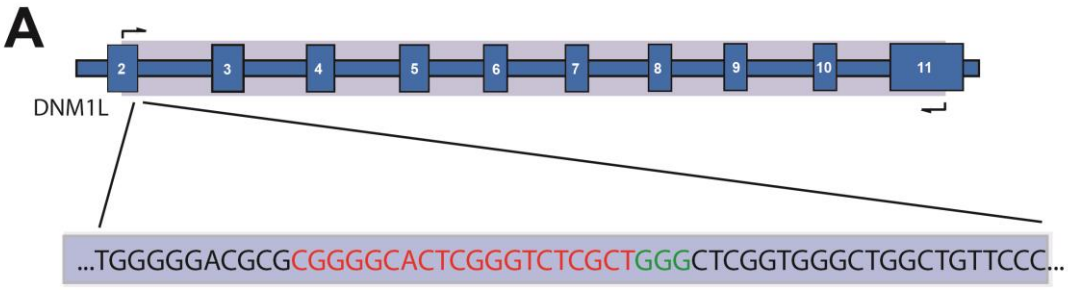

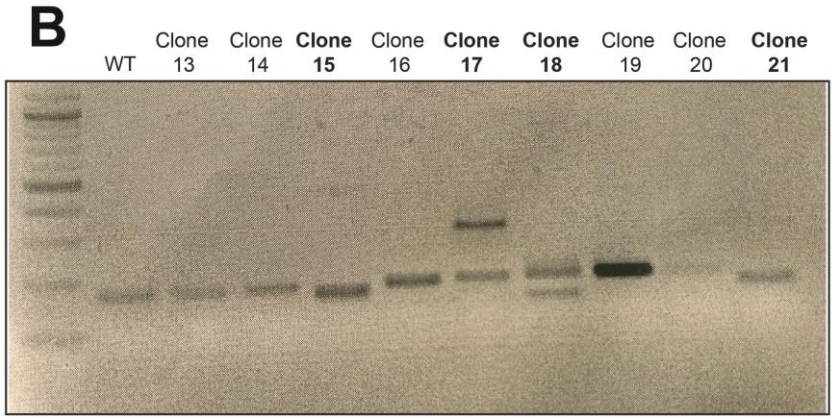

	Clone 15	Clone 17	Clone 18	Clone 21
Allele 1	WT	WT	WT	14bp deletion
Allele 2	13bp deletion	120bp insertion	36bp deletion	18bp deletion

Figure 6.4. Unsuccessful attempt to create a Drp1 knockout MCF10A cell line
A. Schematic of CRISPR targeting site and guide sequence. The *DNM1L* gene was targeted in the first coding exon, exon 2. Red text indicates the guide sequence and green text indicates the PAM site.
B. Agarose gel of PCR amplicons of DNA extracted from WT BadER^{Tam}-GFP-Bcl-XL MCF10As and nine CRISPR clones. The table below indicates specific indels in four of the CRISPR clones.

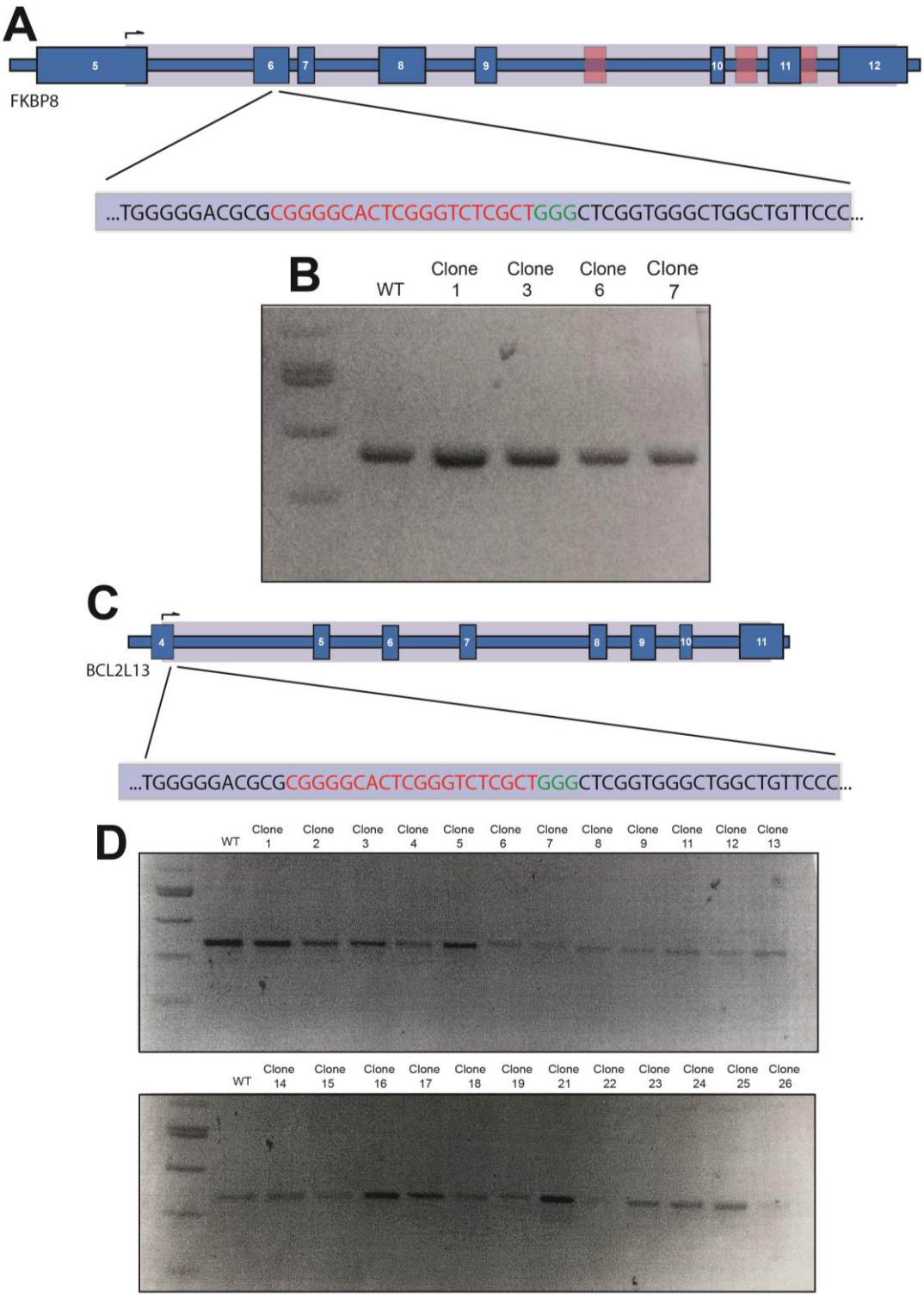

Figure 6.4 Unsuccessful attempt to create an FKBP8 and BCL2L13 knockout MCF10A cell line

A. Schematic of CRISPR targeting site and guide sequence. The FKBP8 gene was targeted in the second coding exon, exon 6. Red text indicates the guide sequence and green text indicates the PAM site. Red boxes indicate a long non-coding RNA sequence running antisense.

B. Agarose gel of PCR amplicons of DNA extracted from WT BadER^{Tam}-GFP-Bcl-XL MCF10As and four CRISPR clones.

C. Schematic as in A of BCL2L13 CRISPR guides targeting the first coding exon, exon 4.

D. Agarose gels as in B of BCL2L13 amplicons extracted from WT cells and CRISPR 24 clones.

mitochondrial localisation of Bcl-XL. As AKAP1 is a key substrate of Drp1 in neurons[362], a lack of AKAP1 would therefore potentially alter mitochondrial morphology and thus affect the localisation of Bcl-XL at the OMM. Immunofluorescence was carried out on wildtype, AKAP1$^{-/-}$ and AKAP1$^{-/+}$ MCF10A cells to determine if any changes in mitochondrial morphology or Bcl-XL localisation were evident (Fig. 6.6). There were no obvious differences in mitochondrial morphology or Bcl-XL localisation between WT, AKAP1$^{-/+}$ or AKAP1$^{-/-}$ MCF10A cells.

To further investigate whether AKAP1 has any role in the regulation of Bcl-XL, we determined whether knocking out AKAP1 had any effect on the dynamics of Bcl-XL in live cells. WT, AKAP1$^{-/+}$ or AKAP1$^{-/-}$ BadER^{Tam}-GFP-Bcl-XL MCF10A cell lines were subjected to FRAP analysis (Fig. 6.7A). Neither the knockout nor heterozygous cell lines showed any significant differences in overall levels of priming or cell-to-cell variation in Bcl-XL dynamics (Fig. 6.7B & 6.7C). As Bcl-XL was overexpressed in BadER^{Tam}-GFP-Bcl-XL MCF10A cells, it was possible that any subtle differences in the dynamics of Bcl-XL may have been masked by the high levels of Bcl-XL expression within the cells. To determine whether lowering this would reveal any differences between WT and AKAP1 KO cells, an siRNA targeting BadER^{Tam} was used to knockdown Bcl-XL expression levels. This siRNA had been originally designed to target endogenous human Bad but instead effectively targets BadER^{Tam} and has been described in Chapter 5. We therefore utilised this siRNA to reduce expression levels of Bcl-XL before carrying out FRAP analysis (Fig. 6.8A). Even after lowering expression levels, no significant differences in overall levels of priming were evident (Fig. 6.8B). An interesting observation was made, however, that although there was no significant difference in priming, the mean Bcl-XL translocation rates were much more consistent between experimental repeats within the AKAP1 KO line compared to the WT cells. This trend was also evident when analysing the variation in Bcl-XL dynamics between cell lines (Fig. 6.8D). Where the apoptotic threshold of a population of cells is set varies over time. This FRAP data potentially suggests that, whilst average levels of priming and cell-to-cell variation in priming are not significantly altered in the absence of AKAP1, the ability of the population of cells to adjust their baseline level of priming over time may be compromised, causing the average Bcl-XL FRAP dynamics of a population to become more consistent between experimental repeats. Analysing FRAP dynamics over longer timeframes may reveal whether this is indeed the case.

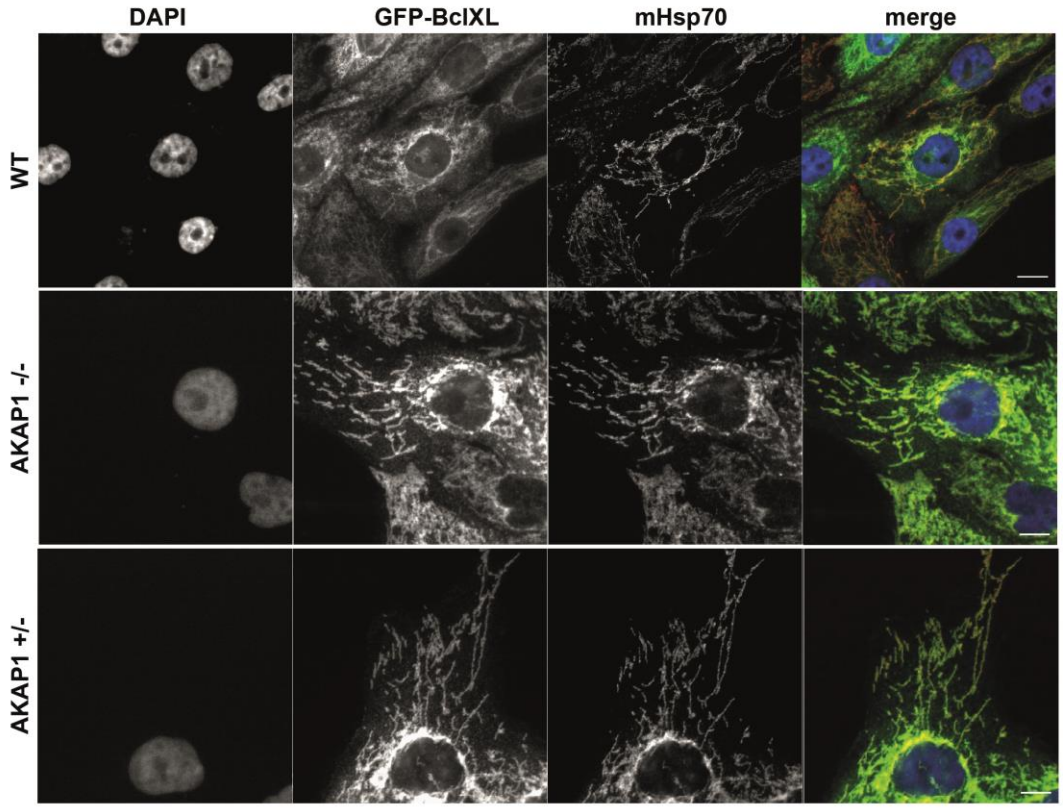

Figure 6.7. AKAP1 knockout has no obvious effect on mitochondrial morphology or Bcl-XL localisation

Immunofluorescence images of WT, AKAP1$^{+/-}$ and AKAP1 KO BadER^{Tam} -GFP-Bcl-XL cells stained for GFP and mHsp70. Scale bar represents 20µm.

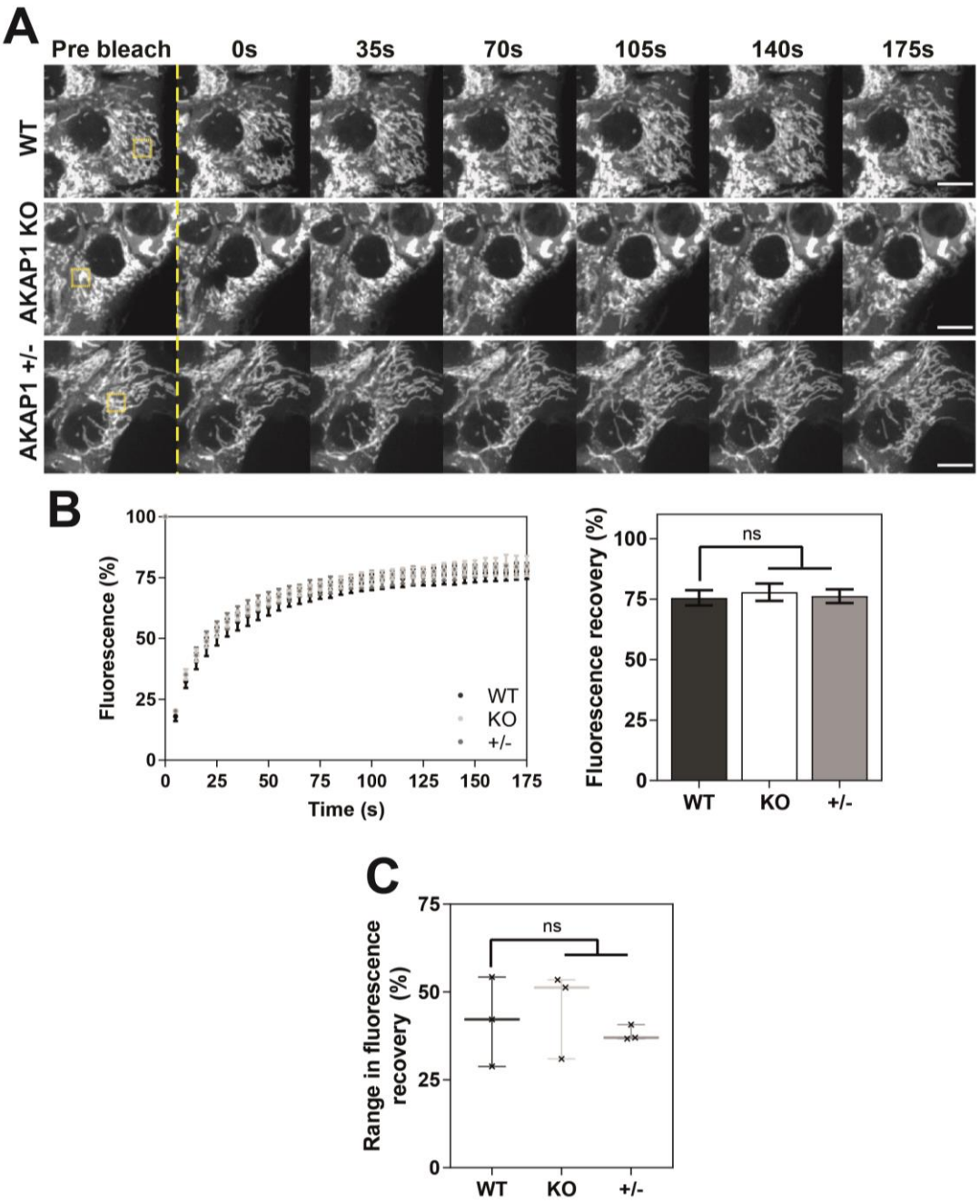

Figure 6.7. AKAP1 does not regulate Bcl-XL dynamics in Bcl-XL-overexpressing cells
A. Representative images showing FRAP analysis carried out on WT, AKAP1$^{+/-}$ and AKAP1KO BadER^{Tam}-GFP-Bcl-XL MCF10A cells. The ROI within the yellow box was photobleached for 10ms using a 488nm laser, and the recovery of fluorescence in the same area measured over time. Images were taken every 5 seconds. Scale bars represent 10µm.
B. Recovery of fluorescence was plotted over time and non-linear regression carried out to calculate the average fluorescence recovery for each cell line. Data was analysed via ANOVA and values represent data from 3 independent experiments, n=120 cells. Error bars represent SD.
C. The range in GFP-Bcl-XL fluorescence recovery was calculated for each experimental repeat from B and each value plotted. Data was analysed via ANOVA.

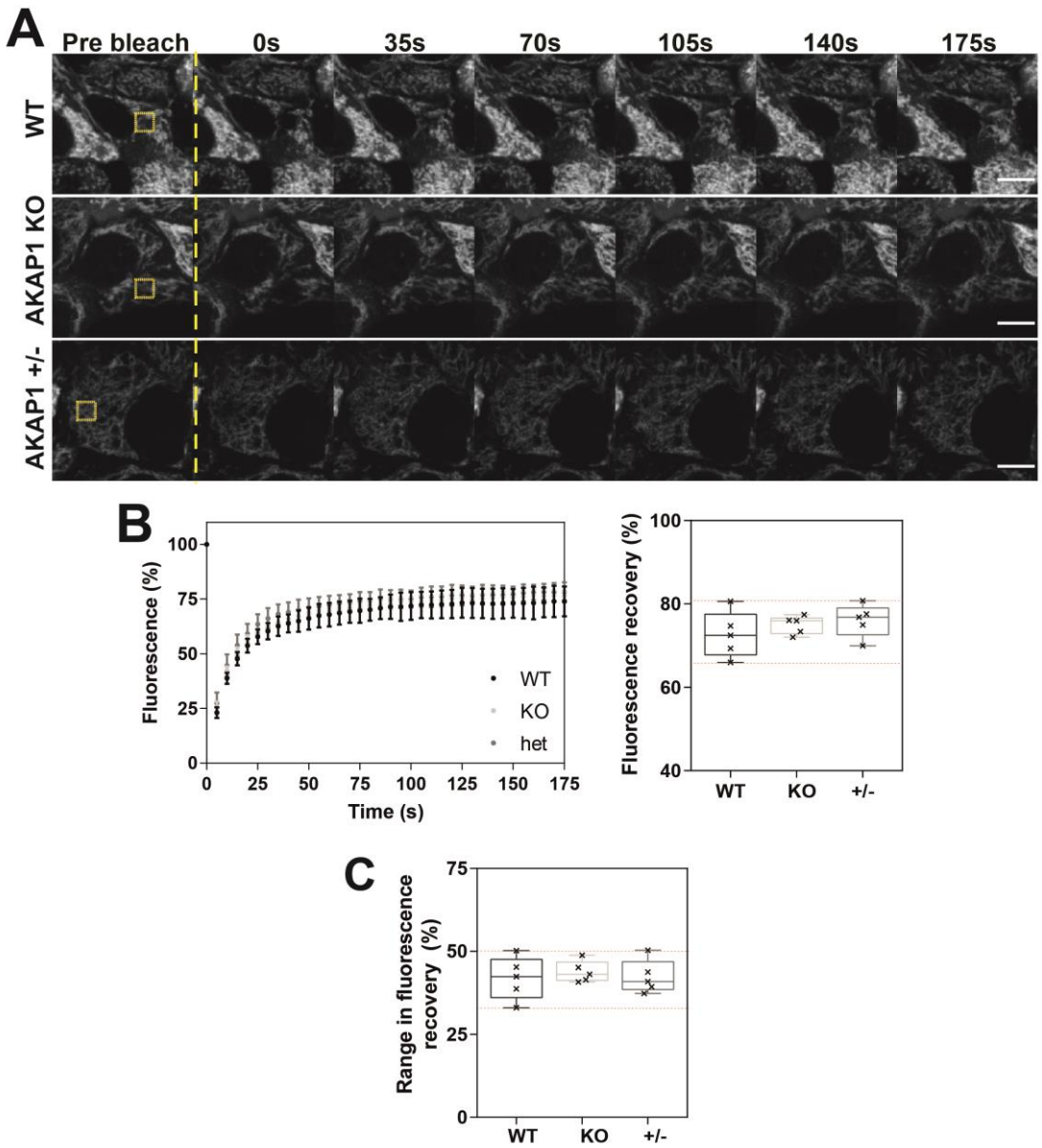

Figure 6.8. AKAP1 does not significantly affect Bcl-XL dynamics in lower expressing cells

A. Representative images showing FRAP analysis carried out on WT, AKAP1$^{+/-}$ and AKAP1KO BadER^{Tam}-GFP-Bcl-XL MCF10A cells after mBad siRNA knockdown. The ROI within the yellow box was photobleached for 10ms using a 488nm laser, and the recovery of fluorescence in the same area measured over time. Images were taken every 5 seconds. Scale bars represent 10µm.

B. Recovery in fluorescence plotted over time and non-linear regression carried out to calculate the average fluorescence recovery for each cell line. Data was analysed via ANOVA and values represent data from 5 independent experiments, n=200 cells per condition. Error bars represent SD.

C. The range in GFP-Bcl-XL fluorescence recovery was calculated for each experimental repeat from B and each value plotted. Data was analysed via ANOVA.

6.5 Drp1 does not regulate Bcl-XL dynamics in MEFs

As AKAP1 KO showed very subtle changes in Bcl-XL dynamics, we next examined the effect of a lack of the mitochondrial fission regulator Drp1 on Bcl-XL in Drp1 knockout MEFs. A lack of Drp1 is known to cause elongated mitochondria[361], so we began by carrying out immunofluorescence analysis to confirm this mitochondrial morphology in the knockout cell lines (Fig. 6.9A). As expected, the Drp1 knockout MEF line appeared to have elongated mitochondria compared to WT MEFs. To examine if altered mitochondrial morphology affected Bcl-XL localisation, WT and Drp1KO MEFs were transiently transfected with a GFP-Bcl-XL vector and immunofluorescence carried out (Fig. 6.9B). There were no obvious differences in GFP-Bcl-XL localisation evident between WT and Drp1KO MEFs.

To determine the effect of Drp1 knockout on Bcl-XL dynamics in live cells, WT and Drp1KO MEFs transiently expressing GFP-Bcl-XL were subjected to FRAP analysis (Fig. 6.10A). There was no significant difference in overall levels of Bcl-XL translocation between WT and Drp1KO cells (Fig. 6.10B). There was also no difference in the average levels of cell-to-cell variation in Bcl-XL dynamics between WT and Drp1KO cells, although the knockout cell line did trend towards having less cell-to-cell variation (Fig. 6.10C). These data suggest that, although in close-proximity to Bcl-XL, Drp1 is likely not a direct regulator of Bcl-XL dynamics in healthy cells. As cells were transiently expressing Bcl-XL, overall expression levels were relatively high, and as such may have been concealing any subtle differences that may have been present. Furthermore, both WT and Drp1KO MEF lines had particularly high mobile fractions of Bcl-XL. Inducing priming either via the BadER^{Tam} lentivirus or an alternative apoptotic stimulus to induce more mitochondrial Bcl-XL may also reveal differences between the cell lines.

6.6 Generation of BioID-Bax MCF10A cell lines for proximity labelling

As the Bcl-XL BioID assay revealed a number of interesting candidate proteins as regulators of Bcl-XL dynamics, we questioned whether we could develop the assay to compare cytosolic versus mitochondrial Bcl-2 protein interactions. A similar assay

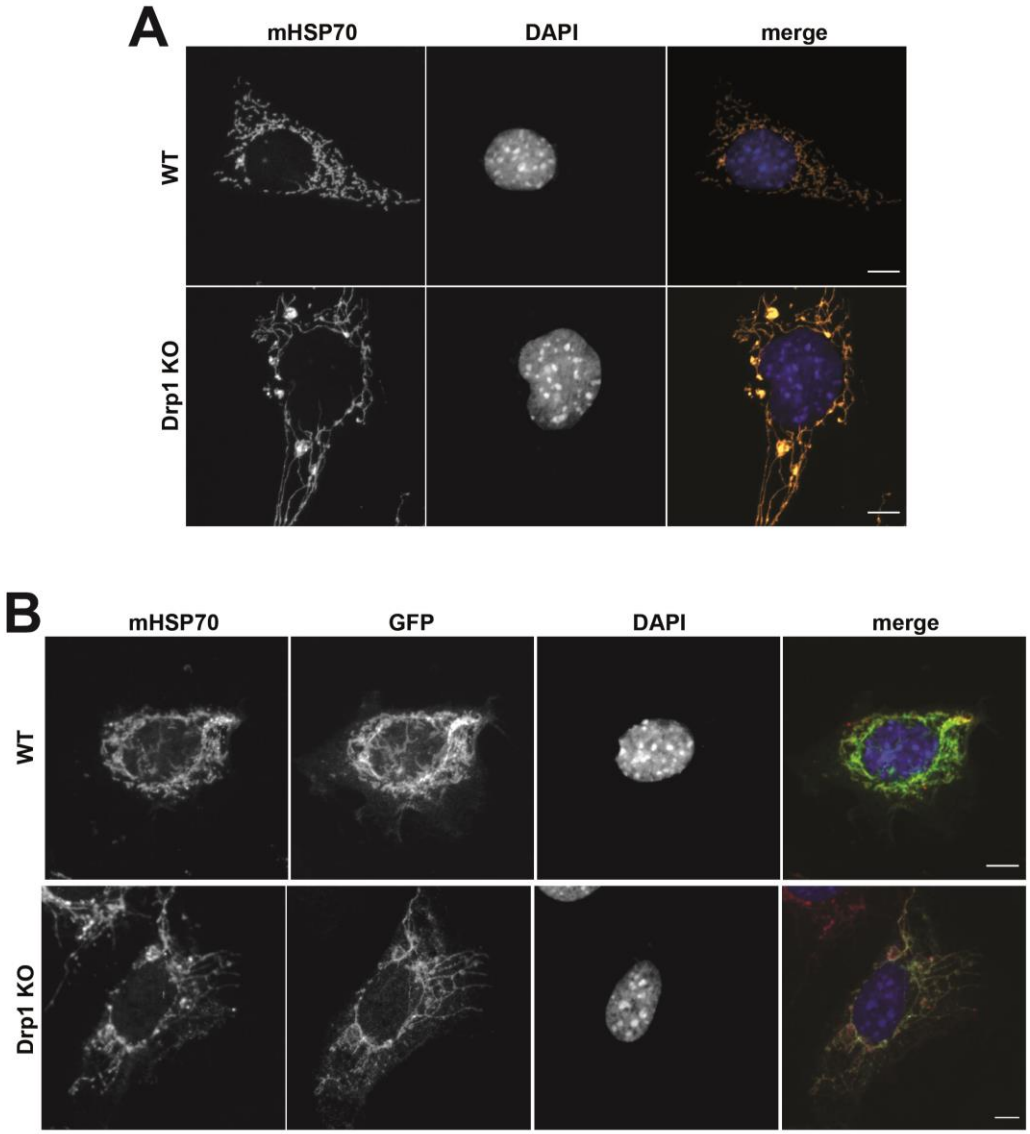

Figure 6.9. Drp1KO MEF appear to have elongated mitochondria which do not affect Bcl-XL localisation

A. Immunofluorescence images of WT and Drp1 KO MEF stained with mHsp70 to visualise mitochondrial localisation. KO cells have elongated mitochondria. Scale bar represents 10µm.

B. Immunofluorescence images of the same cell lines in A transiently transfected with GFP-Bcl-XL and stained for mHsp70 and GFP. Scale bar represents 10µm.

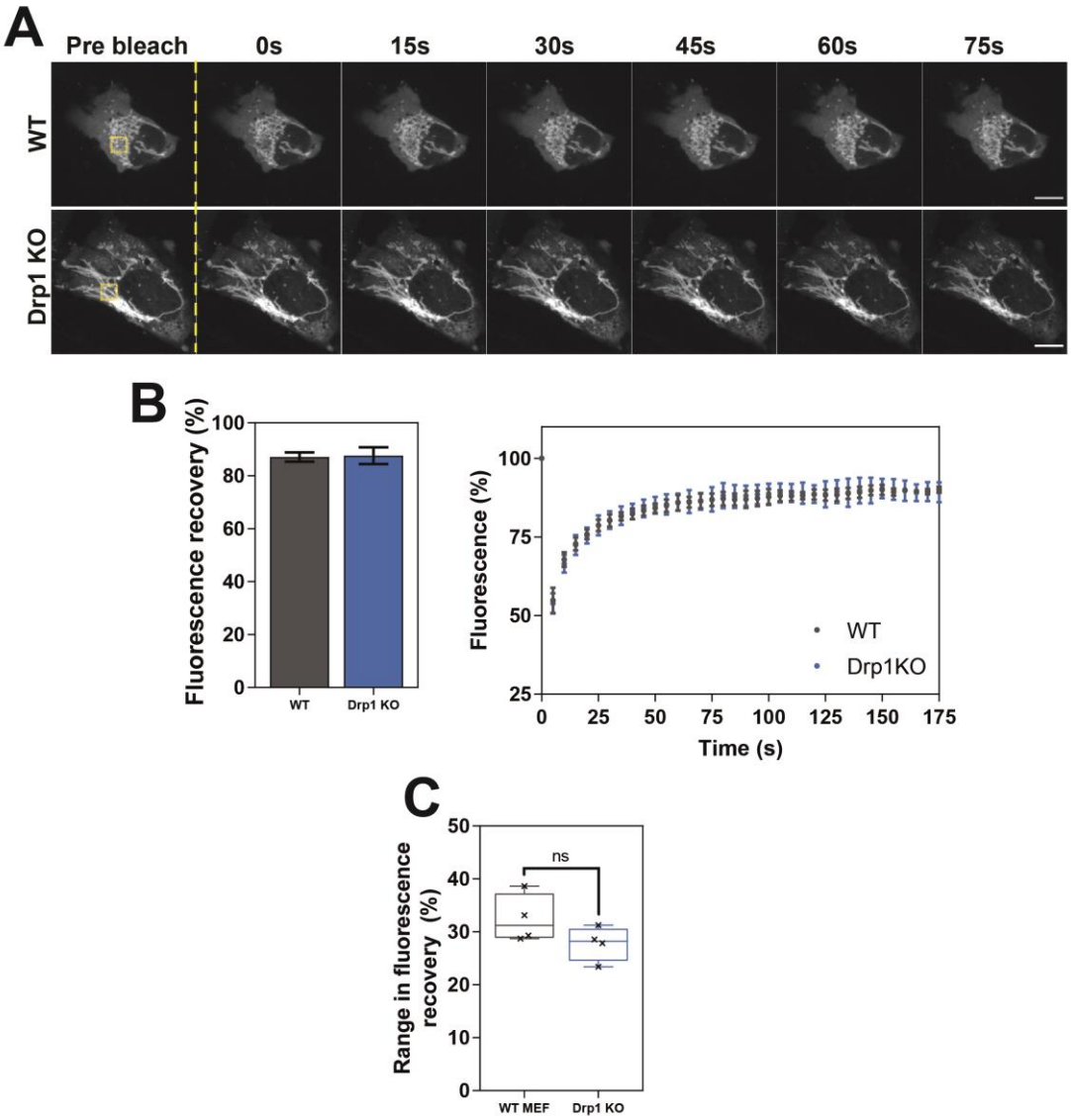

Figure 6.10. Drp1 does not regulate Bcl-XL dynamics

A. Representative images showing FRAP analysis carried out on WT and Drp1KO MEFs transiently expressing GFP-Bcl-XL. The ROI within the yellow box was photobleached for 10ms using a 488nm laser, and the recovery of fluorescence in the same area measured over time. Images were taken every 5 seconds. Scale bars represent 10µm.

B. Recovery in fluorescence plotted over time and non-linear regression carried out to calculate the average fluorescence recovery for each cell line. Data was analysed via ANOVA and values represent data from 4 independent experiments, n=100 cells per condition. Error bars represent SD.

C. The range in GFP-Bcl-XL fluorescence recovery was calculated for each experimental repeat from B and each value plotted. Data was analysed via Student's t-test.

was carried out in our laboratory examining BirA*Bax interactions in MCF10A cells, that showed enrichment of a mix of cytosolic and mitochondrial proteins (Robert Pedley, unpublished data). As Bax is a highly dynamic protein with a mainly cytosolic localisation, interactions with the OMM are relatively transient. We wondered if we could utilise the more mitochondrial S184V Bax that also retrotranslocates from the OMM, but with much slower kinetics, to enrich for mitochondrial proteins[110]. This would allow comparison of the same protein in both an unprimed and primed state, as the S184V Bax mutant increases apoptosis induced via ECM detachment or ABT-737 treatment.

To investigate this, three MCF10A cell lines were produced via lentiviral transduction: one stably expressing the mainly cytosolic BirA*Bax, one expressing the more mitochondrial BirA*S184VBax, and the control VenusBirA* (Fig. 6.11A). The stable lines were sorted via FACS to normalise expression levels relative to the S184V Bax line as this line had the lowest overall levels of tagBFP expression as high expression levels of S184VBax induce apoptosis (Fig. 6.11B). To ensure the Bax variants were localising to the correct cellular compartments, immunofluorescence was carried out on each line (Fig. 6.11C). As expected, BirA*Bax localised between cytosol and mitochondria whereas BirA*S184VBax was more mitochondrial. VenusBirA* was completely cytosolic.

We next wanted to confirm that the BirA* Bax MCF10A cell lines were capable of labelling close-proximity proteins. Each line was seeded so that they were 60-70% confluent 24 hours later. Growth medium was then replaced with medium supplemented with biotin and cells were incubated for 24 hours before replacing with normal growth medium for a minimum of one hour. Cells were then lysed and labelled proteins pulled down overnight using streptavidin beads. Labelled proteins were eluted from the beads and pulldown efficiency examined via SDS-PAGE, with input and flowthrough protein mass normalised to each other (Fig. 6.12). In all three samples there was a visible enrichment of proteins in the elution compared to the flowthrough. Blots were also immunostained for vinculin to ensure normalised loading of input and flowthrough, and to ensure there was no non-specific labelling of proteins, as vinculin is found in focal adhesions and would therefore not be expected to come into proximity with Bax. Vinculin was present at relatively equal

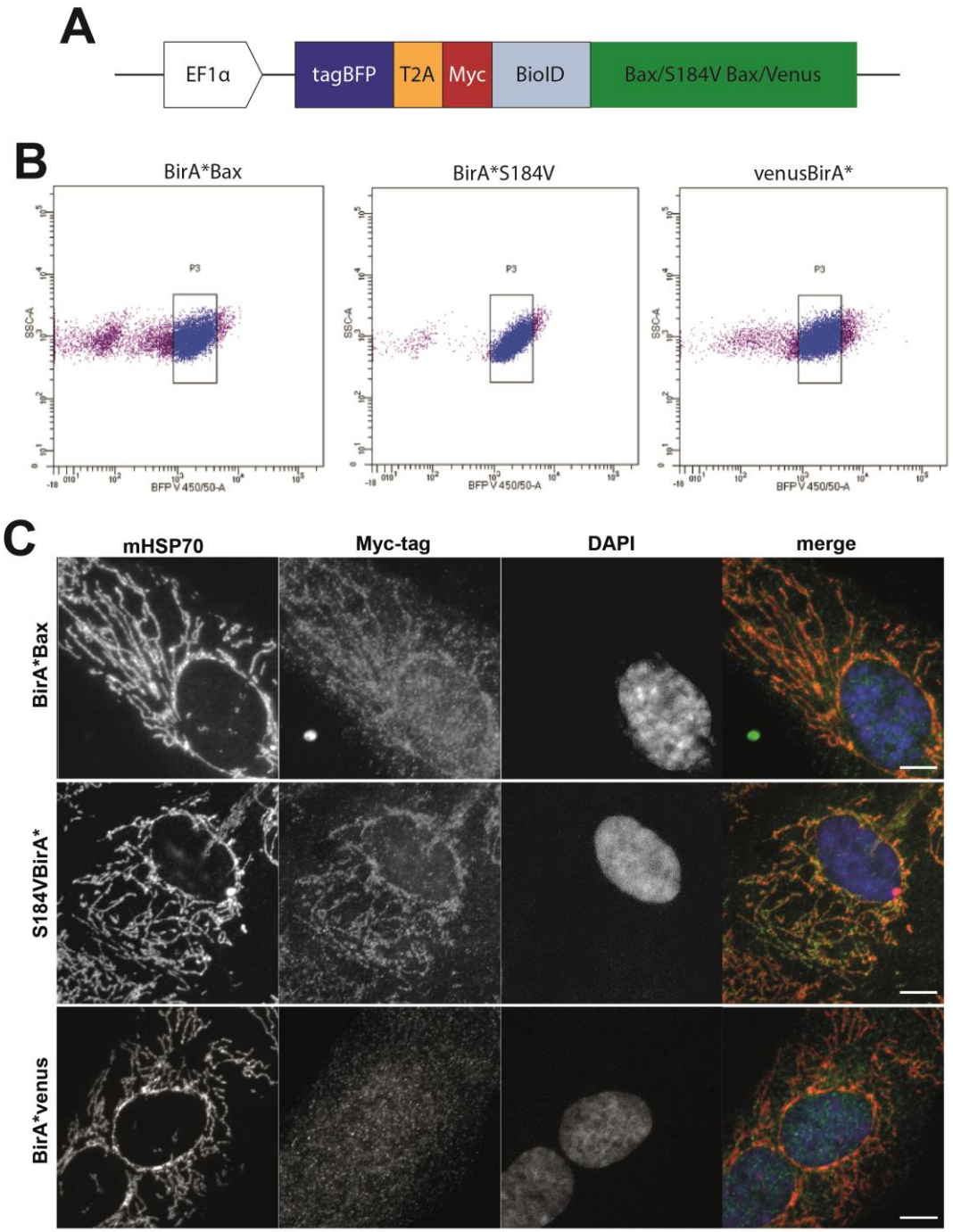

Figure 6.11. Creation of BirA* MCF10A cell lines

A. Schematic of Bax BirA* constructs expressed in cells used for BioID. Under the EF1α promoter, tagBFP is fused to either WT Bax or S184V Bax via a T2A self-cleaving sequence. This allows FACS sorting of stable cells and normalisation of expression levels. BirA* is fused to the N-terminus of Bax which itself is fused to a Myc-tag. As a control for non-specific interactions, Bax is replaced with Venus.

B. FACS plots of BirA*Bax, BirA*S184V and VenusBirA* cell lines. Cells were sorted within the boundary based on BirA*S184V expression levels.

C. Immunofluorescence images of stable BirA* cell lines stained for mHsp70 and Myc-tag. Scale bar represents 20μm.

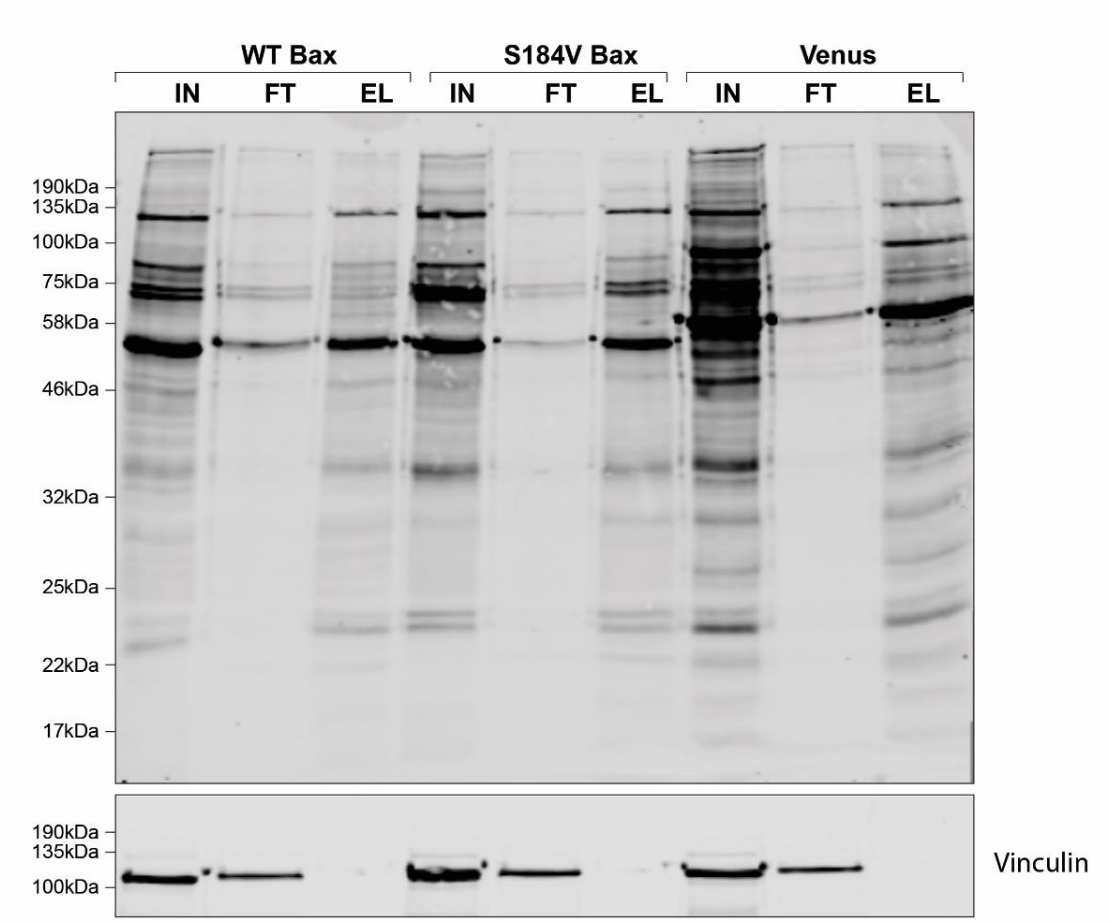

Figure 6.12. Pulldown of BirA* cell lines showing successful biotin labelling and elution from streptavidin beads

Each BirA* cell line was incubated overnight with biotin, lysed and biotinylated proteins purified using streptavidin beads. Pulldown efficiency was tested via Western blot, staining for streptavidin. For each cell line, the input (whole lysates), flowthrough (unbound proteins) and elution (proteins eluted from beads) were run. IN = input, FT = flowthrough, EL = elution. Vinculin was used as a loading control and a control for non-specific biotin labelling.

levels in each input and flowthrough lane, but not present in the elution suggesting successful proximity labelling.

Using the verified MCF10A BirA* Bax cell lines, three independent labelling experiments were conducted as described previously. A test pulldown was carried out for each set of samples to ensure successful labelling and enrichment in the elution (Fig. 6.13A). Biotinylated proteins eluted from each experiment were simultaneously run into the top of an SDS-PAGE gel and then prepped for LC-MS/MS analysis by the BioMS facility. All samples were run as a single batch on the LC-MS/MS to ensure consistency of analysis. Raw data was then analysed using MaxQuant[267] against the human proteome and principal component analysis carried out to ensure consistency between replicates before using SAINTexpress to identify interacting prey. Results from the SAINT analysis identified a similar number of enriched proteins between the samples: 585 enriched proteins in the BirA*Bax samples, and 527 in the BirA*S184V samples. Of these, 479 were common to both BirA*Bax and BirA*S184V (Fig. 6.13B).

Examination of the highest enriched proteins in each cell line identified only one significantly enriched protein in the Bax sample, and 6 in the S184V sample, other than Bax itself (Fig. 6.14A). In the WT Bax screen GSTP1 was identified which has a number of roles including catalysis of the conjunction of endogenous and exogenous compounds to glutathione S-transferases[383], and regulation of various signalling proteins such as MAP kinases[384] and transglutaminase 2[385] (Table 6.2). High expression of GSTP1 is linked to increased tumour cisplatin resistance and a decrease in Bax mitochondrial localisation[386,387], however there is, as of yet, no experimental evidence indicating a direct interaction between Bax and GSTP1. In the S184V screen, multiple mitochondrial proteins were identified, some of which were also present in the original Bcl-XL screen, including AKAP1, DNM1L and MAVS (Table 6.3). One unique protein identified, ALDH3A2, is a fatty acid aldehyde dehydrogenase[388], the deficiency of which causes an accumulation of fatty alcohols in the neurological disorder Sjögren-Larsson syndrome[389,390]. Currently there is no direct link between mitochondrial Bax and ALDH3A2.

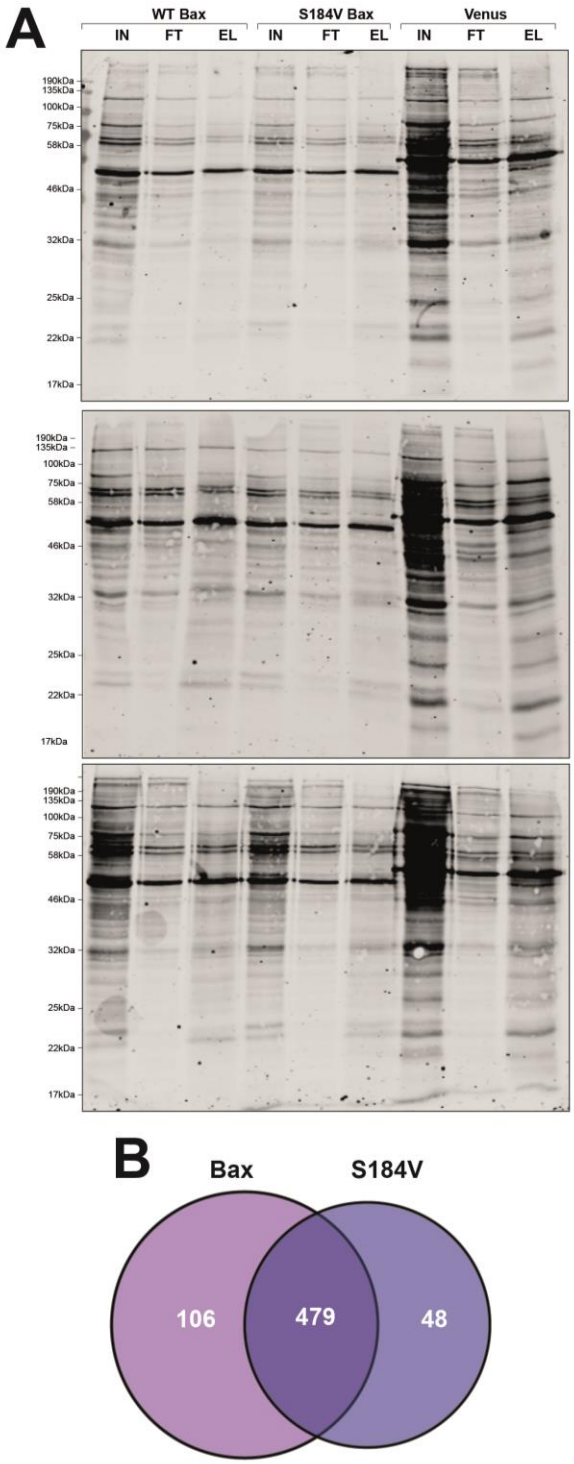

Figure 6.13. Results from BirA*Bax and BirA*S814V Bax mass spectrometry analysis
A. Test pulldown of samples in triplicate prepared for mass spectrometry analysis. Each BirA* cell line was incubated overnight with biotin, lysed and biotinylated proteins purified using streptavidin beads. 1 tenth of each sample was tested via Western blot, probing for streptavidin. IN = input, FT = flowthrough, EL = elution.
B. Venn diagram showing all proteins enriched according to SAINT analysis in the WT Bax and S184V Bax samples compared to VenusBirA.

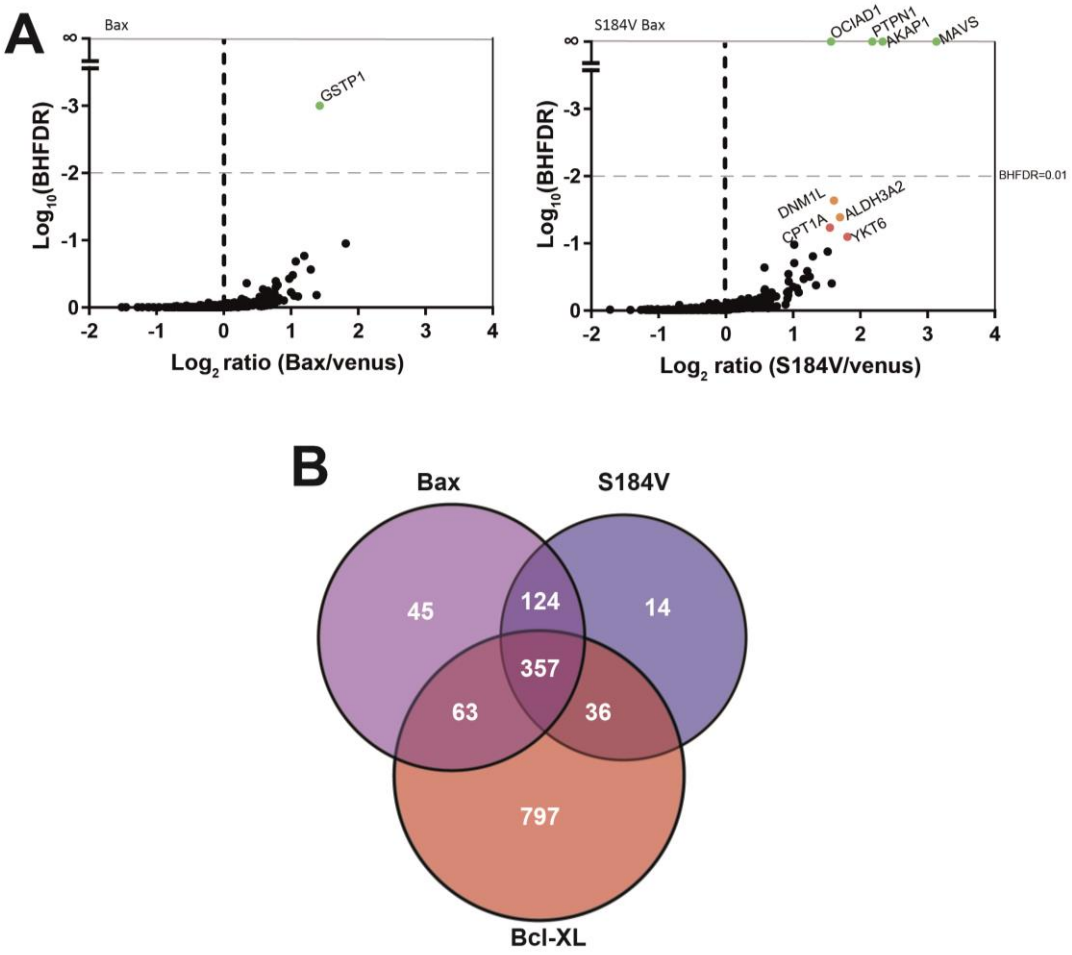

Figure legend on next page.

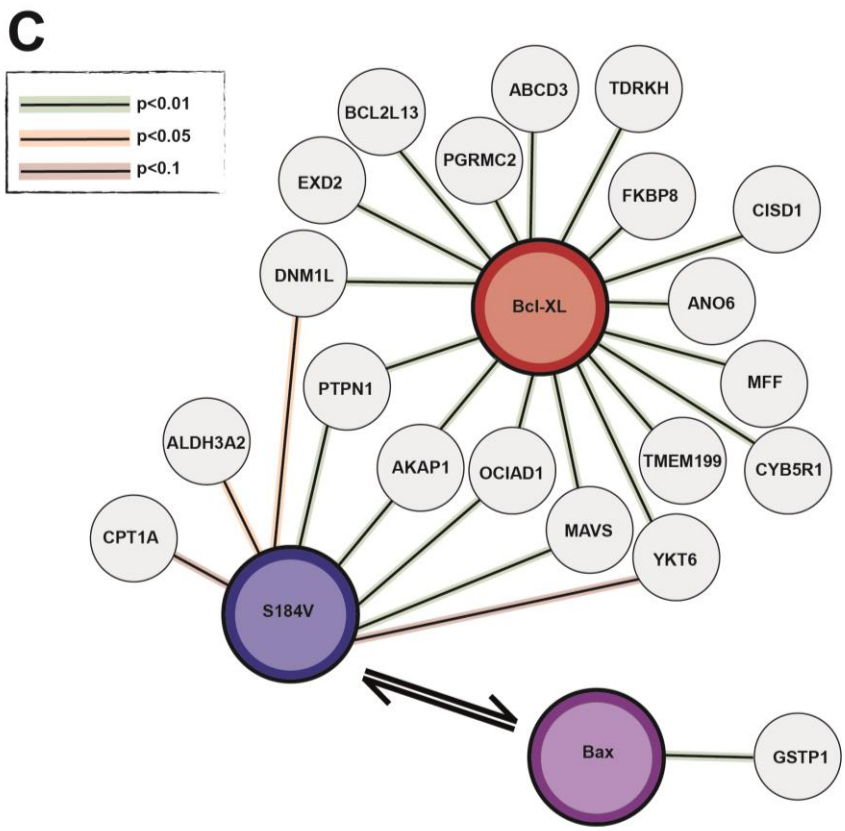

Figure 6.14. BioID identifies multiple commonly enriched proteins between Bcl-XL, Bax and S184V Bax

A. Volcano plots showing mean ratio of biotinylated protein abundance for WT Bax and S184V Bax versus Venus control. A positive ratio indicates enrichment in the Bax/S184V samples. Green points represent $p<0.01$; orange points represent $p<0.05$; red points represent $p<0.1$. Data represents values from 3 independent experiments which were all processed for mass spectrometry analysis at the same time.

B. Venn diagram showing all proteins enriched according to SAINT analysis from Bax, S184V Bax and Venus datasets. There are over 350 proteins identified in all three cell lines.

C. Diagram summarising the significantly enriched proteins from Bcl-XL, Bax and S184V Bax mass spectrometry experiments, highlighting commonly enriched proteins between experiments.

Examining all the enriched proteins from the WT and S184V Bax screens revealed a significant proportion of identified proteins were common between both Bax datasets and the Bcl-XL protein list (Fig. 6.14B). Combining data gathered from all three experiments allows us to begin to create a potential “interactome map” of how Bcl-XL and Bax are regulated (Fig. 6.14C). It is interesting to note that no Bcl-2 family proteins were significantly enriched between all three experiments, although Bcl-Rambo does appear in both the Bcl-XL and Bax S184V datasets, and Bax was enriched in the Bcl-XL dataset. It is also interesting that there are mitochondrial-localised proteins common between Bcl-XL and mitochondrial S184V Bax, as these commonalities may be part of a larger complex, regulating the localisation and thus dynamics of Bcl-2 family proteins at the OMM.

6.7 Discussion

Using BioID proximity labelling to investigate Bcl-2 protein family interactions is advantageous over many other previously used techniques. Unlike co-immunoprecipitation assays or native PAGE gels, it does not require the use of detergents to extract membrane-embedded proteins, which can induce artificial interactions or disrupt genuine ones[209]. More recent live cell microscopy techniques such as FRAP[281] and FRET[351] are advantageous in that they examine protein-protein interactions in live cells and thus are more representative of *in vivo* interactions. However, these require the proteins of interest to be fluorescently tagged and can therefore only be used to examine already known interacting proteins. BioID is therefore a more appropriate method for identifying novel interactions as only the protein of interest requires the BioID fusion, and thus proximal proteins can be labelled in an unbiased manner. Furthermore, this method allows identification of novel protein-protein interactions *in situ*, therefore both the cytosolic and membrane interactions are represented. This method has so far proven successful both in our laboratory examining Bcl-2 family interactions and elsewhere[354,356].

Using previously gathered data from a Bcl-XL BioID screen, proteins known to be enriched as interacting partners with Bcl-XL were selected for further analysis by creating knockout cell lines. CRISPR-Cas9 was used to create these knockout lines, however overall efficiency was poor. Recently some alternative approaches have

Gene name	Description/protein name	Log$_2$ fold change	BHFDR
GSTP1	Glutathione S-Transferase Pi 1	1.43	0.000

Gene name	Description/protein name	Log$_2$ fold change	BHFDR
AKAP1	A-kinase anchor protein 1	3.13	0.000
MAVS	Mitochondrial antiviral-signaling protein	2.33	0.000
OCIAD1	OCIA domain containing 1	2.18	0.000
PTPN1	Tyrosine-protein phosphatase non-receptor type 1	1.57	0.000
DNM1L	Dynamin 1-like (DRP1)	1.61	0.023
ALDH3A2	Aldehyde Dehydrogenase 3 Family Member A2	1.70	0.041
CPT1A	Carnitine Palmitoyltransferase 1A	1.55	0.058
YKT6	Synaptobrevin homolog YKT6	1.81	0.080

Table 6.2 Proteins significantly enriched in Bax MS screens
Table of proteins that were significantly enriched in the BirA*Bax (upper) and BirA*S184VBax (lower) mass spectrometry output, analysed by SAINT. BHFDR of 0 indicates p<0.001 due to rounding.

WT Bax	
Gene name	BHFDR
GSTP1	0.001
PFN1	0.112
MAVS	0.171
TKT	0.207
GLUD1;GLUD2	0.273
PPIA	0.33
YWHAE	0.372
MRPS9	0.405
UBA1	0.436
ENO1	0.463
HSP90AA1	0.501
DSG1	0.535
SERPINB12	0.564
RPSA	0.59
S100A11	0.613
GOT2	0.633
TPI1	0.651
PPIB	0.668
YWHAZ	0.683
STMN2;STMN1	0.697
HSPD1	0.721
ANXA1	0.732
MYOF	0.743
AKAP1	0.752
ALDH3A2	0.761
PRDX3	0.769
ANXA5	0.777
PARK7	0.784
CTSD	0.784
MDH2	0.797

S184V Bax	
Gene name	BHFDR
AKAP1	0
MAVS	0
DNM1L	0.023
ALDH3A2	0.041
CPT1A	0.058
NPM1	0.104
PFN1	0.132
RPS5	0.156
NACA	0.195
KPRP	0.228
P4HB	0.258
CYB5R3	0.286
S100A11	0.313
RPSA	0.338
ANXA1	0.366
TPI1	0.393
YWHAZ	0.418
STMN2;STMN1	0.44
YWHAQ	0.461
YWHAE	0.48
DSG1	0.498
TKT	0.516
GSTP1	0.533
HIST1H1C;HIST1H1E;HIST1H1D;HIST1H1T;HIST1H1A	0.533
ZC3HAV1	0.533
ANXA5	0.578
PPIA	0.591
SET;SETSIP	0.603
DBI	0.614
PPIB	0.614

Table 6.3 Top 30 highest enriched proteins in Bax and S184V Bax datasets
Highest enriched proteins in Bax and S184V datasets analysed by SAINT. Proteins common between both Bax and S184V Bax datasets are highlighted. Those highlighted in pink are either more or less enriched in S184V Bax compared to WT Bax (and therefore appear higher or lower down the list, respectively). BHFDR of 0 indicates p<0.001 due to rounding.

been developed using a newly characterised RNA-guided, RNA-targeting CRISPR system using Cas13[391]. Upon interaction with the target mRNA via a designed crRNA, Cas13 cleaves downstream of the protospacer flanking sequence[392], providing a specific knockdown of target mRNA that is more efficient than siRNA systems[391]. Our laboratory is currently adapting this system to create a Cas13d lentivirus that can be co-transduced with a tetracycline-inducible crRNA designed to target the gene of interest (Matthew Jones – personal communication). This will allow creation of a stable Cas13d cell line that can be used to conditionally knock down the expression of any gene of choice to rapidly assay any candidate genes.

One protein that was successfully knocked out, AKAP1, is of particular interest as it was also significantly enriched in the later S184V Bax BioID screen and was present in the WT Bax screen. As previously mentioned, the link between AKAP1 and apoptosis has been studied in neuronal cells, with AKAP1 regulating Bad pro-apoptotic function, but no direct interaction between AKAP1 with either Bcl-XL or Bax has been identified[363,369]. Bad has been shown to form large complexes at the OMM containing protein kinase A, PP1 catalytic units, the AKAP protein WAVE-1 and glucokinase as part of glucose respiration regulation[156]. There is potential that AKAP1 could also regulate Bad phosphorylation in other mitochondrial complexes including Bax or Bcl-XL. Whilst there appeared to be no effect on Bcl-XL dynamics in the stable BadER^{Tam}-GFP-Bcl-XL MCF10A cell line, reducing expression levels using siRNA revealed subtle differences in the KO line. A lack of AKAP1 did not significantly alter the average mobility of Bcl-XL but did decrease the variation in the average mobile fraction of Bcl-XL between experiments. Cell-to-cell variation in Bcl-XL dynamics is highly varied; as the level of priming of an individual cell is frequently changing, so too is this threshold at a population level. Therefore, the same cell population can have differing apoptotic sensitivities at different points in time. Seeing a more consistent average in Bcl-XL dynamics suggests that AKAP1 may play a role in regulating these temporal changes. To further examine this observation, analysing variation in single cell Bcl-XL dynamics over much longer timeframes would allow quantification of these temporal changes in more detail and could be used to compare between WT and AKAP1 KO cells. Analysing the effect of AKAP1 KO on Bad activation via 4-OHT or Bax mitochondrial retrotranslocation could also provide useful information with regards to AKAP1 being part of a mitochondrial complex involving Bad, Bax and Bcl-XL.

Another protein which appeared significantly enriched in both the Bcl-XL mass spectrometry analysis and subsequent WT and S184V Bax data was Drp1. Although creation of an MCF10A KO line was unsuccessful, MEF knockout cells showed the characteristic elongated mitochondria associated with a lack of mitochondrial fission[393]. A lack of Drp1 had no effect on Bcl-XL dynamics. GFP-Bcl-XL was transiently overexpressed in these cells, and as such, the excess of protein could obscure more subtle changes. Creating a cell line stably expressing Bcl-XL at low levels or lowering expression with siRNA could potentially reveal differences masked in these experiments. FRAP analysis has been carried out on Drp1 and demonstrated that, much like Bcl-2 family proteins, Drp1 is highly dynamic between mitochondria and cytosol, with a more mitochondrial localisation upon an increase in apoptotic signalling[394]. Interestingly, this increase in Drp1 mitochondrial localisation is dependent on previous Bax mitochondrial localisation, and would explain the much higher enrichment found in the S184V dataset compared to WT (Table 6.4). It may also explain a lack of effect on Bcl-XL, as Drp1 may localise to mitochondria after Bcl-XL and Bax localisation. Whilst there does appear to be a direct interaction between Drp1 and Bcl-XL in hippocampal neurons[362], there is a lack of evidence in other cell types. Potentially, whilst in the same complex as Bcl-XL, Drp1 may interact via another protein or proteins within the same complex.

Another protein of interest that appeared highly enriched in all three datasets is Mitochondrial Antiviral Signalling Protein (MAVS). MAVS is an OMM adaptor protein required for the innate immune response against viruses via the regulation of β-interferon expression[395,396]. MAVS contains both a CARD domain and transmembrane domain, and can induce apoptosis when localised to the OMM[397]. Viruses use homologues of Bcl-2 proteins in order to prevent apoptosis of the host cell[398], thus the similar localisation of MAVS to Bcl-2 proteins when protecting cells from viral infections is logical. The role of MAVS outside of this response is unknown, and MAVS could also be involved in normal Bcl-2 protein function. Further examination via siRNA knockdown or knockout via CRISPR-Cas9 may help elucidate such a mechanism.

When examining the Bax datasets it was apparent that only one protein was significantly enriched in the WT Bax screen – GSTP1. GSTP1 is known to localise

mainly in either the cytosol or mitochondria and can protect cells against apoptotic stresses like H_20_2 via regulation of stress kinases such as inhibition of JNK[399]. JNK induces apoptosis via Bax activation when stress is induced[400,401], thus the presence of GSTP1 in healthy cells is not unexpected. GSTP1 may be in a complex with JNK and Bax in the cytosol to inhibit apoptosis in healthy cells. Measuring differences in Bax FLIP kinetics in the presence or absence of GSTP1 could help confirm this observation. As Bax is very mobile within healthy cells, with its equilibrium favouring a mainly cytosolic distribution, many of the interactions between Bax and other proteins will be transient. It is perhaps unsurprising that very few proteins were as highly enriched in the WT Bax samples compared to the S184V samples. This agrees with the previous Bax BioID experiment carried out in our laboratory, which also had very few significantly enriched proteins (Robert Pedley, unpublished data).

It was encouraging that, within the top 30 most enriched proteins in both WT and S184V Bax datasets, 13 proteins were common between both (Table 6.3). Within those proteins it was also interesting to see that mitochondrial proteins that were at the lower end of enrichment in the Bax list were some of the most highly enriched in the S184V list (e.g. AKAP1). Also, cytosolic proteins were more highly enriched in the WT Bax list compared to S184V, such as Transketolase (TKT) and Peptidylprolyl Isomerase A (PPIA). This suggested that the biotin labelling system can enrich for proteins either in the cytosol or mitochondria, depending on the retrotranslocation kinetics of the bait protein. It was surprising that no Bcl-2 family proteins were significantly enriched in either of the Bax datasets, and only Bcl-Rambo and Bax were enriched in the Bcl-XL dataset. This could be because the cells being examined were in an unprimed state, and thus little interaction between pro- and anti-apoptotic Bcl-2 proteins would be occurring, and any that did would potentially be transient. Carrying out a similar BioID screen using the BadER^{Tam}-GFP-Bcl-XL cells in the absence and presence of 4-OHT would induce a Bad-Bcl-XL interaction, and potentially other Bcl-2 family protein binding, and confirm these interactions can still occur with the BirA* fusions. Bax, S184V Bax and Bcl-XL were also being overexpressed in the samples, so interactions with Bcl-2 family proteins could potentially be masked by other interactions taking place. Carrying out BioID at lower expression levels may help account for this. Further use of the BioID system with other Bcl-2 protein variants such as Bax that cannot localise to the OMM, or Bcl-XL in the presence of activated BadER^{Tam} could help us understand more fully the different interactions that occur in unprimed versus primed cells.

Our current understanding of Bcl-2 protein regulation is mainly focussed on Bcl-2 family proteins themselves, and how their interactions with each other regulate MOMP. This is a very simplified view as these models do not consider other factors that regulate these interactions, such as OMM proteins. By using techniques such as BioID, we can begin to understand what larger protein complexes are involved in regulating Bcl-2 protein retrotranslocation, and potential causes of apoptotic heterogeneity within cell populations. Live cell microscopy techniques such as FRAP can then be used to interrogate these interactions in more detail, potentially improving our overall understanding of Bcl-2 protein regulation of apoptosis.

7. General discussion and future work

Heterogeneity in the apoptotic response of a population of cells remains a significant issue in terms of cancer treatment and patient response. Precisely how cells regulate levels of mitochondrial priming at a single cell level and how this varies temporally is unclear. In this thesis we present a novel insight into how Bcl-2 protein dynamics vary significantly between single cells, and how these dynamics alter as cells become more mitochondrially primed. Specifically, we demonstrate that anti-apoptotic Bcl-2 proteins are highly dynamic, much like pro-apoptotic Bax[110], translocating between cytosol and mitochondria in healthy cells. Upon receipt of an apoptotic stimulus like increased pro-apoptotic BH3 protein levels, these dynamics alter, increasing the mitochondrial fraction of the protein due to a decrease in retrotranslocation kinetics, which correlates with increased levels of apoptotic priming. Individual Bcl-2 proteins have varying affinities for their pro-apoptotic partners, which can compete for binding. It appears that BH3-mimetics like ABT-737, whilst designed to recapitulate the interactions of full-length BH3 proteins like Bad, do not do so via the same mechanism as their endogenous counterparts.

The cycling of Bcl-2 proteins between cytosol and mitochondria varies dramatically between individual cells, with cells with inherently slower Bcl-XL dynamics being more susceptible to pro-apoptotic stimuli such as Taxol treatment. What specifically controls this cell-to-cell variation is unclear. What is becoming apparent is that it is most likely not one single factor regulating these dynamics, but a culmination of multiple signalling events. Individual BH3 proteins like Bad, for example, may regulate small subpopulations of cells such as those which are sensitive to fluctuations in growth factor signalling, as was demonstrated via FRAP of BadKO MCF10A cells. Regulation of mitochondrial priming during the cell cycle is an interesting example of multiple Bcl-2 proteins functioning simultaneously as it has been shown that cell cycle stage is an important factor contributing to the efficacy of cancer treatments[402]. p53 controls G1 and G2 checkpoints in response to stimuli such as DNA damage, and activated p53 can induce Fas[403] or DR5[404] transcription, which in turn can activate apoptosis via BH3 proteins like Puma[188]. During mitosis, cells become more mitochondrially primed due to a combination of both Mcl-1 degradation[102] and Bid phosphorylation[172], which correlates with cancer treatments like radiotherapy being most effective at killing cells in late G2 and M-phase[405]. In

agreement with this, we have shown that cancer cells like MDA-MB-231s are more susceptible to Taxol treatment in mitosis than normal cells. Our examination of Bcl-XL dynamics at G1, S and G2 did not reveal any changes in Bcl-XL retrotranslocation, although the high expression levels of Bcl-XL could potentially mask any differences. It is also highly likely that multiple anti-apoptotic proteins are responsible for regulating Bcl-XL dynamics during cell cycle and so removal one protein may cause changes that are too subtle to quantify via the methods used here.

Whilst it is becoming clear that multiple interactions between Bcl-2 family proteins regulate cell fate outcomes, another key component in the dynamic equilibrium of Bcl-2 protein localisation in cells is lipid membranes, with the OMM particularly important in apoptotic regulation. There are a number of studies examining specific interactions between Bcl-2 proteins and OMM components, although how these interactions regulate protein dynamics or contribute to cell-to-cell variation in apoptotic outcome is still not clear. There is evidence suggesting that anti-apoptotic Bcl-2 proteins interact with channel proteins in the OMM to regulate the release of the inter-membrane contents, opposing the activities of the multi-domain proteins. For example, Bcl-XL has been shown to directly interact with the mitochondrial porin VDAC to regulate cytochrome c by closing the channel VDAC forms, whereas Bax and Bak binding opens the channel, releasing cytochrome c[406]. Bcl-2 can inhibit the formation of lipid channels via interaction with the adenine nucleotide translocator (ANT), which is inhibited by Bax[407]. Bcl-XL may also have a role in the regulation of mitochondrial dynamics, at least in neurons, as it has been shown to co-localise with Drp1 at the OMM during mitochondrial fission[362]. How membrane components regulate Bcl-2 protein translocation to the OMM is also not clear, although like Bcl-XL, Drp1 also retrotranslocates between mitochondria and cytosol, potentially via a similar mechanism[394]. FKBP8 is suggested to be a chaperone for both Bcl-XL and Bcl-2[374,375], and two components of the retromer endosomal scaffold complex, VPS35 and VPS26, have been shown to increase Bcl-XL mitochondrial localisation[408].

Multiple studies have identified that both multi-domain and BH3-only pro-apoptotic Bcl-2 proteins can form large multi-protein membrane complexes. For example, Bad forms large complexes to regulate the glucose respiration response[156], and Bax

forms part of 200kDa complexes at the OMM prior to cytochrome c release[128]. The interaction of Bax with OMM components has been the subject of a larger number of studies than other Bcl-2 family members due to efforts in determining its mechanism of activation. For example, Bax interaction with lipids like cardiolipin at the OMM are important for pore formation, at least in cell-free systems[409]. Like Bcl-XL, Bax can also interact with Drp1 as well as Mfn2 at constricted areas of mitochondria[134,410]. Both Bid and Bax have also been shown to form a complex with the mitochondrial carrier homologue 2 (Mtch2) at the OMM[411,412], and Bid can also disrupt Optic Atrophy 1 (OPA1) oligomers forming at cristae junctions during apoptotic cristae remodelling[413]. Whilst direct interactions between Bcl-2 proteins and OMM proteins have been identified, what is still lacking are studies examining the full composition of OMM-Bcl-2 complexes and how they are involved in regulating Bcl-2 protein membrane dynamics. Furthermore, understanding how these differ in unrprimed versus primed cells to alter Bcl-2 protein membrane kinetics could provide some interesting insights into apoptotic regulation. A number of questions, therefore, remain unanswered: What regulates transient versus more stable Bcl-2 protein membrane binding kinetics? How does binding of other Bcl-2 family proteins alter this, and do these interactions differ between mitochondria and cytosol?

Bcl-2 proteins have different distributions between cytosol and mitochondria which seems to be, in part, dictated by the hydrophobicity of the protein's TMD. Protein insertion into lipid membranes depends on multiple additional factors such as the 3D conformation of the protein itself, the change in the mobility of lipids within the membrane and formation of bonds between the two[414]. Many proteins with C-terminal TMDs are targeted to the ER utilising the conserved TMD recognition complex (TRC) targeting pathway[415]. Highly hydrophobic TMDs are believed to be shielded by a deep hydrophobic groove in TRC40, the main component of the TRC pathway[416], and released at the membrane in an ATPase-dependent reaction[417]. Proteins with less hydrophobic TMDs are shielded from this process by calmodulin and thus are more cytosolic[418]. This concept fits with the dynamics seen with Bcl-2 family proteins, in which Bcl-2 is more mitochondrial and has a more hydrophobic TMD than its counterparts, although evidence of the same pathway occurring at the OMM is lacking. Interestingly, a substrate of TRC40, Bat3[419], contains a chaperone-related BAG domain which was first identified via interaction with Bcl-2[420], suggesting Bcl-2 protein membrane localisation may be regulated by BAG-containing proteins.

How proteins like Bax and Bcl-XL can retrotranslocate from the OMM back to the cytosol is not well understood. The mechanism of Bax insertion into, rather than removal from, the OMM has been an area of intense study, with the 3D structure of the process at each stage being delineated[118,129] although some debate as to the exact mechanism still remains. In terms of retrotranslocation from the OMM to the cytosol, the models generally do not consider the contribution of the surrounding lipid membrane or other membrane proteins involved in this process. It is possible that, in order for Bax to release its TMD, it must not only interact with other Bcl-2 proteins, but also specific membrane proteins like VDAC2 to fully activate, as without the presence of VDAC2 Bax localises to other cell compartments[421]. Until this occurs, insertion may not occur and Bax could be retrotranslocated back to the cytosol whereupon it can be degraded by proteins such as 14-3-3 proteins[422] or the E3 ligase parkin[423]. A similar principle could hold true for other mobile Bcl-2 proteins like Bcl-XL. This may also contribute to differences in binding of endogenous BH3 proteins and mimetics like ABT-737. As mentioned previously, live cell studies have revealed that when localised to the OMM, Bcl-XL is much less sensitive to derepression by ABT-737 treatment compared to a more cytosolic distribution[212]. Examination of Bcl-XL in two states – water-soluble and membrane-integrated – highlights differences in the conformation of the C-terminus, but not the soluble domain, with BH3 binding possible in both states[424]. Both membrane insertion and BH4 domain release are regulated by the lipid composition of the membrane such as cardiolipin content[425]. As the molecular structure of ABT-737 is based upon the Bad BH3 peptide, whether binding to Bcl-XL can occur effectively in both cytosolic and membrane-bound states, and how this is affected by the lipid and protein composition of the OMM is yet to be confirmed.

As highlighted throughout this thesis, much of the contradictory data within the literature to date in terms of Bcl-2 protein regulation of apoptosis can be at least partly explained by the different methodologies used to study Bcl-2 family proteins. Much of the previous work examining apoptosis has used dead cells as the assay readout, for example, mitochondrial depolarisation or loss of cytochrome c measured in BH3 profiling[203,257]. Whilst this is useful in determining the effectiveness of specific drug treatments on cells populations, it does not give insight into why certain cells were more susceptible to apoptosis than the survivors; rather than cells

being either sensitive or resistant, they are more likely to be on a continuum of sensitivity that continually changes. Much of the literature also uses BH3 peptides rather than full-length proteins, or purified lipid vesicles rather than endogenous membranes which do not recapitulate the live cell environment. More recently, studies examining full-length proteins in live cells have demonstrated the dynamic nature of Bcl-2 proteins and have emphasised the concept that mitochondrial priming is not an all or nothing process, but a continually shifting equilibrium. For example, studies examining Bax or Bcl-XL retrotranslocation have demonstrated that due to the dynamic changes in mitochondrial priming, any measurements of priming taken at any single point in time may not truly reflect how a population of cells will behave at a later point[110,215,426]. For example, Bim activity is negatively regulated by ERK[300] signalling, and ERK signalling has been shown to occur in asynchronous pulses[337]. Therefore, Bim activity will fluctuate over time, altering levels of apoptotic priming. To fully understand the mechanisms involved, examinations of Bcl-2 protein dynamics in both live cell populations and between single cells over longer timeframes is necessary to understand the dynamic changes occurring within cells.

Live cell microscopy approaches such as FLIM-FRET or FRAP are useful tools to measure interactions of two known proteins but cannot be used to identify novel protein interactions due to the requirement of attached fluorophores. In this thesis we therefore utilised a Biotin proximity labelling mass spectrometry approach to identify other proteins involved in the regulation of Bcl-2 protein dynamics. Our screen identified several mitochondrial proteins which may be involved in regulating the localisation of Bcl-2 proteins at the OMM, a number of which were common between Bcl-XL and Bax, such as MAVS, Drp1 and AKAP1 as discussed previously. It will be interesting to further develop approaches such as this to examine differences between membrane complexes in healthy versus primed cells, or normal versus cancer cells to pick out key differences. It may be possible to utilise the BadER^{Tam}-GFP-Bcl-XL system to artificially prime cells and quantify changes in enriched proteins between inactive and active BadER^{Tam} to determine what regulates changes in Bcl-XL dynamics in primed cells.

Bcl-2 proteins themselves are not the only dynamic component involved in apoptotic regulation. Mitochondria themselves are highly dynamic structures, continually

changing shape and distribution across cells[427]. Differences between mitochondria could alter the binding kinetics of Bcl-2 proteins at the OMM. Differences between mitochondria within the same cell is evident when a cell fails to completely undergo MOMP, termed minority MOMP, whereby only a small proportion of mitochondria permeabilise within a cell, therefore failing to induce apoptosis and instead inducing DNA damage[225]. To date, few studies have examined the heterogeneity between individual mitochondria within the same cell or between different cells within a population and how this relates to variation in Bcl-2 protein dynamics and apoptotic outcome. It has been shown that mitochondrial content varies significantly between cells[428,429] and a recent study by Márquez-Jurado and colleagues has shown that cells with a higher mitochondrial content are more susceptible to TRAIL-induced apoptosis due to increased levels of pro-apoptotic proteins[430]. It is also possible that Bcl-2 proteins do not localise to mitochondria in a homogenous manner. Individual mitochondria may have different Bcl-2 protein profiles, or multiple different Bcl-2 protein complexes could be present on an individual mitochondrion. Super resolution imaging has the power to identify rings of Bax at the OMM[126] and the release of mitochondrial DNA or "herniation" of this DNA out of the pores formed by Bax and Bak[431], thus similar techniques could be used to examine the potential heterogeneity of complexes between and within individual mitochondria. Further examination of how mitochondrial heterogeneity contributes to apoptotic priming, and indeed what causes this heterogeneity may help in our understanding of variations in apoptotic response within a population of cells.

In this thesis and indeed other studies within the literature, methodologies used require overexpression of the proteins in question to enable quantitative measurements. Whilst measuring proteins at this level can provide incredibly useful insights into Bcl-2 family protein dynamics and mechanisms of action, studying these proteins at endogenous levels would provide a more accurate *in vivo* representation of how apoptosis is regulated. With the continual development of the CRISPR-Cas9 system for gene editing, the potential to examine fluorescently labelled Bcl-2 proteins at endogenous levels of expression could provide a more detailed analysis of how interactions between the different proteins differs in healthy cells in the lead up to apoptosis, and indeed between normal and cancer cells. It could also provide a more representative overview of how heterogeneous Bcl-2 protein dynamics are within cells when excess protein is not present. A recent study by Vandemoortele and colleagues outlines the development of a BioID strategy to

examine protein-protein interactions at endogenous levels by using CRISPR-Cas9 to knock in T2A-BirA* to the protein of interest[432]. There is therefore future potential to examine what cytosolic and mitochondrial complexes regulate Bcl-2 proteins in live cells, at endogenous levels, to provide a better understanding of apoptotic regulation and causes of heterogeneity in apoptotic outcome.

References

1. Kerr, J. F., Wyllie, A. H. & Currie, A. R. Apoptosis: a basic biological phenomenon with wide-ranging implications in tissue kinetics. *Br. J. Cancer* **26**, 239–57 (1972).

2. Hanahan, D. & Weinberg, R. A. Hallmarks of cancer: the next generation. *Cell* **144**, 646–74 (2011).

3. Lockshin, R. A. & Williams, C. M. Programmed Cell Death--I. Cytology of Degeneration in the Intersegmental Muscles of The Pernyi Silkmoth. *J. Insect Physiol.* **11**, 123–33 (1965).

4. Wyllie, A. H., Morris, R. G., Smith, A. L. & Dunlop, D. Chromatin cleavage in apoptosis: Association with condensed chromatin morphology and dependence on macromolecular synthesis. *J. Pathol.* **142**, 67–77 (1984).

5. Messam, C. A. & Pittman, R. N. Asynchrony and commitment to die during apoptosis. *Exp. Cell Res.* **238**, 389–398 (1998).

6. Zmasek, C. M. & Godzik, A. Evolution of the Animal Apoptosis Network. *Cold Spring Harb. Perspect. Biol.* **5**, a008649 (2013).

7. D, X. *et al.* The Caenorhabditis elegans cell-death protein CED-3 is a cysteine protease with substrate specificities similar to those of the human CPP32 protease. *Genes Dev.* **10**, 1073–1083 (1996).

8. Earnshaw, W. C., Martins, L. M. & Kaufmann, S. H. Mammalian caspases: structure, activation, substrates, and functions during apoptosis. *Annu. Rev. Biochem.* **68**, 383–424 (1999).

9. Lüthi, A. U. & Martin, S. J. The CASBAH: a searchable database of caspase substrates. *Cell Death Differ.* **14**, 641–650 (2007).

10. Fischer, U., Jänicke, R. U. & Schulze-Osthoff, K. Many cuts to ruin: A comprehensive update of caspase substrates. *Cell Death Differ.* **10**, 76–100 (2003).

11. Blanchard, H. *et al.* The three-dimensional structure of caspase-8: an initiator enzyme in apoptosis. *Structure* **7**, 1125–1133 (1999).

12. Hofmann, K., Bucher, P. & Tschopp, J. The CARD domain: a new apoptotic signalling motif. *Trends Biochem. Sci.* **22**, 155–156 (1997).

13. Renatus, M., Stennicke, H. R., Scott, F. L., Liddington, R. C. & Salvesen, G. S. Dimer formation drives the activation of the cell death protease caspase 9. *Proc. Natl. Acad. Sci. U. S. A.* **98**, 14250–14255 (2001).

14. Riedl, S. J. *et al.* Structural basis for the activation of human procaspase-7. *Proc. Natl. Acad. Sci. U. S. A.* **98**, 14790–5 (2001).

15. Boatright, K. M. *et al.* A unified model for apical caspase activation. *Mol. Cell* **11**, 529–41 (2003).

16. Pop, C. & Salvesen, G. S. Human Caspases: Activation, Specificity, and Regulation. (2009). doi:10.1074/jbc.R800084200

17. Pop, C., Fitzgerald, P., Green, D. R. & Salvesen, G. S. Role of Proteolysis in Caspase-8 Activation and Stabilization †. (2007). doi:10.1021/bi602623b

18. Twiddy, D. & Cain, K. Caspase-9 cleavage, do you need it? *Biochem. J.* **405**, 1–2 (2007).

19. Boucher, D. *et al.* Caspase-1 self-cleavage is an intrinsic mechanism to terminate inflammasome activity. *J. Exp. Med.* **215**, 827–840 (2018).

20. Chai, J. *et al.* Crystal Structure of a Procaspase-7 Zymogen: Mechanisms of

Activation and Substrate Binding. *Cell* **107**, 399–407 (2001).

21. Smith, C. A., Farrah, T. & Goodwin, R. G. The TNF receptor superfamily of cellular and viral proteins: Activation, costimulation, and death. *Cell* **76**, 959–962 (1994).

22. Tartaglia, L. A., Ayres, T. M., Wong, G. H. & Goeddel, D. V. A novel domain within the 55 kd TNF receptor signals cell death. *Cell* **74**, 845–53 (1993).

23. Kischkel, F. C. *et al.* Cytotoxicity-dependent APO-1 (Fas/CD95)-associated proteins form a death-inducing signaling complex (DISC) with the receptor. *EMBO J.* **14**, 5579–5588 (1995).

24. Irmler, M. *et al.* Inhibition of death receptor signals by cellular FLIP. *Nature* **388**, 190–195 (1997).

25. Riedl, S. J. *et al.* Structural basis for the inhibition of caspase-3 by XIAP. *Cell* **104**, 791–800 (2001).

26. Ozören, N. & El-Deiry, W. S. Defining characteristics of Types I and II apoptotic cells in response to TRAIL. *Neoplasia* **4**, 551–7 (2002).

27. Jost, P. J. *et al.* XIAP discriminates between type I and type II FAS-induced apoptosis. *Nature* **460**, 1035–1039 (2009).

28. Kantari, C. & Walczak, H. Caspase-8 and Bid: Caught in the act between death receptors and mitochondria. *Biochim. Biophys. Acta - Mol. Cell Res.* **1813**, 558–563 (2011).

29. Ogasawara, J. *et al.* Lethal effect of the anti-Fas antibody in mice. *Nature* **364**, 806–809 (1993).

30. Galle, P. R. *et al.* Involvement of the CD95 (APO-1/Fas) receptor and ligand in liver damage. *J. Exp. Med.* **182**, 1223–1230 (1995).

31. Creagan, E. T., Kovach, J. S., Moertel, C. G., Frytak, S. & Kvols, L. K. A phase I clinical trial of recombinant human tumor necrosis factor. *Cancer* **62**, 2467–2471 (1988).

32. Hersh, E. M. *et al.* Phase II studies of recombinant human tumor necrosis factor alpha in patients with malignant disease: a summary of the Southwest Oncology Group experience. *J. Immunother. (1991).* **10**, 426–31 (1991).

33. Spierings, D. C. J. *et al.* Expression of TRAIL and TRAIL death receptors in stage III non-small cell lung cancer tumors. *Clin. Cancer Res.* **9**, 3397–405 (2003).

34. Sträter, J. *et al.* Expression of TRAIL and TRAIL receptors in colon carcinoma: TRAIL-R1 is an independent prognostic parameter. *Clin. Cancer Res.* **8**, 3734–40 (2002).

35. Walczak, H. *et al.* Tumoricidal activity of tumor necrosis factor–related apoptosis–inducing ligand in vivo. *Nat. Med.* **5**, 157–163 (1999).

36. Herbst, R. S. *et al.* Phase I Dose-Escalation Study of Recombinant Human Apo2L/TRAIL, a Dual Proapoptotic Receptor Agonist, in Patients With Advanced Cancer. *J. Clin. Oncol.* **28**, 2839–2846 (2010).

37. Soria, J.-C. *et al.* Phase 1b Study of Dulanermin (recombinant human Apo2L/TRAIL) in Combination With Paclitaxel, Carboplatin, and Bevacizumab in Patients With Advanced Non-Squamous Non–Small-Cell Lung Cancer. *J. Clin. Oncol.* **28**, 1527–1533 (2010).

38. de Miguel, D., Lemke, J., Anel, A., Walczak, H. & Martinez-Lostao, L. Onto better TRAILs for cancer treatment. *Cell Death Differ.* **23**, 733–747 (2016).

39. Goldstein, J. C., Waterhouse, N. J., Juin, P., Evan, G. I. & Green, D. R. The coordinate release of cytochrome c during apoptosis is rapid, complete and kinetically

invariant. *Nat. Cell Biol.* **2**, 156–162 (2000).

40. Zou, H., Li, Y., Liu, X. & Wang, X. An APAF-1·Cytochrome c Multimeric Complex Is a Functional Apoptosome That Activates Procaspase-9. *J. Biol. Chem.* **274**, 11549–11556 (1999).

41. Rodriguez, J. & Lazebnik, Y. Caspase-9 and APAF-1 form an active holoenzyme. *Genes Dev.* **13**, 3179–84 (1999).

42. Li, Y. *et al.* Mechanistic insights into caspase-9 activation by the structure of the apoptosome holoenzyme. *Proc. Natl. Acad. Sci.* **114**, 1542–1547 (2017).

43. Li, P. *et al.* Cytochrome c and dATP-dependent formation of Apaf-1/caspase-9 complex initiates an apoptotic protease cascade. *Cell* **91**, 479–89 (1997).

44. Du, C., Fang, M., Li, Y., Li, L. & Wang, X. Smac, a mitochondrial protein that promotes cytochrome c-dependent caspase activation by eliminating IAP inhibition. *Cell* **102**, 33–42 (2000).

45. Verhagen, A. M. *et al.* Identification of DIABLO, a mammalian protein that promotes apoptosis by binding to and antagonizing IAP proteins. *Cell* **102**, 43–53 (2000).

46. Youle, R. J. & Strasser, A. The BCL-2 protein family: Opposing activities that mediate cell death. *Nat. Rev. Mol. Cell Biol.* **9**, 47–59 (2008).

47. Tsujimoto, Y., Cossman, J., Jaffe, E. & Croce, C. M. Involvement of the bcl-2 gene in human follicular lymphoma. *Science* **228**, 1440–3 (1985).

48. Bakhshi, A. *et al.* Cloning the chromosomal breakpoint of t(14;18) human lymphomas: clustering around Jhon chromosome 14 and near a transcriptional unit on 18. *Cell* **41**, 899–906 (1985).

49. Vaux, D. L., Cory, S. & Adams, J. M. Bcl-2 gene promotes haemopoietic cell survival and cooperates with c-myc to immortalize pre-B cells. *Nature* **335**, 440–442 (1988).

50. Merry, D. E. *et al.* bcl-2 protein expression is widespread in the developing nervous system and retained in the adult PNS. *Development* **120**, 301–311 (1994).

51. Gratiot-Deans, J., Merino, R., Nuñez, G. & Turka, L. A. Bcl-2 expression during T-cell development: early loss and late return occur at specific stages of commitment to differentiation and survival. *Proc. Natl. Acad. Sci.* **91**, (1994).

52. Hockenbery, D. M., Zutter, M., Hickey, W., Nahm, M. & Korsmeyer, S. J. BCL2 protein is topographically restricted in tissues characterized by apoptotic cell death. *Proc. Natl. Acad. Sci.* **88**, 6961–6965 (1991).

53. Hockenbery, D., Nuñez, G., Milliman, C., Schreiber, R. D. & Korsmeyer, S. J. Bcl-2 is an inner mitochondrial membrane protein that blocks programmed cell death. *Nature* **348**, 334–336 (1990).

54. Krajewski, S. *et al.* Investigation of the subcellular distribution of the bcl-2 oncoprotein: residence in the nuclear envelope, endoplasmic reticulum, and outer mitochondrial membranes. *Cancer Res.* **53**, 4701–14 (1993).

55. Veis, D. J. *et al.* Bcl-2-deficient mice demonstrate fulminant lymphoid apoptosis, polycystic kidneys, and hypopigmented hair. *Cell* **75**, 229–240 (1993).

56. Martinou, J. *et al.* Overexpression of BCL - 2 in transgenic mice protects neurons from naturally occurring cell death and experimental ischemia. *Neuron* **13**, 1017–1030 (1994).

57. Hotchkiss, R. S. *et al.* Overexpression of Bcl-2 in transgenic mice decreases apoptosis and improves survival in sepsis. *J. Immunol.* **162**, 4148–56 (1999).

58. Hanada, M., Delia, D., Aiello, A., Stadtmauer, E. & Reed, J. C. bcl-2 gene hypomethylation and high-level expression in B-cell chronic lymphocytic leukemia.

Blood **82**, 1820–8 (1993).

59. Ikegaki N, Katsumata M, Minna J, T. Y. Expression of bcl-2 in small cell lung carcinoma cells. *Cancer Res.* 6–8 (1994).

60. Castle, V. P. *et al.* Expression of the apoptosis-suppressing protein bcl-2, in neuroblastoma is associated with unfavorable histology and N-myc amplification. *Am. J. Pathol.* **143**, 1543–50 (1993).

61. Petros, A. M. *et al.* Solution structure of the antiapoptotic protein bcl-2. *Proc. Natl. Acad. Sci.* **98**, 3012–3017 (2001).

62. Yin, X. M., Oltvai, Z. N. & Korsmeyer, S. J. BH1 and BH2 domains of Bcl-2 are required for inhibition of apoptosis and heterodimerization with Bax. *Nature* **3676**, 321–323 (1994).

63. Nguyen, M., Millar, D. G., Yong, V. W., Korsmeyer, S. J. & Shore, G. C. Targeting of Bcl-2 to the mitochondrial outer membrane by a COOH-terminal signal anchor sequence. *J. Biol. Chem.* **268**, 25265–8 (1993).

64. Yamamoto, K., Ichijo, H. & Korsmeyer, S. J. BCL-2 is phosphorylated and inactivated by an ASK1/Jun N-terminal protein kinase pathway normally activated at G(2)/M. *Mol. Cell. Biol.* **19**, 8469–78 (1999).

65. Gross, A. & Katz, S. G. Non-apoptotic functions of BCL-2 family proteins. *Cell Death Differ.* **24**, 1348–1358 (2017).

66. Hardwick, J. M. & Soane, L. Multiple functions of BCL-2 family proteins. *Cold Spring Harb. Perspect. Biol.* **5**, 1–22 (2013).

67. Boise, L. H. *et al.* bcl-x, a bcl-2-Related Gene That Functions as a Dominant Regulator of Apoptotic Cell Death. *Cell* **74**, 597–606 (1993).

68. Muchmore, S. W. *et al.* X-ray and NMR structure of human Bcl-xu an inhibitor of programmed cell death. *Nature* **381**, 1747–1754 (1996).

69. Sattler, M. Structure of Bcl-xL-Bak Peptide Complex: Recognition Between Regulators of Apoptosis. *Science (80-.).* **275**, 983–986 (1997).

70. Liu, X., Dai, S., Zhu, Y., Marrack, P. & Kappler, J. W. The Structure of a Bcl-xL/Bim Fragment Complex: Implications for Bim Function. *Immunity* **19**, 341–352 (2003).

71. Jeong, S.-Y. *et al.* Bcl-x L sequesters its C-terminal membrane anchor in soluble, cytosolic homodimers. *EMBO J.* **23**, 2146–2155 (2004).

72. Fiebig, A. A., Zhu, W., Hollerbach, C., Leber, B. & Andrews, D. W. Bcl-XL is qualitatively different from and ten times more effective than Bcl-2 when expressed in a breast cancer cell line. (2006). doi:10.1186/1471-2407-6-213

73. González-García, M. *et al.* bcl-XL is the major bcl-x mRNA form expressed during murine development and its product localizes to mitochondria. *Development* **120**, 3033–42 (1994).

74. Motoyama, N. *et al.* Massive cell death of immature hematopoietic cells and neurons in Bcl-x-deficient mice. *Science* **267**, 1506–10 (1995).

75. Park, H. *et al.* Genomic alterations in BCL2L1 and DLC1 contribute to drug sensitivity in gastric cancer. *Proc. Natl. Acad. Sci. U. S. A.* **112**, 12492–7 (2015).

76. De Carné Trécesson, S. *et al.* BCL-X L directly modulates RAS signalling to favour cancer cell stemness. doi:10.1038/s41467-017-01079-1

77. Scherr, A.-L. *et al.* Bcl-xL is an oncogenic driver in colorectal cancer. *Cell Death Dis.* **7**, e2342–e2342 (2016).

78. Grad, J. M., Zeng, X. R. & Boise, L. H. Regulation of Bcl-xL: a little bit of this and a

little bit of STAT. *Curr. Opin. Oncol.* **12**, 543–9 (2000).

79. Terrano, D. T., Upreti, M. & Chambers, T. C. Cyclin-Dependent Kinase 1-Mediated Bcl-xL/Bcl-2 Phosphorylation Acts as a Functional Link Coupling Mitotic Arrest and Apoptosis. *Mol. Cell. Biol.* **30**, 640–656 (2010).

80. Jonas, E. BCL-xL Regulates Synaptic Plasticity. *Mol. Interv.* **6**, 208–222 (2006).

81. White, C. *et al.* The endoplasmic reticulum gateway to apoptosis by Bcl-XL modulation of the InsP3R. *Nat. Cell Biol.* **7**, 1021–1028 (2005).

82. Gibson, L. *et al.* bcl-w, a novel member of the bcl-2 family, promotes cell survival. *Oncogene* **13**, 665–75 (1996).

83. Denisov, A. Y. *et al.* Solution structure of human BCL-w: modulation of ligand binding by the C-terminal helix. *J. Biol. Chem.* **278**, 21124–8 (2003).

84. Wilson-Annan, J. *et al.* Proapoptotic BH3-only proteins trigger membrane integration of prosurvival Bcl-w and neutralize its activity. *J. Cell Biol.* **162**, 877–887 (2003).

85. Hinds, M. G. *et al.* The structure of Bcl-w reveals a role for the C-terminal residues in modulating biological activity. *EMBO J.* **22**, 1497–507 (2003).

86. Print, C. G. *et al.* Apoptosis regulator Bcl-w is essential for spermatogenesis but appears otherwise redundant. *Proc. Natl. Acad. Sci.* **95**, 12424–12431 (1998).

87. Adams, C. M. *et al.* BCL-W has a fundamental role in B cell survival and lymphomagenesis. *J. Clin. Invest.* **127**, 635–650 (2017).

88. Bae, I. H. *et al.* Signaling components involved in Bcl-w-induced migration of gastric cancer cells. *Cancer Lett.* **277**, 22–28 (2009).

89. G. Middleton, S. Wyatt, N. N. and A. D. Reciprocal developmental changes in the roles of Bcl-w and Bcl-xL and in regulating sensory neuron survival. *Development* **128**, 447–457 (2001).

90. Kozopas, K. M., Yang, T., Buchan, H. L., Zhou, P. & Craig, R. W. MCL1, a gene expressed in programmed myeloid cell differentiation, has sequence similarity to BCL2. *Proc. Natl. Acad. Sci. USA* **90**, 3516–3520 (1993).

91. Day, C. L. *et al.* Solution Structure of Prosurvival Mcl-1 and Characterization of Its Binding by Proapoptotic BH3-only Ligands. *J. Biol. Chem.* **280**, 4738–4744 (2005).

92. Rogers, S., Wells, R. & Rechsteiner, M. Amino acid sequences common to rapidly degraded proteins: the PEST hypothesis. *Science (80-.).* **234**, 364–368 (1986).

93. Thomas, L. W., Lam, C. & Edwards, S. W. Mcl-1; the molecular regulation of protein function. *FEBS Lett.* **584**, 2981–2989 (2010).

94. Perciavalle, R. M. *et al.* Anti-apoptotic MCL-1 localizes to the mitochondrial matrix and couples mitochondrial fusion to respiration. *Nat. Cell Biol.* **14**, 575–583 (2012).

95. Yang, T., Kozopas, K. M. & Craig, R. W. The intracellular distribution and pattern of expression of Mcl-1 overlap with, but are not identical to, those of Bcl-2. *J. Cell Biol.* **128**, 1173–1184 (1995).

96. Krajewski, S. *et al.* Immunohistochemical Analysis of Mci-1 Protein in Human Tissues - Differential regulation of Mcl-1 and Bcl-2 protein production suggests a unique role for Mcl-1 in control of programmed cell death in vivo. *Am. J. Pathol.* **146**, (1995).

97. Rinkenberger, J. L., Horning, S., Klocke, B., Roth, K. & Korsmeyer, S. J. Mcl-1 deficiency results in peri-implantation embryonic lethality. *Genes Dev.* **14**, 23–7 (2000).

98. Campbell, K. J. *et al.* MCL-1 is a prognostic indicator and drug target in breast cancer. *Cell Death Dis.* **9**, 19 (2018).

99. Reiner, T. *et al.* Mcl-1 protects prostate cancer cells from cell death mediated by chemotherapy-induced DNA damage. *Oncoscience* **2**, 703–15 (2015).

100. Zervantonakis, I. K. *et al.* Systems analysis of apoptotic priming in ovarian cancer identifies vulnerabilities and predictors of drug response. *Nat. Commun.* **8**, 365 (2017).

101. Fujise, K., Zhang, D., Liu, J. & Yeh, E. T. Regulation of apoptosis and cell cycle progression by MCL1. Differential role of proliferating cell nuclear antigen. *J. Biol. Chem.* **275**, 39458–65 (2000).

102. Sloss, O., Topham, C., Diez, M. & Taylor, S. Mcl-1 dynamics influence mitotic slippage and death in mitosis. *Oncotarget* **7**, 5176–92 (2016).

103. Kvansakul, M. *et al.* Vaccinia virus anti-apoptotic F1L is a novel Bcl-2-like domain-swapped dimer that binds a highly selective subset of BH3-containing death ligands. *Cell Death Differ.* **15**, 1564–1571 (2008).

104. Llambi, F., Wang, Y.-M., Moldoveanu, T., Chen, T. & Green Correspondence, D. R. BOK Is a Non-canonical BCL-2 Family Effector of Apoptosis Regulated by ER-Associated Degradation. *Cell* **165**, 421–433 (2016).

105. Hsu, S. Y., Kaipia, A., McGee, E., Lomeli, M. & Hsueh, A. J. Bok is a pro-apoptotic Bcl-2 protein with restricted expression in reproductive tissues and heterodimerizes with selective anti-apoptotic Bcl-2 family members. *Proc. Natl. Acad. Sci. U. S. A.* **94**, 12401–6 (1997).

106. Zheng, J. H. *et al.* Intrinsic Instability of BOK Enables Membrane Permeabilization in Apoptosis Data and Software Availability 6CKV. *CellReports* **23**, 2083-2094.e6 (2018).

107. Oltvai, Z. N., Milliman, C. L. & Korsmeyer, S. J. Bcl-2 heterodimerizes in vivo with a conserved homolog, Bax, that accelerates programmed cell death. *Cell* **74**, 609–19 (1993).

108. Suzuki, M., Youle, R. J. & Tjandra, N. Structure of Bax: coregulation of dimer formation and intracellular localization. *Cell* **103**, 645–54 (2000).

109. Hsu, Y. T., Wolter, K. G. & Youle, R. J. Cytosol-to-membrane redistribution of Bax and Bcl-X(L) during apoptosis. *Proc. Natl. Acad. Sci. U. S. A.* **94**, 3668–72 (1997).

110. Schellenberg, B. *et al.* Bax Exists in a Dynamic Equilibrium between the Cytosol and Mitochondria to Control Apoptotic Priming. *Mol. Cell* **49**, 959–971 (2013).

111. Todt, F. *et al.* Differential retrotranslocation of mitochondrial Bax and Bak. *EMBO J.* **34**, 67–80 (2015).

112. Soriano, M. E. E. & Scorrano, L. Traveling Bax and Forth from Mitochondria to Control Apoptosis. *Cell* **145**, 15–17 (2011).

113. Valentijn, A. J., Metcalfe, A. D., Kott, J., Streuli, C. H. & Gilmore, A. P. Spatial and temporal changes in Bax subcellular localization during anoikis. *J. Cell Biol.* **162**, 599–612 (2003).

114. Owens, T. W. *et al.* Apoptosis commitment and activation of mitochondrial Bax during anoikis is regulated by p38MAPK. *Cell Death Differ.* **16**, 1551–1562 (2009).

115. Miyashita, T. *et al.* Tumor suppressor p53 is a regulator of bcl-2 and bax gene expression in vitro and in vivo. *Oncogene* **9**, 1799–805 (1994).

116. Gavathiotis, E. *et al.* BAX activation is initiated at a novel interaction site. *Nature* **455**, 1076–1081 (2008).

117. Cartron, P.-F. *et al.* The first alpha helix of Bax plays a necessary role in its ligand-induced activation by the BH3-only proteins Bid and PUMA. *Mol. Cell* **16**, 807–18 (2004).

118. Czabotar, P. E. *et al.* Bax crystal structures reveal how BH3 domains activate Bax and nucleate its oligomerization to induce apoptosis. *Cell* **152**, 519–31 (2013).

119. Chen, H.-C. *et al.* An interconnected hierarchical model of cell death regulation by the BCL-2 family. *Nat. Cell Biol.* **17**, 1270–1281 (2015).

120. Schinzel, A. *et al.* Conformational control of Bax localization and apoptotic activity by Pro168. *J. Cell Biol.* **164**, (2004).

121. Nechushtan, A., Smith, C. L., Hsu, Y.-T. T. & Youle, R. J. Conformation of the Bax C-terminus regulates subcellular location and cell death. *EMBO J.* **18**, 2330–41 (1999).

122. George, N. M., Evans, J. J. D. D. & Luo, X. A three-helix homo-oligomerization domain containing BH3 and BH1 is responsible for the apoptotic activity of Bax. *Genes Dev.* **21**, 1937–48 (2007).

123. Westphal, D. *et al.* Apoptotic pore formation is associated with in-plane insertion of Bak or Bax central helices into the mitochondrial outer membrane. *Proc. Natl. Acad. Sci. U. S. A.* **111**, E4076–E4085 (2014).

124. Dewson, G. *et al.* Bax dimerizes via a symmetric BH3:groove interface during apoptosis. *Cell Death Differ.* **19**, 661–670 (2012).

125. Zhang, Z. *et al.* BH 3-in-groove dimerization initiates and helix 9 dimerization expands Bax pore assembly in membranes . *EMBO J.* **35**, 208–236 (2016).

126. Große, L. *et al.* Bax assembles into large ring-like structures remodeling the mitochondrial outer membrane in apoptosis. *EMBO J.* **35**, 402–413 (2016).

127. Subburaj, Y. *et al.* Bax monomers form dimer units in the membrane that further self-assemble into multiple oligomeric species. *Nat. Commun.* **6**, 1–11 (2015).

128. Valentijn, A. J., Upton, J.-P. & Gilmore, A. P. Analysis of endogenous Bax complexes during apoptosis using blue native PAGE: implications for Bax activation and oligomerization. *Biochem. J.* **412**, 347–357 (2008).

129. Bleicken, S. *et al.* Structural Model of Active Bax at the Membrane. *Mol. Cell* **56**, 496–505 (2014).

130. Knudson, C. M. *et al.* Bax-deficient mice with lymphoid hyperplasia and male germ cell death. *Science* **270**, 96–9 (1995).

131. Sun, W., Gould, T. W., Vinsant, S., Prevette, D. & Oppenheim, R. W. Neuromuscular development after the prevention of naturally occurring neuronal death by Bax deletion. *J. Neurosci.* **23**, 7298–310 (2003).

132. Scorrano, L. *et al.* BAX and BAK regulation of endoplasmic reticulum Ca2+: a control point for apoptosis. *Science* **300**, 135–9 (2003).

133. Zong, W.-X. *et al.* Bax and Bak can localize to the endoplasmic reticulum to initiate apoptosis. *J. Cell Biol.* **162**, 59–69 (2003).

134. Karbowski, M. *et al.* Spatial and temporal association of Bax with mitochondrial fission sites, Drp1, and Mfn2 during apoptosis. *J. Cell Biol.* **159**, 931–8 (2002).

135. Farrow, S. N. *et al.* Cloning of a bcl-2 homologue by interaction with adenovirus E1B 19K. *Nature* **374**, 731–733 (1995).

136. Griffiths, G. J. *et al.* Cell Damage-induced Conformational Changes of the Pro-Apoptotic Protein Bak In Vivo Precede the Onset of Apoptosis. *J. Cell Biol.* **144**, 903–914 (1999).

137. Setoguchi, K., Otera, H. & Mihara, K. Cytosolic factor- and TOM-independent import of C-tail-anchored mitochondrial outer membrane proteins. *EMBO J.* **25**, 5635–5647 (2006).

138. Chittenden, T. *et al.* A conserved domain in Bak, distinct from BH1 and BH2, mediates cell death and protein binding functions. *EMBO J.* **14**, 5589–5596 (1995).

139. Moldoveanu, T. *et al.* The X-ray structure of a BAK homodimer reveals an inhibitory zinc binding site. *Mol. Cell* **24**, 677–688 (2006).

140. Wang, H. *et al.* Novel dimerization mode of the human Bcl-2 family protein Bak, a mitochondrial apoptosis regulator. *J. Struct. Biol.* **166**, 32–37 (2009).

141. Zhou, L. & Chang, D. C. Dynamics and structure of the Bax-Bak complex responsible for releasing mitochondrial proteins during apoptosis. *J. Cell Sci.* **121**, 2186–96 (2008).

142. Iyer, S. *et al.* Identification of an activation site in Bak and mitochondrial Bax triggered by antibodies. *Nat. Commun.* **7**, 11734 (2016).

143. Lindsten, T. *et al.* The combined functions of proapoptotic Bcl-2 family members bak and bax are essential for normal development of multiple tissues. *Mol. Cell* **6**, 1389–99 (2000).

144. Karbowski, M., Norris, K. L., Cleland, M. M., Jeong, S.-Y. & Youle, R. J. Role of Bax and Bak in mitochondrial morphogenesis. *Nature* **443**, 658–662 (2006).

145. Yang, E. *et al.* Bad, a Heterodimeric Partner for Bcl-x, and Bcl-2, Displaces Bax and Promotes Cell Death. *Cell* **80**, 285–291 (1995).

146. Zha, J. *et al.* BH3 domain of BAD is required for heterodimerization with BCL-X(L) and pro-apoptotic activity. *J. Biol. Chem.* **272**, 24101–24104 (1997).

147. Polzien, L. *et al.* Identification of novel in vivo phosphorylation sites of the human proapoptotic protein BAD. Pore-forming activity of bad is regulated by phosphorylation. *J. Biol. Chem.* **284**, 28004–28020 (2009).

148. Zha, J., Harada, H., Yang, E., Jockel, J. & Korsmeyer, S. J. Serine phosphorylation of death agonist BAD in response to survival factor results in binding to 14-3-3 not BCL-X(L). *Cell* **87**, 619–628 (1996).

149. Tan, Y., Demeter, M. R., Ruan, H. & Comb, M. J. BAD Ser-155 phosphorylation regulates BAD/Bcl-XL interaction and cell survival. *J. Biol. Chem.* **275**, 25865–25869 (2000).

150. Ranger, A. M. *et al.* Bad-deficient mice develop diffuse large B cell lymphoma. *Proc. Natl. Acad. Sci.* **100**, 9324–9329 (2003).

151. Idogawa, M., Adachi, M., Minami, T., Yasui, H. & Imai, K. Overexpression of BAD preferentially augments anoikis. *Int. J. Cancer* **107**, 215–223 (2003).

152. Jiang, L. *et al.* BAD overexpression inhibits cell growth and induces apoptosis via mitochondrial-dependent pathway in non-small cell lung cancer. *Cancer Cell Int.* **13**, 1 (2013).

153. Taghiyev, A. F. *et al.* Overexpression of BAD Potentiates Sensitivity to Tumor Necrosis Factor-Related Apoptosis-Inducing Ligand Treatment in the Prostatic Carcinoma Cell Line LNCaP. *Mol. Cancer Res.* **1**, 500–507 (2003).

154. Jan, M.-S., Liu, H.-S. & Lin, Y.-S. Bad Overexpression Sensitizes NIH/3T3 Cells to Undergo Apoptosis Which Involves Caspase Activation and ERK Inactivation. *Biochem. Biophys. Res. Commun.* **264**, 724–729 (1999).

155. Chattopadhyay, A., Chiang, C.-W. & Yang, E. BAD/BCL-xL heterodimerization leads to bypass of G0/G1 arrest. *Oncogene* **20**, 4507–4518 (2001).

156. Danial, N. N. *et al.* BAD and glucokinase reside in a mitochondrial complex that integrates glycolysis and apoptosis. *Nature* **424**, 1–5 (2003).

157. Oda, E. Noxa, a BH3-Only Member of the Bcl-2 Family and Candidate Mediator of

p53-Induced Apoptosis. *Science (80-.).* **288**, 1053–1058 (2000).

158. Shibue, T. *et al.* Integral role of Noxa in p53-mediated apoptotic response. *Genes Dev.* **17**, 2233–2238 (2003).

159. Chen, L. *et al.* Differential Targeting of Prosurvival Bcl-2 Proteins by Their BH3-Only Ligands Allows Complementary Apoptotic Function. *Mol. Cell* **17**, 393–403 (2005).

160. Kim, J.-Y., Ahn, H.-J., Ryu, J.-H., Suk, K. & Park, J.-H. BH3-only protein Noxa is a mediator of hypoxic cell death induced by hypoxia-inducible factor 1alpha. *J. Exp. Med.* **199**, 113–24 (2004).

161. Hershko, T. & Ginsberg, D. Up-regulation of Bcl-2 homology 3 (BH3)-only proteins by E2F1 mediates apoptosis. *J. Biol. Chem.* **279**, 8627–34 (2004).

162. Nikiforov, M. A. *et al.* Tumor cell-selective regulation of NOXA by c-MYC in response to proteasome inhibition. *Proc. Natl. Acad. Sci. U. S. A.* **104**, 19488–93 (2007).

163. Bouillet, P. *et al.* Proapoptotic Bcl-2 relative Bim required for certain apoptotic responses, leukocyte homeostasis, and to preclude autoimmunity. *Science* **286**, 1735–8 (1999).

164. Lowman, X. H. *et al.* The Proapoptotic Function of Noxa in Human Leukemia Cells Is Regulated by the Kinase Cdk5 and by Glucose. *Mol. Cell* **40**, 823–833 (2010).

165. Wang, K., Yin, X. M., Chao, D. T., Milliman, C. L. & Korsmeyer, S. J. BID: a novel BH3 domain-only death agonist. *Genes Dev.* **10**, 2859–2869 (1996).

166. Chou, J. J., Li, H., Salvesen, G. S., Yuan, J. & Wagner, G. Solution structure of BID, an intracellular amplifier of apoptotic signaling. *Cell* **96**, 615–24 (1999).

167. Hinds, M. G. *et al.* Bim, Bad and Bmf: intrinsically unstructured BH3-only proteins that undergo a localized conformational change upon binding to prosurvival Bcl-2 targets. *Cell Death Differ.* **14**, 128–136 (2007).

168. Li, H., Zhu, H., Xu, C.-J. & Yuan, J. Cleavage of BID by Caspase 8 Mediates the Mitochondrial Damage in the Fas Pathway of Apoptosis. *Cell* **94**, 491–501 (1998).

169. Eskes, R., Desagher, S., Antonsson, B. & Martinou, J.-C. Bid Induces the Oligomerization and Insertion of Bax into the Outer Mitochondrial Membrane. *Mol. Cell. Biol.* **20**, 929–935 (2000).

170. Sarig, R. *et al.* BID-D59A is a potent inducer of apoptosis in primary embryonic fibroblasts. *J. Biol. Chem.* **278**, 10707–15 (2003).

171. Valentijn, A. J. & Gilmore, A. P. Translocation of Full-length Bid to Mitochondria during Anoikis. *J. Biol. Chem.* **279**, 32848–32857 (2004).

172. Wang, P. *et al.* Phosphorylation of the proapoptotic BH3-only protein Bid primes mitochondria for apoptosis during mitotic arrest. *Cell Rep.* **7**, 661–71 (2014).

173. Yin, X. M. *et al.* Bid-deficient mice are resistant to Fas-induced hepatocellular apoptosis. *Nature* **400**, 886–91 (1999).

174. Esposti, M. D., Erler, J. T., Hickman, J. A. & Dive, C. Bid, a Widely Expressed Proapoptotic Protein of the Bcl-2 Family, Displays Lipid Transfer Activity. *Mol. Cell. Biol.* **21**, 7268–7276 (2001).

175. Yeretssian, G. *et al.* Non-apoptotic role of BID in inflammation and innate immunity. *Nature* **474**, 96–99 (2011).

176. Luo, W. *et al.* Bid Mediates Anti-Apoptotic COX-2 Induction Through the IKKβ/NFκB Pathway Due to 5-MCDE Exposure. *Curr. Cancer Drug Targets* **10**, 96–106 (2010).

177. O'Connor, L. *et al.* Bim: a novel member of the Bcl-2 family that promotes apoptosis. *EMBO J.* **17**, 384–395 (1998).

178. U, M., Miyashita, T., Shikama, Y., Tadokoro, K. & Yamada, M. Molecular cloning and characterization of six novel isoforms of human Bim, a member of the proapoptotic Bcl-2 family. *FEBS Lett.* **509**, 135–41 (2001).

179. Hildeman, D. A. *et al.* Activated T cell death in vivo mediated by proapoptotic Bcl-2 family member Bim. *Immunity* **16**, 759–767 (2002).

180. Snow, A. L. *et al.* Critical role for BIM in T cell receptor restimulation-induced death. *Biol. Direct* **3**, (2008).

181. Herold, M. J. *et al.* Impact of conditional deletion of the pro-apoptotic BCL-2 family member BIM in mice. *Cell Death Dis.* **5**, (2014).

182. Gogada, R. *et al.* Bim, a proapoptotic protein, up-regulated via transcription factor E2F1-dependent mechanism, functions as a prosurvival molecule in cancer. *J. Biol. Chem.* **288**, 368–381 (2013).

183. O'Reilly, L. A. *et al.* Rapid hybridoma screening method for the identification of monoclonal antibodies to low-abundance cytoplasmic proteins. *Biotechniques* **25**, 824–30 (1998).

184. Puthalakath, H., Huang, D. C. S., O'Reilly, L. A., King, S. M. & Strasser, A. The proapoptotic activity of the Bcl-2 family member Bim is regulated by interaction with the dynein motor complex. *Mol. Cell* **3**, 287–296 (1999).

185. Ruppert, S. M. *et al.* The major isoforms of Bim contribute to distinct biological activities that govern the processes of autophagy and apoptosis in interleukin-7 dependent lymphocytes. *Biochim. Biophys. Acta - Mol. Cell Res.* **1823**, 1877–1893 (2012).

186. Rodriguez, D. A. *et al.* BH3-only proteins are part of a regulatory network that control the sustained signalling of the unfolded protein response sensor IRE1α. *EMBO J.* **31**, 2322–2335 (2012).

187. Herold, M. J. *et al.* Evidence against upstream regulation of the unfolded protein response (UPR) by pro-apoptotic BIM and PUMA. *Cell Death and Disease* **5**, (2014).

188. Nakano, K. & Vousden, K. H. PUMA, a Novel Proapoptotic Gene, Is Induced by p53. *Mol. Cell* **7**, 683–694 (2001).

189. Jeffers, J. R. *et al.* Puma is an essential mediator of p53-dependent and -independent apoptotic pathways. *Cancer Cell* **4**, 321–328 (2003).

190. Villunger, A. *et al.* p53-and Drug-Induced Apoptotic Responses Mediated by BH3-Only Proteins Puma and Noxa. doi:10.1126/science.1090072

191. Ekoff, M. *et al.* The BH3-only protein Puma plays an essential role in cytokine deprivation induced apoptosis of mast cells. *Blood* **110**, 3209–17 (2007).

192. Jabbour, A. M. *et al.* Myeloid progenitor cells lacking p53 exhibit delayed up-regulation of Puma and prolonged survival after cytokine deprivation. *Blood* **115**, 344–52 (2010).

193. Garrison, S. P. *et al.* Selection against PUMA gene expression in Myc-driven B-cell lymphomagenesis. *Mol. Cell. Biol.* **28**, 5391–402 (2008).

194. Bean, G. R. *et al.* PUMA and BIM are required for oncogene inactivation-induced apoptosis. *Sci. Signal.* **6**, ra20 (2013).

195. Gallenne, T. *et al.* Bax activation by the BH3-only protein Puma promotes cell dependence on antiapoptotic Bcl-2 family members. *J. Cell Biol.* **185**, 279–290 (2009).

196. Dai, H., Pang, Y. P., Ramirez-Alvarado, M. & Kaufmann, S. H. Evaluation of the BH3-only protein Puma as a direct Bak activator. *J. Biol. Chem.* **289**, 89–99 (2014).

197. Ren, D. *et al.* BID, BIM, and PUMA are essential for activation of the BAX- and BAK-dependent cell death program. *Science* **330**, 1390–3 (2010).

198. Ma, B. *et al.* Over-Expression of PUMA Correlates with the Apoptosis of Spinal Cord Cells in Rat Neuropathic Intermittent Claudication Model. *PLoS One* **8**, (2013).

199. Liu, Z. *et al.* PUMA overexpression induces reactive oxygen species generation and proteasome-mediated stathmin degradation in colorectal cancer cells. *Cancer Res.* **65**, 1647–54 (2005).

200. Zhang, F. *et al.* Proliferative and Survival Effects of PUMA Promote Angiogenesis. *Cell Rep.* **2**, 1272–1285 (2012).

201. Aouacheria, A., Rech de Laval, V., Combet, C. & Hardwick, J. M. Evolution of Bcl-2 homology motifs: homology versus homoplasy. *Trends Cell Biol.* **23**, 103–11 (2013).

202. Bae, J., Leo, C. P., Hsu, Y. & Hsueh, A. J. W. MCL-1S, a Splicing Variant of the Antiapoptotic BCL-2 Family Member MCL-1, Encodes a Proapoptotic Protein Possessing Only the BH3 Domain. (2000). doi:10.1074/jbc.M909826199

203. Letai, A. *et al.* Distinct BH3 domains either sensitize or activate mitochondrial apoptosis, serving as prototype cancer therapeutics. *Cancer Cell* **2**, 183–192 (2002).

204. Kuwana, T. *et al.* BH3 Domains of BH3-Only Proteins Differentially Regulate Bax-Mediated Mitochondrial Membrane Permeabilization Both Directly and Indirectly. *Mol. Cell* **17**, 525–535 (2005).

205. Willis, S. N. *et al.* Apoptosis Initiated When BH3 Ligands Engage Multiple Bcl-2 Homologs, Not Bax or Bak. *Science (80-.).* **315**, 856–859 (2007).

206. Uren, R. T. *et al.* Mitochondrial permeabilization relies on BH3 ligands engaging multiple prosurvival Bcl-2 relatives, not Bak. *J. Cell Biol.* **177**, 277–287 (2007).

207. Llambi, F. *et al.* A Unified Model of Mammalian BCL-2 Protein Family Interactions at the Mitochondria. *Mol. Cell* **44**, 517–531 (2011).

208. O'Neill, K. L., Huang, K., Zhang, J., Chen, Y. & Luo, X. Inactivation of prosurvival Bcl-2 proteins activates Bax/Bak through the outer mitochondrial membrane. *Genes Dev.* **30**, 973–88 (2016).

209. Hsu, Y. T. & Youle, R. J. Nonionic detergents induce dimerization among members of the Bcl-2 family. *J. Biol. Chem.* **272**, 13829–34 (1997).

210. Walensky, L. D. *et al.* Activation of apoptosis in vivo by a hydrocarbon-stapled BH3 helix. *Science* **305**, 1466–70 (2004).

211. Dai, H., Meng, X. W., Lee, S.-H., Schneider, P. A. & Kaufmann, S. H. Context-dependent Bcl-2/Bak Interactions Regulate Lymphoid Cell Apoptosis. *J. Biol. Chem.* **284**, 18311–18322 (2009).

212. Pécot, J. *et al.* Tight Sequestration of BH3 Proteins by BCL-xL at Subcellular Membranes Contributes to Apoptotic Resistance. *Cell Rep.* **17**, 3347–3358 (2016).

213. Rooswinkel, R. W. *et al.* Antiapoptotic potency of Bcl-2 proteins primarily relies on their stability, not binding selectivity. *Blood* **123**, 2806–2815 (2014).

214. Lovell, J. F. *et al.* Membrane Binding by tBid Initiates an Ordered Series of Events Culminating in Membrane Permeabilization by Bax. *Cell* **135**, 1074–1084 (2008).

215. Edlich, F. *et al.* Bcl-xL Retrotranslocates Bax from the Mitochondria into the Cytosol. *Cell* **145**, 104–116 (2011).

216. Gilmore, A. P., Metcalfe, A. D., Romer, L. H. & Streuli, C. H. Integrin-mediated survival signals regulate the apoptotic function of Bax through its conformation and subcellular localization. *J. Cell Biol.* **149**, 431–46 (2000).

217. Chonghaile, T. N. N. *et al.* Pretreatment Mitochondrial Priming Correlates with Clinical Response to Cytotoxic Chemotherapy. *Science* **334**, 1129–1134 (2011).

218. Deng, J. *et al.* BH3 Profiling Identifies Three Distinct Classes of Apoptotic Blocks to Predict Response to ABT-737 and Conventional Chemotherapeutic Agents. *Cancer Cell* **12**, 171–185 (2007).

219. Vo, T. T. *et al.* Relative mitochondrial priming of myeloblasts and normal HSCs determines chemotherapeutic success in AML. *Cell* **151**, 344–355 (2012).

220. Del Gaizo Moore, V., Schlis, K. D., Sallan, S. E., Armstrong, S. A. & Letai, A. BCL-2 dependence and ABT-737 sensitivity in acute lymphoblastic leukemia. *Blood* **111**, 2300–2309 (2008).

221. Del Gaizo Moore, V. *et al.* Chronic lymphocytic leukemia requires BCL2 to sequester prodeath BIM, explaining sensitivity to BCL2 antagonist ABT-737. *J. Clin. Invest.* **117**, 112–121 (2007).

222. Lithgow, T. & Wattenberg, B. Targeting of C-terminal (tail)-anchored proteins: understanding how cytoplasmic activities are anchored to intracellular membranes. *Traffic* **2**, 66–71 (2001).

223. Borgese, N., Gazzoni, I., Barberi, M., Colombo, S. & Pedrazzini, E. Targeting of a Tail-anchored Protein to Endoplasmic Reticulum and Mitochondrial Outer Membrane by Independent but Competing Pathways. *Mol. Biol. Cell* **12**, 2482–2496 (2001).

224. Wang, P. *et al.* Dynamin-related protein Drp1 is required for Bax translocation to mitochondria in response to irradiation-induced apoptosis. *Oncotarget* **6**, 22598–612 (2015).

225. Ichim, G. *et al.* Limited Mitochondrial Permeabilization Causes DNA Damage and Genomic Instability in the Absence of Cell Death. *Mol. Cell* **57**, 860–872 (2015).

226. Lebedeva, I., Rando, R., Ojwang, J., Cossum, P. & Stein, C. A. Bcl-xL in Prostate Cancer Cells: Effects of Overexpression and Down-Regulation on Chemosensitivity. *CANCER Res.* **60**, 6052–6060 (2000).

227. Beroukhim, R. *et al.* The landscape of somatic copy-number alteration across human cancers. *Nature* **463**, 899–905 (2010).

228. Liu, Y., Hernandez, A. M., Shibata, D. & Cortopassi, G. A. BCL2 translocation frequency rises with age in humans. *Proc. Natl. Acad. Sci. U. S. A.* **91**, 8910–4 (1994).

229. Dölken, G., Illerhaus, G., Hirt, C. & Mertelsmann, R. BCL-2/JH rearrangements in circulating B cells of healthy blood donors and patients with nonmalignant diseases. *J. Clin. Oncol.* **14**, 1333–1344 (1996).

230. Strasser, A., Harris, A. W. & Cory, S. E mu-bcl-2 transgene facilitates spontaneous transformation of early pre-B and immunoglobulin-secreting cells but not T cells. *Oncogene* **8**, 1–9 (1993).

231. Johnson, N. A. *et al.* Lymphomas with concurrent BCL2 and MYC translocations: the critical factors associated with survival. (2009). doi:10.1182/blood-2009-03-212191

232. Zantl, N. *et al.* Frequent loss of expression of the pro-apoptotic protein Bim in renal cell carcinoma: evidence for contribution to apoptosis resistance. *Oncogene* **26**, 7038–7048 (2007).

233. Fitzsimmons, L. *et al.* Coordinated repression of BIM and PUMA by Epstein–Barr virus latent genes maintains the survival of Burkitt lymphoma cells. *Cell Death Differ.* **25**, 241–254 (2018).

234. Zhang, C.-Z. *et al.* MiR-221 and miR-222 target PUMA to induce cell survival in glioblastoma. *Mol. Cancer* **9**, 229 (2010).

235. Sawai, H. *et al.* Somatic Frameshift Mutations in the BAX Gene in Colon Cancers of the Microsatellite Mutator Phenotype . *Science (80-.).* **275**, 967–969 (2002).

236. Miquel, C. *et al.* Role of bax Mutations in Apoptosis in Colorectal Cancers With Microsatellite Instability. *Am. J. Clin. Pathol.* **123**, 562–570 (2005).

237. Zhou, L., Gao, R., Wang, Y., Zhou, M. & Ding, Z. Loss of BAX by miR-365 Promotes Cutaneous Squamous Cell Carcinoma Progression by Suppressing Apoptosis. *Int. J. Mol. Sci. Artic.* **18**, 1–13 (2017).

238. Oltersdorf, T. *et al.* An inhibitor of Bcl-2 family proteins induces regression of solid tumours. *Nature* **435**, 677–81 (2005).

239. Gilormini, M. *et al.* Preferential targeting of cancer stem cells in the radiosensitizing effect of ABT-737 on HNSCC. *Oncotarget* **7**, 16731–44 (2016).

240. Park, C.-M. *et al.* Discovery of an Orally Bioavailable Small Molecule Inhibitor of Prosurvival B-Cell Lymphoma 2 Proteins. *J. Med. Chem.* **51**, 6902–6915 (2008).

241. Tse, C. *et al.* ABT-263: A Potent and Orally Bioavailable Bcl-2 Family Inhibitor. *Cancer Res.* **68**, 3421–3428 (2008).

242. Shoemaker, A. R. *et al.* The Bcl-2 Family Inhibitor ABT-263 Shows Significant but Reversible Thrombocytopenia in Mice. *Blood* **108**, (2006).

243. Wilson, W. H. *et al.* Navitoclax, a targeted high-affinity inhibitor of BCL-2, in lymphoid malignancies: a phase 1 dose-escalation study of safety, pharmacokinetics, pharmacodynamics, and antitumour activity. *Lancet Oncol.* **11**, 1149–1159 (2010).

244. Kaefer, A. *et al.* Mechanism-based pharmacokinetic/pharmacodynamic meta-analysis of navitoclax (ABT-263) induced thrombocytopenia. *Cancer Chemother. Pharmacol.* **74**, 593–602 (2014).

245. Mason, K. D. *et al.* Programmed Anuclear Cell Death Delimits Platelet Life Span. *Cell* **128**, 1173–1186 (2007).

246. Vogler, M. *et al.* Diminished Sensitivity of Chronic Lymphocytic Leukemia Cells to ABT-737 and ABT-263 Due to Albumin Binding in Blood. *Clin. Cancer Res.* **16**, 4217–4225 (2010).

247. Souers, A. J. *et al.* ABT-199, a potent and selective BCL-2 inhibitor, achieves antitumor activity while sparing platelets. *Nat. Med.* **19**, 202–208 (2013).

248. Henz, K. *et al.* Selective BH3-mimetics targeting BCL-2, BCL-XL or MCL-1 induce severe mitochondrial perturbations. *Biol. Chem.* **400**, 181–185 (2019).

249. Faqar-Uz-Zaman, S. F., Heinicke, U., Meister, M. T., Vogler, M. & Fulda, S. BCL-xL-selective BH3 mimetic sensitizes rhabdomyosarcoma cells to chemotherapeutics by activation of the mitochondrial pathway of apoptosis. *Cancer Lett.* **412**, 131–142 (2018).

250. Lessene, G. *et al.* Structure-guided design of a selective BCL-XL inhibitor. *Nat. Chem. Biol.* **9**, 390–397 (2013).

251. Levesley, J. *et al.* Selective BCL-XL inhibition promotes apoptosis in combination with MLN8237 in medulloblastoma and pediatric glioblastoma cells. *Neuro. Oncol.* **20**, 203–214 (2018).

252. Tao, Z.-F. *et al.* Discovery of a Potent and Selective BCL-X L Inhibitor with in Vivo Activity. *ACS Med. Chem. Lett* **5**, 9 (2014).

253. Xiang, W., Yang, C.-Y. & Bai, L. MCL-1 inhibition in cancer treatment. *Onco. Targets. Ther.* **11**, 7301–7314 (2018).

254. Montero, J. *et al.* Drug-Induced Death Signaling Strategy Rapidly Predicts Cancer Response to Chemotherapy. *Cell* **160**, 977–989 (2015).

255. Butterworth, M., Pettitt, A., Varadarajan, S. & Cohen, G. M. BH3 profiling and a toolkit of BH3-mimetic drugs predict anti-apoptotic dependence of cancer cells. *Br. J. Cancer* **114**, 638–641 (2016).

256. Crombie, J. *et al.* Dynamic BH3 Profiling Reveals Novel Therapeutic Strategies for the Treatment of Double-Hit Lymphoma. *Blood* **130**, (2017).

257. Certo, M. *et al.* Mitochondria primed by death signals determine cellular addiction to antiapoptotic BCL-2 family members. *Cancer Cell* **9**, 351–365 (2006).

258. Grabow, S. *et al.* Subtle Changes in the Levels of BCL-2 Proteins Cause Severe Craniofacial Abnormalities. *Cell Rep.* **24**, 3285-3295.e4 (2018).

259. Lessene, G., Czabotar, P. E. & Colman, P. M. BCL-2 family antagonists for cancer therapy. *Nat. Rev. Drug Discov.* **7**, 989–1000 (2008).

260. Blombery, P. *et al. Characterization of a novel venetoclax resistance mutation (BCL2 Phe104Ile) observed in follicular lymphoma*. *British Journal of Haematology* **186**, 188–191 (2019).

261. Tausch, E. *et al.* Venetoclax resistance and acquired BCL2 mutations in chronic lymphocytic leukemia. *Haematologica* **104**, 434–437 (2019).

262. Liu, Q. *et al.* Bim escapes displacement by BH3-mimetic anti-cancer drugs by double-bolt locking both Bcl-XL and Bcl-2. *Elife* **8**, (2019).

263. Casara, P. *et al.* S55746 is a novel orally active BCL-2 selective and potent inhibitor that impairs hematological tumor growth. *Oncotarget* **9**, 20075–20088 (2018).

264. Flusberg, D. A., Roux, J., Spencer, S. L. & Sorger, P. K. Cells surviving fractional killing by TRAIL exhibit transient but sustainable resistance and inflammatory phenotypes. *Mol. Biol. Cell* **24**, 2186–2200 (2013).

265. Littlewood, T. D. *et al.* A modified oestrogen receptor ligand-binding domain as an improved switch for the regulation of heterologous proteins. *Nucleic Acids Res.* **23**, 1686–90 (1995).

266. Ran, F. A. *et al.* Genome engineering using the CRISPR-Cas9 system. *Nat. Protoc.* **8**, 2281–308 (2013).

267. Tyanova, S., Temu, T. & Cox, J. The MaxQuant computational platform for mass spectrometry-based shotgun proteomics. *Nat. Protoc.* **11**, 2301–2319 (2016).

268. Teo, G. *et al.* SAINTexpress: improvements and additional features in Significance Analysis of INTeractome software. *J. Proteomics* **100**, 37–43 (2014).

269. Todt, F., Cakir, Z., Reichenbach, F., Youle, R. J. & Edlich, F. The C-terminal helix of Bcl-xL mediates Bax retrotranslocation from the mitochondria. *Cell Death Differ.* **20**, 333–342 (2012).

270. Liu, Q., Leber, B. & Andrews, D. W. Interactions of pro-apoptotic BH3 proteins with anti-apoptotic Bcl-2 family proteins measured in live MCF-7 cells using FLIM FRET. *Cell Cycle* **1119**, 3536–3542 (2012).

271. Vuillier, C. *et al.* E2F1 interacts with BCL - xL and regulates its subcellular localization dynamics to trigger cell death. *EMBO Rep.* **19**, 234–243 (2018).

272. Hessa, T. *et al.* Molecular code for transmembrane-helix recognition by the Sec61 translocon. *Nature* **450**, 1026–1030 (2007).

273. Kaufmann, T. *et al.* Characterization of the signal that directs Bcl-x(L), but not Bcl-2, to the mitochondrial outer membrane. *J. Cell Biol.* **160**, 53–64 (2003).

274. Borner, C. *et al.* The protein bcl-2 alpha does not require membrane attachment, but two conserved domains to suppress apoptosis. *J. Cell Biol.* **126**, 1059–1068 (1994).

275. Wolter, K. G. *et al.* Movement of Bax from the Cytosol to Mitochondria during Apoptosis. *J. Cell Biol.* **139**, 1281–1292 (1997).

276. Kim, H. *et al.* Hierarchical regulation of mitochondrion-dependent apoptosis by BCL-2 subfamilies. *Nat. Cell Biol.* **8**, 1348–1358 (2006).

277. Aranovich, A. *et al.* Differences in the Mechanisms of Proapoptotic BH3 Proteins Binding to Bcl-XL and Bcl-2 Quantified in Live MCF-7 Cells. *Mol. Cell* **45**, 754–763 (2012).

278. Reginato, M. J. *et al.* Integrins and EGFR coordinately regulate the pro-apoptotic protein Bim to prevent anoikis. *Nat. Cell Biol.* **5**, 733–740 (2003).

279. Zhou, X.-M., Liu, Y., Payne, G., Lutz, R. J. & Chittenden, T. Growth Factors Inactivate the Cell Death Promoter BAD by Phosphorylation of Its BH3 Domain on Ser155. *J. Biol. Chem.* **275**, 25046–25051 (2000).

280. Reits, E. A. J. & Neefjes, J. J. From fixed to FRAP: Measuring protein mobility and activity in living cells. *Nat. Cell Biol.* **3**, (2001).

281. Sprague, B. L. & McNally, J. G. FRAP analysis of binding: Proper and fitting. *Trends Cell Biol.* **15**, 84–91 (2005).

282. Beckman Anderson Fellow, M., Patterson, G. H. & Lippincott-Schwartz, J. A Photoactivatable GFP for Selective Photolabeling of Proteins and Cells. *Proc. Natl. Acad. Sci. U.S.A* **293**, 727 (1999).

283. Mihara, K. Targeting and insertion of nuclear-encoded preproteins into the mitochondrial outer membrane. *BioEssays* **22**, 364–371 (2000).

284. Lithgow, T., Strasser, A., Driel, V. & Bertram, J. F. The Protein Component Endoplasmic Mitochondrial Product of the Oncogene of the Nuclear Envelope , the Membrane Is a. **5**, (1994).

285. Ruggiano, A., Foresti, O. & Carvalho, P. ER-associated degradation: Protein quality control and beyond. *J. Cell Biol.* **204**, 869–879 (2014).

286. Chin, H. S. *et al.* VDAC2 enables BAX to mediate apoptosis and limit tumor development. *Nat. Commun.* **9**, 4976 (2018).

287. Akgul, C., Moulding, D. A., White, M. R. . & Edwards, S. W. In vivo localisation and stability of human Mcl-1 using green fluorescent protein (GFP) fusion proteins. *FEBS Lett.* **478**, 72–76 (2000).

288. Thomas, L. W. *et al.* Serine 162, an Essential Residue for the Mitochondrial Localization, Stability and Anti-Apoptotic Function of Mcl-1. *PLoS One* **7**, 1–10 (2012).

289. Ku, B., Liang, C., Jung, J. U. & Oh, B.-H. Evidence that inhibition of BAX activation by BCL-2 involves its tight and preferential interaction with the BH3 domain of BAX. *Cell Res.* **21**, 627–641 (2011).

290. Lopez, H. *et al.* Perturbation of the Bcl-2 Network and an Induced Noxa/Bcl-xL Interaction Trigger Mitochondrial Dysfunction after DNA Damage * □ S Downloaded from. *J. Biol. Chem.* **285**, 15016–15026 (2010).

291. Zhang, L. *et al.* Selective involvement of BH3-only proteins and differential targets of Noxa in diverse apoptotic pathways. *Cell Death Differ.* **18**, (2010).

292. Smith, A. J. *et al.* Noxa/Bcl-2 protein interactions contribute to bortezomib resistance in human lymphoid cells. *J. Biol. Chem.* **286**, 17682–92 (2011).

293. Yan, W. *et al.* Bcl-w Forms Complexes with Bax and Bak, and Elevated Ratios of Bax/Bcl-w and Bak/Bcl-w Correspond to Spermatogonial and Spermatocyte Apoptosis in the Testis. *Mol. Endocrinol.* **14**, 682–699 (2000).

294. Petros, A. M. *et al.* Rationale for Bcl-X $_L$ /Bad peptide complex formation from structure, mutagenesis, and biophysical studies. *Protein Sci.* **9**, 2528–2534 (2000).

295. Shamas-Din, A. *et al.* tBid Undergoes Multiple Conformational Changes at the Membrane Required for Bax Activation. *J. Biol. Chem.* **288**, 22111–22127 (2013).

296. Billen, L. P., Kokoski, C. L., Lovell, J. F., Leber, B. & Andrews, D. W. Bcl-XL Inhibits Membrane Permeabilization by Competing with Bax. *PLoS Biol.* **6**, e147 (2008).

297. Lopez, J. *et al.* Mito-priming as a method to engineer Bcl-2 addiction. *Nat. Commun.* **7**, 10538 (2016).

298. Bouillet, P. *et al.* The Role of the Pro-Apoptotic Bcl-2 Family Member Bim in Physiological Cell Death. *Ann. N. Y. Acad. Sci.* **926**, 83–89 (2006).

299. STRASSER, A. *et al.* The Role of Bim, a Proapoptotic BH3-Only Member of the Bcl-2 Family, in Cell-Death Control. *Ann. N. Y. Acad. Sci.* **917**, 541–548 (2006).

300. Ley, R., Balmanno, K., Hadfield, K., Weston, C. & Cook, S. J. Activation of the ERK1/2 Signaling Pathway Promotes Phosphorylation and Proteasome-dependent Degradation of the BH3-only Protein, Bim. *J. Biol. Chem.* **278**, 18811–18816 (2003).

301. Albert, M.-C., Brinkmann, K. & Kashkar, H. Noxa and cancer therapy: Tuning up the mitochondrial death machinery in response to chemotherapy. *Mol. Cell. Oncol.* **1**, e29906 (2014).

302. Carrington, J. C. & Dougherty, W. G. A viral cleavage site cassette: Identification of amino acid sequences required for tobacco etch virus polyprotein processing (potyvirus proteinase/celi-free expression/cleavage site requirements/protein engineering). *Proc. Nadl. Acad. Sci. USA* **85**, 3391–3395 (1988).

303. Gray, D. C., Mahrus, S. & Wells, J. A. Activation of Specific Apoptotic Caspases with an Engineered Small-Molecule-Activated Protease. *Cell* **142**, 637–646 (2010).

304. Danielian, P. S., White, R., Hoare, S. A., Fawell, S. E. & Parker, M. G. Identification of residues in the estrogen receptor that confer differential sensitivity to estrogen and hydroxytamoxifen. *Mol. Endocrinol.* **7**, 232–240 (1993).

305. Burden, D. A. *et al.* Topoisomerase II.etoposide interactions direct the formation of drug-induced enzyme-DNA cleavage complexes. *J. Biol. Chem.* **271**, 29238–44 (1996).

306. Clifford, B., Beljin, M., Stark, G. R. & Taylor, W. R. G2 arrest in response to topoisomerase II inhibitors: the role of p53. *Cancer Res.* **63**, 4074–81 (2003).

307. Schreiber, G., Haran, G. & Zhou, H.-X. Fundamental Aspects of Protein−Protein Association Kinetics. *Chem. Rev.* **109**, 839–860 (2009).

308. Ries, J. & Schwille, P. Fluorescence correlation spectroscopy. *BioEssays* **34**, 361–368 (2012).

309. Soderquist, R. S. *et al.* Systematic mapping of BCL-2 gene dependencies in cancer reveals molecular determinants of BH3 mimetic sensitivity. *Nat. Commun.* **9**, 1–13 (2018).

310. Kumar, R., Mandal, M., Lipton, A., Harvey, H. & Thompson, C. B. Overexpression of HER2 Modulates Bcl-2, Bcl-XL, and Tamoxifen-induced Apoptosis in Human MCF-7 Breast Cancer Cells. **2**, 12–17 (1996).

311. Hudson, S. G. *et al.* Microarray determination of Bcl-2 family protein inhibition sensitivity in breast cancer cells. *Exp. Biol. Med.* **238**, 248–256 (2013).

312. Downward, J. How BAD phosphorylation is good for survival. *Nat. Cell Biol.* **1**, E33–E35 (1999).

313. Ezzoukhry, Z. *et al.* The Bcl-2 Homology Domain 3 (BH3) Mimetic ABT-737 Reveals

the Dynamic Regulation of Bad, a Proapoptotic Protein of the Bcl-2 Family, by Bcl-xL. *Mol. Pharmacol.* **79**, 997–1004 (2011).

314. Rieder, C. L. & Maiato, H. Stuck in division or passing through: what happens when cells cannot satisfy the spindle assembly checkpoint. *Dev. Cell* **7**, 637–51 (2004).

315. Gascoigne, K. E. & Taylor, S. S. Cancer Cells Display Profound Intra-and Interline Variation following Prolonged Exposure to Antimitotic Drugs. *Cancer Cell* **14**, 111–122 (2008).

316. Spencer, S. L., Gaudet, S., Albeck, J. G., Burke, J. M. & Sorger, P. K. Non-genetic origins of cell-to-cell variability in TRAIL-induced apoptosis. *Nature* **459**, 428–432 (2009).

317. Schmid, J. *et al.* Systems Analysis of Cancer Cell Heterogeneity in Caspase-dependent Apoptosis Subsequent to Mitochondrial Outer Membrane Permeabilization. *J. Biol. Chem.* **287**, 41546–41559 (2012).

318. Rehm, M. *et al.* Single-cell Fluorescence Resonance Energy Transfer Analysis Demonstrates That Caspase Activation during Apoptosis Is a Rapid Process. *J. Biol. Chem.* **277**, 24506–24514 (2002).

319. Albeck, J. G., Burke, J. M., Spencer, S. L., Lauffenburger, D. A. & Sorger, P. K. Modeling a Snap-Action, Variable-Delay Switch Controlling Extrinsic Cell Death. *PLoS Biol.* **6**, e299 (2008).

320. Rehm, M. *et al.* Dynamics of outer mitochondrial membrane permeabilization during apoptosis. *Cell Death Differ.* **16**, 613–623 (2009).

321. Weaver, B. A. How Taxol/paclitaxel kills cancer cells. *Mol. Biol. Cell* **25**, 2677–81 (2014).

322. Pedley, R. & Gilmore, A. P. Mitosis and mitochondrial priming for apoptosis. *Biol. Chem.* **397**, 595–605 (2016).

323. Cagalinec, M. *et al.* Principles of the mitochondrial fusion and fission cycle in neurons. *J. Cell Sci.* **126**, 2187–2197 (2013).

324. Karbowski, M. *et al.* Quantitation of mitochondrial dynamics by photolabeling of individual organelles shows that mitochondrial fusion is blocked during the Bax activation phase of apoptosis. *J. Cell Biol.* **164**, 493–499 (2004).

325. Youle, R. J. & Karbowski, M. Mitochondrial fission in apoptosis. *Nat. Rev. Mol. Cell Biol.* **6**, 657–663 (2005).

326. Nechushtan, A., Smith, C. L., Lamensdorf, I., Yoon, S.-H. & Youle, R. J. Bax and Bak Coalesce into Novel Mitochondria-Associated Clusters during Apoptosis. *J. Cell Biol.* **153**, 1265–1276 (2001).

327. Mitra, K., Wunder, C., Roysam, B., Lin, G. & Lippincott-Schwartz, J. A hyperfused mitochondrial state achieved at G1-S regulates cyclin E buildup and entry into S phase. *Proc. Natl. Acad. Sci. U. S. A.* **106**, 11960–5 (2009).

328. Taguchi, N., Ishihara, N., Jofuku, A., Oka, T. & Mihara, K. Mitotic Phosphorylation of Dynamin-related GTPase Drp1 Participates in Mitochondrial Fission. *J. Biol. Chem.* **282**, 11521–11529 (2007).

329. Alenzi, F. Q. B. Links between apoptosis, proliferation and the cell cycle. *Br. J. Biomed. Sci.* **61**, 99–102 (2004).

330. Mellor, H. R., Ferguson, D. & Callaghan, R. A model of quiescent tumour microregions for evaluating multicellular resistance to chemotherapeutic drugs. *Br. J. Cancer* **93**, 302–309 (2005).

331. Evan, G. I. *et al.* Induction of apoptosis in fibroblasts by c-myc protein. *Cell* **69**, 119–28 (1992).

332. Vasquez, R. J., Howell, B., Yvon, A. M., Wadsworth, P. & Cassimeris, L. Nanomolar concentrations of nocodazole alter microtubule dynamic instability in vivo and in vitro. *Mol. Biol. Cell* **8**, 973–85 (1997).

333. Schvartzman, J. B., Krimer, D. B. & Van't Hof, J. The effects of different thymidine concentrations on DNA replication in pea-root cells synchronized by a protracted 5-fluorodeoxyuridine treatment. *Exp. Cell Res.* **150**, 379–389 (1984).

334. Kurose, A., Tanaka, T., Huang, X., Traganos, F. & Darzynkiewicz, Z. Synchronization in the cell cycle by inhibitors of DNA replication induces histone H2AX phosphorylation: an indication of DNA damage. *Cell Prolif.* **39**, 231–240 (2006).

335. Sakaue-Sawano, A. *et al.* Visualizing Spatiotemporal Dynamics of Multicellular Cell-Cycle Progression. *Cell* **132**, 487–498 (2008).

336. Bajar, B. T. *et al.* Fluorescent indicators for simultaneous reporting of all four cell cycle phases. *Nat. Methods* **13**, 993–996 (2016).

337. Albeck, J. G., Mills, G. B. & Brugge, J. S. Frequency-Modulated Pulses of ERK Activity Transmit Quantitative Proliferation Signals. *Mol. Cell* **49**, 249–261 (2013).

338. Niepel, M. *et al.* Analysis of growth factor signaling in genetically diverse breast cancer lines. *BMC Biol.* **12**, 20 (2014).

339. Howells, C. C., Baumann, W. T., Samuels, D. C. & Finkielstein, C. V. The Bcl-2-associated death promoter (BAD) lowers the threshold at which the Bcl-2-interacting domain death agonist (BID) triggers mitochondria disintegration. *J. Theor. Biol.* **271**, 114–123 (2011).

340. Adachi, M. & Imai, K. The proapoptotic BH3-only protein BAD transduces cell death signals independently of its interaction with Bcl-2. *Cell Death Differ.* **9**, 1240–1247 (2002).

341. Niepel, M., Spencer, S. L. & Sorger, P. K. Non-genetic cell-to-cell variability and the consequences for pharmacology. *Curr. Opin. Chem. Biol.* **13**, 556–61 (2009).

342. Harley, M. E., Allan, L. A., Sanderson, H. S. & Clarke, P. R. Phosphorylation of Mcl-1 by CDK1-cyclin B1 initiates its Cdc20-dependent destruction during mitotic arrest. *EMBO J.* **29**, 2407–20 (2010).

343. Wertz, I. E. *et al.* Sensitivity to antitubulin chemotherapeutics is regulated by MCL1 and FBW7. *Nature* **471**, 110–114 (2011).

344. O'Reilly, L. A., Huang, D. C. & Strasser, A. The cell death inhibitor Bcl-2 and its homologues influence control of cell cycle entry. *EMBO J.* **15**, 6979–6990 (1996).

345. Greider, C., Chattopadhyay, A., Parkhurst, C. & Yang, E. BCL-xL and BCL2 delay Myc-induced cell cycle entry through elevation of p27 and inhibition of G1 cyclin-dependent kinases. *Oncogene* **21**, 7765–7775 (2002).

346. Linette, G. P., Li, Y., Roth, K. & Korsmeyer, S. J. Cross talk between cell death and cell cycle progression: BCL-2 regulates NFAT-mediated activation. *Proc. Natl. Acad. Sci. U. S. A.* **93**, 9545–52 (1996).

347. Vail, M. E., Chaisson, M. L., Thompson, J. & Fausto, N. Bcl-2 expression delays hepatocyte cell cycle progression during liver regeneration. *Oncogene* **21**, 1548–1555 (2002).

348. Dawson, S.-J. *et al.* BCL2 in breast cancer: a favourable prognostic marker across molecular subtypes and independent of adjuvant therapy received. *Br. J. Cancer* **103**, 668–675 (2010).

349. Huang, D. C., O'Reilly, L. A., Strasser, A. & Cory, S. The anti-apoptosis function of Bcl-2 can be genetically separated from its inhibitory effect on cell cycle entry. *EMBO J.* **16**, 4628–38 (1997).

350. Lindsay, J., Esposti, M. D. & Gilmore, A. P. Bcl-2 proteins and mitochondria--specificity in membrane targeting for death. *Biochim. Biophys. Acta* **1813**, 532–9 (2011).

351. Sekar, R. B. & Periasamy, A. Fluorescence resonance energy transfer (FRET) microscopy imaging of live cell protein localizations. *J. Cell Biol.* **160**, 629–33 (2003).

352. Pedley, R. *et al.* BioID based proteomic screen identifies VDAC2 as a coordinator of Bid dependent apoptotic priming during mitosis. *bioRxiv* 529685 (2019). doi:https://doi.org/10.1101/529685

353. Choi-Rhee, E., Schulman, H. & Cronan, J. E. Promiscuous protein biotinylation by Escherichia coli biotin protein ligase. *Protein Sci.* **13**, 3043–3050 (2008).

354. Agircan, F. G., Hata, S., Nussbaum-Krammer, C., Atorino, E. & Schiebel, E. Proximity mapping of human separase by the BioID approach. *Biochem. Biophys. Res. Commun.* **478**, 656–662 (2016).

355. Roux, K. J., Kim, D. I., Raida, M. & Burke, B. A promiscuous biotin ligase fusion protein identifies proximal and interacting proteins in mammalian cells. *J. Cell Biol.* **196**, 801–810 (2012).

356. Dong, J.-M. *et al.* Proximity biotinylation provides insight into the molecular composition of focal adhesions at the nanometer scale. *Sci. Signal.* **9**, 1–13 (2016).

357. Shin, H.-W., Shinotsuka, C., Torii, S., Murakami, K. & Nakayama, K. Identification and Subcellular Localization of a Novel Mammalian Dynamin-Related Protein Homologous to Yeast Vps1p and Dnm1p. *J. Biochem.* **122**, 525–530 (1997).

358. Smirnova, E., Shurland, D.-L., Ryazantsev, S. N. & Van Der Bliek, A. M. A Human Dynamin-related Protein Controls the Distribution of Mitochondria. *J. Cell Biol.* **143**, 351–358 (1998).

359. Wakabayashi, J. *et al.* The dynamin-related GTPase Drp1 is required for embryonic and brain development in mice. *J. Cell Biol.* **186**, 805–816 (2009).

360. Ishihara, N. *et al.* Mitochondrial fission factor Drp1 is essential for embryonic development and synapse formation in mice. *Nat. Cell Biol.* **11**, 958–966 (2009).

361. Estaquier, J. & Arnoult, D. Inhibiting Drp1-mediated mitochondrial fission selectively prevents the release of cytochrome c during apoptosis. *Cell Death Differ.* **14**, 1086–1094 (2007).

362. Li, H. *et al.* Bcl-xL induces Drp1-dependent synapse formation in cultured hippocampal neurons. *Proc. Natl. Acad. Sci. U. S. A.* **105**, 2169–74 (2008).

363. Merrill, R. A. *et al.* Mechanism of Neuroprotective Mitochondrial Remodeling by PKA/AKAP1. *PLoS Biol.* **9**, 1–19 (2011).

364. Flippo, K. H. *et al.* AKAP1 Protects from Cerebral Ischemic Stroke by Inhibiting Drp1-Dependent Mitochondrial Fission. **38**, 8233–8242 (2018).

365. Trendelenburg, G., Hummel, M., Riecken, E.-O. & Hanski, C. Molecular Characterization of AKAP149, a Novel A Kinase Anchor Protein with a KH Domain. *Biochem. Biophys. Res. Commun.* **225**, 313–319 (1996).

366. Jun, Y.-W. *et al.* D-AKAP1a is a signal-anchored protein in the mitochondrial outer membrane. *FEBS Lett.* **590**, 954–961 (2016).

367. Huang, L. J. *et al.* NH_2 -Terminal Targeting Motifs Direct Dual Specificity A-Kinase–anchoring Protein 1 (D-AKAP1) to Either Mitochondria or Endoplasmic Reticulum. *J. Cell Biol.* **145**, 951–959 (1999).

368. Harada, H. *et al.* Phosphorylation and Inactivation of BAD by Mitochondria-Anchored Protein Kinase A. *Mol. Cell* **3**, 413–422 (1999).

369. Affaitati, A. *et al.* Essential role of A-kinase anchor protein 121 for cAMP signaling to mitochondria. *J. Biol. Chem.* **278**, 4286–94 (2003).

370. Lam, E., Martin, M. & Wiederrecht, G. Isolation of a cDNA encoding a novel human FK506-binding protein homolog containing leucine zipper and tetratricopeptide repeat motifs. *Gene* **160**, 297–302 (1995).

371. Fischer, G., Bang, H. & Mech, C. [Determination of enzymatic catalysis for the cis-trans-isomerization of peptide binding in proline-containing peptides]. *Biomed. Biochim. Acta* **43**, 1101–11 (1984).

372. Shirane-Kitsuji, M. & Nakayama, K. I. Mitochondria: FKBP38 and mitochondrial degradation. *Int. J. Biochem. Cell Biol.* **51**, 19–22 (2014).

373. Edlich, F. *et al.* Bcl-2 regulator FKBP38 is activated by Ca2+/calmodulin. *EMBO J.* **24**, 2688–2699 (2005).

374. Shirane, M. & Nakayama, K. I. Inherent calcineurin inhibitor FKBP38 targets Bcl-2 to mitochondria and inhibits apoptosis. *Nat. Cell Biol.* **5**, 28–37 (2003).

375. Chen, Y., Sternberg, P. & Cai, J. Characterization of a Bcl-XL-interacting protein FKBP8 and its splice variant in human RPE cells. *Invest. Ophthalmol. Vis. Sci.* **49**, 1721–7 (2008).

376. Edlich, F. *et al.* The Bcl-2 regulator FKBP38-calmodulin-Ca2+ is inhibited by Hsp90. *J. Biol. Chem.* **282**, 15341–8 (2007).

377. Yuan, H., Li, X., Zhang, X., Kang, R. & Tang, D. CISD1 inhibits ferroptosis by protection against mitochondrial lipid peroxidation. *Biochem. Biophys. Res. Commun.* **478**, 838–844 (2016).

378. Chang, N. C., Nguyen, M., Germain, M. & Shore, G. C. Antagonism of Beclin 1-dependent autophagy by BCL-2 at the endoplasmic reticulum requires NAF-1. *EMBO J.* **29**, 606–618 (2010).

379. King, S. D. *et al.* The cisd gene family regulates physiological germline apoptosis through ced-13 and the canonical cell death pathway in Caenorhabditis elegans. *Cell Death Differ.* **26**, 162–178 (2019).

380. Kataoka, T. *et al.* Bcl-rambo, a Novel Bcl-2 Homologue That Induces Apoptosis via Its Unique C-terminal Extension. *J. Biol. Chem.* **276**, 19548–19554 (2001).

381. Kim, J.-Y., So, K.-J., Lee, S. & Park, J.-H. Bcl-rambo induces apoptosis via interaction with the adenine nucleotide translocator. *FEBS Lett.* **586**, 3142–3149 (2012).

382. Murakawa, T. *et al.* Bcl-2-like protein 13 is a mammalian Atg32 homologue that mediates mitophagy and mitochondrial fragmentation. *Nat. Commun.* **6**, 7527 (2015).

383. Coles, B. F. & Kadlubar, F. F. Detoxification of electrophilic compounds by glutathione S-transferase catalysis: Determinants of individual response to chemical carcinogens and chemotherapeutic drugs? *BioFactors* **17**, 115–130 (2003).

384. Adler, V. Regulation of JNK signaling by GSTp. *EMBO J.* **18**, 1321–1334 (1999).

385. Lo, H.-W. & Ali-Osman, F. Genetic polymorphism and function of glutathione S-transferases in tumor drug resistance. *Curr. Opin. Pharmacol.* **7**, 367–374 (2007).

386. Singh, S., Okamura, T. & Ali-Osman, F. Serine phosphorylation of glutathione S-transferase P1 (GSTP1) by PKCα enhances GSTP1-dependent cisplatin metabolism and resistance in human glioma cells. *Biochem. Pharmacol.* **80**, 1343–1355 (2010).

387. Lin, C., Xie, L., Lu, Y., Hu, Z. & Chang, J. miR-133b reverses cisplatin resistance by targeting GSTP1 in cisplatin-resistant lung cancer cells. *Int. J. Mol. Med.* **41**, 2050 (2018).

388. Kelson, T. L., Secor McVoy, J. R. & Rizzo, W. B. Human liver fatty aldehyde dehydrogenase: microsomal localization, purification, and biochemical characterization. *Biochim. Biophys. Acta - Gen. Subj.* **1335**, 99–110 (1997).

389. Verhoeven, N. M. *et al.* Involvement of microsomal fatty aldehyde dehydrogenase in the α-oxidation of phytanic acid. *FEBS Lett.* **429**, 225–228 (1998).

390. Lloyd, M. D. *et al.* Characterisation of recombinant human fatty aldehyde dehydrogenase: Implications for Sjögren-Larsson syndrome. *J. Enzyme Inhib. Med. Chem.* **22**, 584–590 (2007).

391. Konermann, S. *et al.* Transcriptome Engineering with RNA-Targeting Type VI-D CRISPR Effectors. *Cell* **173**, 665–676 (2018).

392. Granados-Riveron, J. T. & Aquino-Jarquin, G. CRISPR–Cas13 Precision Transcriptome Engineering in Cancer. *Cancer Res.* **78**, 4107–4113 (2018).

393. Bleazard, W. *et al.* The dynamin-related GTPase Dnm1 regulates mitochondrial fission in yeast. *Nat. Cell Biol.* **1**, 298–304 (1999).

394. Wasiak, S., Zunino, R. & McBride, H. M. Bax/Bak promote sumoylation of DRP1 and its stable association with mitochondria during apoptotic cell death. *J. Cell Biol.* **177**, 439–450 (2007).

395. Kawai, T. *et al.* IPS-1, an adaptor triggering RIG-I- and Mda5-mediated type I interferon induction. *Nat. Immunol.* **6**, 981–988 (2005).

396. Xu, L.-G. *et al.* VISA Is an Adapter Protein Required for Virus-Triggered IFN-β Signaling. *Mol. Cell* **19**, 727–740 (2005).

397. Lei, Y. *et al.* MAVS-mediated apoptosis and its inhibition by viral proteins. *PLoS One* **4**, e5466 (2009).

398. Cuconati, A. & White, E. Viral homologs of BCL-2: role of apoptosis in the regulation of virus infection. *Genes Dev.* **16**, 2465–78 (2002).

399. Yin, Z., Ivanov, V. N., Habelhah, H., Tew, K. & Ronai, Z. Glutathione S-Transferase p Elicits Protection against H2O2-induced Cell Death via Coordinated Regulation of Stress Kinases. *Cancer Res.* **54**, 4313–4320 (2000).

400. Papadakis, E. S. *et al.* The regulation of Bax by c-Jun N-terminal protein kinase (JNK) is a prerequisite to the mitochondrial-induced apoptotic pathway. *FEBS Lett.* **580**, 1320–1326 (2006).

401. Lei, K. *et al.* The Bax Subfamily of Bcl2-Related Proteins Is Essential for Apoptotic Signal Transduction by c-Jun NH2-Terminal Kinase. *Mol. Cell. Biol.* **22**, 4929–4942 (2002).

402. Otani, K. *et al.* Cell-cycle-controlled radiation therapy was effective for treating a murine malignant melanoma cell line in vitro and in vivo. *Sci. Rep.* **6**, 30689 (2016).

403. Owen-Schaub, L. B. *et al.* Wild-type human p53 and a temperature-sensitive mutant induce Fas/APO-1 expression. *Mol. Cell. Biol.* **15**, 3032–40 (1995).

404. Wu, G. S. *et al.* KILLER/DR5 is a DNA damage–inducible p53–regulated death receptor gene. *Nat. Genet.* **17**, 141–143 (1997).

405. Gogineni, V. R. *et al.* Chk2-mediated G2/M cell cycle arrest maintains radiation resistance in malignant meningioma cells. *Cancer Lett.* **313**, 64–75 (2011).

406. Shimizu, S., Narita, M., Tsujimoto, Y. & Tsujimoto, Y. Bcl-2 family proteins regulate the release of apoptogenic cytochrome c by the mitochondrial channel VDAC. *Nature* **399**, 483–487 (1999).

407. Brenner, C. *et al.* Bcl-2 and Bax regulate the channel activity of the mitochondrial adenine nucleotide translocator. *Oncogene* **19**, 329–336 (2000).

408. Farmer, T. *et al.* Retromer facilitates the localization of Bcl-xL to the mitochondrial outer membrane. *Mol. Biol. Cell* **30**, (2019).

409. Kuwana, T. *et al.* Bid, Bax, and lipids cooperate to form supramolecular openings in the outer mitochondrial membrane. *Cell* **111**, 331–42 (2002).

410. Montessuit, S. *et al.* Membrane Remodeling Induced by the Dynamin-Related Protein Drp1 Stimulates Bax Oligomerization. *Cell* **142**, 889–901 (2010).

411. Grinberg, M. *et al.* Mitochondrial Carrier Homolog 2 Is a Target of tBID in Cells Signaled To Die by Tumor Necrosis Factor Alpha. *Mol. Cell. Biol.* **25**, 4579–4590 (2005).

412. Zaltsman, Y. *et al.* MTCH2/MIMP is a major facilitator of tBID recruitment to mitochondria. *Nat. Cell Biol.* **12**, 553–562 (2010).

413. Frezza, C. *et al.* OPA1 controls apoptotic cristae remodeling independently from mitochondrial fusion. *Cell* **126**, 177–89 (2006).

414. Jahnig, F. Thermodynamics and kinetics of protein incorporation into membranes. *Proc. Natl. Acad. Sci.* **80**, 3691–3695 (1983).

415. Hegde, R. S. & Keenan, R. J. Tail-anchored membrane protein insertion into the endoplasmic reticulum. *Nat. Rev. Mol. Cell Biol.* **12**, 787–798 (2011).

416. Mateja, A. *et al.* Protein targeting. Structure of the Get3 targeting factor in complex with its membrane protein cargo. *Science* **347**, 1152–5 (2015).

417. Mariappan, M. *et al.* The mechanism of membrane-associated steps in tail-anchored protein insertion. *Nature* **477**, 61–66 (2011).

418. Guna, A., Volkmar, N., Christianson, J. C. & Hegde, R. S. The ER membrane protein complex is a transmembrane domain insertase. *Science* **359**, 470–473 (2018).

419. Leznicki, P., Clancy, A., Schwappach, B. & High, S. Bat3 promotes the membrane integration of tail-anchored proteins. *J. Cell Sci.* **123**, 2170–8 (2010).

420. Janiak, F., Leber, B. & Andrews, D. W. Assembly of Bcl-2 into microsomal and outer mitochondrial membranes. *J. Biol. Chem.* **269**, 9842–9 (1994).

421. Lauterwasser, J. *et al.* The porin VDAC2 is the mitochondrial platform for Bax retrotranslocation. *Sci. Rep.* **6**, 32994 (2016).

422. Tsuruta, F. *et al.* JNK promotes Bax translocation to mitochondria through phosphorylation of 14-3-3 proteins. *EMBO J.* **23**, 1889–1899 (2004).

423. Cakir, Z. *et al.* Parkin promotes proteasomal degradation of misregulated BAX. *J. Cell Sci.* **130**, 2903–2913 (2017).

424. Yao, M. *et al.* Mechanical activation of vinculin binding to talin locks talin in an unfolded conformation. *Sci. Rep.* **4**, 4610 (2014).

425. Vasquez-Montes, V. *et al.* Lipid-modulation of membrane insertion and refolding of the apoptotic inhibitor Bcl-xL. *Biochim. Biophys. Acta - Proteins Proteomics* **1867**, 691–700 (2019).

426. Hantusch, A., Das, K. K., García-Sáez, A. J., Brunner, T. & Rehm, M. Bax retrotranslocation potentiates Bcl-xL's antiapoptotic activity and is essential for switch-like transitions between MOMP competency and resistance. *Cell Death Dis.* **9**, 430 (2018).

427. Lackner, L. L. Shaping the dynamic mitochondrial network. *BMC Biol.* **12**, 35 (2014).

428. das Neves, R. P. *et al.* Connecting Variability in Global Transcription Rate to Mitochondrial Variability. *PLoS Biol.* **8**, 1–11 (2010).

429. Johnston, I. G. *et al.* Mitochondrial Variability as a Source of Extrinsic Cellular Noise.

PLoS Comput. Biol. **8**, 1–14 (2012).

430. Márquez-Jurado, S. *et al.* Mitochondrial levels determine variability in cell death by modulating apoptotic gene expression. *Nat. Commun.* **9**, 389 (2018).

431. McArthur, K. *et al.* BAK/BAX macropores facilitate mitochondrial herniation and mtDNA efflux during apoptosis. *Science (80-.).* **359**, 1–12 (2018).

432. Vandemoortele, G. *et al.* A Well-Controlled BioID Design for Endogenous Bait Proteins. *J. Proteome Res.* **18**, 95–106 (2018).